

A STUDY OF HYDRAULIC FILL PERFORMANCE IN HONG KONG - PHASE 2

GEO REPORT No. 64

C.K. Shen, K.M. Lee & X.S. Li

**GEOTECHNICAL ENGINEERING OFFICE
CIVIL ENGINEERING DEPARTMENT
THE GOVERNMENT OF THE HONG KONG
SPECIAL ADMINISTRATIVE REGION**

A STUDY OF HYDRAULIC FILL PERFORMANCE IN HONG KONG - PHASE 2

GEO REPORT No. 64

C.K. Shen, K.M. Lee & X.S. Li

**This report was originally produced in July 1996
under Consultancy Agreement CE 51/94**

© The Government of the Hong Kong Special Administrative Region

First published, November 1997

Prepared by:

Geotechnical Engineering Office,
Civil Engineering Department,
Civil Engineering Building,
101 Princess Margaret Road,
Homantin, Kowloon,
Hong Kong.

This publication is available from:

Government Publications Centre,
Ground Floor, Low Block,
Queensway Government Offices,
66 Queensway,
Hong Kong.

Overseas orders should be placed with:

Publications (Sales) Office,
Information Services Department,
28th Floor, Siu On Centre,
188 Lockhart Road, Wan Chai,
Hong Kong.

Price in Hong Kong: HK\$150

Price overseas: US\$25 (including surface postage)

An additional bank charge of **HK\$50** or **US\$6.50** is required per cheque made in currencies other than Hong Kong dollars.

Cheques, bank drafts or money orders must be made payable to
The Government of the Hong Kong Special Administrative Region

PREFACE

In keeping with our policy of releasing information of general technical interest, we make available some of our internal reports in a series of publications termed the GEO Report series. The reports in this series, of which this is one, are selected from a wide range of reports produced by the staff of the Office and our consultants. A charge is made to cover the cost of printing.

The Geotechnical Engineering Office also publishes guidance documents and presents the results of research work of general interest in GEO Publications. These publications and the GEO Reports may be obtained from the Government's Information Services Department. Information on how to purchase these publications is given on the last page of this report.

A handwritten signature in black ink, appearing to read 'A.W. Malone', with a stylized, cursive script.

A.W. Malone
Principal Government Geotechnical Engineer
November 1997

FOREWORD

This report is the first volume of a set of three reports on the phase 2 study of performance of hydraulic fill in Hong Kong. The phase 1 study has been published as GEO Report No. 40. The phase 2 study was carried out by Professor C.K. Shen, Dr K.M. Lee and Dr X.S. Li of the Hong Kong University of Science and Technology (HKUST) as consultants to the Geotechnical Engineering Office (GEO) of the Civil Engineering Department. Professor J.K. Mitchell of the University of California at Berkeley, USA, Professor M. Jamiolkowski of the University of Turin, Italy and Dr. K. Been of Golder Associates Limited, UK assisted as sub-consultants. The project was partly funded by a Research Infrastructure Grant from HKUST.

The study was coordinated and reviewed by Mr Y.C. Chan, Dr J. Premchitt, Dr J. Kwong and Mr M. Shaw of the GEO.

Mr P.H. Ho of Binnie Consultants Limited, Mr J. Mckinlay of Mott MacDonald Hong Kong Limited, Mr D.B. Douglass of Maunsell Consultants Asia Limited, Mr M. Broadgate of Mott MacDonald Hong Kong Limited, and Mr R. Newman, Dr A. Pickles, Mr C. Covil and Mr N. Ng of the Airport Authority provided site specific data and assistance in field investigation and sampling at the Tin Shui Wai, West Kowloon, Tseung Kwan O, Tung Chung and Chek Lap Kok Reclamation Sites respectively.

Postgraduate students Mr D.C.K. Yu, Mr A. Ma, Ms Y. Wang, Mr R. Sun and Ms Y. Wang, and Senior Technician Mr K. Ma and Technician Mr M. Chung of the Department of Civil and Structural Engineering, HKUST assisted the authors in carrying out most of the field and experimental work, computer analysis, and preparation of figures and drawings presented in the report. The Drafting Unit of the Special Projects Division, GEO converted the figures and drawings into GEO format for the printing of this report.

Detailed test results and other information relevant to this report are provided in Appendices in Volumes 2 and 3 of the study reports. They are available for viewing in the Civil Engineering Library.



A.W. Malone
Principal Government Geotechnical Engineer
November 1997

CONTENTS

	Page No.
Title Page	1
PREFACE	3
FOREWORD	4
CONTENTS	5
1. INTRODUCTION	8
1.1 General	8
1.2 Background	8
1.3 Site Locations	8
2. BULK SAMPLING AND FIELD TESTING	8
2.1 Site Visits for Bulk Sampling	8
2.2 Bulk Sampling	9
2.3 Transport	9
2.4 Field Test (The Tung Chung Site)	9
2.5 Results of Drilling	10
2.6 Standard Penetration Tests (SPT)	10
2.7 Undisturbed Sampling of Hydraulic Sand Fill	10
2.8 Seismic Cone Penetration Tests (SCPT)	11
2.9 Correlation of Field Test Results	11
2.10 Field Test Data at Chek Lap Kok	13
3. CASE HISTORIES AND SURVEY QUESTIONNAIRE	14
3.1 New Airport at Chek Lap Kok	15
3.2 Tung Chung Reclamation Area	17
3.3 Findings from Surveys of the Five Sites	19
3.3.1 Effects of Grading of the Borrow Materials	19
3.3.2 Seabed Preparation Work	20
3.3.3 Effects of Bottom-dumping	21

	Page No.
3.3.4 Subaqueous Placement by Rainbowing and Pipeline	26
3.3.5 Subaerial Placed Sand	27
4. LABORATORY TESTS	27
4.1 Physical Properties Determination	27
4.2 Triaxial Static Tests	29
4.2.1 Static Triaxial Tests - Tung Chung Sand	30
4.2.2 Static Triaxial Tests - Chek Lap Kok Sand	31
4.3 Cyclic Triaxial Tests	31
4.3.1 Cyclic Triaxial Tests - Tung Chung Sands	32
4.3.2 Cyclic Triaxial Tests - Chek Lap Kok Sand	33
5. RELATIONSHIP BETWEEN VOID RATIO AND SHEAR WAVE VELOCITY	33
5.1 Shear Wave Velocity Measurement	33
5.2 Laboratory Shear Wave Velocity Measurement	34
5.3 Set-up of Laboratory Shear Wave Velocity Measurement	34
5.4 Scheme of Work	35
5.5 Results of Measurement	35
6. STEADY STATE OF HYDRAULIC FILL SANDS IN HONG KONG	36
6.1 Introduction	36
6.2 Terminology	37
6.3 Steady State Line Determination at Medium Stress Range (about 200 kPa to about 1000 kPa)	38
6.4 Non-linear Steady State Lines for the Hong Kong Marine Sands	40
6.5 Linear Representation of Steady State Lines for the Marine Sands in Hong Kong	43
7. CALIBRATION CHAMBER TESTS	48
7.1 Introduction	48
7.2 Calibration Chamber Testing Procedure	48
7.3 Correction for Boundary Conditions	49

	Page No.
7.4 Correlation with Cone Tip Resistance	50
7.5 Correlation with Shear Wave Velocity	53
8. SITE RESPONSE TO DYNAMIC LOADS	55
9. DEVELOPMENT OF QUALITY CONTROL GUIDELINE FOR HYDRAULIC SAND FILL PLACEMENT	56
9.1 Introduction	56
9.2 "Dense" Sand versus "Loose" Sand	57
9.3 Cone Penetration Test (CPT) to Evaluate In-situ State	58
9.4 Cone Penetration Test (CPT) to Evaluate Relative Density of Soils	61
9.5 Shear Wave Velocity to Evaluate In-situ State	62
9.6 Evaluation of the Proposed Relationships	64
9.7 Proposed Application	65
9.8 Recommended Soil Constants to be Used for Quality Control	67
10. SUMMARY AND CONCLUSIONS	68
10.1 Estimating the Needed Density	69
10.2 Estimating the Likely CPT- q_c Achievable by the Given Material Type and Placement Method	70
10.3 Verifying the In-situ Density on the Basis of Field Test Results	72
10.4 Optimization of Hydraulic Fill Properties During Placement	73
10.5 Conclusion	74
11. REFERENCES	75
LIST OF TABLES	80
LIST OF FIGURES	102
LIST OF PLATES	260

1. INTRODUCTION

1.1 General

This report presents the results and findings of an investigation on "Hydraulic Fill Performance in Hong Kong, Phase 2", under the Agreement No. CE 51/94 with the Civil Engineering Department of the Hong Kong Government.

1.2 Background

In Phase 1 of the study, the behaviour of hydraulic fill sands from West Kowloon (CS1), Tseung Kwan O (TKO) and Tin Shui Wai (TSW) were evaluated and their responses to the various types of loadings were studied. In Phase 2, a similar study of sands from Tung Chung (TC) and Chek Lap Kok (CLK) was proposed including a literature review; site visits and interviews; stress chamber tests; field tests; laboratory tests; and the inclusion of the state parameter concept in forming a theoretical framework to interpret the operation and control of placement of hydraulic sand fill.

1.3 Site Locations

Locations of the two reclamation sites (Chek Lap Kok and Tung Chung) are shown in the site plans Figures 1.1 and 1.2 respectively.

The CLK marine sand was obtained from a stockpile not necessarily representing the sand from a specific borrow pit. No field testing has been conducted at CLK except those carried out at HAECO site, but large amount of previous test data from two study areas within the new airport site at CLK have been obtained from the Airport Authority (AA).

2. BULK SAMPLING AND FIELD TESTING

2.1 Site Visits for Bulk Sampling

During the period from November to December 1994, a number of site visits were made to the Tung Chung (TC) and Chek Lap Kok (CLK) reclamation sites

- to carry out discussions with site engineers
- to review all the relevant background data and information of the sites
- to familiarize with site conditions and construction processes of the sites
- to locate areas for field work and bulk sampling.

2.2 Bulk Sampling

Bulk samples of hydraulic sand fill material were obtained at the Tung Chung reclamation area (TC) and at the new airport at Chek Lap Kok (CLK) between 17 and 18 of February 1995. The location where the TC bulk sample was taken is shown in Figure 2.1; whereas, the CLK bulk sample was taken from the stockpile area near Area D3/1 just to the north of Works Order No. 38 (information provided by I-P Foundation Ltd.) and in between the haul roads as shown in Figure 2.2, where sand mixture from four different marine sand borrow sources (Tsing Yi, Poi Toi, Sha Chau, and Brother Islands) were stacked (see Plate 2.1). The bulk sample obtained from the stockpile area can be considered fairly representative of the marine sand used in the new replacement airport at Chek Lap Kok. Bulk samples for TC were obtained from a depth of 2 to 3 m below the ground surface (see Plate 2.2). Mechanical excavators were used to load the bulk sand sample into steel barrels of 0.2 cubic metres in volume. The steel barrels were then capped and sealed. Each barrel was carefully checked and labeled in the field. A total of 20 barrels each from Tung Chung and Chek Lap Kok were obtained and placed in a 20-ft long container for shipment.

2.3 Transport

The shipment was handled by Danzas Freight (H.K.) Ltd and was transported overseas on-board the carrier 'MED SINGAPORE V.05'. The shipment arrived in Milano, Italy in April 1995 which was subsequently transported over land to the Ente Nazionale per l'Energia Elettrica, Centro Ricerca Idraulica E Strutturali (ENEL) for stress chamber testing.

2.4 Field Test (The Tung Chung Site)

This section should be read in conjunction with the report entitled : "Ground Investigation New Territories West, Term Contract (Works Order No. GE/93/08.57) : Study of Hydraulic Fill Performance for Marine Reclamation Tung Chung New Town Development Phase I" prepared by Lam Geotechnics Limited.

The location of the proposed field investigation station in Tung Chung was determined on the basis that it has to be free from construction disturbance, deep compaction and/or rock fill surcharging. The final location shown in Figure 2.3 is in the vicinity of where the bulk sample was taken.

The field work was carried out between 24 - 29 December 1994, and 23 February 1995. The following site investigation works were carried out :

- i) one drillhole, where Standard Penetration Test (SPT) was carried out at 1.5 m intervals with "undisturbed" tube samples obtained by Mazier sampler (76 mm in diameter, one-metre long sampler, using polymer drill mud) taken in-between each SPT reading; and

- ii) one 15 cm² Seismic Cone Penetration Test (SCPT) was performed. In addition to the standard cone tip resistance and sleeve friction with continuous reading, the SCPT also measured both pore water pressure and shear wave velocity.

The SPT was undertaken by Lam Geotechnics Ltd; whereas the SCPT was carried out by Fugro McClelland Ltd.

2.5 Results of Drilling

The drillhole record was logged by the technical staff from Lam Geotechnics Ltd. in accordance with Geoguide 3 "Guide to Rock and Soil Description". The drillhole log is shown in Figure 2.4 and a summary of the soil stratification is given in Table 2.1.

As revealed from the drillhole log, approximately 8.5 m of hydraulic sand fill overlying marine deposits was recovered at Tung Chung. The fill material is mainly fine to coarse sand with fragmented shells and occasional lenses of clayey sandy silt.

2.6 Standard Penetration Tests (SPT)

SPTs (according to GEOGUIDE 2, 1987) were carried out at 1.5 m intervals on the Tung Chung site. The results of penetration resistance (N) value versus depth are plotted in Figure 2.5. The densities of the fills are much higher above mean sea level (0.78 mPD) than those below the mean sea level.

2.7 Undisturbed Sampling of Hydraulic Sand Fill

In this study, Mazier samples (76 mm diameter) were taken in between the SPT measurements. The Mazier sampler is a triple-core-barrel which contains detachable plastic PVC liners within the inner barrel that protect the core from drilling fluid and damage during transportation and extrusion. Of particular importance of this sampling technique utilized in the study is that a stabilizer of Polyacrylamide Polymer was used as drilling fluid and a spring core-catcher was attached at the inner barrel cutting shoe. The percentage of total core recovery of Mazier samples from the Tung Chung site is indicated on the drillhole record shown in Figure 2.4. It should be noted that the percentage of total core recovery of Mazier samples was quite low from ground surface to about 5 m depth. Upon inspection of samples at the site, the fine content of the samples were found to be high. It was considered that the use of spring core-catcher attached at the inner barrel cutting shoe might result in poor core recovery for fine grain soils. The core-catcher was subsequently removed and much higher core recovery (almost 100%) was obtained for the rest of the Mazier samples. (It should be noted that removal of core-catcher may result in very high core recovery or complete loss of core).

All Mazier samples were drained free of water before being waxed and capped to avoid damage due to disturbance during transportation and extrusion. Samples of fill materials were

hand carried back to Hong Kong University of Science and Technology and all other Mazier samples were subsequently shipped and stored by Lam Geotechnics Ltd.

2.8 Seismic Cone Penetration Tests (SCPT)

One seismic cone penetration test (15 sq. cm cone) was conducted on the Tung Chung site. The details of the seismic piezocone and the method statement of the seismic piezocone penetration testing can be found in Appendix III of the report entitled : "Study of Hydraulic Fill Performance for Marine Reclamation - Tung Chung New Town Development Phase I" (Works Order No. GE/93/0857) prepared by Lam Geotechnics Limited. The location of the SCPT was 3 metres from the SPT drillhole. The penetration rate was set at a constant speed of 2 cm/sec with a sampling frequency of 1 second. Shear wave velocity measurements during the SCPT were taken at every metre of penetration. The position of porous element was on the shaft between the piezocone and the sleeve (see Figure 2.6 for cone filter position), and glycerine was used as the system de-airing fluid.

In this study, the shear wave velocity measurements were obtained by seismic piezocone which involves a penetrating cone in which geophones are incorporated to detect a shear wave generated at the ground surface. Figure 2.7 shows the principle of the operation. A shear wave is generated by means of a hammer blow against a wooden block rested under the static load of the CPT truck. The shear wave travels to the piezocone in which three seismometers are incorporated (as shown in the x,y,z directions in Figure 2.6). A seismograph is triggered by the hammer blow and records the arrival of the shear and pressure waves. In this study, the so-called stacking method was employed which involves repeating the procedure at the two sides of the wooden block (i.e. at the left and right sides of the CPT truck) in order to improve the signal to noise ratio. After taking one set of measurements the piezocone was pushed to the next depth of one metre further. Subsequently the next measurement was taken. The difference in arrival time of the shear wave for the two measurements is the actual travel time through the one metre soil interval between the two measurements. In this manner a shear wave velocity profile can be made with one metre intervals. For the recording of the data a seismograph has to be added to the standard cone data acquisition equipment, which records the cone resistance, sleeve friction and pore pressure.

The results of the CPT's and the shear wave velocity profile are included in Figures 2.8 (a)-(c) and 2.9, respectively. Results of the cone tip resistance (q_c) and the shear wave velocity (V_s) above the mean sea level were significantly greater than those below the sea level. These findings seem to be consistent with that obtained from the SPT measurements and the results from the Phase 1 study.

2.9 Correlation of Field Test Results

The results of q_c (in MPa) obtained from the Tung Chung reclamation site were plotted against the SPT-N value in Figure 2.10 (It should be noted that q_c is estimated by averaging the values of sounding for a depth of about 300 mm at the corresponding SPT drive depth). It can be seen that a reasonable correlation between the cone tip resistance values and N values

can be obtained. For the overall soil profile up to a depth of 20 m, a relationship between q_c and N is found as follow :

$$q_c = 0.44 N \dots\dots\dots(2.1)$$

Since only the upper 9 m of the soil profile can be considered as hydraulic fill sand, and the remaining soils were consisted of marine deposit/sand fill mixture and marine deposit. Two separate linear regression analyses were carried out on each of the upper sand fill layer and the lower marine deposit layer. The relationships are found as follow :

$$(\text{for the Marine Deposit}) \quad q_c = 0.38 N \dots\dots\dots(2.2)$$

$$(\text{for the Sand Fill}) \quad q_c = 0.53 N \dots\dots\dots(2.3)$$

The relationship of $q_c = 0.53 N$ for the hydraulic sand fill layer is compared with the relationship of $q_c = 0.7 N$ obtained from the Phase 1 study (for the West Kowloon sand, Tin Shui Wai sand, and Tseung Kwan O sand), the lower value of coefficient obtained in this study seems to indicate that the Tung Chung sand is more compressible than the other three silica sands obtained from the Phase 1 study. It has been suggested previously (Robertson and Campanella, 1983) that compressibility has a major effect on the cone resistance, and compressible soils generally exhibit lower cone tip resistance values than less compressible soils at a given relative density. The compressible nature of the Tung Chung sand is attributed to the higher fine content and finer grain size, and it also contains significantly more broken shell fragments and carbonate than the other four sands examined in this study (see sections on physical properties tests for details).

The result obtained for the Tung Chung sand is also plotted on the q_c/N versus average grain size, D_{50} , relationship as proposed by Burland and Burbidge (1985) in Figure 2.11. The proposed relationship of $q_c/N = 0.53$ with $D_{50} = 0.33$ mm seems to be in good agreement with the results obtained from Burland and Burbidge (1985).

Robertson et al. (1995) suggested that the compressibility of a sand can be estimated from a comparison between normalized shear wave velocity (V_{sl}) and normalized cone penetration resistance (q_{cl}). The normalized shear wave velocity (V_{sl}) is defined as :

$$V_{sl} = V_s \cdot \left(\frac{P_a}{\sigma_v'}\right)^{na} \cdot \left(\frac{P_a}{\sigma_h'}\right)^{nb} \dots\dots\dots(2.4)$$

where V_s = shear wave velocity, in m/sec
 σ_v' = vertical effective stress, in kPa
 σ_h' = horizontal effective stress, in kPa
 P_a = atmospheric pressure, typically 100 kPa
na and nb = stress exponents; typically, na = nb = 0.125

and the normalized cone penetration resistance (q_{cl}) is defined as :

$$q_{cl} = q_c \left(\frac{P_a}{\sigma_v'} \right)^{0.5} \dots\dots\dots(2.5)$$

A plot of normalized shear wave velocity (V_{sl}) and normalized cone penetration resistance (q_{cl}) is shown in Figure 2.12. A linear regression analysis is carried out on the data and a relationship between normalized shear wave velocity (V_{sl}) and normalized cone penetration resistance (q_{cl}) for the Tung Chung sand is proposed as (with coefficient of correlation, $R^2 = 0.626$) :

$$V_{sl} = 140 (q_{cl})^{0.25} \text{ (in m/s)} \dots\dots\dots(2.6)$$

Robertson et al. (1992) suggested a general correlation for sub-rounded to sub-angular quartz sands as :

$$V_{sl} = 102 (q_{cl})^{0.25} \text{ (in m/s)} \dots\dots\dots(2.7)$$

Newman et al. (1996) also reported a similar relationship between normalized V_{sl} and q_{cl} from a number of SCPTs conducted in the sand fill at the Chek Lap Kok new airport. Their results are reproduced in Figure 2.13 and the following relationship were proposed by Newman et al (1996) for the Chek Lap Kok sand :

$$V_{sl} = 115 (q_{cl})^{0.25} \text{ (in m/s)} \dots\dots\dots(2.8)$$

Based on this comparison it appears that the marine sands encounter at the Tung Chung reclamation site are more compressible than the others. This finding is consistent with the CPT versus SPT results as discussed previously.

2.10 Field Test Data at Chek Lap Kok

A five-volume report on the "Works Order No 255/016 - Marine Sand Specialized Study" prepared by Intrusion-Prepakt (Far East) Limited in conjunction with ConeTec Investigation Ltd. on two test areas in the new airport at Chek Lap Kok was forwarded from AA to us on 19 January 1996.

An additional arrangement with HAECO through Meinhardt Consulting Engineers and Golder Associates to carry out Spectral Analysis of Surface Waves (SASW) tests and in-situ density measurements along the slopes of an open trench at the HAECO Base Maintenance Facility on the Chek Lap Kok replacement airport site had been obtained (details of field tests arrangement are included in Appendix A). Field tests were carried out by the staff of HKUST on 24 and 25 January 1996. Detailed test arrangement is outlined as follows :

- 1) The HKUST carried out three SASW measurements - two in the densified Type-C sand fill; and one in the Type A/B rockfill at the HAECO site.
- 2) The HKUST provided the necessary equipments for SASW and in-situ density testing. The I-P Foundations supplied us with a backhoe on site and the necessary sea and on-site transportation.
- 3) A 4 m deep test trench with gentle side slopes was excavated. In-situ density measurements by sand replacement technique and nuclear density gauge were taken at every 0.5 m interval along the slope to the depth of 3.3 m.
- 4) The HKUST have access to the CPT and SCPT data that have been collected at the site.

3. CASE HISTORIES AND SURVEY QUESTIONNAIRE

A survey questionnaire was developed with the aim to obtain detailed site specific information at the five reclamation sites undertaken in the current study. Comments suggested by Dr. Ken Been were incorporated in the questionnaire. The final version of the survey questionnaire is shown in Figure 3.1. The survey questionnaire is divided into seven sections : they are :

- 1.0 Location of site
- 2.0 Soil Stratigraphy at the site
- 3.0 Extraction and Rehandling of fill material
- 4.0 Site preparation work
- 5.0 Reclamation and filling methods
 - 5.1 Bottom-dump method
 - 5.2 High-velocity (spigotting or rainbow) discharge
 - 5.3 LowContainment -velocity pipe-line (pump-out) discharge
- 6.0 Subsequent ground improvement work
- 7.0 Remarks

The survey questionnaire was sent to the chief resident engineers of the five sites. The following personnel from various offices were served as contacts :

- Mr. P.H. Ho of Binnie Consultants Limited at the Tin Shui Wai Reclamation Site.
- Mr. John Mckinlay of Mott MacDonald (HK) Limited at the West Kowloon (CS1) Reclamation Site.
- Mr. D.B. Douglass of Maunsel Consultants Asia Limited at the Tseung Kwan O Reclamation Site.
- Mr. Martin Broadgate of Mott MacDonald (HK) Limited at the Tung Chung Reclamation Site.
- Mr. Richard Newman/Andrew Pickles of the Airport Authority Hong Kong at the Chek Lap Kok Replacement Airport Site.

Much of the problems associated with completing the questionnaire were due to the fact that most of the resident geotechnical engineers in charge of the reclamation works had left their companies. Therefore, much more efforts were required to review the previous construction records or interview with former contractor's staff. Some of the detail information may be very difficult to obtain. The returned survey questionnaires are attached in Appendix B.

3.1 New Airport at Chek Lap Kok

The new airport at Chek Lap Kok is located on the Northern coast of Lantau Island, and covers two islands namely Chek Lap Kok and the Lam Chau Island. The new airport site is separated from the Lantau Island by a navigation channel, but is jointed by two vehicular bridges across the channel to the Tung Chung New Town as shown in Figure 3.2. The new airport is being constructed on the 1248 hectare site of which 938 hectares is reclaimed land. The extent of the reclamation is shown in Figure 3.3. The reclamation comprises 197 Mm³ of fill of which 60 Mm³ is sand fill placed by bottom dumping from barges, pipeline deposition and "rainbowing" from dredgers. The following sections describe the geology and reclamation construction details about the new airport at Chek Lap Kok. This information is largely extracted from two technical papers (Newman et al., 1996a, and Newman et al., 1996b). Additional information was also obtained from interviews with site staff of AA.

Geology

According to Newman et al. (1996b), the Quaternary geology of the airport site has been classified (BGS, 1991) as soft clay (marine mud) of the Hang Hau (QHH) and Sham Wat (QSW) Formations overlying firmer clays and sands alluvium of the Chek Lap Kok (QCK) formation.

The Hang Hau Formation is the youngest formation and consists predominantly of very soft to soft, greenish grey, silty clay and forms a blanket of sediment over most of offshore Hong Kong. It is a highly compressible clay with a moisture content of typically 100% and a liquidity index close to 1. Its undrained shear strength increases from less than 5 kPa near the

surface at a rate of about 1 kPa/m. It has a relatively high sensitivity of 10 and is essentially normally consolidated.

The Sham Wat Formation occurs in the southwest part of the reclamation, where it infills a large channel system with over 18 m of generally firm, grey silty clay. Lithologically it is distinguishable from the overlying Hang Hau Formation by its slightly higher shear strength, slightly lower moisture content and lower shell content. The Sham Wat exhibits a liquid limit of 60%, a plastic limit of 21% and a moisture content of 52%. It is a slightly overconsolidated clay with an average undrained shear strength of 35 kPa.

The Chek Lap Kok Formation includes a range of lithologies from silty clay through silt and sand to gravel. In many areas it can exhibit abrupt variation in sediment type, both laterally as well as vertically. A number of erosion surfaces and channel systems were identified within the formation. The plastic and liquid limits of the alluvium within this formation range from 20 to 30%, and 40 to 65%, respectively, while its moisture content is typically 40%. Its undrained shear strength in the upper 5 m is 35 to 40 kPa and then it increases at approximately 5 kPa/m. Its geological history is variable and OCR's are generally in the range of 2 to 3.

Extraction of fill material

The marine sands were won from Tsing Yi, Poi Toi, Sha Chau, and Brother Islands borrow areas. The geological origin of the borrow materials is mainly marine sand deposits. Trailer suction hopper dredgers (TSHD) were used to remove the overburden deposits (marine mud and alluvial clays) in order to win sand from the borrow pits. Overflowing of fines (until specified density achieved) was allowed from the hoppers as a way of ensuring the quality of the marine sands. The dredged marine sands were transported to the site by dump barge and trailer hopper suction dredger. Bottom dumping was first conducted by trailer suction hopper dredgers to depths of -4 mPD to -6 mPD. Above this level sand was dumped in a rehandling basin and pumped by cutter suction dredger to required level in the reclamation site. Material in the upper 2 m of the capping layer was pumped by pipeline and then rehandled and leveled by bulldozer.

Construction of the reclamation

The mean sea level is approximately 1.3 mPD with a tidal variation typically in the range of 0 mPD to 2.6 mPD. The original seabed level varied from approximately -3 mPD to -8 mPD and was covered by a blanket of soft marine mud with a typical thickness of 8 m. The marine mud was largely removed prior to construction of the reclamation. Figure 3.3 shows the areas of the reclamation construction using marine sand fill. The remainder of the reclamation was constructed using hard, durable granite rockfill and finer rockfills containing varying amounts of decomposed rock. The nature of the fill and its location in the reclamation were dictated by both design and construction considerations.

Although the sand was derived from four marine borrow areas, the mineralogy was found to be similar due to the large amount of re-mixing between materials from different borrow areas. There are some zones which show variance, this is usually due to the placement method and tidal range and the fact that some pockets of sand have not been well mixed. The

specification for the sand fill was governed by a limit of 20% fines and a maximum size of 100 mm.

Three methods of deposition were used to place the sand fill. Bottom dumping from barges was adopted in areas where the sand was placed directly on the dredged surface. This was the preferred method of placement where navigational and operational constraints permitted. Beneath the northern runway bottom dumping was used to raise the sand to a level of about -9 mPD but elsewhere bottom dumping took place to a level of between -6 mPD and -4 mPD. At the location of Study Area 1 a sand island was formed by "rainbowing" of the sand directly onto the bottom dumped material, while in Study Area 2 the sand was pumped as a slurry by pipeline method to form a beach deposit. These methods of deposition were used to bring the fill in the reclamation to a level of approximately +4 mPD. Sand fill above this level was placed by pipeline method and bull-dozed into final position achieving a final formation level of typically +6.5 mPD. The upper 2 m of fill is designated as the capping layer and was specified to be placed at 95% standard Proctor density.

Subsequent ground improvement work

Surcharges were carried out at designated areas as indicated in Figure 3.4. Generally rockfill was used as surcharge material, and the thickness of surcharging layers are generally 3 m, 6 m or 10 m. The surcharge periods are varying from 3 to 12 months depending on the follow-on structural requirements and programme constraints. Vibrocompaction was only carried out in areas where foundation pads for future structures are required as shown in Figure 3.4. The acceptance criteria of vibro-compaction adopted by AA are shown in Table 3.1. Final reclamation levels varied between +5.5 mPD to +6 mPD.

3.2 Tung Chung Reclamation Area

The studied location is within the Tung Chung Development - Phase 1 area. Primary focus of the site records is given to the area near B4 of the MTRC site area (co-ordinates near E811693 and N816853, see Figure 2.3).

Soil stratigraphy

The mean sea level at the Tung Chung reclamation area is approximately +1.2 mPD with tidal variation typically in the range of 0 mPD to 2.3 mPD. The whole site area is covered by a layer of marine deposit at a depth of about -3 mPD to -4 mPD. The thickness of this marine deposit is ranging from 8 m to 15 m with an average of about 11 m. The layer of marine deposit can be described as soft, greenish grey, slightly fine to medium sandy silty clay with some thin layer of medium to fine sand and shell fragments. This is underlain by a layer of alluvium of various thickness of 8 m to 20 m. The average thickness near the study area is about 19 m. The materials within this alluvium layer consist of rounded to subrounded cobbles and gravel with silty clayey fine matrix, to medium dense clayey fine to coarse sand with small gravels of quartz grains. The alluvium layer is in turn underlain by a layer of completely decomposed volcanic rock of various thicknesses. The materials within this layer can be described as medium dense to dense, reddish brown to brownish grey slight clayey fine sandy silt with relict joint, to medium to very dense light grey, pink and brownish yellow

mottled, silty fine to medium sand. The average thickness of the completely decomposed rock at the study area is about 10 m.

Extraction of fill material

Marine sands were won from a borrow site near Soko Islands on the south-west side of Lantau Island. The sands are of marine origin. Dredging of the sand was carried out by a cutter suction dredger and grabs. The general depth of extraction of marine sand was about 6 to 7 m below sea level. The dredged marine sands were then pipelined from the cutter suction dredger to a stationary discharge barge located about 20 - 30 m away through a single pipeline system connecting between the cutter suction dredger and the stationary discharge barge called "spider" as shown in plate 3.1. The sand/water mixture was then discharged to flat bottom hopper barges docked on the sides of the stationary discharge barge. Difficulty in controlling the speed of discharge from the "spider" onto hopper barges was reported. It was found that if the speed of discharge was too fast, significant overflow of the sand/water mixture from the hopper barge could be resulted; however, if the speed was too slow, hydraulic pressure might not be enough to transport the mixture through the pipeline into the "spider". Consequently, extraction of marine sand by grabbing was used more frequently. Dredged marine sands were transported to the site by hopper barges. The carrying capacity of hopper barges is about 1000 m³, but because of the high fine content of the marine materials, the barges were actually carrying about 700 m³ of sand and the upper portion of the barge was full of water/fine mixture. Most of the marine sands were bottom dumped to a rehandling basin near the site. Some were directly bottom dumped at the filling area.

Construction sequences and reclamation work

For the general reclamation area within the site, a sand blanket layer of about 1 m thick was spread on top of the marine mud to prevent excessive mud wave generation. Bottom dumping from barges was adopted in areas where the sand was placed directly on the sand blanket. This was the preferred method of placement where navigational and operational constraints permitted. The carrying capacity of the barges were 700 to 1000 m³. Discharge operation was usually conducted in one single opening operation; for most of the time, the barge remained stationary. In the mass hydraulic filling operation, pipeline discharge was employed to reclaim the landfill to +5.5 mPD. Marine sands were extracted from the rehandling basin by a cutter suction dredger and transported by a 700 mm diameter pipeline to various areas for rainbowing. The sand-water mixture ratio was about 1:4. A discharge gate was attached to the discharge point of the pipeline to control the distribution and velocity of the sand/water mixture. A smaller pipeline system of 600 mm diameter was also employed on the site. bunds were constructed by bulldozers around the perimeter of the filling area. The general size of the containment pond was about 200 m². Leveling and compaction above the sea level were conducted by bulldozers.

Subsequent ground improvement work

Wick drains (AMERDRAIN 407) were installed at +5.5 mPD in a triangular pattern with 1.5 to 2.0 m centre-to-centre spacing for the entire site. In some areas, surcharge loading was then placed to +11 mPD for a period of about 7 to 8 months. No surcharging was

conducted on the MTRC tunnel channel alignment, but the sand fill was improved by deep compaction (vibro-compaction) along the channel alignment.

3.3 Findings from Surveys of the Five Sites

3.3.1 Effects of Grading of the Borrow Materials

From the surveys of the five reclamation sites and a large number of grain size distribution curves obtained from the five sites, the effects of fill gradation and fine content on the processes of winning of marine sand, loading of dredged sand onto hopper and quality control on hopper barges have been examined. General findings are summarized in the following table :

Site	Marine Sand Sources	Grain size D ₅₀ (mm)	Fine Content (%)	Extraction Problems
TSW	Urmston Road	0.9 to 2.0 Average : 1.6	0 to 3 Average : 2%	No difficulty
CS1	South Tathong Channel and Nine Pin Group	0.2 to 0.85 Average : 0.72	2 to 9 Average : 4%	Mostly no difficulty, except some overflow problems with finer materials
TKO	South Tathong Channel	0.2 to 0.9 Average : 0.55	1 to 10 Average : 4.5%	Mostly no difficulty, except some overflow problems with finer materials
TC	Soko Island	0.15 to 0.7 Average : 0.33	10 to >20% Average : 15%	Significant overflow problems due to fines suspended in sand/water mixture for long time, control of discharge/loading of dredged sands on hopper was difficult to achieve.
CLK	Tsing Yi, Poi Toi, Sha Chau, Brother Islands	0.3 to 1.5 Average : 0.8	0 to 10 Average : 3%	No difficulty

The locations of the marine sand borrow areas for the five reclamation sites in Hong Kong are shown in Figure 3.5. Based on the general information obtained from the five reclamation sites in Hong Kong, an empirical relationship between the expected degree of difficulty during sand winning operation with the gradation and fine content of the dredged sands is proposed as shown in Figure 3.6. Based on this figure, the following observations can be stated :

- 1) The ease of marine sand winning and dredging operations does not seem to be dependent upon the average size of dredged sands, up to D_{50} value of 2 mm (maximum size may be as large as 20 mm as observed in the TSW site).
- 2) Sand winning and dredging operations can be significantly affected by the presence of fine contents. Based on the information obtained from the current study, the following three groups can be classified :

<u>Operation Level</u>	<u>Range of fine content</u>
No difficulty	0% to about 10%
Moderate difficulty	10% to about 15%
Difficult	more than about 15%

Based on this correlation, sand winning and dredging operations at the Soko Island borrow area is expected to be more difficult. Within the South Tathong Channel borrow area, pockets of finer sands with higher fine content could be expected, this may occasionally impose slight difficulty during sand dredging operation, otherwise, the dredged sand can be considered as high quality. It should be noted that, however, the fine content is only one of a number of factors which could affect the difficulty of sand winning. Two other classes of factors which may also affect the efficiency of sand winning; namely, material factor and equipment factor. Material factor such as depth of dredging, angularity of the sand, presence of coarse material, density of the in-situ material, and occurrence of silt and clay lenses could affect the ease of operation and quality of dredged sand. Equipment factors such as type of dredger and configuration of the pumps, hopper, overflow weirs, distance between borrow area and reclamation, type of drag head and skill of operation may affect the efficiency of operation. Detail information about these factors, however, is not available at the present study.

3.3.2 Seabed Preparation Work

Reclamations in Hong Kong are largely carried out by bottom dumping from hopper barges followed by rainbowing and pipeline discharge. Problems of fill materials punching into the seabed causing mud-wave formation have been reported. This can lead to subsequent problems of differential settlement and reclamation stability (Ng, 1991). The use of a geotextile on the seabed prior to filling operation to reduce the mud-wave problems had been demonstrated in the Tseung Kwan O reclamation site.

According to the description of the site engineers and staff, the geotextile (Mirafi 400 woven) was installed by placing a layer of fabric on the seabed and covered with two initial layers of fill, each of 0.5 m thickness. This initial one metre fill also acts as the drainage blanket for the vertical drains. As described by Ng (1991), geotextiles in rolls were mounted on a working platform on the side of the barges, where they were unrolled and sunk onto the seabed. There was another alternative where the geotextiles in rolls were lowered onto the

seabed along two vertical H-beams secured in position by collars to the side of the barges. The H-beams were able to move vertically and could be locked into position when the geotextiles were at the correct level.

The uniformity of the initial sand layer is of greater importance for the correct functioning of the drains. Sounding of the sea bottom was used to check the thickness of the fill placement. Divers were also sent down to probe the actual thickness of the fill placed above the geotextile by pushing a probe through the fill. This served as a confirmation of the sounding results. Results have indicated that the geotextile has fulfilled its function to prevent fill punching and maintain a uniform thickness of the initial fill. Reclamation with the use of geotextile in the TKO site has not encountered serious problems of mud-wave formation. Boreholes sunk after the completion of the reclamation indicated that the fill/mud interface within the area was fairly uniform thus giving a generally more uniform settlement of the seabed instead of large differences due to fill penetrations and mud-wave formation. Results of CPT sounding carried out in the Phase 1 study also indicated a very clear fill/mud interface at the TKO site. These results are reproduced at Figure 3.7. It should be noted that the two CPT tests, which were carried out 3 m apart, all indicated a clear sand/mud interface at a depth of 12.3 m. These results are consistent with that of Ng (1991).

The CPT sounding from the Tung Chung reclamation site as shown in Figure 2.8 can be used to illustrate the problems of fill penetration and mud-wave generation when geotextile was not used. Despite the similarity of the geological conditions and reclamation methods adopted for the TKO and TC sites, a zone of intermixed fill/marine deposit of 3 m thick (from about -2.5 mPD to -5.5 mPD) was observed from the Tung Chung site. This may indicate the possible fill penetration and mud-wave generation problems occurred at the Tung Chung site when geotextile was not used.

Marine mud was fully dredged before bottom dumping at the Chek Lap Kok and West Kowloon sites, therefore mud-wave was not a problem and geotextile was not required. At the Tin Shui Wai site, marine sand was directly filled on top of the fish ponds. Fish pond bunds were first cleared of vegetation and they were cut down and allowed to drain. The ponds were drained and the bottom were allowed to dry out and form a reasonably strong crust such that mud waves would not be formed during filling. This technique seems to work very well and the CPT sounding showed a clear transition of sand fills and marine deposits.

3.3.3 Effects of Bottom-dumping

Based on the observation obtained from the Phase 1 study together with published results from various case histories (Sladen, 1990; Jefferies et al, 1988; Massarch, 1985; and Wallays, 1983), a general sequence of highest to lowest post-placement density for a given material according to placement method commonly used in Hong Kong was proposed as shown in the following (with possible range of relative density as observed from the Phase 1 Study) :

1. Above water with traffic compaction (with $D_{r(ASM)}$ above 80%).

2. Hopper dumping below water (with $D_{r(ASM)}$ in the range of 35% to 65%).
3. Beach above water - no compaction (with $D_{r(ASM)}$ in the range of 30% to 60%).
4. Below water - pipeline deposition above fill surface (with $D_{r(ASM)}$ in the range of 25% to 55%).

Based on the average CPT profiles of over thirty soundings from the Chek Lap Kok new airport (as shown in Figures 3.8 and 3.9), Newman et al. (1996b) concluded that there is no perceptible difference between the q_c values measured in subaqueous fill placed by bottom dumping, rainbowing or pipeline discharge. The characteristics of the sand fills as observed in the West Kowloon reclamation site and in the Beaufort Sea reported by Sladen and Hewitt (1989), showed that placement technique had a strong influence on in situ density with q_c values in the bottom dumped fill being significantly different depending on the total thickness of the bottom dumped sand.

Based on the wealth of information available from the five reclamation sites undertaken in the current study, the mechanisms of the bottom dumping process and the factors affecting the "as placed" density is re-examined. A hypothetical mechanism of the bottom dumping process is postulated as in the following.

The dredged sand in hopper barge, though relatively loose and nearly saturated, probably has a bulk density as suggested by Sladen (1990) of around 18 to 19 kN/m³. The relatively quick opening of valves or doors of the hopper dredger will cause the sand to fall from the hopper as a slug rather than as individual particles. The simultaneous falling motion of the sand body will inhibit or minimize the entrainment of "fresh" seawater into the slug that would reduce its fall velocity and expand its size. The kinetic energy of this discharge is likely dissipated in compaction to the soil layers underneath the falling sand body through impact and shearing. The bottom dumping method as suggested by Sladen (1990) is in itself a form of soil compaction. During the moment of impact of the falling sand body with the underlying soil layer, instantaneous pore water pressure will develop within the sand body. Since the falling sand body has a relatively loose structure, flow liquefaction will develop within the sand body. A final equilibrium state of the sand body will take the shape as shown in Figure 3.10. The two sides of the sand body will develop two gentle slopes marking an angle around 30° from the horizontal (probably corresponds to the f_{cv} of the marine sand). The centre part (the crest) of the berm will probably have a width (W_{berm}) similar to the width of the hopper barge (W_{barge}). Since a significant part of the sand body was liquefied and flow down to form the side slopes of the berm, the maximum height (H_{berm}) at the centre of the berm should be smaller than the height of the hopper (H_{barge}). The actual height of the berm is rather difficult to predict, but based on the examination over a few hundreds of CPT soundings from the five hydraulic sand fill sites, the maximum height of the berm was found to be within 30% to 50% of the height of the sand hopper ($H_{berm} = H_{barge}/3$ to $H_{barge}/2$).

The driving force from the impact of each falling sand body is likely to be small. However, as the number of sand layers increase, the impact forces and the increased load of the sand layers may cause a re-positioning of the sand grains in lower layers. After dissipation

of the pore water pressure, these impact forces will increase the densities and cause some settlements to develop at the lower sand layers. The compaction and densification of the lower layers can be improved as the total thickness of the bottom dumped soil layers increased. It should be noted that, however, the locations of the bottom dumping processes are rather random. The resulting layered configurations of the bottom dumped sand berms are considered to be stacked up in a rather random fashion (probably as illustrated in Figure 3.11). The likelihood of the crest of a berm stacks directly on top of the crest of a lower berm is not too high, and along any given vertical profile, the layer thickness should vary rather randomly (as illustrated in the hypothetical CPT profile along the vertical line A-A as shown in Figure 3.11).

As fill material is dumped, segregation of fine and coarse material will occur. The segregation process was probably already developed when the fill material was stored inside the hopper with the coarser particles settled at the bottom of the hopper and finer particles near the top. If the fine content of the dredged sand fill is quite high, the fine will remain as suspension in water forming fine/water slurry sitting near the top of the fill mass. Segregation is further developed during the dumping process with the coarser particles quickly falling to the bottom of the berm and the finer particles taking longer time to settle near the top of the berm. This segregated profile will result in a higher cone tip resistance q_c near the bottom of the berm (with low friction ratio) and a much lower q_c near the top of the berm layer (with considerable higher friction ratio because of the high fine content). The amount of segregation of a given filling material will depend on the gradation, average grain size, fine content of the materials, etc.

With the proposed hypothetical bottom dumping mechanism in mind, one can re-examine the CPT results obtained from the CLK, CS1, and TC reclamation sites (all these three sites were first reclaimed by bottom dumping technique). At the Chek Lap Kok site, detailed site investigations were carried out at two study areas; namely Study Area 1 and Study Area 2 as shown in Figure 3.3. Bottom dumping from barges was adopted in areas where the sand was placed directly on the dredged surfaces. At the location of Study Area 1, bottom dumping was used from about -16 mPD to -7 mPD for a total bottom dumped fill thickness of about 9 m. This was followed by rainbow discharge to about +4 mPD. Sand fill above this level was placed by pipeline method and bull-dozed into final position achieving a final formation level of typically +6.5 mPD. At the location of Study Area 2, bottom dumping was used from about -14 mPD to -10.5 mPD for a total bottom dumped fill thickness of about 3.5 m. It was followed by pipeline discharge to final formation level.

Typical CPT results from the Study Areas 1 and 2 of the CLK site are shown in Figures 3.12 to 3.14, inclusively. Figures 3.12(a) and 3.12(b) show the results with the total bottom dumped fill thickness of 10.5 m and 14 m, respectively. The cone tip resistance along the bottom dumped fill varied significantly, which clearly reflected the segregation problems resulted from the bottom dumping process. The areas with lower q_c values together with higher friction ratio (f_s) indicate the locations of higher fine content at the top of each bottom dumped berm and possibly indicate "clayball" inclusions. Whereas the areas with higher q_c values and lower f_s indicate the locations of coarser particles at the bottom levels of each bottom dumped layer. In fact, one can make use of this as a guide to delineate the approximate number of bottom dumped lifts being placed at a given location. Despite the bottom 1 to 2 m thick of intermixed fill/un-dredged sea mud zone, the cone tip resistance

profiles along the bottom dumped zones were approximately linearly increasing with depth. Because of the large variation of q_c values due to segregation, the maximum q_c values can be approximately connected by an upper bound straight line, while the minimum q_c values were connected by a lower bound line. The average q_c values can also be approximated by a linear relationship with q_c about 5 to 7.5 MPa at the top of the bottom dumped zone and increases with a rate of about 0.48 MPa/m. The increase of cone tip resistance with depth can be considered as a result of the successive compaction efforts from each layer of bottom dumped sand mass together with the increase in overburden stress. Results from Figures 3.12 (a) and (b) clearly indicate that the average q_c values along the bottom dumped zone are higher than that of the rainbow discharged zones. This finding is consistent with the results observed from the West Kowloon reclamation site as discussed in the Phase 1 study.

Figures 3.13 (a) and (b) show the results with the bottom dumped fill thickness of 8 m and 9 m, respectively. The cone tip resistance profiles are quite similar to that of the thicker bottom dumped zones as shown in Figures 3.12 (a) and (b). However, the average q_c values along the bottom dumped zone were only slightly higher than that of the rainbow discharged zones, and the increase of q_c with depth were quite moderate (at a rate of about 0.35 MPa/m). The CPT results for the total bottom dumped fill thickness of 4.0 m and 4.5 m are shown in Figures 3.14 (a) and (b). It can be seen that the cone tip resistance profiles along the bottom dumped zones differ only slightly with that of the pipeline discharged sand fill. This indicates that the advantageous effect of bottom dumping process was not observed if the total thickness of the bottom dumped zone was not large enough. The adverse effects of segregation of soil particles were somehow outweighing the compaction and densification efforts of the bottom dumping process. This may further be complicated by the intermixing of un-dredged soft marine mud leaving at the bottom of the seabed with bottom dumped sand fill. To substantiate these findings, all 33 CPT results from Study Areas 1 and 2 from CLK were classified according to the improvement of q_c values along the bottom dumped zones as compared with that of the rainbow discharge or pipeline discharge zones as : GOOD; FAIR; and POOR. The results are summarized in Table 3.2. Based on these results, the following trend can be observed :

- If the total thickness of the bottom dumped sand fill is more than about 9 m, improvement in cone tip resistance (and thereby the post-placement in-situ density) is likely to result from the bottom dumping process.
- If the total thickness of the bottom dumped sand fill is between about 6 m to 9 m, only slight improvement in cone tip resistance (and the post-placement in-situ density) is likely to result from the bottom dumping process.
- If the total thickness of the bottom dumped sand fill is less than about 6 m, no noticeable improvement in cone tip resistance (and the post-placement in-situ density) is expected to result from the bottom dumping process.

It should be noted that the above observations were obtained based on CPT results from the CLK sand ($D_{50} = 0.8$ mm, $C_u = 4.5$, and average fine content = 4%) and bottom

dumped at a maximum water depth of about 13 m to 20 m. To examine the effects of water depth, additional CPT results from the West Kowloon (CS1) reclamation site were examined. The CS1 sand has a typical grain size of $D_{50} = 0.72$ mm ($C_u = 6.0$, and average fine content = 4%) and it was bottom dumped at water depths of about 10 m to 15 m. Classification of the 14 CPT results from the CS1 site were summarized in Table 3.3. It is interesting to note that all 14 test results can be classified as GOOD. Some fills with bottom dumped thickness of only 4 m did indicate a significant improvement in q_c when the water depths were at 10 to 11 m. The beneficial effects of bottom dumping at shallow water depths may be due to the fact that the entrainment of "fresh" water into the slug of falling soil mass was significantly reduced. There would be very little reduction of falling velocity or volume expansion of falling soil mass. Therefore, the fall energy and soil compaction efficiency was maximized under such conditions. Based on these findings, the following guideline for soil compaction resulting from bottom dumping process was tentatively proposed :

Maximum Water Depth of Fill Deposition	Total Thickness of Bottom Dumped Sand Fill		
	Compaction effort - GOOD	Compaction effort - FAIR	Compaction effort - POOR
15 m to 20 m	> 9 m Average $q_c = 5$ to 7.5 MPa at the top of the bottom dumped fill and increased at a rate of 0.4 to 0.55 MPa/m	6 m to 9 m Average $q_c = 4.5$ MPa to 5.5 MPa at the top of the bottom dumped fill and increased at a rate of 0.3 to 0.45 MPa/m	< 6 m Very little difference in q_c between bottom dumped fill and pipeline discharged fill
Less than 10 to 11 m	> 5 m Average $q_c = 7$ to 12 MPa at the top of the bottom dumped fill and increased at a rate of 0.4 to 0.8 MPa/m (or almost constant with depth at shallower depth)	< 5 m Average $q_c = 5$ to 7 MPa at the top of the bottom dumped fill and remains almost constant with depth	---
Note : The above table is only applicable to dredged marine sands with average fine content about 4% to 5%. The fill constructed by bottom dumping method would most likely to be highly segregated with minimum $q_{c (min)}$ value about 50% lower than the average q_c , and maximum $q_{c (max)}$ value about 50% higher than the average q_c .			

It should be noted that the above guideline may not be applicable to relatively uniform, clean sands, where segregation is generally not a problem, or bottom dumping at a much greater water depth where hydrodynamic effects become more significant.

3.3.4 Subaqueous Placement by Rainbowing and Pipeline

Study Areas 1 and 2 at CLK also provides an excellent opportunity to examine the effects of subaqueous placement by rainbowing or pipeline discharge. Typical CPT soundings are shown in Figures 3.12 (a)-(b) and 3.13 (a)-(b) for Study Area 1, and Figures 3.14 (a)-(b) for Study Area 2. At the location of Study Area 1 a sand island was formed by rainbowing of the sand directly onto the bottom dumped material, while in Study Area 2 the sand was pumped as a slurry by pipeline method to form a beach deposit. Based on these results, the following observations were made :

- 1) There is a substantial difference in the q_c values between subaerial and subaqueous fills, with subaqueous fills generally having a lower q_c value than that of subaerial fills.
- 2) Subaqueous placement by rainbowing generally produces relatively low q_c values of about 3 to 4 MPa just below the sea level and increases almost linearly to values of 5 to 6 MPa just before reaching the bottom dumped material.
- 3) Subaqueous placement by pipeline discharge generally produces slightly higher q_c values than that of rainbowing discharge. The q_c values generally remain constant with depth ranging between 5 to 7 MPa. But it may occasionally vary linearly with depth. The difference between subaqueous placement by rainbowing and pipeline discharge is, however, generally quite small.
- 4) One noticeable difference between subaqueous placement by rainbowing and pipeline discharge is the fact that the q_c profiles for sand fills constructed by rainbowing technique are generally much smoother than that constructed by pipeline discharge. This implies that pipeline discharge generally resulted in slightly more segregated sand fills.
- 5) It should be noted that pipeline discharge involves pumping of sand/water slurry from rehandling basin or stockpile area by (commonly) cutter-suction dredger to various discharge points through a pipeline. The sands stored in the rehandling basin were generally bottom dumped on location by hopper barges. This bottom dumping process would induce natural segregation of sand particles in the rehandling basin. Subsequent pumping and discharging of these stockpile materials by pipe-line deposition method might induce further degrees of segregation on discharged materials, and therefore resulting in more heterogeneous and segregated sand fills. Rainbowing process involves pumping of sand slurry directly from cutter suction dredger or trailer suction dredger, the dredged sands stored in the

hopper of the suction dredger are generally subjected to circulating water. The sand/water mixture was less likely to be segregated and therefore the resulting sand fills are generally more homogenous and less segregated.

These observations are generally applicable to the other four reclamation sites undertaken in the current study.

3.3.5 Subaerial Placed Sand

The deposition process of subaerial placed sand is quite different from the subaqueous deposition. After leaving the pipeline, the sand-water mixture will form a crater lined with the coarsest fraction of the soil. The soil water mixture will flow over the edge of the crater and the sand will deposit on the outside slopes (see Figure 3.15). The slope angle is dependent upon the average grain size of filling material, mixture concentration and discharge velocity (de Groot et al. 1988). Along the slope individual grain settles in a turbulent current while the sand mass is subjected to a downward seepage due to the drainage effect of the sand body. Each grain will finally rest in a stable position, forming a sand body with a lower void ratio than under the submerged deposition process. Compaction is further increased by the bulldozers which work on the slope to guide the mixture flow. Usually this will result in cone tip resistance q_c values in the range of 10 MPa to 20 MPa (in relative density of about 60 to 90 percent or in Proctor densities of 95 percent or above) as suggested by Verkerke and Volbeda (1991). However, it should be noted that, if compaction was not properly done by bulldozers or other leveling equipments, q_c values as low as 1 to 2 MPa have been reported at the CS1 site (see Figure 3.16).

Segregation in hydraulic fills above water level will inevitably take place, with the coarse fractions mainly settling in the upper parts of the slope and the finer fractions mainly at the lower parts. In the end, the top layers of the fill will consist of coarser material than the lower layers close to water level. If fine fraction is presented in open fills, it may be washed out of the fill area and settled below the water level. In enclosed fill ponds the fine fraction will settle near the overflow weir (see Figure 3.17). If the formation of such deposits of fines are to be prevented, careful planning of the filling method is required. The free water level in the fill area should be kept as low as possible to minimize the quantity of stagnant water and to maximize the layer thickness with high compaction.

4. LABORATORY TESTS

4.1 Physical Properties Determination

All the laboratory tests described in the following sections were conducted using the well-blended mixture of the bulk samples from the field. All particles of the mixture passed the 5 mm sieve. The results of all physical properties tests are summarized and tabulated in Table 4.1. It should be noted that the results presented in this study only represent the behaviour of the bulk sample obtained from one sampling location at each particular site. It does not represent the large variability of geotechnical behaviour of fill sand for the entire reclamation.

Sieve analysis :

The well-blended mixture was quartered down to provide representative samples for particle size distribution test 2.9.2A in GEO Report No. 36 for wet-sieving. The grading results for the four batches of CLK sand and the three batches of TC sand are summarised in Tables 4.2 and 4.3 respectively. The grain size distribution curves of the bulk samples obtained from the two sites are given in Figure 4.1.

The sands from the four batch samples of CLK are very similar, all comprising mainly siliceous material derived from the weathering and decomposition of volcanic rocks. The particle shapes are sub-angular, and the particle sizes are fine to coarse with some shell fragments. The sands from the three batch samples of TC are also very similar, all comprising mainly fine to coarse sand with fragmented shells. The coefficient of uniformity C_u , defined as

$$C_u = \frac{D_{60}}{D_{10}} \dots\dots\dots(4.1)$$

where D_{60} = grain size (in mm) corresponding to 60% passing,
and D_{10} = grain size (in mm) corresponding to 10% passing, by weight;

the coefficient of curvature, defined as

$$C_c = \frac{(D_{30})^2}{(D_{10})(D_{60})} \dots\dots\dots(4.2)$$

where D_{30} = grain size (in mm) corresponding to 30% passing by weight;

and the average grain size, D_{50} (= grain size in mm corresponding to 50% passing by weight), are calculated and summarized in Table 4.4. It should be noted that the C_u and C_c values were determined based on the bulk samples obtained from shallow depths from the two sites; thus, these values may not be representative of the relatively heterogeneous nature of the sand mixture commonly observed from the two reclamation sites.

Specific Gravity (G_s) :

Three specific gravity tests in accordance with Part 2, Test no. 8.3 of BS 1377 (1990) on oven-dry samples were conducted and the results of G_s were found to be 2.64 and 2.67 for Chek Lap Kok and Tung Chung sand, respectively.

Minimum Density :

Minimum density test in accordance with Part 4:4.3 of BS 1377(1990) was performed. The minimum density $\rho_{D,min}$ was found to be 1.578 and 1.343 g/cm³ for Chek Lap Kok and Tung Chung sand respectively.

Maximum Density :

Maximum density test in accordance with Part 4:4.2 of BS 1377 (1990) was performed. The maximum density was determined by compacting the soil under water into a CBR compaction mould with a vibrating hammer. All together three maximum density tests for both CLK and TC samples were performed, and the maximum density $\rho_{D,max}$ by averaging the three tests was found to be 1.930 and 1.732 g/cm³, respectively.

Compaction Tests :

The relationships between dry density and moisture content for both CLK and TC samples were determined by the standard compaction test as detailed in test 12 of 4.3.3B in GEO Report No. 36. The results are shown in Figures 4.2 and 4.3 respectively. The maximum dry densities determined by the compaction test (Standard Proctor) were found to be 1.85 g/cm³ at an optimum water content of 14.1%, and 1.67 g/cm³ at 23.72%, respectively. The 100% saturation (zero air-void) lines are also plotted in Figures 4.2 and 4.3 for reference.

Permeability Tests :

The coefficients of permeability for CLK and TC samples were determined by the constant head permeability tests according to Akroyd (1969). Three tests on CLK sand and four tests on TC sand were performed at different relative densities. The air pluviation sample preparation technique was utilized to prepare specimens of different densities. This sample preparation procedure is very similar to that used for making cylindrical triaxial specimens. The results of the permeability tests are tabulated in Table 4.5 and are shown in Figures 4.4 and 4.5.

Carbonate Content :

Because of the significant amount of broken shell fragments present in the TC and CLK marine sands, rapid titration method in accordance with Part 3 of BS 1377 (1990) was used to determine carbonate content of the marine sand specimens. The results of these tests are summarized as in the following :

Chek Lap Kok sand Carbonate Content = 2.435%

Tung Chung sand Carbonate Content = 5.78%

4.2 Triaxial Static Tests

In this study, the static tests were performed using the Wykeham Farrance triaxial testing system. This system includes one AT2000 Data Logger, one Trittech 50 Digital load

frame and a WF17044 Volume change unit. The dynamic tests were performed using the CKC automated triaxial testing system. Details of the CKC testing system and the sample preparation method have been discussed in the Phase 1 report.

4.2.1 Static Triaxial Tests - Tung Chung Sand

Undrained triaxial tests were performed on saturated samples (with a "B" value of at least 0.97) of the Tung Chung sand to establish the stress-strain, and strength characteristics of the hydraulic fill sand. Three groups of samples with relative densities (in British Standard) of approximately 30% - 40%, 45% - 55% and 60% - 70% were tested under isotropic consolidation pressures of 100 kPa, 200 kPa and 300 kPa. To better define the stress-strain characteristics, especially for the case of strain-softening material, the strain-controlled static triaxial testing with pore pressure measurement was employed. The strain rate was kept constant at 0.5 mm/min for all tests.

Behaviour of sand at relatively low range of D_r (30 - 40%)

The $s' - t'$ ($s' = (\sigma'_1 + \sigma'_3)/2$ and $t' = (\sigma'_1 - \sigma'_3)/2$) stress path plots of the Tung Chung sand with relative densities in the range of 31.9% - 38.9% are shown in Figure 4.6. The effective stress shear strength parameter (ϕ') for the material was found to be about 36.0° . The stress-strain, pore water pressure response for each undrained test are plotted in Figures 4.6 (a) - (d) for consolidation pressures of 100 kPa, 200 kPa, and 300 kPa. The results indicated that shearing first caused the sand to have a tendency to decrease in volume (compression) thus a corresponding increase in pore pressure. Within about 2% axial strain, the rate of pore pressure increase was very rapid. Following this initial phase of rapid increase in pore pressure, further shearing only caused the pore pressure to increase very gradually to the maximum value at about 4 - 6% axial strain. Upon reaching the phase transformation line (volume change tendency reverses from compression to dilation) at an axial strain level of about 4 - 6%, further loading caused the sand to have a tendency to slightly increase in volume (dilation) thus a corresponding gradual decrease in pore pressure. The net change in pore water pressure (Δu), during undrained testing, however, remained positive for all three tests. The results of these three tests are summarized in Table 4.6. Detailed test results are given in Appendix C.

Behaviour of sand at intermediate range of D_r (45 - 55%)

The $s' - t'$ stress path plots of the Tung Chung sand with relative densities in the range of 47.3% - 53.0% are shown in Figure 4.7. The effective stress shear strength parameter (ϕ') for the material was found to be about 39.0° . The stress-strain, pore water pressure response for each undrained test are plotted in Figures 4.7 (a) - (d) for consolidation pressures of 100 kPa, 200 kPa, and 300 kPa. The results of stress-strain and pore water pressure response of the medium dense sand samples are generally quite similar to that of the loose samples, except that, the rate of soil dilatancy (reflected by decrease in pore water pressure) after the phase transformation, was higher than that of loose sand. The net change of pore water pressure (Δu) at the end of the tests was slightly negative. The results of these three tests are summarized in Table 4.6. Detailed test results are given in Appendix C.

Behaviour of sand at relatively high range of D_r (60 - 70%)

Figure 4.8 shows the $s'-t'$ stress path plot for the Tung Chung sand with relative densities in the range of 67.1% - 69.5%. The effective stress shear strength parameter (ϕ') was found to be about 40.5° . The stress-strain, pore water pressure response for each undrained test are plotted in Figures 4.8 (a) - (d) for consolidation pressures of 100 kPa, 200 kPa, and 300 kPa. The results clearly indicate that before reaching the phase transformation line, shearing of samples caused a slight tendency of the sample to decrease in volume thus a corresponding slight increase in pore pressure (occurred within 1% axial strain). As the sample approached the failure condition, further loading caused the sand to have a tendency to increase in volume (dilation) thus a corresponding (more significant) decrease in pore pressure. The net change in pore water pressure (Δu) was negative in this case indicating a net volume increase tendency during shearing. Table 4.6 summarizes the stress-strain and strength response of the sand at a range of relative densities of 67.1% - 69.5%. Detailed test results are given in Appendix C.

4.2.2 Static Triaxial Tests - Chek Lap Kok Sand

Thirteen consolidated undrained tests were performed on the CLK sand to define and to characterize the static behaviour of the material. These triaxial static test results can also be used to define the steady state line for the purpose of interpreting the material behaviour within the framework of the state parameter concept. Three groups of samples with relative densities of approximately 30%, 50% and 70% were tested with a range of isotropic consolidation pressures of 100kPa, 200kPa, 300kPa and 400kPa. All specimens were tested under strain-controlled conditions and shearing were carried to axial strains exceeding 25%. The strain rate is kept constant at 0.5mm/min. Table 4.7 summarized the results of all triaxial static tests on the CLK sand. Detailed records of the results of these tests are included in Appendix C.

Apart from the tests listed above, isotropically consolidated undrained triaxial compression (CIU) tests on samples obtained from the West Kowloon site (CS1), Tseung Kwan O site (TKO), and Tin Shui Wai site (TSW) were performed to determine the steady state lines of the three materials for use with the state parameter approach. Results of these triaxial tests on the three reclamation sites are summarized in Tables 4.8, 4.9, and 4.10 for CS1, TKO and TSW sands, respectively. Detailed records of test results for these three sands are included in Appendix C. Details for the establishment of the steady state lines for the five marine sands undertaken in the Phases 1 and 2 studies will be discussed in Chapter 6.

4.3 Cyclic Triaxial Tests

Samples prepared the same way as those used in static loading tests were fabricated for cyclic triaxial tests. After consolidation to an effective stress (σ_e') of 150kPa, a cyclic axial load was applied to the specimen while holding the cell pressure constant. The undrained loading response was monitored and recorded in terms of the cyclic deviator stress, axial deformation, and pore pressure (or effective stress) change. From the recorded data on the

response of the soil to cyclic loading of various stress levels, the liquefaction potential of the soil could be evaluated and established.

4.3.1 Cyclic Triaxial Tests - Tung Chung Sands

A total of 20 stress-controlled cyclic loading tests at a frequency of 1Hz were performed on the Tung Chung (TC) hydraulic sand fill samples with relative densities of about 30%, 50%, and 70%. For different relative density samples, different cyclic deviator stresses (σ_{dp}) were applied to determine the liquefaction potential of the samples. The cyclic stress level applied to the specimen is commonly quantified by the stress ratio, SR, defined as :

$$SR = \frac{\sigma_{dp}}{2(\sigma_c')} \dots\dots\dots(4.3)$$

where σ_{dp} = cyclic or pulsating deviator stress, i.e., the amplitude of the applied cyclic loading.

σ_c' = effective normal stress at the end of isotropic consolidation.

Thus normalized liquefaction curves (SR versus number of loading cycles to liquefaction , N) can be established for a given relative density and material.

The results of cyclic triaxial tests for the TC samples are summarized in Table 4.11. The normalized liquefaction curves (SR versus N) for D_r of 30%, 50% and 70% at an isotropic consolidation pressure of 150kPa are shown in Figure 4.9. When the level of cyclic deviator stress was increased, the number of cycles needed to cause liquefaction decreased, and vice versa. At a constant stress ratio, the number of cycles needed to cause initial liquefaction increased as the relative density of the material increased. These findings are consistent with those obtained by DeAlba et al. (1976) and Seed and Lee (1966).

The results of a typical cyclic loading test of loose sand (with $D_r = 30.80\%$ and $SR=0.145$) are shown in Figures 4.10a and 4.10b. In this test, a cyclic deviator stress, σ_{dp} , of constant amplitude (± 43.5 kPa), was applied at a frequency of 1Hz to a sample of saturated sand under a confining pressure of 150kPa. The resulting changes in axial strain and pore-water pressure were recorded. Figures 4.10a shows the changes in stress, strain, and pore-water pressure with the number of loading cycles. The number of cycles required to cause initial liquefaction was defined as the loading cycles needed to cause the excess pore water pressure to reach the value of the confining pressure. At this time, the effective confining stress would be zero. Based on the test data shown in Figures 4.10a and 4.10b, it can be seen that the development of axial strains was negligible until the initiation of liquefaction. The pore-water pressure, however, built up steadily as the number of stress cycles increased, until there was a sudden jump denoting the onset of initial liquefaction at $N = 14$. Figure 4.10b shows the effective stress paths and the shear stress-shear strain loops during a test. Large shear strains were associated with stress paths approaching the phase transformation line under very small effective confinement. The shear strain built up was slow and gradual before

the phase transformation. The reduction in shear resistance with increasing loading cycles was also evident. Results of stress, strain and pore-water pressure responses with loading cycles for the rest of the cyclic loading tests are given in Appendix D.

4.3.2 Cyclic Triaxial Tests - Chek Lap Kok Sand

A total of 19 samples were prepared of Chek Lap Kok (CLK) Sand for undrained cyclic triaxial tests. The results of these tests are summarized in Table 4.12. The normalized liquefaction curves (SR versus N) for relative densities of approximately 30%, 50% and 70% are shown in Figure 4.11. Samples were saturated and consolidated under an effective confining pressure of 150 kPa. Comparing with the results of the TC sand, it appears that the CLK sand is slightly lower in liquefaction resistance under the same cyclic stress ratio. The relatively higher in liquefaction resistance of the TC sand is probably due to the fact that the TC sand has a higher fine content than the other marine sands undertaken in the Phases 1 and 2 studies. Detailed cyclic triaxial test results for the CLK sand are given in Appendix D.

5. RELATIONSHIP BETWEEN VOID RATIO AND SHEAR WAVE VELOCITY

5.1 Shear Wave Velocity Measurement

The propagation of shear wave in a soil mass depends mainly on the void ratio, the effective confining stress, the intrinsic characteristics of the soil and its structure. The shear wave velocity can also be regarded as a characteristic parameter for cohesionless soils. In general, shear wave velocity can be expressed in terms of shear modulus (G) and mass density (ρ) as in the following equation

$$V_s = \sqrt{\frac{G}{\rho}} \dots\dots\dots(5.1)$$

Hardins and Richarts (1963) suggested that the small strain shear modulus (G_o) and the shear wave velocity can be related to on effective mean normal stress and void ratio by

$$V_s = (m_1 - m_2 e)(p')^n \dots\dots\dots(5.2)$$

where V_s = shear wave velocity; e = void ratio, p' = effective mean normal stress; m_1 , m_2 and n are material constants. By plotting the V_s and p' on a log-log scale, n becomes the slope of the line. Hardins and Richarts (1963) suggested that the n value for sub-rounded to rounded silica sands was typically around 0.25.

Rosler (1979) later proposed an alternative equation based his results from cubic specimens. Rosler proposed that

$$V_s = (A - Be) \left(\frac{\sigma_a'}{p_a} \right)^{na} \left(\frac{\sigma_b'}{p_a} \right)^{nb} \dots\dots\dots(5.3)$$

where σ_a' = vertical effective stress; σ_b' = horizontal effective stress p_a = atmospheric pressure (typically 100kPa); na and nb = stress exponents (typically, $na = nb = 0.125$). Under an isotropic condition, where $\sigma_a' = \sigma_b' = \sigma_c'$ (σ_c' = the confining pressure) and $na = nb = n/2$, the above equation (5.3) becomes

$$V_s = (A - Be) \left(\frac{\sigma_c'}{p_a} \right)^n \dots\dots\dots(5.4)$$

It is found that for different types of sand, the above material constants, A, B and n are different. Therefore, A, B and n actually characterize a specific material. Experiments can be setup to measure the shear wave velocities as different specific void ratios (or densities) under different confining pressures, the material constants A, B and n can then be readily determined.

5.2 Laboratory Shear Wave Velocity Measurement

Recently, a new piece of equipment was added to our laboratory which measures the shear wave velocity in a cylindrical sample using the bender elements. Each bender element is constructed from two longitudinally-expanding piezoelectric ceramics which are separated by an insulating layer (see Plate 5.1). When a voltage is applied across the bender element one plate elongates and the other contracts. The net result is a bending displacement which is greater in magnitude than the length change in either plate. If this element is inserted in a soil sample, the bending impulse can generate a shear wave propagating perpendicular to the plane of particle motion. On the other hand, a bender element can be used as a receiver as a voltage ; is induced in a bender element when it receives a shear wave. Therefore, by mounting one bender element each in the top and bottom platens of a cylindrical sample and measuring the time elapsed between the generation and reception of the shear wave and the separation between the two bender elements, the shear wave velocity can be calculated (see Plate 5.2).

5.3 Set-up of Laboratory Shear Wave Velocity Measurement

A typical setup of the equipment is given in Figure 5.1 and Plate 5.3. A pulse is generated from a pulse generator. The voltage is then amplified through an amplifier to a higher voltage about 200V. This high voltage is connected to a display unit and applied across the bender element at the bottom platen. A shear wave is then generated and travels along the sample. When the second bender element, which is fixed at the top platen, receives

this shear wave, a voltage will be induced. This voltage is then connected to another channel of the display unit.

A Control System Analyzer 3565A manufactured by Hewlett Packard is used as a display unit. This device is also capable of minimizing unwanted random noises by taking the average value of a large number of individual measurements.

In this study, dry samples were prepared to different relative densities. Each sample was placed inside a CKC automated triaxial testing machine. The chamber pressure (cell pressure) was adjusted to give different confining pressures.

5.4 Scheme of Work

To establish the relationships between confining pressure and shear wave velocity, shear wave velocities of dry samples of different relative densities under confining pressures of 50, 100, 150 up to 400 kPa were measured. The shear wave velocity measurements were performed on both the CLK and TC sands; in addition tests were also conducted on the three previously studies sands, ie. CS1, TKO and TSW.

5.5 Results of Measurement

The results of these measurements are given in Appendix E and are plotted as shown in Figures 5.2 to 5.16.

Figures 5.2 to 5.6 show the relationships between the shear wave velocity and the confining pressure of the five materials on a log-log scale. In general, the velocity increases as the confining pressure increases for a given density. Linear relationships can be approximated as shown on the plots. Furthermore, the slopes of the linear relationships are virtually the same for different relative densities of each material. The slopes of the straight lines on log-log scale can be used to determine the material constant n , which range from 0.20 to 0.33 for the five materials.

Figures 5.7 to 5.11 show the plot of shear-wave velocity versus void ratio in linear scale. It can be seen that the shear wave velocity is inversely proportional to the void ratio for a given confining pressure. However, because of the scatter in the results, it is quite difficult to develop any correlation between V_s and e . To further study the results, the shear-wave velocities were normalized with respect to the effective confining stress using the following modified form as suggested by Robertson et al. (1992).

$$V_{sl} = V_s \left(\frac{p_a}{\sigma_c'} \right)^n \dots\dots\dots (5.5)$$

where V_{sl} = normalized shear wave velocity
 V_s = shear wave velocity
 p_a = reference pressure = 100 kPa
 σ_c' = effective confining stress;
 n = slope of the line of V_s versus σ_c' on a log-log scale
(instance of $n=0.25$ as suggested by Robertson et al. 1992)

The relationship between the V_{sl} and e can be expressed as the following linear relationship :

$$V_{sl} = A - B \cdot e \dots\dots\dots(5.6)$$

Figures 5.12 to 5.16 show the plots of the proposed linear relationship of the five materials. The material constant, A , can be determined from the y-intercept of the straight line, while the material constant, B , can be determined from the slope of the linear relationship. The three material constants (A , B and n) determined for the five sands undertaken in the Phases 1 and 2 studies are summarized in Table 5.1.

6. STEADY STATE OF HYDRAULIC FILL SANDS IN HONG KONG

6.1 Introduction

Marine sands have been used as fill materials for land reclamation in Hong Kong. Geotechnical evaluation of these deposits requires a knowledge of the in-situ state of the soil deposit which may be defined by the combination of void ratio and effective stress conditions. Been and Jefferies (1985) introduced the state parameter (Ψ) to describe the large strain behaviour of a sand based on the combined influence of the initial void ratio, effective confining stress and their relation to the "steady state" void ratio at the same stress level. Been and Jefferies showed that the initial state of a sand controls the large strain behaviour of the material.

A loose cohesionless soil loaded in shear will contract to reach the steady state condition, whereas a dense soil will dilate and move toward the steady state condition. When a loose cohesionless soil is sheared undrained under an initial consolidation pressure which is higher than the steady state pressure p' for that particular void ratio, it will tend to contract thus causing an increase in pore pressure and leading to a reduction in effective confining pressure. The soil will reach its peak strength and drop rapidly to the steady state in strain-softening mode. At the steady state there is a state of constant void ratio, constant effective mean normal stress and constant shear stress (Castro, 1969). While dense cohesionless soils are typically dilative in nature they will generally not exhibit large deformations under normal loading conditions if properly designed.

6.2 Terminology

To avoid confusion in the terminology used in this report, the terminology as suggested by Been et al. (1991) were adopted, and a brief discussion is given as follows :

The *state* of a sand is the description of the physical conditions under which it exists. Void ratio (density) and initial in-situ stresses are the primary state variables for soils. Fabric is also a state variable of importance.

Fabric is the term used to describe the arrangement of sand grains on a particulate scale. This would include a description of particle contacts, their orientations and distribution, and cementation at the contacts, if any.

The *steady state* of deformation for any mass of particles as suggested by Poulos (1981) is that state in which the mass is continuously deforming at constant volume, constant normal effective stress, and constant shear stress. The steady state of deformation is achieved only after the orientation of all particle has reached a statistically steady state condition and after degradation of particles, if any, is completed, so that the shear stress needed to continue deformation and the velocity of deformation remain constant.

The *steady state line* is the locus of steady state points in void ratio/stress space. For convenience, the stress invariants $p' = (\sigma_1' + \sigma_2' + \sigma_3')/3$ and $q = (\sigma_1' - \sigma_3')$ are used to describe the stress state of a sand following the logic of Wood (1984), and the projection of the steady state line on to the e - p' plane is used for data presentation and definition of the state parameter Ψ .

The *state parameter* Ψ defines the void ratio (e) and mean normal effective stress level (p') of a sand relative to a reference state (the steady state) as shown in Figure 6.1 (Been and Jefferies, 1985). Therefore, the state parameter Ψ is simply the void ratio difference between the current void ratio and the steady state void ratio at the same stress level. Additional parameters describing the fabric and stress anisotropy are necessary to define the state of a sand uniquely, but in practice these parameters are generally unknown.

The *critical state* has been defined as the state at which the soil "continues to deform at constant stress and constant void ratio" (Roscoe et al., 1958). The steady state has traditionally been measured using undrained tests on loose sand samples, while the critical state is generally inferred from drained tests on dense sands.

Flow liquefaction as defined by Robertson (1994) is given as follows :

- Requires strain softening response in undrained loading resulting in constant shear stress and effective mean stress (i.e. at steady state).
- Requires that shear stress is greater than undrained residual or steady state shear strength.

- Flow liquefaction can be triggered by either monotonic or cyclic loading.
- For failure of an earth structure due to flow liquefaction to occur, such as a dam or a slope, a sufficient volume of material must show strain softening response. The resulting failure can be a slide or a flow depending on the material characteristics and slope geometry. The resulting movements are due to internal causes and can occur after the trigger mechanism.
- Flow liquefaction can occur in saturated, very loose granular deposits, very sensitive clays and loose loess deposits.

In this report, following the suggestion by Been et al. (1991), the critical and steady states are assumed to be equal and independent of stress path, sample preparation method and initial void ratio. The words critical state and steady state therefore represent the same conditions and can be inter-changed with each others.

6.3 Steady State Line Determination at Medium Stress Range (about 200 kPa to about 1000 kPa)

In order to define the state parameter Ψ of steady state line (SSL) must first be determined. In defining the steady state line, the stress invariants $p' = \sigma_{oct}' = (\sigma_1' + \sigma_2' + \sigma_3')/3$ and $q = (\sigma_1 - \sigma_3)/2$ are commonly used to describe the stress states of a sand following the logic of Wood (1984). It should be noted that the stress invariant p' commonly adopted for state parameter interpretation is actually the octahedral normal effective stress $\sigma_{oct}' = (\sigma_1' + \sigma_2' + \sigma_3')/3$, which is different from $p' = (\sigma_1' + \sigma_3')/2$ normally used in Hong Kong and from those used elsewhere in this and previous report of this study.

In the original concept of steady state of sands as defined by Been and Jefferies (1985), the e - $\log p'$ plane is used for data presentation and definition of the state parameter Ψ . The state parameter Ψ defines the void ratio (e) and mean normal effective stress level (p') of a sand relative to a reference state (the steady state) as shown in Figure 6.1 (Been and Jefferies, 1985).

The triaxial test results obtained in the previous section are used to determine the steady state lines of the five marine sands undertaken in this study. For all the static triaxial tests carried out in this study, the soil samples were sheared to 20% to 30% axial strains in order to reach the steady state condition. The steady state is the ultimate state at which the sample will undergo large strains at a constant volume under monotonic loading. However, it should be noted that even at strain levels up to 30%, sometimes, it is uncertain as to whether the ultimate state is indeed reached or whether further changes would occur at even larger strains.

The results of void ratio (e) and p' at the steady state condition (or at the end of the test if steady state condition cannot be clearly defined) are summarized in Tables 4.6 to 4.10

for the five marine sands. In some tests, the so-called "quasi-steady state" condition as defined by Been et al. (1991) and illustrated in Figure 6.2 can be detected. The quasi-steady state is in fact more like the phase transformation state, thus is not included in defining the steady state line. In other tests there was a mild tendency for the sample to dilate at the end of the test. It is possible that this apparent dilatancy is the result of sample non-uniformities and other testing effects, rather than the real soil behaviour. In these cases, the conditions at the end of the test are assumed to be representative of the steady state.

Some of the test results shown in Tables 4.6 to 4.10 (also included in Appendix C) were subjected to significant amount of sample tilting at large axial strain levels (around 15% to 20%), this adverse test condition would induce significant amount of eccentric and non-uniform stresses in the specimens; results with such conditions were discarded from the steady state line determination. It should also be noted that some of the test results in high relative density ranges were affected by cavitation when the pore water pressure reached a value about -100 kPa. These results therefore cannot be used for steady state line determination.

The steady state points determined by triaxial undrained tests for the Tung Chung sand are plotted in the e -log p' space as shown in Figures 6.3. The steady state line of a cohesionless material can be approximated by a straight line within the stress range of 200 kPa to about 800 kPa in e -log p' space. This is generally a reasonable approximation for sub-angular or sub-rounded quartz sands in the stress range up to about 1000 kPa as suggested by Been et al. (1991).

It should be noted that, because of the scarcity of steady state points and the concentration of data points at void ratios (e) of 0.67 to 0.83, the steady state line defined for Tung Chung sand as shown in Figure 6.3 is only applicable to the stress range of about 200 to 800 kPa. The steady state parameters at this stress range defined in e -log p' space are summarized as in the following :

The slope of the steady state line, $\lambda_{ss} = 0.26$
Void ratio at reference pressure of 1 kPa, $e_{ss} = 1.43$

In order to define the steady state lines for all the marine sands undertaken in the Phases 1 and 2 of the project, four series of additional triaxial undrained tests were conducted on all the other four marine sands as described in Chapter 4. For all the static triaxial tests carried out in this study, the soil samples were sheared to 25% to 30% axial strains in order to reach the steady state condition. The results of these triaxial undrained tests are summarized in Tables 4.7, 4.8, 4.9, and 4.10 for the Chek Lap Kok (CLK), West Kowloon (CS1), Tseung Kwan O (TKO), and Tin Shui Wai (TSW) marine sands, respectively. The interpretation for steady state lines in e -log p' space are shown in Figures 6.4 to 6.7 for the four marine sands, respectively. Because of the imposed test conditions in these series of CIU tests and the initial void ratios of the samples, all the steady state points were concentrated in the stress range of 200 kPa to 1000 kPa (with relative densities in the range of 30% to 60%). The approximated steady states parameters in e -log p' space defined from these figures are summarized as in the following (in the stress range of 200 to 1000 kPa) :

Chek Lap Kok (CLK) sand :

The slope of the steady state line, $\lambda_{ss} = 0.13$

Void ratio at reference pressure of 1 kPa, $e_{ss} = 0.905$

West Kowloon (CS1) sand :

The slope of the steady state line, $\lambda_{ss} = 0.185$

Void ratio at reference pressure of 1 kPa, $e_{ss} = 0.971$

Tseung Kwan O (TKO) sand :

The slope of the steady state line, $\lambda_{ss} = 0.181$

Void ratio at reference pressure of 1 kPa, $e_{ss} = 1.221$

Tin Shui Wai (TSW) sand :

The slope of the steady state line, $\lambda_{ss} = 0.118$

Void ratio at reference pressure of 1 kPa, $e_{ss} = 0.85$

It is clear that the data shown in Figures 6.3 to 6.7 are in a very narrow range of void ratios. Additional tests at low relative density range of $D_r = 10\%$ to 30% and at higher relative density range of above 60% were carried out as discussed in the following section.

6.4 Non-linear Steady State Lines for the Hong Kong Marine Sands

The measured steady state line for sands is frequently approximated by a straight line in e -log p' space. Been et al. (1991) suggested that this linear approximation is reasonable for sub-angular or sub-rounded quartz sands in the stress range up to about 1000 kPa. However, some second-order curvature of the line is often apparent, as shown in Figure 6.8 for a series of tests on Leighton Buzzard sand tested by Been et al. (1991). The authors also found that the steady state line curves abruptly at a stress level of about 1000 kPa (1 MPa) for both Erksak 330/0.7 sand (as shown in Figure 6.9) and Leighton Buzzard sand. They suggested that this abrupt change in the slopes of the steady state line can be attributed to some breakage of grains at stress level above 1 MPa.

Likewise, to define the steady state lines for the five Hong Kong marine sands with confidence, the shape of the steady state lines over a wider stress range must be considered. The steady state points at higher stress levels (and with lower void ratios) can be easily determined by triaxial undrained/drained tests on samples with lower initial void ratios (must be conducted at high back pressure levels to avoid cavitation problem). These additional tests were obtained with results summarized in Tables 4.6 to 4.10. On the other hands, the steady state points at high void ratio and low stress level are commonly determined from triaxial undrained tests on very loose samples. These test conditions will usually result in strain softening of the soil sample at failure (see Figure 6.10 for typical test result of strain softening soil). Interpretation of steady state points for such strain softening test results always present great challenge and uncertainty. These are briefly discussed as follows :

- 1) It is difficult to determine the small deviatoric stress (undrained residual or steady state shear strength) accurately after the strain softening behaviour. It is especially true when stress levels are less than about 10 kPa (Been et al. 1991).
- 2) The problems with membrane compliance make the determination of deviatoric stress from undrained tests on very loose specimens much complicated (Verdugo, 1992). Up to present, there is no reliable technique to correct the membrane force for such membrane compliance conditions.
- 3) The inertia effect of the load cell during strain softening deformation of the specimens may cause erratic determination in axial stress. This problem can only be eliminated with external load cell mounted at the bottom of the triaxial cell. However, such a triaxial testing facility is not commonly available (including our laboratory and, therefore, all the undrained tests were conducted by strain controlled tests).
- 4) The relevance of the linear assumption of the steady state line at low stress levels with very loose density range is highly questionable. This linear portion of the steady state line is commonly determined by undrained tests on contractive loose sand specimens. The very loose states for such tests have to be prepared by moist tamping technique, and the initial void ratios are commonly required to prepare at values greater than the maximum void ratio defined by ASTM or BS standards (i.e. looser than the maximum void ratio as indicated in Figure 6.9 for Erksak 330/0.7 sand tested by Been et al., 1991). The implications of steady state concepts that are inaccessible to them in the water pluviated state, and hence are of questionable relevance to the design of hydraulic fill earth structures.
- 5) A potential systematic error in laboratory testing of very loose sands if membrane penetration is not corrected properly as suggested by Sladen and Handford (1987).
- 6) The fundamental concepts of non-homogeneous deformation, particularly along the thin layers of shear bands or slip planes, during strain softening deformation is still uncertain. Chu and Lo (1992) have shown that non-homogeneous deformation could develop in dense sand tested under triaxial drained conditions. If we accept the non-homogeneous deformation field in the shear bands of a soil under large strains can exist, under the classical

plasticity theory (Drucker's stability postulate) in work-softening conditions, non-homogenous soil deformations along the slip planes are possible under both drained and undrained conditions. If one determines the steady state points for very loose sand under undrained conditions (that experienced strain softening behaviour) and assuming the void ratio along the shear band remained the same as with the bulk of the sample, one could over-estimate the actual steady state at low stress levels and high void ratio range (see Figure 6.11). This is generally the case for most of the steady state line interpretation made in the existing literature.

In here, in order to avoid the difficulties and unresolved problems as stated previously, steady state points at low stress level and high void ratio range were determined by stress-path controlled constant p' (p' defined as : $p' = (\sigma_1' + 2\sigma_3')/3$) tests for specimens with medium-dense to medium-loose initial void ratio (i.e, $D_r = 30\%$ to 40%). The constant p' tests are stress controlled triaxial drained stress-path tests with σ_1' increased monotonically while continuously changing the cell pressure σ_3' so that the resulting p' remained constant. These tests can be used to determine the steady state points at pre-defined p' values and allowing the soil specimen sheared either in dilative mode (for sands with initial void ratios smaller than the steady state) or in contractive mode (for sands with initial void ratios greater than the steady state) to the steady state conditions. This test mode can eliminate a lot of the ambiguities as stated above.

A typical constant p' test results for the Tung Chung (TC) sand with $e_0 = 0.858$ and initial confining pressure of 25 kPa are shown in Figures 6.12 (a)-(c). The stress path for the test is simply a vertical line increased from $q = 0$ to the steady state condition. The void ratio versus axial strain as shown in Figure 6.12 (c) indicates that the void ratio increased due to dilation from the initial value of 0.858 to a final void ratio of 0.875 at an axial strain of about 20%. The steady state conditions (see Figure 6.12 (a) and (c)) can be easily identified for this test at axial strain of above 15%. The constant p' test results for the five Hong Kong marine sands are summarized in Table 6.1 and detail test results are given in Appendix F.

Combining the results of constant p' tests and the convention triaxial tests, the steady state points for the five Hong Kong marine sands were plotted in the e -log p' space as shown in Figures 6.13 to 6.17, respectively. Results of the five sands all indicate that non-linear steady state lines can be observed in the e -log p' space. The data suggested that the steady state line becomes flatter at stress levels lower than about 100 kPa. The curvatures of the steady state lines seem to increase at a stress range about 500 to 1000 kPa, and the slopes of the lines are much steeper at high levels of pressure. The non-linear steady state behaviours determined for the five sands may be caused by their higher fine contents and more sub-angular shapes than the sands undertaken by Been et al. (1991). The significantly higher percentage of broken shell fragments and minute carbonates particles found in the five marine sands also make the sands more compressible than the silica sands commonly examined by other researchers. The flatter steady state lines at lower stress levels may also indicate the actual steady state behaviour which can be readily determined under the constant p'

conditions, whereas this soil behaviour might be difficult to observe by conventional triaxial compression tests.

It is considered, however, that when a small range of pressure is under study, the steady state line can be represented by a linear relationship in e -log p' space (typically around 200 kPa to 800 kPa for the five marine sands undertaken in this study). On the other hand, when the range of pressure under consideration is not small, especially under lower stress level, a better representation of the steady state line must be sought.

6.5 Linear Representation of Steady State Lines for the Marine Sands in Hong Kong

In the development of the original state parameter concepts for sands by Been and Jefferies (1985), the state of a sand at a given void ratio (e) and mean normal stress level (p') is related to a reference state of the steady state line in the e -log p' space. The reason for using a semi-logarithmic plot is rooted in the empirical observation that soil stiffness is generally proportional to pressure. In fact, this relationship was largely based on observations made in the deformation behaviour of cohesive soils.

Janbu (1963) has shown that the relationship between soil stiffness and confining pressure for cohesionless soils can be expressed by the following empirical relationship :

$$E = K \cdot p_a \cdot \left(\frac{\sigma_c'}{p_a} \right)^n \dots\dots\dots(6.1)$$

where E is the elastic modulus of a soil;
 K is the modulus number;
 n is the modulus exponent;
 p_a is the reference stress = 100 kPa; and
 σ_c' is the effective confining stress.

In a more general term, this relationship implies that the shear modulus (G) of a cohesionless soil is proportional to the mean normal effective stress (p') as in the following form :

$$G \propto (p')^n \dots\dots\dots(6.2)$$

Following the logistics of Been and Jefferies (1985) that a general relationship between e and p' of a cohesionless soil at the steady state condition can be assumed to take a similar form as the relationship between soil stiffness and applied pressure. One can thus assume that the steady state void ratio (e_{ss}) of a cohesionless soil can be related to the mean normal effective stress (p') as in the following form :

$$e_{ss} \propto (p')^\alpha \dots\dots\dots(6.3)$$

Where α is an exponential constant of the soil. This constant, however, can only be determined by trial-and-error approach. In order to develop a representation between void ratio (e) and stress level (p') at steady state conditions under a wider stress range and with a simple mathematical relationship, a linear equation between e and $(p')^\alpha$ is assumed to exist as in the following form :

$$e = a + b(p')^\alpha \dots\dots\dots(6.4)$$

The soil constants a and b can be determined by linear regression analysis if a linear relationship does exist as in the form of Equation 6.4. If the soil parameters a and b are determined, the exponential constant α can be determined by the least-squares optimization technique as shown in the following equation :

$$\sum [y_i - \hat{y}_i]^2 = \sum \left[e_i - \left(a + b(p'_i)^\alpha \right) \right]^2 = \text{Min} \dots\dots\dots(6.5)$$

where $i = 1$ to n ,
and $n =$ total number of steady state points.

Optimized linear regression analyses as described by Equations 6.4 and 6.5 were carried out on the steady state points as shown in Figures 6.13 to 6.17 for the five Hong Kong marine sands, respectively. The search for the optimized α value for the Tung Chung sand is shown in Figure 6.18. The optimum α value of 0.75 resulted in the maximum coefficient of correlation (R^2) of 0.9432. The steady state line defined by the relationship $e = 0.9017 - 0.0016 (p')^{0.75}$ (where p' is expressed in kPa and $a = 0.9017$ and $b = -0.0016$) is shown in Figure 6.19. It can be seen that a linear relationship (with a highly acceptable coefficient of correlation, R^2 , of 0.9432) over the entire tested stress range can be found to represent the void ratio (e) and stress level (p') at steady state conditions for the Tung Chung sand. Similar analyses were carried out on the remaining four marine sands, and the results are shown in Figures 6.20 to 6.23, respectively. All test results indicate that the steady state conditions of soils can be expressed by a linear relationship as proposed in Equation 6.4. The following table summarized all the soil constants and R^2 of the five marine sands undertaken in this study :

SAND	α	a	b	R^2
Tung Chung	0.75	0.9017	-0.0016	0.9432
Chek Lap Kok	0.56	0.6438	-0.0029	0.9566
West Kowloon	0.95	0.5515	-0.0001	0.9572
Tseung Kwan O	0.86	0.8086	-0.0003	0.9869
Tin Shui Wai	0.55	0.6141	-0.0026	0.9692

Although the linear relationship proposed in Equation 6.4 defines the steady state lines for all five Hong Kong sands very well, a close examination of the procedure and the resulting soil constants reveal the following difficulties in the proposed analytical procedure :

- 1) The α parameters are different for the five sands and it varied from 0.55 to 0.95. If different a values were adopted for various sands, it will make direct comparison of the state parameters (Ψ) for various sands under different initial states very difficult. It would be much more convenient to adopt a constant α common for all sands, if possible.
- 2) The slope of the straight line (b) expressed in Equation 6.4 can be used to indicate the compressibility of the material as in the case of the parameter λ in the original steady state line proposed by Been et al. (1991) in e-log p' space. The value of the parameter (b), however, under the current mathematical expression is a very small value (in the range of -0.0001 to 0.0029). Such a small value will be inconvenient to use in engineering analysis and error prompt. A better form of mathematical expression should be developed to better reflect the potential compressibility of the material and be practical to be adopted by the profession.
- 3) More importantly, the soil parameters (a) and (b) as defined in Eq. (6.4) are not dimensionless constants. It would be much more convenient to develop a relationship with dimensionless material constants.

An examination of the α values for the five marine sands indicates an average value of 0.734. For simplicity, the parameter α can be assumed to be constant for the five Hong Kong marine sands. One can assume a constant α value of 0.75 for all five sands. A comparison in terms of the coefficient of correlation (R^2) by adopting optimum α values as defined by the optimization procedure described in Equation 8.5 for each individual sands with those adopting a constant α value of 0.75 for all five sands is given in the following table :

Sand	R^2 if optimum were α used in the linear equation	R^2 if a constant $\alpha =$ 0.75 were used for all sands	Error in R^2 values (%)
Tung Chung	0.9432	0.9432	0.0
Chek Lap Kok	0.9566	0.9458	1.14
West Kowloon	0.9572	0.9523	0.51
Tseung Kwan O	0.9869	0.9809	0.61
Tin Shui Wai	0.9692	0.9686	0.07

It is found that by adopting a constant α value of 0.75 for all five sands, it would only result in very minor error of within 1.5%. This level of error seems to be rather insignificant for most of the engineering analyses. It is therefore proposed to adopt a constant $\alpha = 0.75$ for all sands undertaken in this study. Furthermore, the slope of the straight line can be represented in a more convenient and meaningful way by expressing the mean principal stress invariants $p' = (\sigma_1' + 2\sigma_3')/3$ in a normalized way as :

$$p_l' = (p'/p_a) \text{ (in kPa)} \dots\dots\dots (6.6)$$

where p_a is a reference pressure, typically $p_a = 100$ kPa.

Based on these two modifications, the proposed linear relationship between void ratio (e) and normalized stress level (p_l') for steady state line of a sand can be expressed as :

$$e = \Gamma - \lambda (p_l')^{0.75} \text{ (in kPa)} \dots\dots\dots (6.7a)$$

or

$$e = \Gamma - \lambda (p'/p_a)^{0.75} \text{ (in kPa)} \dots\dots\dots (6.7b)$$

Where Γ is the value of void ratio at $p' = 0$, and

λ is the slope of the steady state line in $e-(p_l')^{0.75}$ space.

Equation 6.7 are used to re-examine the results of steady state points for the five marine sands, and the results are shown in Figures 6.24 to 6.28. Again, linear relationships can be developed for all five marine sands undertaken in the current study. The soil parameters obtained are shown as follows :

SAND	α	Γ	λ	R^2
Tung Chung	0.75	0.9017	0.0491	0.9432
Chek Lap Kok	0.75	0.6221	0.0191	0.9458
West Kowloon	0.75	0.5591	0.0165	0.9701
Tseung Kwan O	0.75	0.8181	0.0248	0.9809
Tin Shui Wai	0.75	0.5946	0.0173	0.9686

It is interesting to note that Γ represents the void ratio at the steady state conditions with zero confining stress. In other words, if the initial void ratio in the field is higher (at a looser state) than Γ , flow liquefaction would be induced in the soil when it was subjected to monotonic loading or cyclic loading, regardless of the magnitude of the overburden pressure at the site. To substantiate this concept, a series of CIU tests were conducted on Tung Chung sand with initial void ratio higher than Γ . Figure 6.29 shows a conventional CIU test on the Tung Chung sand with initial void ratio 0.905 (which is just slightly greater than Γ of 0.9017) and $p' = 200$ kPa. It can be seen that significant strain softening deformation were developed when the soil was sheared to an axial strain above 1.5%. Since the test was conducted under undrained conditions, excess pore pressure was developed rapidly until it reached the confining pressure, after which a significant reduction in the deviator stress was observed. Furthermore the post-liquefaction undrained residual shear strength (s_u) or the steady state shear strength of the sand was quite small with s_u about 7 to 8 kPa. This test result seems to agree with the above mentioned concept.

With the new form of the linear expression as defined by Eq. (6.7), the slopes of the straight lines λ are now much more sensible than the one defined by Eq. (6.4). The λ values of the five marine sands defined by Eq. (6.7) seem to correlate with the compressibility of the sand very well.

The applicability of the proposed relationship for other silica sands are also examined. The results of comparison for the Erksak 330/0.7 sand (Been et al., 1991), Leighton Buzzard sand (Been et al., 1991), Toyoura sand (Verdugo, 1992), and the CLK sand tested by Prof. Robertson at the University of Alberta are shown in Figures 6.30 to 6.33, respectively. The results of these comparisons are summarized in Table 6.2. The proposed linear relationship seems to perform very well for these additional sands, which indicates that the proposed relationship can be used to define the steady state line for most of the silica sands as well as marine sands.

The proposed linear steady state relationship as defined in Eq. (6.7) will be used as the basic framework in the development of quality control guideline for hydraulic sand fills in Hong Kong as discussed in Chapter 9.

7. CALIBRATION CHAMBER TESTS

7.1 Introduction

The cone penetration test (CPT) is one of the most common methods for site investigation work in Hong Kong. The results of CPT tests can provide a quantitative index of the compactness of reclaimed sand fill. The CPT sounding is a direct and effective way to assess the competence of hydraulic fill for field control, however, measured q_c (cone tip resistance) and f_s (shaft resistance) values are not basic soil parameters. Empirical correlations are therefore required in order to make use of the q_c and/or f_s values to characterize the state and, to some extent, the engineering behaviour of the soil being investigated. Numerous empirical correlations exist to estimate the in-situ state of cohesionless soils from penetration test results. However, for granular soil in the field, its behaviour is heavily influenced by the combined effect of in-situ effective confining stress (p') and density (or void ratio, e) of the soils. To make the penetration test results more meaningful, it is desirable if correlation among q_c and the in-situ state of cohesionless soils (i.e. p' and e) can be established. The calibration chamber test is designed to furnish this very information.

Other more recent in-situ testing involve the measurements of shear wave velocity (V_s) such as SCPT or SASW, to generate a profile of V_s with depth. However, there is only limited information on the use of V_s for the evaluation of in-situ state and liquefaction susceptibility of a soil. Based on a limited number of historical database where V_s was measured at sites where liquefaction was or was not reported, a normalized shear wave velocity value of V_{sl} less than 160 m/s was suggested by Robertson et al. (1992) as a value below which the potential for flow liquefaction is high.

This chapter describes the use of calibration chamber tests to estimate in-situ state of the Tung Chung (TC) and Chek Lap Kok (CLK) sands with shear wave velocity (V_s) and cone penetration (q_c) measurements. Experimental relationships between the void ratio (e), the mean normal effective stress (p'), with V_s or q_c were developed through a series of laboratory controlled calibration chamber tests on TC and CLK sands. The proposed relationships were also used to re-examine the calibration chamber test results for the West Kowloon (CS1), Tseung Kwan O (TKO) and Tin Shiu Wai (TSW) sands obtained from the Phase 1 study.

7.2 Calibration Chamber Testing Procedure

The calibration chamber test is performed in a large calibration chamber with the aim of calibration, under carefully controlled stress and strain conditions, various in-situ testing devices in sand. A detailed description of the design, construction and use of the ENEL Calibration Chamber is given by Bellotti et al. (1982). Specimens of approximately 1.2 m in diameter and 1.5 m high were prepared in the calibration chamber by air pluviation method. A deposition tube (22 mm in diameter) maintained at height 6 m above the plane of deposition was used to prepare soil specimens for the calibrating chamber. Samples with various relative densities were obtained by adjusting the drop height between the nozzle of the deposition tube and the actual surface of soil deposition, as shown in Figure 7.1. Detailed description of this air pluviation technique is given by Fretti et al. (1995).

All specimens were saturated by back pressures prior to performing the CPT test and shear wave velocity measurement. A 20 mm diameter cone at a penetration rate of 2 cm/sec was adopted for the CPT tests. Two sets of CPT were performed on each specimen under the boundary condition 1 (BC1, $\sigma_v' = \text{constant}$, $\sigma_h' = \text{constant}$). The penetration of the cone under the first stage stress conditions was carried to a depth of 64 cm and stopped; the stress conditions were increased (increase in both σ_v' and σ_h' with a constant K_o) before further penetration of the cone was proceeded.

Shear wave velocities in the vertical direction (V_{zx}) and in the horizontal direction (V_{xz}) were determined by two series of geophones installed in the calibration chamber specimen as shown in Figure 7.2. For the vertical direction, three geophones (i.e. No. 15, 27 and 34 as shown in Figure 7.2) were installed to measure the shear wave travelled in the vertical (z) direction with particle motion in the horizontal direction (V_{zx}). During each measurement, the top geophone (No. 15) acted as the source, and the difference in first arrival times between the bottom two geophones was recorded (No. 27 and 34). Since the distance between the bottom two geophones was known, the shear wave velocity (V_{zx}) can then be readily determined. This procedure was repeated with the bottom geophone (No. 34) acted as the source and the top two geophones (No. 27 and 15) as the receivers. These two sets of shear wave velocities (V_{zx}) were generally very close to each other with a difference less than 2.5% in all cases. Similarly, another three sets of geophones were installed in the horizontal direction (No. 33, 4 and 14) to determine the shear wave velocity travelled in the horizontal direction with particle motion in the vertical direction (V_{xz}). These two independent series of geophone arrangement were designed to investigate the effect of stress induced anisotropy on shear wave velocity determination.

During the consolidation phase, the consolidation pressures (σ_v' and σ_h') were increased in a number of steps until the final designated values. Shear wave velocity measurements (in both V_{zx} and V_{xz} directions) were determined at each steps. Once the specimen consolidated to the final designated confining pressures and shear wave velocity measurements were completed, the cone penetration test was then carried out up to a depth of 64 cm. After the first penetration test was completed, the consolidation pressures were then further increased in steps (with corresponding shear wave velocity determinations in each step). Under the second stage of consolidation pressure, the cone penetration test was further proceeded to a depth up to 125 cm. The results of calibration chamber tests on the Tung Chung sand and Chek Lap Kok sand are summarized in Tables 7.1 and 7.2, respectively. Detailed test results are given in Appendix G.

7.3 Correction for Boundary Conditions

In this study, all the calibration chamber test results were obtained by the use of a miniature 20 mm cone. The use of such a small size cone is aimed at reducing the chamber size effect on CPT readings which is accomplished by increasing the ratio of the diameter of the test specimen to the diameter of the cone ($D/d = 60$). According to the work by Parkin and Lune (1982), Salgado (1993), and previous studies at the ENEL, the chamber size effect under constant σ_v' and σ_h' (BC1) can under-estimate the free field penetration resistance value (q_{eff}) by an amount up to 15% for uniformly graded clean silica sands. In this study, the correction for chamber size effect for penetration resistance values was obtained by a computer code

based on the theory of cavity expansion analysis and cavity limit pressure developed by Rodrigues (1993). The calibration chamber test results of the TC and CLK sands were selected to properly calibrate the required soil parameters using the back calculation approach for computer simulation and validation. Results of the predicted cone penetration resistance values (q_{cp}) under the simulated calibration chamber conditions are tabulated in Tables 7.3 and 7.4; and were plotted against the corresponding actual chamber test results (q_c) as shown in Figures 7.3 and 7.4 for TC and CLK sands, respectively. As seen from the results, the predicted values were in reasonable agreement with the test data. To correct for free field boundary conditions, the computer program also predict a q_{cpff}/q_{cp} ratio for each set of test (as indicated in Tables 7.3 and 7.4), where q_{cpff} is the predicted free field cone penetration resistance values. The corrected free field penetration resistance value q_{cff} can then be determined by multiplying the ratio q_{cpff}/q_{cp} to the calibration chamber test (q_c) results. Comparisons of the predicted free field penetration resistance values q_{cff} to the measured penetration resistance values q_c are shown in Figure 7.5 for TC sand and Figure 7.6 for CLK sand. The computer simulation yielded average correction factors (slope of the dotted linear regression line) of 1.07 for the TC sand and 1.056 for the CLK sand. These factors are lower than the value of 1.13 obtained for the West Kowloon (CS1) sand obtained in the Phase 1 study.

7.4 Correlation with Cone Tip Resistance

The cone penetration resistance (q_c) value obtained from CPT is controlled primarily by the void ratio, the effective confining stresses, the intrinsic characteristics of the soil (grain size distribution, grain shape, angularity, surface roughness, and mineralogical composition), and the structure (fabric, inter-particle forces, and bonds) of the soils. As suggested by Robertson et al. (1995), unless significant grain crushing occurs, the intrinsic characteristics of the soil does not change with changes in the void ratio and effective confining stresses, although the structure can change. In spite of this, in many freshly deposited, uncemented hydraulic fill sands, the cone penetration resistance (q_c) can be used to define the in-situ state (void ratio, and effective confining stresses) of a deposit.

To develop a simple correlation between $q_c - p' - e$ (or $q_c - p' - D_r$), it would be advantageous to define a normalized cone tip resistance (q_{cl}) as in the following (in-line with the normalization scheme used for the shear wave velocity as discussed in Chapter 5) :

$$q_{cl} = q_c \cdot \left(\frac{p_a}{p'} \right)^{0.5} \dots\dots\dots(7.1)$$

where q_{cl} is the normalized cone tip resistance

q_c is the cone penetration resistance value determined by CPT

p' is the mean normal effective stress $p' = (\sigma_1' + 2\sigma_3')/3$

p_a is the atmospheric pressure (typically $p_a = 100$ kPa)

The results of laboratory determined shear wave velocities (as shown in Chapter 5) indicate a strong linear relationship between the void ratio (e) and the normalized shear wave velocity (V_{sl}) for the five marine sands as :

$$V_{sl} = A - Be \dots\dots\dots(7.2)$$

Furthermore, Robertson et al. (1992a) suggest a correlation between normalized shear wave velocity (V_{sl}) and normalized cone penetration resistance (q_{cl}) for clean uniformly graded silica sands in the form as :

$$q_{cl} = \left(\frac{V_{sl}}{102} \right)^4 \dots\dots\dots(7.3)$$

where q_c is in MPa and V_s is in m/s.

Fear and Robertson (1995) show that the site specific correlation between q_{cl} and V_{sl} obtainedd from field SCPT tests for the Alaska sand is in the following form :

$$q_{cl} = \left(\frac{V_{sl}}{135} \right)^4 \dots\dots\dots(7.4)$$

Results from the site investigation works conducted at the Tung Chung site and Chek Lap Kok site as discussed in Chapter 2 also indicated similar relationships.
At the Tung Chung site :

$$q_{cl} = \left(\frac{V_{sl}}{140} \right)^4 \dots\dots\dots(7.5)$$

and at the Chek Lap Kok site :

$$q_{cl} = \left(\frac{V_{sl}}{115} \right)^4 \dots\dots\dots(7.6)$$

Therefore, it can be assumed that the normalized cone penetration resistance (q_{cl}) can be correlated with the normalized shear wave velocity (V_{sl}) as in the following form :

$$q_{cl} = \left(\frac{V_{sl}}{m} \right)^4 \dots\dots\dots(7.7)$$

where m is a correlation constant,
 q_c is in MPa and V_s is in m/s.

Combining Eqs. (7.2) and (7.7), it can be shown that the void ratio (e) and the normalized cone penetration resistance (q_{cl}) can be correlated as in the following form :

$$e = C_1 - C_2 (q_{cl})^{0.25} \dots\dots\dots(7.8)$$

where C_1 and C_2 are two correlation constants.

Results of the cone tip resistance (corrected for far field effect, q_{cff}) obtained from calibration chamber tests with pre-defined void ratio (e) and initial confining pressure (p') for the Tung Chung sand are plotted in the e versus $q_{cl}^{0.25}$ relationship as shown in Figure 7.7. It can be seen that a well defined linear relationship is observed between e and q_{cl} as follows :

$$e = 1.1258 - 0.0425 q_{cl}^{0.25} \dots\dots\dots(7.9)$$

where q_c is in kPa.

Similar analyses were carried out for the Chek Lap Kok sand calibration chamber test results, and for the other three sands obtained from the Phase 1 study. Results of correlation analysis are shown in Figures 7.8 to 7.11 for CLK, CS1, TKO and TSW sands, respectively. All five results show a well defined linear relationship between e and q_{cl} . The following table summarizes the results for the five sands undertaken in this study :

Sand	C_1	C_2	Coefficient of correlation R^2
Tung Chung	1.1258	0.0425	0.9476
Chek Lap Kok	0.8938	0.0391	0.8965
West Kowloon	0.8247	0.0305	0.6886
Tseung Kwan O	1.2550	0.0539	0.9422
Tin Shui Wai	0.9563	0.0446	0.8871

Furthermore, it is common to express the results from calibration chamber tests in the $q_c - p' - D_r$ space, which can be readily obtained since the void ratio (e) can be directly related to the relative density (D_r) of a soil. Results from the five Hong Kong sands were plotted in the $D_r - q_{cl}^{0.25}$ space as shown in Figures 7.12 to 7.16, inclusively. It can be seen that a linear relationship can be defined as in the following :

$$D_r = C_3 + C_4 q_{cl}^{0.25} \dots\dots\dots (7.10a)$$

where q_c is in kPa.

or

$$D_r = C_3 + C_4 \cdot q_c^{0.25} \cdot \left(\frac{p_a}{p'} \right)^{0.125} \dots\dots\dots (7.10b)$$

where C_3 and C_4 are two correlation constants.

The results from these analyses on the five Hong Kong sands are summarized in the following table :

Sand	C_3	C_4	Coefficient of correlation R^2
Tung Chung	-23.2	9.4078	0.9368
Chek Lap Kok	-78.43	14.441	0.8972
West Kowloon	-56.7	12.61	0.6860
Tseung Kwan O	-86.5	14.67	0.9422
Tin Shui Wai	-96.3	15.67	0.8867

Eq. (7.10 a-b) can be used to fit all the data over a wide range of relative densities and initial confining pressures obtained from the calibration chamber test results. Figures 7.17 to 7.21 show the calibration chamber test results in the form of cone penetration resistance (q_c) versus initial confining pressures (p') for the five Hong Kong marine sands. Curves of relative density ($D_r = 30\%, 40\%, 50\%, 60\%$, and 70%) predicted by Eq. (7.10 b) are also included in the same plot for cross comparison. Adjacent to each data point is the tested value of D_r for comparison with the predicted value. In general, good agreement is seen between measured and predicted D_r values. In another form, comparisons between measured relative densities and predicted relative densities from Eq. (7.10 b) are shown in Figures 7.22 to 7.26. In general, the predicted relative density is within $\pm 20\%$ from the observed values.

7.5 Correlation with Shear Wave Velocity

Shear wave velocity is predominantly a function of the void ratio and the effective confining stress in the soil. Soil compressibility, which can have a large effect on CPT penetration resistance, has little or no effect on shear wave velocity. Fabric, aging, and cementation of the soil can also have an effect on shear wave velocity. However, one of the objectives of this study is to estimate the in-situ state of hydraulic fill sands for land reclamation in Hong Kong. Such sands are likely to be young and uncemented, thus cementation is unlikely to be of major concern. On the other hand, it has been shown that

aging of freshly deposited sand can increase the cone tip resistance by about 20% in 15 days for certain type of silica sand (Dowding and Hryciw, 1986; Mesri et al., 1990). Thus aging could have an influence on the behaviour of freshly deposited hydraulic sand fill. It is the authors' opinion that the effects of aging mechanism on hydraulic sand fills are probably dependent upon among the others, the method of sand deposition, ground densification technique employed, grain size distribution and mineralogy of sand grains. Micro-vibrations induced by nearby construction activities and construction vehicles may also improve the frictional contact on the macro-arrangement of the sand grains as well as the micro-arrangement of the inter-particle surface contact. The exact aging mechanisms, however, is highly uncertain, and warrant further research investigations.

Results of shear wave velocity measurement on isotropically consolidated triaxial samples as discussed in Chapter 5 have shown that the initial sample void ratio (e) can be estimated by measuring shear wave velocity (V_s) and using the relationship :

$$V_{sl} = A - B \cdot e \dots\dots\dots(7.11)$$

and

$$V_{sl} = V_s \left(\frac{p_a}{p'} \right)^n \dots\dots\dots(7.12)$$

where V_s is in m/s.

The validity of this linear relationship can be evaluated from the results of shear wave velocities determined from large size calibration chamber (1.2 m diameter x 1.5 m height) tests. The shear wave velocities obtained in the V_{zx} direction were normalized according to Eq. (7.12) with $n = 0.25$ and plotted against the void ratio as shown in Figures 7.27 and 7.28 for Tung Chung sand ($A = 669.68$ and $B = 589.01$) and Chek Lap Kok sand ($A = 379.36$ and $B = 312.27$), respectively. It can be seen that the relationship between e and the V_{sl} determined from calibration chamber tests can be reasonably described by the linear equation as in Eq. (7.11). This implies that the shear wave velocity can be a very useful parameter to estimate the in-situ state (in terms of e and p') of freshly deposited hydraulic fill sand by the following relationship :

$$e = \frac{A}{B} - \frac{V_s}{B} \cdot \left(\frac{p_a}{p'} \right)^n \dots\dots\dots(7.13)$$

where V_s is the shear wave velocity, in m/s;
A and B are constants for a given sand;
n is stress exponent; typically $n = 0.25$;
 p_a is the reference stress, typically $p_a = 100$ kPa;
 p' is the mean normal effective stress, and $p' = (\sigma_1' + 2\sigma_3') / 3$
 σ_1' is the effective stress in the direction of wave propagation, in kPa; and
 σ_3' is the effective stress in the direction of particle motion, in kPa

The results of calibration chamber tests can also be used to verify the correlation between normalized shear wave velocity (V_{sl}) and normalized cone penetration resistance (q_{cl}) in a form as proposed by Eq. (7.7).

$$\text{i.e.} \quad q_{cl} = \left(\frac{V_{sl}}{m} \right)^4$$

where V_{sl} is in m/s and q_{cl} is in MPa.

Comparisons of calibration chamber test results for the Tung Chung sand and Chek Lap Kok sand are shown in Figures 7.29 and 7.30, respectively. In general, good correlation between the two normalized parameters V_{sl} and q_{cl} is observed. The correlation constant (m) is equal to 147 for the Tung Chung sand, while $m = 110$ for the Chek Lap Kok sand.

The difference in the m values between the two sands reflects the difference in compressibility, of which the Tung Chung sand is more compressible. For a given in-situ state and, hence, in-situ shear wave velocity, the Tung Chung sand will have a smaller penetration resistance (q_c) due to the high compressibility.

8. SITE RESPONSE TO DYNAMIC LOADS

The site response of sandy soil to dynamic loads was extensively studied and discussed in the Final Report of the Phase 1 study. The two questions that were addressed in the Phase 1 study were the liquefaction potential during possible seismic events and the surface settlement resulting from dynamic loads such as vehicular traffic loading and other types of vibratory disturbances. It was concluded that, given the fact that Hong Kong is not a seismically active region, the likelihood of any earthquake induced liquefaction in the hydraulic fill sand is quite low. In addition, a simple analysis of the West Kowloon sand results indicated that the surface settlement of the sandy fill would be small and it should be tolerable under normal conditions. Of course, settlement in the vicinity of pile driving or heavy impact loads must be considered separately.

In this Chapter, we shall present the results of seismic response analyses of the Tung Chung (TC) site and the Chek Lap Kok (CLK) site. These analyses were carried out using the SUMDES finite element programme (Li et al., 1992). The generalized soil profiles of the TC and CLK sites are given in Figures 8.1 and 8.2, respectively. The pertinent soil properties of

each soil layer were either determined in the laboratory on bulk samples or deduced from available site information.

The procedures to develop the input parameters (including shear modulus and modulus degradation curves) for the SUMDES finite element code for the two sites are given in Appendix H. As in the Phase 1 study, the N - S direction horizontal motions of the November 1986 Lotung earthquake record was used as input. However, in order to limit the maximum ground acceleration to 0.07 g, a scaling factor of 0.45 was applied to the original record for both sites.

The time history of excess pore water pressure and effective mean normal stress at different depths in the hydraulic fills are shown in Figures 8.3 to 8.5 for the TC site and Figures 8.6 to 8.12 for the CLK site respectively. It is quite obvious that the induced pore water pressure is smaller than the effective mean normal stress at all depths for both sites. The cumulative ground settlements shown in Figures 8.13 and 8.14 are for TC and CLK sites, respectively. They are no more than 2 mm in magnitude at TC and 8 mm at CLK. Figures 8.15 and 8.16 show the ground surface response spectra for the TC site and CLK site, respectively. The curves represent the response spectra having damping ratios of 1%, 2% and 5%. It is clear that the predominant period at the maximum ground acceleration for both sites is approximately 0.3 seconds, which is characteristic for soft soil deposit.

From the above information, it would be safe to conclude that when the fills are properly placed, they are not prone to earthquake induced liquefaction. The layer just below the mean sea level, though relatively loose, is still adequate to withstand the earthquake disturbance likely to be experienced in Hong Kong. This, however, does not implies that the "weak" zone below the sea level needs no further ground improvement for other reasons.

No attempt has been made in this study to estimate the surface settlement of the fill due to vibratory type of loading, because the estimated settlement of the West Kowloon site was only 2 cm for a 10 m thick fill deposit. Furthermore, it is the authors' opinion, that significant on site settlement is likely to develop in the compressible sea mud layers or the alluvial deposits below the sand fill.

9. DEVELOPMENT OF QUALITY CONTROL GUIDELINE FOR HYDRAULIC SAND FILL PLACEMENT

9.1 Introduction

Hydraulic sand fills have been commonly used for land reclamation work in Hong Kong. Geotechnical evaluation of these sand fills requires a knowledge of the in-situ "state" of the soil deposits. "State" is a description of the physical conditions under which a material exists; the material behavior is controlled by these "state" conditions. As suggested by Been et al. (1986), void ratio (e) and in-situ stress level (p') are the most important physical conditions which define the current state of the soil and therefore control its behavior. It is the location of this "state" relative to the steady state that provides an estimate of the large strain behavior of the soil. For any deposit the evaluation of in-situ state can be undertaken by either obtaining undisturbed samples of the soil for laboratory testing or by performing in-situ tests.

High-quality undisturbed samples of cohesionless soils can be difficult and expensive to obtain. Ground freezing is one method to obtain the highest quality samples available (Sego et al. 1994; Yoshimi et al. 1989). However, due to the high cost associated with obtaining these undisturbed samples, this approach has been reserved for large budget engineering projects. Polymer impregnation technique to assist undisturbed sampling of cohesionless soils (Sutterer et al. 1994; Sutterer et al. 1995) seems to be a very promising method, however, the field sampling technique and equipment is still under research development.

The primary in-situ test for hydraulic sand fills in Hong Kong is the cone penetration test (CPT). As is the case with other mechanical in-situ tests, the cone penetration test does not measure any particular property of the soil; rather, the local responses in terms of the cone tip resistance (q_c) and sleeve friction (f_s) to an imposed penetration are measured. Therefore empirical correlations are normally used to derive geotechnical properties from the CPT (such as Baldi et al., 1982; Schmertmann, 1978; Villet and Mitchell, 1981; and Jamiolkowski et al., 1985). These existing empirical correlations between cone tip resistance q_c and behavioral properties of sands are based on large diameter calibration chamber test results. However, the application of such correlations in general assumes that all sands behave in a similar manner at the same relative density and stress level.

To examine the correlations of the Hong Kong marine sands and the other sands that have been tested in calibration chambers, the calibration chamber test results obtained from this study were compared with the empirical relationship developed by Jamiolkowski et al. (1985) for uncemented normally-consolidated quartz sand. The results are shown in Figure 9.1. It may be seen that on this basis the five sands do not define the same relationship and that the CS1 and TC sands appear to be much more compressible than the other sands. The sand data points shown in Figure 9.1 are plotted on the basis of the relative density being defined by the ASTM method. These findings suggest that it would be unwise to consider previously published correlations between relative density, confining pressure, and penetration resistance as generally applicable to all sands. Special sets of correlations are required for the Hong Kong hydraulic fill sands.

9.2 "Dense" Sand versus "Loose" Sand

In this report, the definitions of dense and loose sand behaviors were defined according to that suggested by Cunnings et al. (1995). In general, a cohesionless soil element exists in a state of void ratio and effective stress such that it is either loose or dense of the steady state. A three-dimensional space of e , p' , and deviator stress (q) can be used to describe boundaries that separate the state at which a soil can or cannot exist. When a soil is sheared the void ratio and effective stress move toward the steady state line at large strains.

A cohesionless soil that is loose of the steady state and loaded in shear will contract to reach the steady state condition; likewise, a soil that is dense of the steady state will dilate toward the steady state condition. Loose cohesionless soils can produce large deformations thus can be more critical for design considerations. Dense cohesionless soils are typically not a design problem, as they will generally not exhibit large deformations upon most normal loading conditions. When a cohesionless soil is loose of the steady state and is

sheared undrained, it tends to contract and causing increase in pore water pressure, which can result in strain softening, flow liquefaction behavior. The soil reaches its peak strength then decreasing rapidly to the steady state (with residual strength) under large deformation. Thus the investigation of cohesionless soils is often directed toward quantifying how loose the soil deposit is in-situ.

Been and Jefferies (1985) introduced the state parameter (Ψ) to describe the large strain behavior of a sand based on the combined influence of the initial void ratio, effective confining stress, and their relation to the steady state void ratio at the same stress. The state parameter (Ψ), as defined by Been and Jefferies (1985), is the difference between the initial void ratio and the void ratio of the point at the steady state line (e_{ss}) under the same mean normal effective stress (p'), i.e.

$$\Psi = e - e_{ss} \dots\dots\dots(9.1)$$

Been and Jefferies (1985) showed that the initial state of a sand controls the large strain behavior. A negative (-ve) Ψ value indicates an initial state of the soil that is dense of the steady state thus it can be considered as a "dense" sand, while a positive (+ve) Ψ value indicates an initial state of the soil that is loose of the steady state and it can be considered as a "loose" sand.

9.3 Cone Penetration Test (CPT) to Evaluate In-situ State

As discussed in section 7.4, results from the calibration chamber tests on the five Hong Kong hydraulic fill sands indicated an approximately linear relationship between the normalized cone tip resistance (q_{cl}) with the void ratio (e), as

$$e = C_1 - C_2 (q_{cl})^{0.25} \dots\dots\dots(9.2)$$

where q_c is in kPa, C_1 and C_2 are two correlation constants, and q_{cl} is defined as :

$$q_{cl} = q_c \left(\frac{p_a}{p'} \right)^{0.5} \dots\dots\dots(9.3)$$

where q_c is the cone penetration resistance value determined from CPT (in kPa)

p' is the mean normal effective stress,

$p' = (\sigma_1' + 2\sigma_3')/3$ (in kPa)

p_a is the atmospheric pressure (typically 100 kPa)

Combining Eq. (9.2) and (9.4) yields,

$$e = C_1 - C_2 q_c^{0.25} \cdot \left(\frac{p_a}{p'} \right)^{0.125} \dots\dots\dots (9.4)$$

Eq. (9.4) express a relationship between the cone tip resistance (q_c) determined from field CPT results with the state of the soil under in-situ conditions (i.e. e and p'). For freshly deposited and uncemented cohesionless soils, the behaviors of the soils under laboratory controlled calibration chamber testing conditions can be assumed to be similar to that at the site. Therefore, the soil constants C_1 and C_2 determined from calibration chamber tests (corrected for chamber size effects) can be used in Eq. (9.4) for the correlation between field determined q_c values with the in-situ state of the soils (in terms of e and p'). The soil constants C_1 and C_2 determined from laboratory calibration chamber tests for the five Hong Kong sands are summarized in Table 9.1.

As shown in Chapter 6, the steady state line can be defined as follows :

$$e_{ss} = \Gamma - \lambda (p_1')^\alpha \dots\dots\dots (9.5)$$

where Γ is the intercept of the steady state line at $p' = 0$ kPa;
 λ is the slope of the steady state line in $e - (p_1')^\alpha$ space; and
 α is the exponential constant (typically, $\alpha = 0.75$)

and

$$p_1' = \frac{p'}{p_a} \dots\dots\dots (9.6)$$

Combining Eqs. (9.1) and (9.4) to (9.6), the state parameter (Ψ) can be expressed as :

$$\Psi = C_1 - C_2 q_{cl}^{0.25} - \Gamma + \lambda (p_1')^{0.75} \dots\dots\dots (9.7)$$

or

$$\Psi = (C_1 - \Gamma) - \left(C_2 q_c^{0.25} \left(\frac{p_a}{p'} \right)^{0.125} - \lambda \left(\frac{p'}{p_a} \right)^{0.75} \right) \dots\dots\dots (9.8)$$

The state parameter based on cone penetration resistance for each sand can be evaluated using the soil constants, C_1 , C_2 , Γ and λ . Since the mean normal effective stress (p') has been used in the development of the above relationships, and both the vertical effective stress (σ_1') and horizontal effective stress (σ_3') are required to determine p' , therefore the coefficient of earth pressure at rest, K_o has an influence on the determination of Ψ (i.e. $\sigma_3' = K_o \sigma_1'$).

Figures 9.2 and 9.3 show the $q_c - p'$ relationship for various values of state parameter (Ψ) using the C_1 and C_2 constants determined by calibration chamber tests for the Tung Chung and Chek Lap Kok sands. The contour defined by $\Psi = 0$ in these figures represents an important boundary. When the q_c and p' values obtained from site fell to the left side of the $\Psi = 0$ curve ($\Psi = +ve$ value), the soil can be considered as "loose" sand and it will deform in contractive mode when sheared. On the other hand, if the q_c and p' values fell to the right side of the $\Psi = 0$ curve ($\Psi = -ve$ value), the soil can be considered as "dense" sand and it will deform in dilative mode when sheared. Therefore the $\Psi = 0$ line can be considered as the contractive/dilative boundary for a given sand in terms of q_c against p' .

If one adopts the $\Psi = 0$ line as the contractive/dilative boundary for a given sand, the cone tip resistance value q_c (in kPa) obtained by CPT from site investigation may be used to define the acceptance criteria or quality control criteria for hydraulic sand fills. For the hydraulic sand fills to deform in dilative mode under shear loading; the $q_{c(min)}$ is defined as in the following equation :

$$q_{c(min)} = \left[\frac{(C_1 - \Gamma)}{C_2} \left(\frac{p'}{p_a} \right)^{1/8} + \frac{\lambda}{C_2} \left(\frac{p'}{p_a} \right)^{7/8} \right]^4 \quad (\text{kPa}) \dots \dots \dots (9.9)$$

The $q_{c(min)}$ versus p' profiles defined by Eq. (9.9) for the five Hong Kong hydraulic fill sands are shown in Figure 9.4. It should be noted that $q_{c(min)}$ defined in Eq. (9.9) for a given soil (with soil parameters C_1 , C_2 , Γ and λ) is not a constant value, but it depends on the value of the mean normal effective stress p' ; which in turn depends on the overburden effective stress σ_v' , and coefficient of earth pressure at rest K_o . Figures 9.5 and 9.6 show the $q_{c(min)}$ versus effective vertical overburden pressure σ_v' profile for the Tung Chung sand and Chek Lap Kok sand under the cases of $K_o = 0.4, 0.6, 0.8$ and 1.0 , respectively. The maximum difference in $q_{c(min)}$ between $K_o = 0.4$ and $K_o = 1.0$ is approximately 660 kPa for TC sand and 750 kPa for CLK sand at σ_v' of 100 kPa. This difference increases slowly as σ_v' increases. For a deposit with a high K_o , a higher q_c value is required for the soil to remain on the dilative side of the steady state.

For most of the engineering design work conducted by the geotechnical engineering profession, a factor of safety (FS) is commonly applied to the estimated value to get the allowable design value. Thus one would expect to apply a safety factor to the $q_{c(min)}$ value determined by Eq (9.9) into the design specification. However, the relationship between $q_{c(min)}$ and the mean effective stress p' as defined in Eq (9.9) is highly non-linear, and there is

little guidance on how to select an appropriate value of safety factor to account for the uncertainties in design. One way to account for the uncertainties that might occur in the experimental procedure and to increase the degree of confidence level of the specified minimum q_c requirement, the 20 minimum cone tip resistance profile specified in the acceptance criteria $q_{c(min)}^*$ can then take the following form :

$$q_{c(min)}^* = \left[\frac{(C_1 - \Gamma - \Psi_{FS})}{C_2} \left(\frac{p'}{p_a} \right)^{1/8} + \frac{\lambda}{C_2} \left(\frac{p'}{p_a} \right)^{7/8} \right]^4 \quad (\text{kPa}) \dots\dots\dots (9.10)$$

where Ψ_{FS} is the additional state parameter to account for the added degree of confidence in ensuring the soil to remain on the dilative side of the steady state.

Based on the results of undrained triaxial compression tests on the five Hong Kong sands as discussed in section 4.2, the Ψ_{FS} is recommended to be up to about -0.05. The relationships between the specified $q_{c(min)}^*$ versus p' for $\Psi_{FS} = -0.05$ for the TC and CLK sands are shown in Figures 9.7 and 9.8, respectively. At $p' = 100$ kPa, a $\Psi_{FS} = -0.05$ will cause the $q_{c(min)}^*$ to increase by +1.6 MPa for TC sand and +2.6 MPa for CLK sand.

9.4 Cone Penetration Test (CPT) to Evaluate Relative Density of Soils

As shown in section 7.4, the results of calibration chamber tests also indicated an approximately linear relationship between the relative density (D_r) of the soils and the normalized cone tip resistance (q_{cl}) as :

$$D_r = C_3 + C_4 q_{cl}^{0.25} \dots\dots\dots (9.11)$$

where q_c is in kPa, C_3 and C_4 are two correlation constants and these values are summarized in Table 9.1 for the five Hong Kong sands undertaken in this study.

Since,

$$q_{cl} = q_c \left(\frac{p_a}{p'} \right)^{0.5} \dots\dots\dots (9.12)$$

Combining Eqs (9.11) and (9.12), the relative density of a soil (D_r) can be related with the cone tip resistance value (q_c) determined from field CPT results and the in-situ mean effective stress (p'), viz :

$$D_r = C_3 + C_4 q_c^{0.25} \left(\frac{p_a}{p'} \right)^{0.125} \dots\dots\dots (9.13)$$

where D_r is in %, p' and q_c are in kPa.

The cone penetration resistance value (q_c) can be expressed in terms of D_r and p' , viz :

$$q_c = \left[\left(\frac{D_r - C_3}{C_4} \right) \left(\frac{p'}{p_a} \right)^{1/8} \right]^4 \dots\dots\dots (9.14)$$

where D_r is in %, p' and q_c are in kPa.

For illustration proposes, the $q_c - p'$ relationship at $D_r = 40\%$ (the boundary between loose and medium dense sand as defined by Meyerhof, 1956) estimated by Eq (9.14) for the five Hong Kong sands are shown in Figure 9.9. It should be noted that because of the difference in physical properties of the five sands (including compressibility, grain size shape and distribution, mineralogy and friction angle), the $q_c - p'$ relationships are very different for the five sands. The Tung Chung sand seems to be most compressible and experienced a very gentle $q_c - p'$ response, while the Tin Shui Wai sand is most incompressible and displayed a steep $q_c - p'$ response. In the engineering design analysis of hydraulic sand fills, the minimum relative density value ($D_{r(min)}$) can be specified based on certain acceptable criteria. This minimum acceptable criteria can be estimated based on the results of static/dynamic triaxial tests on the given soils tested at various relative density values. The relationships such as D_r - deformation modulus (E), D_r - angle of internal friction (ϕ), D_r - constrained modulus (M_s) and D_r - liquefaction potential can be obtained from a well planned triaxial testing programme with various D_r and confining pressures. Various empirical correlations between D_r with various soil parameters (friction angle, deformation modulus compressibility of soil etc.) have been developed, and some of these correlations already reported in Volume II of the Phase 1 report. These empirical correlations should be used with extreme cautions, as the relative density of a soil is not only a function of the physical properties and the mechanical testing parameters (q_c or N), but it also depends on the in-situ stress state of the soil (p') as shown in Eq (9.14).

9.5 Shear Wave Velocity to Evaluate In-situ State

Results of shear wave velocity measurements obtained from the calibration chamber tests (as described in section 7.5) and laboratory bender element tests on triaxial specimens (as described in Chapter 5) indicated that a linear relationship between the normalized shear wave velocity (V_{sl}) and void ratio of the soil (e) can be defined as :

$$V_{sl} = A - Be \dots\dots\dots (9.15)$$

where

$$V_{sl} = V_s \cdot \left(\frac{p_a}{p'} \right)^n \dots\dots\dots (9.16)$$

where p' is in kPa and V_s is in m/s

The correlation constants A and B and the stress exponents n for the five Hong Kong sands determined from the laboratory bender element tests on triaxial specimens are summarized in Table 9.1. Combining Eqs. (9.15) and (9.16) yields :

$$e = \frac{A}{B} - \frac{V_s}{B} \left(\frac{p_a}{p'} \right)^n \dots\dots\dots (9.17)$$

Following a similar line of development as described in section 9.3 and the work of Cunning et al. (1995) and Robertson et al. (1995), the state parameter (Ψ) of a soil determined by the shear wave velocity (V_s) can be defined as :

$$\Psi = \left(\frac{A}{B} - \Gamma \right) - \left(\frac{V_s}{B} \left(\frac{p_a}{p'} \right)^n - \lambda \left(\frac{p'}{p_a} \right)^\alpha \right) \dots\dots\dots (9.18)$$

where n is the stress exponential constant determined from the slope of the V_s versus p' line on a log-log scale (typically $n=0.25$); and
 α is an exponential constant of the soil obtained by the optimization technique of the linear relationship between steady state void ratio and $(p_l')^\alpha$ as described in section 6.6 (typically, α can be assumed as 0.75).

The state parameter based on the shear wave velocity of the soil can be evaluated using the soil constants A , B , n , Γ , λ and assuming $\alpha = 0.75$. Figure 9.10 shows the contractive/dilative boundaries (Ψ) for the Tung Chung and Chek Lap Kok sands using the soil parameters A and B determined by bender element tests on triaxial specimens (as summarized in Table 9.1). It can be seen that the $V_{s(min)}$ profiles for the five marine sands are all concentrated in a relatively narrow range. This is due to the fact that the general range of shear wave velocities for most of the marine sands are quite similar to each together, as observed from the results of bender element tests as discussed in Chapter 5.

If the shear wave velocity profile can be determined by SCPT or SASW tests in the field, the shear wave velocity values V_s obtained from the site investigation can be used to check against the proposed acceptance criteria or quality control criteria of hydraulic sand fills based on laboratory determined soil constants n , A , B , λ and Γ . For the soils to deform in

dilative mode under shear loadings, the shear wave velocity V_s (in m/sec) profile obtained from SASW or SCPT test must be greater than the minimum acceptable shear wave velocity $V_{s(\min)}$ profile defined by the following equation :

$$V_{s(\min)} = (A - B\Gamma) \cdot \left(\frac{p'}{p_a} \right)^n + \lambda B \cdot \left(\frac{p'}{p_a} \right)^{\alpha+n} \dots\dots\dots (9.19)$$

Assuming $\alpha = 0.75$, Eq. (9.19) can be written as :

$$V_{s(\min)} = (A - B\Gamma) \cdot \left(\frac{p'}{p_a} \right)^n + \lambda B \cdot \left(\frac{p'}{p_a} \right)^{0.75+n} \dots\dots\dots (9.20)$$

where V_s is in m/s and p' is in kPa.

The $V_{s(\min)}$ versus p' profiles defined by Eq (9.20) for the five Hong Kong marine sands, in fact, are the same as the $\Psi = 0$ boundaries as shown in Figure 9.10. The CLK sand is representative of a coarse, less compressible, silica sand. However, the TKO and TC sands are more compressible soils which display lower V_s versus p' responses.

9.6 Evaluation of the Proposed Relationships

Eqs (9.9) and (9.20) defined the minimum field investigation acceptance criteria based on, respectively, the cone penetration resistance (q_c) and shear wave velocity (V_s) under the condition of $\Psi = 0$ (the contractive/dilative boundary). The applicability of these proposed equations to determine where potential for flow liquefaction exists on the site under the in-situ state will be examined through the site investigation data at the Tung Chung site and Chek Lap Kok site.

For both sites, field data on the seismic cone penetration test (SCPT) profiles were obtained. Both the cone penetration resistance (q_c) profile as well as the shear wave velocity (V_s) profile were determined from the same SCPT sounding. The steady state line constants Γ and λ were determined from the results of laboratory triaxial tests as described in Chapter 6, while the soil constants C_1 and C_2 were obtained from the results of cone penetration measurements in calibration chamber tests. The soil constants A and B for the $V_{sl} - e$ relationship have been obtained from both the calibration chamber tests as well as the bender element tests in triaxial specimens. These two different series of tests yielded slightly different values of the soil constants, and they are summarized as in the following :

Results obtained from calibration chamber tests				Results obtained from bender element tests in triaxial specimens		
Sand	n	A	B	n	A	B
TC	0.25	669.68	589.01	0.24	687	618
CLK	0.25	379.36	312.27	0.24	459	431

Since the mean normal effective stress (p') defined in Eqs (9.9) and (9.20) requires values of effective overburden pressure (σ_v') and the coefficient of earth pressure at rest (K_0). The σ_v' was calculated based on an estimated bulk density of kN/m^3 and with the mean sea level located at +1.2 mPD. The K_0 is assumed to be equal to 1.0 above the mean sea level and reduced to $K_0 = 0.5$ below the mean sea level to reflect the different in compaction efforts resulted from various fill depositional modes. The field SCPT determined q_c profiles are plotted against the $q_{c(\min)}$ profiles defined by Eq. (9.9) in Figures 9.11 and 9.12 for the TC site and CLK site, respectively. Both figures indicated that regions of sand fills at depths about 2 to 3 meters below the mean sea level are looser than the $q_{c(\min)}$ defined by Eq. (9.9) at the time of testing. This indicates that the soils at these regions should deform under contractive mode when sheared.

The in-situ measured V_s profiles are compared with the $V_{s(\min)}$ profile defined by Eq. (9.20) in Figures 9.13 and 9.14 for the two sites. The $V_{s(\min)}$ profiles defined by the parameters (n , A , and B) obtained from the two different series of tests are quite similar (with difference less than 10% to 15%) at the time of testing. Similar to the previous findings, the results from these analyses also indicated that there are regions of sand fills below the mean sea level with V_s values smaller than the $V_{s(\min)}$ defined by Eq. (9.20). Therefore, prior to improvement by compaction, the soils in these regions of loose zones could deform in contractive mode when subjected to shear loading.

9.7 Proposed Application

Ideally, in order to evaluate in-situ strength and large-strain behavior of sands, it is important to conduct laboratory tests on high-quality undisturbed specimens. High quality undisturbed specimens of sand can be obtained using in-situ ground freezing technique. the cost of in-situ ground freezing is high, the need to obtain high-quality undisturbed specimens would depend on the project requirements. However, it is possible to estimate the in-situ state and large-strain behavior of a fresh and uncemented sand deposits using in-situ cone penetration resistance measurements and/or shear wave velocity measurements as proposed in this chapter.

The relationships proposed in this study have been developed based on reconstituted laboratory samples. Hence, the resulting relationships will only represent young, uncemented cohesionless soil. The in-situ materials could be aged or cemented and have a different behavior. Both aging and cementation will tend to increase the measured cone penetration resistance and shear wave velocity. As suggested by Cunning et al. (1995), aging generally decreases the void ratio of a cohesionless soil and can result in a more dilatant response. Cementation can increase the small strain stiffness of a soil; however, when strains are

sufficient to break the cementation bonds, the large strain behavior can be contractive or dilatant depending on the actual void ratio. Caution should be used to apply the shear wave velocity correlation to cemented soils. On the other hand, the proposed correlation based on cone penetration tests can avoid this potential problem, since the relationship developed based on cone penetration tests were obtained at strain level large enough to break the cementation bonds.

The proposed approach of using normalized q_c values obtained from site CPT tests requires the determination of the soil parameters C_1 and C_2 from large calibration chamber testing for a given soil, which are expensive and are subjected to boundary size effects and corrections. Once these two soil parameters were determined, the results from in-situ cone penetration tests can provide an estimate of whether the soil is either loose of the steady state and therefore contractive or dense of steady state and dilative. It should be noted that the issue of uncertainty in the interpretation of penetration tests in cohesionless soils due to variations in soil compressibility as suggested by Robertson and Campanella (1983) has been resolved in the proposed relationship by the incorporation of the steady state concepts.

On the other hand, shear wave velocity is an attractive parameter, since it can be easily measured both in the field and the laboratory. No corrections are required for boundary effects and the normalized procedure for in-situ confining pressure is developed directly. However based on the results obtained in this study, the normal range of shear wave velocity for the five Hong Kong marine sands was in the order of 200 to 400 m/s for a vertical effective stress from 50 to 400 kPa (under dry sand condition). At a given void ratio, the change in shear wave velocity (ΔV_s) is typically varied within the range of 100 to 150 m/s for a vertical effective stress from 50 to 400 kPa. This relative narrow range of shear wave velocity variation over change in confining stresses implies that highly accurate in situ testing and laboratory bender element testing devices are required (the HKUST is equipped with the most state-of-the-art equipment for shear wave velocity determination). Nevertheless, the results from this research study indicated that the laboratory determined shear wave velocity is dependent upon the following factors :

- i) sample reconstitution techniques;
- ii) degree of saturation of the sample (dry, moist, or fully saturated);
- iii) stress anisotropy;
- iv) sample size effect (or accuracy of measurement in small size sample such as triaxial specimens); and
- v) consolidation time before actual shear wave velocity measurement.

Additional research investigation is currently undergoing to examine the potential effects of the above mentioned factors on the laboratory determination of shear wave velocity.

9.8 Recommended Soil Constants to be Used for Quality Control

- i) For quality control of the hydraulic sand fills, site investigation work is recommended to be carried out by cone penetration tests (CPT), or seismic cone penetration tests (SCPT) or CPT with shear wave velocity profile at the site determined by SASW tests.
- ii) As an initial screening, if the physical properties of the marine sands at the proposed site are similar to (or obtained from the same sand borrow areas) the five Hong Kong sands examined in this study, the soil constants listed in Table 9.1 may be used as reference for a particular site. However, the properties of a sand from a particular borrow area can be extremely variable, the soil parameters Γ and λ to describe the steady state line of the soil should be determined from triaxial tests on representative samples obtained from the site.
- iii) For a more detailed evaluation of a given sand, it should be possible to develop a material specific relationship among shear wave velocity, void ratio, and effective confining stress based on a number of isotropic consolidation tests on fully saturated reconstituted specimens of the sand using a similar procedure adopted in this study. The shear wave velocity should be measured throughout a series of consolidation pressures covering a possible range of in-situ confining stresses and various initial void ratios (or relative densities). Several of the specimens can then be loaded in triaxial compression to reach the steady state. These tests can be performed drained or undrained to provide parameters that defines the steady state line (i.e. Γ and λ). These parameters can then be combined with the constants A , B , and n obtained from shear wave velocity measurements to produce the relationship to estimate the in-situ void ratio (as described by Eq. 9.17), the state parameter Ψ (as described by Eq. 9.18), and the $V_{s(\min)}$ (as described by Eq. 9.20).
- iv) For important project a detailed evaluation of the soil is required. A large bulk sample should be obtained from the site. The bulk sample should be taken preferable at a depth close to mean sea level. Sampling at shallow depth close to fill surface should be avoided. This bulk sample should be used for calibration chamber testing, and the material specific relationships among cone tip resistance (q_c), shear wave velocity (V_s), void ratio (e), and effective confining stress (p') can be developed based on the calibration

chamber test results. For description of the steady state line of the soil, the soil parameters Γ and λ should be determined from triaxial tests on representative samples obtained from the site. These parameters can then be combined with the constants A, B, and n obtained from shear wave velocity measurements and the soil constants C_1 , C_2 , C_3 , and C_4 obtained from cone penetration resistance in calibration chamber tests to produce the relationships to estimate the in-situ void ratio (as described by eqs. 9.3 and 9.17), the state parameter Ψ (as described by eqs. 9.8 and 9.18), the in-situ relative density D_r (as described by eq. 9.13), the $V_{s(\min)}$ (as described by eq. 9.20), and the $q_{c(\min)}$ (as described by eq. 9.9).

- v) Factor of safety may be considered by the incorporation of Ψ_{fs} as described by Eq. (9.10). The Ψ_{fs} is recommended up to a value of -0.05.

Provided that the in-situ sand deposit is fresh and uncemented, the proposed approach should provide a reasonable estimate of the minimum acceptance criteria in terms of $q_{c(\min)}$ or $V_{s(\min)}$ of the sand. For aged or cemented sands the relationship based on reconstituted specimens may not be valid, as these effects are very difficult to simulate in laboratory conditions. Since most of the hydraulic sand fills in Hong Kong are young and relatively uncemented, the proposed approach should be applicable as an initial evaluation of such deposits.

10. SUMMARY AND CONCLUSIONS

The second phase of study aiming at the development of design guidelines for hydraulic sand fill placement in Hong Kong has been completed. The proposed guidelines were developed on the basis of a comprehensive interpretation of all data collected in both phases of the study. These data sources were obtained from an extensive review of existing site construction records at the five reclamation sites, interviews with site staff, results from a number of in-situ testing and sampling, an extensive laboratory static and dynamic triaxial testing programme, a series of shear wave velocity determinations of the soils at the sites and in the laboratory, and calibration chamber test results. The proposed guidelines should be useful in assisting engineers in :

- i) estimating the needed density suitable for reclamation uses,
- ii) estimating the likely density achievable by the given material type and placement method and the need for post-placement improvement,
- iii) verifying the in-situ density on the basis of field test results, and

- iv) drawing up specification for the fill based largely on methods of fill placement and material type.

10.1 Estimating the Needed Density

A properly engineered hydraulic sand fill should satisfy both the stability and serviceability requirements under the given design loads. As the effective friction angles of the five Hong Kong marine sands are quite high (at least 35° for all sands) for relative densities as low as 35%, stability problems such as inadequate bearing capacity are unlikely to be encountered. The most important design criterion for the construction of hydraulic sand fills, therefore, would be the serviceability requirement. In other words, it would be important for engineers to estimate the deformation behaviours of the sand fills when subjected to shear loading. Similarly, the likelihood of flow liquefaction and the associated post-liquefaction type of large deformation resulting from impact loads or strong dynamic loads imposed on the fill deposits, though to be small, must also be considered.

The basic framework of the proposed guideline is based on the definition of a contractive/dilative boundary ($\Psi = 0$), or the steady state line of a soil. A cohesionless soil that is loose of the steady state (the $\Psi = +ve$) and loaded in shear will contract to reach the steady state condition, and a soil that is dense of the steady state ($\Psi = -ve$) will dilate to the steady state condition. Loose cohesionless soils can produce large deformations thus can be more critical for design considerations. Dense cohesionless soils are typically not a design problem, as they will generally not exhibit large deformations under most of the normal loading conditions. When a cohesionless soil is loose of the steady state and is sheared undrained, it tends to contract and causing increase in pore water pressure, which can result in strain softening, flow liquefaction behaviour. Thus the investigation of the needed density of a marine sand suitable for reclamation uses should be directed toward quantifying the as-placed density which must not be looser than that on the steady state line (i.e. the state parameter Ψ must not be +ve).

The details for the determination of the steady state lines for the five Hong Kong sands were given in Chapter 6. The development of minimum acceptance criteria based on in-situ field tests to ensure the soil deposits are dense of the steady state condition was given in Chapter 9.

It should be noted that although a sand fill may be suitable in its as-placed state for the support of most structures and facilities, deep foundations will be needed for settlement sensitive structures if the fill is placed over soft compressible layers. If driven piles are used, then "displacement type" piles are desirable to further densify the sand during driving. Similarly, if preloading and precompression are used to reduce the future settlements from underlying compressible layers beneath a hydraulic fill, then sand drains or wick drains should be installed using vibratory methods to further densify the sand. Mitchell et al. (1995) summarized the experiences in the recent Kobe earthquake which showed significant reduction in settlements of hydraulic fills in areas where precompression and sand drains had been used to treat the soft clay beneath the fill.

10.2 Estimating the Likely CPT- q_c Achievable by the Given Material Type and Placement Method

From the surveys of the five reclamation sites, the effects of fill gradation and fine content on the processes of winning of marine sand, loading of dredged sand onto hopper, and quality control on hopper barges have been examined. Based on this study, the following conclusions can be drawn :

- 1) The ease of marine sand winning and dredging operations does not seem to be dependent upon the average size of dredged sands, up to an average grain size D_{50} of 2 mm (maximum size may be as large as 20 mm as observed in the TSW site).
- 2) Sand winning and dredging operations can be significantly affected by the proportion of fines. Based on the information obtained from the current study, the following three groups can be classified :

<u>Operation Level</u>	<u>Range of fine content</u>
No difficulty	0% to about 10%
Moderate difficulty	about 10% to 15%
Difficult	more than 15%

In this study, the mechanism of the bottom dumping process and the factors affecting the as-placed density is examined. A hypothetical mechanism of the bottom dumping process is also postulated. By using the general framework of the proposed mechanism to examine the available CPT results on the five sites, it was found that the as-placed density and the amount of soil segregation of the bottom-dumped fills are affected by : i) the gradation and fine content of the soil; ii) the total thickness of the bottom dumped sand fill; and iii) the maximum water depth of the bottom-dumped fill. Based on these findings, the following guideline for soil compaction resulting from bottom dumping process is proposed :

Maximum Water Depth of Fill Deposition	Total Thickness of Bottom Dumped Sand Fill		
	Compaction effort - GOOD	Compaction effort - FAIR	Compaction effort - POOR
15 m to 20 m	> 9 m Average $q_c = 5$ to 7.5 MPa at the top of the bottom dumped fill and increased at a rate of 0.4 to 0.55 MPa/m	6 m to 9 m Average $q_c = 4.5$ MPa to 5.5 MPa at the top of the bottom dumped fill and increased at a rate of 0.3 to 0.45 MPa/m	< 6 m Very little difference in q_c between bottom dumped fill and pipeline discharged fill
Less than 10 to 11 m	> 5 m Average $q_c = 7$ to 12 MPa at the top of the bottom dumped fill and increased at a rate of 0.4 to 0.8 MPa/m (or almost constant with depth at shallower depth)	< 5 m Average $q_c = 5$ to 7 MPa at the top of the bottom dumped fill and remains almost constant with depth	---
Note : The above table is only applicable to dredged marine sands with fine content less than 15% (average about 4% to 5%). The fill constructed by bottom dumping method would most likely to be highly segregated with the minimum q_c value about 50% lower than the average q_c , and the maximum q_c value about 50% higher than the average q_c .			

The effects of subaqueous placement by rainbowing and pipeline discharge also had been examined in this study. It was found that subaqueous placement by pipeline discharge generally produced slightly higher q_c values than that of rainbowing discharge. However, the difference between subaqueous placement by rainbowing and pipeline discharge are generally quite small. But one noticeable difference between subaqueous placement by rainbowing and pipeline discharge is the fact that the q_c profiles for sand fills constructed by rainbowing technique are generally much smoother than that constructed by pipeline discharge. This implies that pipeline discharge generally resulted in slightly more segregated sand fills as compared to the rainbowing method.

Based on the observation obtained from this study, a general sequence from highest to lowest post-placement density for a given material according to placement method commonly used in Hong Kong was proposed as shown in the following :

1. Above water with traffic compaction.
2. Hopper dumping below water.
3. Beach above water - no compaction.

4. Below water - subaqueous pipeline or rainbowing discharge.

10.3 Verifying the In-situ Density on the Basis of Field Test Results

In this study, techniques for the estimation of in-situ density based on the field test results had been developed. Correlations were developed between the in-situ state of the soils (e and p') with the results obtained from two kinds of field tests, namely : 1) cone tip resistance (q_c) profile determined by CPT tests; and 2) shear wave velocity (V_s) profile determined by SCPT or SASW tests.

Calibration chamber test results have shown that the cone tip resistance (q_c) of a sand, besides the compressibility of the soils, is primarily controlled by the effective confining stress and void ratio. The q_c data obtained from the calibration chamber tests was used to develop sand specific e - p' - q_c relationships. Based on the relationship between void ratio, effective confining stress, and the penetration resistance plus the establishment of the steady state line, the in-situ state of the sand can be estimated. Hence, the contractive/dilative behaviour of a sand can be evaluated from the in-situ q_c obtained from CPT and effective vertical overburden stress with an estimate of K_o value.

On the other hand, laboratory studies by the bender element technique have been shown that the shear wave velocity of a sand is controlled primarily by the effective confining stress and void ratio. Since shear-wave velocity can be readily measured both in the field and in the laboratory, it can be used to define the in-situ state of a sand. An experimental study of the shear wave velocity measurements was conducted on the five Hong Kong sands. The results show that a linear relationship can be developed between the normalized shear wave velocity (V_{sl}) and the in-situ state (e and p') of a soil. Combining with the steady state concept, the large-strain behaviour of the sands can be estimated using shear wave velocity measurements together with a knowledge of in-situ effective stress. Knowledge of the in-situ state of a sand makes it possible to estimate the contractive/dilative boundary of the soil at large strain. Based on these findings, a method to evaluate the potential for flow liquefaction using shear wave velocity measurement was developed.

Based on these studies, the following empirical correlations have been developed :

- i) the in-situ void ratio (e) of a soil can be determined by Eq. (9.3) with cone penetration resistance (q_c) determined by field CPT results,
- ii) alternatively, the in-situ void ratio (e) of a soil can be determined by Eq. (9.17) with shear wave velocity (V_{sl}) determined by field SCPT or SASW test results,
- iii) the relative density (D_r) profile of a sand fill can be determined by the q_c profile obtained by field CPT results together with the relationship as expressed in Eq. (9.13).

- iv) the cone penetration resistance value (q_c) obtained from site CPT test can be checked against the minimum acceptance criteria or quality control criteria of hydraulic sand fills as defined by the minimum cone penetration resistance ($q_{c(min)}$) value as defined in Eq. (9.9). If the q_c value obtained in the site is lower than the $q_{c(min)}$, -placement soil improvement is recommended.
- v) For a soil to deform in dilative mode (or deform in dense sand behaviour) under loadings, the shear wave velocity (V_s) profile obtained from the field SASW or SCPT tests must be greater than the minimum shear wave velocity ($V_{s(min)}$) as defined in Eq. (9.19); otherwise, post-placement soil improvement is recommended.

Provided that the in-situ sand deposit is fresh and uncemented, the proposed approaches as described in this study should provide a reasonable estimate of the minimum acceptance criteria in terms of $q_{c(min)}$ or $V_{s(min)}$ of the sand. For aged or cemented sands the relationship based on reconstituted specimens may not be valid, as these effects are very difficult to simulate in laboratory conditions. Since most of the hydraulic sand fills are young and uncemented sands, the proposed approach should be applicable as an initial evaluation of such deposits in Hong Kong. However, it should be noted that further research investigation is warranted to examine the effect of aging of sand and the associated increase in cone tip resistance in young deposit as reported by Mesri et al. (1990) (and how the aging mechanism might affect the interpretation of the in-situ void ratio of the sand fill by the proposed theory).

10.4 Optimization of Hydraulic Fill Properties During Placement

As noted previously, the hydraulic fills as conventionally placed have adequate density except for a zone extending over about a few meters depth below the water surface. In this region the water is too shallow to permit bottom dumping from barges, which generally produces a high enough relative density. Above the water surface, construction equipment or rollers can be used to achieve high density.

Thus the major problem is to achieve a higher density in the material that is placed by pipeline on a beach below water. To mitigate problems from insufficient density in this zone, there would appear to be two approaches; namely, improving the density during placement or increasing density after completion of the fill. The latter can be accomplished using very heavy vibratory rollers, by application of deep densification techniques (such as vibro-compaction, compaction piles, vibro-rod) or possibly blasting. Deep dynamic compaction is also well-suited for this purpose. The problems with any of these methods, however, are the added cost and construction time associated with their use.

Thus, modifications in the placement procedures might realize the greatest benefits and economics; however, just what modifications are needed remain to be determined. In the authors' views, a number of possible ways may be able to improve the soil density in the

"weak zone" during placement; however, there is very little information available to indicate the feasibility and construction implementation details of such approaches, future research studies of these methods are warranted;

- i) rather than allowing the placement by the beach below water method over a large area, deposition of large stockpiles of fill above the water level and followed by pushing them into the water may produce denser layers;
- ii) bring the fill above water across the width of an area to be filled and then continuing the pipeline discharge by the beach above water method into the pool to be filled;
- iii) consideration might also be given to discharging the hydraulic sand fill by beach below water in thin layer (around 1 m thick) then densify this layer by under-water vibrators in alternate sequence with the pipeline discharge.

Zoning of both the borrow and the placement areas to ensure that the most desirable material goes to the areas requiring the highest quality should be used whenever feasible. By doing this, it should be possible to minimize the areas of ground treatment for hydraulic fills.

10.5 Conclusion

In light of the above discussion, general statements pertaining to the construction treatment, control and stability of the five Hong Kong reclamation sites examined in this study may be summarized as follows :

- (a) It is prudent to acknowledge that hydraulic fills are heterogeneous. The method used for fill placement and the details of its application, the conditions of discharge, the total thickness of the bottom-dumped fill, the water depth, and the variability of source materials are all important in forming the resulting fill properties.
- (b) The placement technique is probably the single most important factor controlling the as-placed density of a given sand when placed as a hydraulic fill. Typical q_c values resulted by various deposition methods under different conditions had been suggested for typical marine sands in Hong Kong. However, the zone with lower density is generally located beneath water level where fill deposition is made by pipeline discharge.
- (c) It follows that for economic and effective control of the quality of hydraulic fills, attention must be paid to improve

the zone with lower density situated just below the water level.

- (d) There seems a need to develop techniques capable of densifying the fill during the process of fill deposition and monitoring the improvement for quality control.
- (e) Based on the calibration chamber tests and laboratory bender element tests, correlations of $e - p' - q_c$ and $e - p' - V_s$ together with quality control guidelines for Hong Kong marine sands have been established. Field tests which are capable of measuring the cone penetration resistance (q_c) and shear wave velocity (V_s) of soil deposits (such as SCPT tests) would be valuable for future site investigation work on reclaimed land placed by hydraulic fill sands in Hong Kong.
- (f) Because of the good quality of source material and the fact that Hong Kong is not a seismically active zone, the dynamic stability of the five Hong Kong hydraulic sand fill sites appears to be sound.

11. REFERENCES

- Akroyd, T.N.W. (1969), Laboratory Testing in Soil Engineering, Soil Mechanics Ltd., London, 249 pp.
- Baldi, G., Bellotti, R., Ghionna, V., Jamiolkowski, M. and Pasqualini, E. (1982), "Design Parameters for Sand from CPT", Proc. 2nd Eur. Symp. Penetration Testing, Amsterdam, Vol. 2, pp. 425-438.
- Been, K., Crooks, J.H.A., Becker, D.E., and Jefferies, M.G. (1986), "The Cone Penetration Test in Sands: Part I, State Parameter Interpretation", Geotechnique, Vol. 36, No. 2, pp. 239-249.
- Been, K., and Jefferies, M.G. (1985), "A State Parameter for Sands", Geotechnique, Vol. 35, No. 2, pp. 99-112.
- Been, K., Jefferies, M.G., and Hachey, J. (1991), "The Critical State of Sands", Geotechnique, Vol. 41, No. 3, pp. 365-381.
- Bellotti, R., Bizzi, G. and Ghionna, V. (1982), "Design, Construction and Use of a Calibration Chamber", Proceedings for the Second European Symposium on Penetration Testing, Amsterdam, pp. 439-446.
- BGS (1991), An Interpretation of Marine Geology for the Replacement Airport at Chek Lap Kok, Hong Kong", Provisional Airport Authority, Hong Kong.

- Burland, J.B. and Burbidge, M.C. (1985), "Settlement of Foundation on Sand and Gravel", Proc. Instu. Civ. Engrs., Dec. 1985, 78, Part I, pp. 1325-381.
- Castro, G. (1969), "Liquefaction of Sands", Harvard University, Cambridge, Mass., Harvard Soil Mechanics Series No. 81.
- Chu, J. and Lo, S.-C.R. (1992), "Discussion: The Critical State of Sands", Geotechnique, Vol. 42, No. 4, pp. 655-663.
- Cunning, J.C., Robertson, P.K. and Sego, D.C. (1995), "Shear Wave Velocity to Evaluate In-situ State of Cohesionless Soils", Canadian Geotechnical Journal, Vol. 32, pp. 849-858.
- DeAlba, P., Seed, H.B. and Chan, C.K. (1976), "Sand Liquefaction in Large Scale Simple Shear Tests", ASCE Journal of Geotechnical Engineering, Vol. 102, No. GTa, pp. 909-927.
- de Groot, M.B., Heezen, F.T., Mastbergen, D.R. and Stefess, H. (1988), "Slopes and Densities of Hydraulically Placed Sands", Proceedings of the Conference - Hydraulic Fill Structures, ASE, Fort Collin, pp. 32-51.
- Dowding, C.H., and Hryciw, R.D. (1986), "A Laboratory Study of Blast Densification of Saturated Sand", ASCE Journal of Geotechnical Engineering, Vol. 112, No. 2, pp. 187-199.
- Fear, C.E. and Robertson, P.K. (1995), "Estimating the Undrained Strength of Sand: a theoretical framework", Canadian Geotechnical Journal, Vol. 32, pp. 859-870.
- Fretti, C., Lo Presti, D.C.F. and Pedroni, S. (1995), "A Pluvial Deposition Method to Reconstitute Well-Graded Sand Specimens", Geotechnical Testing Journal, GTJODJ, Vol. 18, No. 2, pp. 292-298.
- Hardin, B.O. and Richart, F.E.Jr. (1963), "Elastic Wave Velocities in Granular Soils", Journal of Soil Mechanics and Foundation Division, ASCE, Vol. 89, No. 1, pp. 33-65.
- Jamiolkowski, M., Baldi, G., Bellotti, R., Ghionna, V. and Pasqualini, E. (1985), "Penetration Resistance and Liquefaction of Sands", Proceedings of the 11th International Conference on Soil Mechanics and Foundation Engineering, San Francisco, Vol. 4, pp. 1891-1896.
- Janbu, N. (1963), "Soil Compressibility as Determined by Oedometer and Triaxial Tests", Proceedings, 3rd ECSMFE, Wiesbaden.
- Jefferies, M.G., Rogers, B.T. and Stewart, H.R. (1988), "Island Construction in the Canadian Beanfort Sea", ASEE Geotechnical Special Publication, No. 21, Fort Collin,s Colorado.

- Li, X.S., Wand, Z.L. and Shan, C.K. (1992), User's Manual for SUMDES - A nonlinear Procedure for Response Analysis of Horizontally-Layered Sites Subjected to Multi-directional Earthquake Loading, University California, Davis.
- Massarch, K.R. (1985), "Deep Compaction of Sand Using Vibratory Probes", Third International Geotechnical Seminar, Soil Improvement Methods, Singapore.
- Mitchell, J.K., Baxter, C.D.P, and Travis, C.M. (1995), "Performance of Improved Ground During Earthquakes", Soil Improvement for Liquefaction Hazard Mitigation, ASCE Annual Convention, San Diego, CA, October.
- Mesri, G., Feng, T.W., and Benal, J.M. (1990), "Postdensification Penetration Resistance of Clean Sands", Journal of Geotechnical Engineering, ASCE, Vol. 116, No. 7, pp. 1095 - 1115.
- Meyerhof, G.G. (1956), "Penetration Tests and Bearing Capacity of Cohesionless Soils, Journal of the Soil Mechanics and Foundations Division, ASCE, Vol. 82, No. SMI, pp. 1-19.
- Newman, R., Covil, C., Ng, N., and Pickles, A. (1996), "Characteristics of the Sand Fill Used in the Reclamation for Hong Kong's New Airport at Chek Lap Kok", Provisional Airport Authority, Hong Kong.
- Newman, R., Covil, C., Wood, R., Ng, N. and Berner, P.C. (1996), "CPT Testing at Hong Kong's New Airport at Chek Lap Kok", Provisional Airport Authority, Hong Kong.
- Ng, H.Y. (1991), "Case Histories of Reclamation Techniques", Reclamation - Important Current Issues, HKIE, Geotechnical Division, 14 May, pp. 57-74.
- Parkin, A.K. and Lune, T. (1982), "Boundary Effects in the Laboratory Calibration of Cone Penetrometer for Sand", Proc. ESOPT, Amsterdam.
- Poulos, S.J. (1981), "The Steady State of Deformation", Journal of Geotechnical Engineering, ASCE, Vol. 17, GT5, pp. 553-562.
- Robertson, P.K. (1994), "Suggested Terminology for Liquefaction", Proceeding 46th Canadian Geotechnical Conference, Canadian Geotechnical Society, Ottawa, Canada.
- Robertson, P.K. and Campanella, R.G. (1983), "Interpretation of Core Penetration Tests", Canadian Geotechnical Journal, Vol. 20, No. 4, pp. 718-733.
- Robertson, P.K. Sasitharan, S., Cunning J.C. and Sego, D.C. (1985), "Shear-wave Velocity to Evaluate In-situ State of Ottawa Sand", ASCE Journal of Geotechnical Engineering, Vol. 121, No. 3, pp. 262-273.
- Robertson, P.K., Woeller, D.I. and Finn, W.D.L. (1992), "Seismic Cone Penetration Test for Evaluating Liquefaction Potential under Cyclic Loading", Canadian Geotechnical Journal, Vol. 29, pp. 686-695.

- Robertson, P.K., Woeller, D.J., Kokan, M., Hunter, J. and Luternauer, J. (1992), "Seismic Techniques to Evaluate Liquefaction Potential", 45th Canadian Geotechnical Conference, Toronto, Ont., October 26-28, pp. 5:1-5:9.
- Rodrigues, R.S. (1993), "Analysis of Penetration Resistance in Sands", Ph.D. Dissertation, University of California at Berkeley.
- Roscoe, K.H., Schofield, A.N. and Wroth, C.P. (1958), "On the Yielding of Soils", Geotechnique, Vol. 8, No. 1, pp. 22-53.
- Rosler, S.K. (1979), "Anisotropic Shear Wave Modulus due to Stress Anisotropy", Journal of Geotechnical Engineering, ASCE, Vol. 105, No.7, pp. 871-880.
- Salgado, R. (1993), Analysis of Penetration Resistance in Sands, Ph.D. Thesis, University of California at Berkeley.
- Schmertmann, J.H. (1978), "Study of Feasibility of Using Wissa -Type Piezometer Probe to Identify Liquefaction Potential of Saturated Fine Sands", Report S-78-2, US Army Engineer Waterways Experiment Station.
- Seed, H.B. and Lee, K.L. (1996), "Liquefaction of Saturated Sands During Cyclic Loading", Journal of Soil Mechanics and Foundation Division, ASCE, Vol. 92, No. SM6, pp. 105-134.
- Sego, D.C., Robertson, P.K., Sasitharan, S., Kilpatrick, B.I. and Pillai, V.S. (1994), "Ground Freezing and Sampling of Foundation Soils at Duncan Dam", Canadian Geotechnical Journal, Vol. 31, No. 6, pp. 939-950.
- Sladen, J.A. (1990), "Effect of Placement Method on the Liquefaction Potential of Hydraulic Sand Fill", Proceedings of the Port of Los Angeles Seismic Workshop, March 1990.
- Sladen, J.A. and Handford, G. (1987), "A Potential Systematic Error in Laboratory Testing of Very Loose Sands", Canadian Geotechnical Journal, Vol. 24, No. 3, pp. 462-466.
- Sladen, J.A. and Hewitt, K.J. (1989), "Influence of Placement Method on the In-situ Density of Hydraulic Sand Fills", Canadian Geotechnical Journal, Vol. 26, pp. 453-466.
- Sutterer, K., Chameau, J.-L. and Frost, J.D. (1994), "Sampling of Granular Soils Using a Polymer", XIII ICSMFE, New Delhi, India.
- Sutterer, K.G., Frost, J.D. and Chameau, J.-L. (1995), "Polymer Impregnation to Assist Undisturbed Sampling of Cohesionless Soils", Submitted to the Journal of Geotechnical Engineering, ASCE.
- Verdugo, R. (1992), "Discussion: The Critical State of Sands", Geotechnique, Vol. 42, No. 4, pp. 655-663.

- Verkerke, U.F. and Volbeda, J.H. (1991), "Design and Quality Control of Hydraulic Fill - a Contractor's Perspective, Proceeding of the Seminar in Reclamation - Important Current Issues, HKIE Geotechnical Division, May 14.
- Villet, W.C.B. and Mitchell, J.K. (1981), "Cone resistance, Relative Density and Friction Angle", Proc. Am. Soc. Civ. Engrs. Specialty Session Cone Penetration Testing and Experience, St. Louis, pp. 178-208.
- Wallays, M. (1983), "Deep Compaction by Vertical and Horizontal Vibration", Geotechnical Engineering, Vol. 14.
- Wood, D.M. (1984), "On Stress Parameters", Geotechnique, Vol. 34, No. 2, pp. 282-287.
- Yoshimi, Y., Tokimatsu, K. and Hosaka, Y. (1989), "Evaluation of Liquefaction Resistance of Clean Sands Based on High-Quality Undisturbed Samples, Soils and Foundations, Vol. 29, No. 1, pp. 93-104.

LIST OF TABLES

Table No.		Page No.
2.1	Summary of Soil Stratification for TC Site	82
3.1	Acceptance Criteria for Various Compaction Efforts Adopted by the Airport Authority Hong Kong in the CLK Site	82
3.2	Summary of CPT Results at Study Areas 1 and 2 of the CLK Site	83
3.3	Summary of CPT Results at the West Kowloon (CS1) Site	84
4.1	Summary of Physical Properties	85
4.2	Grain Size Distribution of CLK Sand	85
4.3	Grain Size Distribution of TC Sand	86
4.4	Summary of Coefficients Derived from Grain Size Distribution	86
4.5	Summary of Permeability Test Results	87
4.6	Summary of Static Triaxial Undrained Test Results for Tung Chung (TC) Samples	88
4.7	Summary of Static Triaxial Undrained Test Results for Chek Lap Kok (CLK) Samples	89
4.8	Summary of Static Triaxial Undrained Test Results for West Kowloon (CS1) Samples	90
4.9	Summary of Static Triaxial Undrained Test Results for Tseung Kwan O (TKO) Samples	91
4.10	Summary of Static Triaxial Undrained Test Results for Tin Shui Wai (TSW) Samples	92
4.11	Summary of Cyclic Tests on TC Sand	93
4.12	Summary of Cyclic Test on CLK Sand	94

Table No.		Page No.
5.1	Summary of Soil Contants Determined by Bender Element Tests	95
6.1	Summary of Constant p' Tests Conducted on the Five Marine Sands	95
6.2	Index Properties of Additional Silica Sands	96
7.1	Summary of Calibration Chamber Test Results for the TC Sand	97
7.2	Summary of Calibration Chamber Test Results for the CLK Sand	98
7.3	Summary of Computer Predicted Cone Penetration Resistance Values for TC Sand	99
7.4	Summary of Computer Predicted Cone Penetration Resistance Values for CLK Sand	100
9.1	Summary of Soil Parameters Used for the Proposed Correlations for the Five Hong Kong Sands	101

Table 2.1 - Summary of Soil Stratification for TC Site

Drillhole No.	Ground Level (mPD)	Base of Fill (mPD)	Base of the Mixed Marine Deposits and Fill (mPD)	Base of Marine Deposits/Top of Alluvium (mPD)	End Level (mPD)
DH1	6.02	-2.48	-6.18	-12.58	-14.13

Table 3.1 - Acceptance Criteria for Various Compaction Efforts Adopted by the Airport Authority Hong Kong in the CLK Site

Acceptance Criteria	Light Compaction	Heavy Compaction
Vibroftolt	V32	V32
Grid Spacing	4.6 m triangular	3.7 triangular
Compaction time and Amperage (pulling criteria)	30 seconds for 0.5 m lift of 200A, whichever comes first	30 seconds for 0.5 m lift of 200A, whichever comes first

Compaction Type	V32 (BSG) Grid Spacing	S300 (IPK) Grid Spacing
Light (8 MPa)	4.6 m	4.0 m
Heavy (15 MPa)	3.7 m	3.5 m

Table 3.2 - Summary of CPT Results at Study Areas 1 and 2 of the CLK Site

Classification	CPT No.	Total thickness of bottom dumped fill (m)	Maximum water depth of deposition (m)	Averaged q_c at the top of bottom dumped fill (MPa)	Rate of q_c increases with depth (MPa/m)
GOOD (Study Area 1)	C01	14.0	21.0	5.0	0.55
	C02	8.0	16.0	5.0	0.55
	C03	9.0	15.5	5.0	0.55
	C04	12.0	17.5	5.5	0.4
	C07	10.0	20.5	7.5	0.4
	C10	14.0	20.5	7.5	0.4
	C26	11.5	18.6	5.0	0.5
	C27	12.0	19.0	6.5	0.5
FAIR (Study Area 1)	C05	8.0	16.2	8.0 ⁽¹⁾	0.37
	C06	9.0	16.0	5.5	0.45
	C08	9.0	16.2	4.5	0.45
	C09	9.0	16.0	4.5	0.3
	C12	9.0	16.7	5.0	0.4
	C28	13.5	17.4	6.0 ⁽²⁾	0.3
	C29	9.0	16.6	7.5	0.17
	C30	8.0	15.6	4.5	0.4
POOR (Study Area 2) ⁽³⁾	C13	4.5	14.4	6.0	-
	C14	3.0	15.2	6.5	-
	C16	3.5	12.5	8.0	-
	C17	4.5	14.2	7.0	-
	C18	4.0	14.0	7.0	-
	C19	4.5	13.2	6.0	-
	C20	4.0	13.0	4.5	-
	C22	4.5	14.2	6.0	-
	C23	4.0	13.5	6.5	-
	C24	4.0	13.7	6.5	-
	C31	4.5	14.7	7.5	-
	C32	4.0	17.3	7.5	-
Notes : (1) Grain size is noticeably larger. (2) Grain size is noticeably smaller. (3) Average grain size at Study Area 2 is slightly larger than that at Study Area 1.					

Table 3.3 - Summary of CPT Results at the West Kowloon (CS1) Site

Classification	CPT No.	Total thickness of bottom dumped fill (m)	Maximum water depth of deposition (m)	Averaged q_c at the top of bottom dumped fill (MPa)	Rate of q_c increases with depth (MPa/m)
GOOD	WK1	8.0	13.5	9.0	0.25
	WK2	8.0	14.0	7.0	0.38
	BCS2	5.0	14.0	8.0	0.8
	BCS3	7.5	13.0	7.5	0.6
	BCS4	10.0	14.0	12.0	0.2
	BCS5	9.0	13.0	10.0	0.2
	BCS6	9.0	18.0	6.0	0.45
	BLC15	9.0	17.0	10.0	0.55
	BCS8	7.0	11.0 (shallow water)	8.0	0.6
	BCS9	5.0	10.5 (shallow water)	7.0	0.6
	BCS28	6.0	10.5 (shallow water)	10.0	0.1
	BCS29	4.5	7.5 (shallow water)	10.0	0.6
	BCS30	4.0	12.0 (shallow water)	8.0	1.2
	BCS33	3.5	7.5 (shallow water)	10.0	0.1

Table 4.1 - Summary of Physical Properties

Type of Test, unit	Chek Lap Kok	Tung Chung
Specific Gravity	2.64	2.67
Maximum Dry Density, Mg/m ³	1.93	1.732
Minimum Dry Density, Mg/m ³	1.578	1.342
Compaction Test, Mg/m ³ @ OMC	1.85 @ 14.1%	1.64 @ 22.4%
Permeability Test:		
Void Ratio (e)	0.469 - 0.577	0.750 - 0.896
Coefficient of Permeability, cm/s	9.1×10^{-3} - 2.30×10^{-2}	2.95×10^{-3} - 4.82×10^{-3}

Table 4.2 - Grain Size Distribution of CLK Sand

Size of sieve (mm)	% passing	% passing	% passing	% passing
6.3	100.00	100.00	100.00	100.00
5.0	100.00	100.00	100.00	100.00
3.35	91.24	92.32	92.75	92.52
2	74.27	75.34	76.66	76.89
1.18	54.20	53.74	56.08	56.11
0.6	30.25	28.60	30.66	30.77
0.425	18.75	17.17	18.90	18.71
0.3	10.41	9.47	10.94	10.57
0.212	5.07	4.50	5.82	5.18
0.15	2.36	2.14	2.12	2.54
0.063	0.41	0.40	0.38	0.70
< 0.063	0.00	0.00	0.00	0.00

Table 4.3 - Grain Size Distribution of TC Sand

Size of sieve (mm)	% passing	% passing	% passing
6.3	100.00	100.00	100.00
5	100.00	100.00	100.00
3.35	98.63	98.08	98.29
2	94.50	93.17	94.32
1.18	87.31	85.66	86.98
0.6	73.92	71.70	74.03
0.425	61.71	58.97	61.53
0.3	48.18	44.25	48.80
0.212	32.00	30.68	32.75
0.15	15.01	16.63	16.62
0.063	2.35	3.43	2.38
< 0.063	0.00	0.00	0.00

Table 4.4 - Summary of Coefficients Derived from Grain Size Distribution

	Tung Chung	Chek Lap Kok
Average grain size D_{50} (mm)	0.33	1.00
Coefficient of uniformity, C_u	4.36	4.33
Coefficient of curvature, C_c	0.98	0.92

Table 4.5 - Summary of Permeability Test Results

CLK sand			TC sand		
Dr (%)	Void ratio	k (cm/s)	Dr (%)	Void ratio	k (cm/s)
31.37	0.577	2.30x10 ⁻²	20.66	0.896	4.82x10 ⁻³
54.30	0.507	1.52x10 ⁻²	33.36	0.839	3.13x10 ⁻³
66.94	0.469	9.10x10 ⁻³	48.62	0.771	2.95x10 ⁻³
			63.29	0.750	2.61x10 ⁻³

Table 4.6 - Summary of Static Triaxial Undrained Test Results for Tung Chung (TC) Samples

Test No.	Consolidation Pressure σ'_c	Relative Density D_r (%)	Void ratio e	$(\sigma'_1 - \sigma'_3)_f/2$ (kPa)	$(\sigma'_3)_f$ (kPa)	$(\Delta u)_f$ (kPa)	$(\sigma'_1)_f$ (kPa)	$(p')_{ss}$ or $(p')_f$	ϕ' (degree)
1	100	31.90	0.847	84	36	64	204	92	36.0
2	200	36.20	0.828	182	94.5	105.5	458.5	216	36.0
3	300	38.90	0.816	222	100	200	544	248	36.0
4	100	47.30	0.778	262	132	-32	656	307	39.0
5	200	49.70	0.767	283	150	50	716	339	39.0
6	300	53.00	0.753	343	167	133	853	396	39.0
7	100	69.5	0.679	627	344	-244	1598	762	40.5
8	200	67.1	0.689	582	301	-101	1465	689	40.5
9	300	69.30	0.680	655	357	-57	1667	794	40.5
Remarks : (?) value determined at the point just before the termination of test, and the soil may not reach the steady state condition. ** results affected by cavitation $(p')_{ss} = (\sigma'_1 + \sigma'_2 + \sigma'_3)/3$									

Table 4.7 - Summary of Static Triaxial Undrained Test Results for Chek Lap Kok (CLK) Samples

Test No.	Consolidation Pressure σ'_c	Relative Density D_r (%)	Void ratio e	$(\sigma'_1 - \sigma'_3)_f/2$ (kPa)	$(\sigma'_3)_f$	$(\Delta u)_f$ (kPa)	$(\sigma'_1)_f$	$(p')_{ss}$ or $(p')_f$	ϕ' (degree)
1	100	36.6	0.561	280	159	-59	719	345	36
2	200	35.1	0.566	350	204	-4	904	437	36
3	300	32.1	0.575	392	230	70	1014	491	36
4	100	38.7	0.555	342	200	-100	884	428	37.5
5	200	41.4	0.547	480	273	-73	1233	593	37.5
6	400	42.6	0.543	542	314	86	1398	675	37.5
7	100	50.2	0.520	753	433	-333	1939	935	38.5
8	200	51.9	0.515	857	468	-268	2182	1039	38.5
9	300	50.5	0.519	585	312	-12	1482	702	38.5
10	100	48.2	0.526	713	400	-300	1826	875	38.0
11	300	66.30	0.471	1412	788	-488	3611	1729	
12	300	69.15	0.460	***					
13	300	55.80	0.503	858	466	-166	2182	1038	
<p>Remarks : (?) value determined at the point just before the termination of test, and the soil may not reach the steady state condition. ** results affected by cavitation *** results affected by significant sample tilting $(p')_{ss} = (\sigma'_1 + \sigma'_2 + \sigma'_3)/3$</p>									

Table 4.8 - Summary of Static Triaxial Undrained Test Results for West Kowloon (CS1) Samples

Test No.	Consolidation Pressure σ'_c	Relative Density D_r (%)	Void ratio e	$(\sigma'_1 - \sigma'_3)_f/2$ (kPa)	$(\sigma'_3)_f$	$(\Delta u)_f$ (kPa)	$(\sigma'_1)_f$	$(p')_{ss}$ or $(p')_f$	ϕ' (degree)
1	450	25	0.545	300(?)	170	280	770	370	-
2	450	23.8	0.549	325(?)	200	250	850	417	-
3	100	33.3	0.520	195(?)	120	-20	510	250	38.1
4	200	37.4	0.508	319(?)	178	22	816	390	38.1
5	300	33.8	0.519	490	265	35	1245	592	38.1
6	100	51.6	0.465	825	440	-340	2090	990	38.7
7	200	52.8	0.461	1030	545	-345	2605	1232	38.7
8	300	52.8	0.461	**					38.7
9	300	58.5	0.444	**					38.7
10	100	60.2	0.439	**					39.5
11	200	63.6	0.428	**					39.5
12	300	68.6	0.413	**					39.5
13	300	45.9	0.482	750	392	-92	1892	892	
14	300	58.1	0.445	1000	560	-260	2560	1227	
15	300	62	0.433	1165	649	-349	2979	1426	
Remarks : (?) value determined at the point just before the termination of test, and the soil may not reach the steady state condition. ** results affected by cavitation $(p')_{ss} = (\sigma'_1 + \sigma'_2 + \sigma'_3)/3$									

Table 4.9 - Summary of Static Triaxial Undrained Test Results for Tseung Kwan O (TKO) Samples

Test No.	Consolidation Pressure σ'_c	Relative Density D_r (%)	Void ratio e	$(\sigma'_1 - \sigma'_3)_f/2$ (kPa)	$(\sigma'_3)_f$	$(\Delta u)_f$ (kPa)	$(\sigma'_1)_f$	$(p')_{ss}$ or $(p')_f$	ϕ' (degree)
1	100	26.2	0.769	264	149	-49	677	325	36.9
2	200	29.5	0.756	277	158	42	712	343	36.9
3	300	31.9	0.746	377	212	88	966	463	36.9
4	100	52.9	0.664	880	485	-385	2245	1072	38.7
5	200	51.3	0.670	880	503	-303	2263	1090	38.7
6	300	54.0	0.660	1045	575	-275	2665	1272	38.7
7	100	64.5	0.619	**					39.5
8	200	65.2	0.616	**					39.5
9	300	68.0	0.605	**					39.5
10	300	46.3	0.694	857	490	-190	1904	961.3	
11	300	61.6	0.630	1155	685	-385	2995	1455	
12	300	67.0	0.690	≈ 1600	≈ 900	≈ -600	≈ 3800	≈ 1870	
Remarks : (?) value determined at the point just before the termination of test, and the soil may not reach the steady state condition. ** results affected by cavitation $(p')_{ss} = (\sigma'_1 + \sigma'_2 + \sigma'_3)/3$									

Table 4.10 - Summary of Static Triaxial Undrained Test Results for Tin Shui Wai (TSW) Samples

Test No.	Consolidation Pressure σ'_c	Relative Density D_r (%)	Void ratio e	$(\sigma'_1 - \sigma'_3)_f / 2$ (kPa)	$(\sigma'_3)_f$	$(\Delta u)_f$ (kPa)	$(\sigma'_1)_f$	$(p')_{ss}$ or $(p')_f$	ϕ' (degree)
1	100	41.6	0.529	400	233	-133	1033	500	36.9
2	200	45.7	0.513	543	318	-118	1404	680	36.9
3	300	43.4	0.522	615	335	-35	1565	745	36.9
4	100	51.7	0.490	820	466	-366	2106	1013	38.1
5	200	49.5	0.498	857	468	-268	2182	1039	38.1
6	300	51.7	0.490	923	491	-191	2337	1106	38.1
7	100	68.7	0.424	**					40.5
8	200	70.1	0.419	**					40.5
9	300	71.3	0.414	**					40.5
10	300	56.9	0.470	≈ 1200	≈ 780	≈ -480	≈ 3180	≈ 1580	
11	300	63.0	0.446	***					
Remarks : (?) value determined at the point just before the termination of test, and the soil may not reach the steady state condition. ** results affected by cavitation *** results affected by sample tilting $(p')_{ss} = (\sigma'_1 + \sigma'_2 + \sigma'_3) / 3$									

Table 4.11 - Summary of Cyclic Tests on TC Sand

Soil Type	Relative Density, Dr (%)	Stress Ratio	Number of Cycle (N)
Loose	30.80	0.145	13
	30.51	0.115	42
	28.78	0.095	104
	30.80	0.127	21
	29.65	0.163	7
	29.94	0.190	2
	31.08	0.103	66
Medium	52.26	0.145	49
	50.45	0.175	10
	53.04	0.110	93
	51.49	0.147	22
	50.97	0.205	5
	51.75	0.13	49
	47.04	0.225	3
Dense	69.27	0.200	17
	68.32	0.150	71
	67.61	0.235	7
	68.56	0.27	5
	69.03	0.175	46
	68.56	0.255	5

Table 4.12 - Summary of Cyclic Test on CLK Sand

Soil Type	Relative Density, Dr (%)	Stress Ratio	Number of Cycle (N)
Loose	31.99	0.18	8
	30.45	0.14	17
	30.45	0.15	11
	31.99	0.12	30
	28.90	0.16	11
	29.83	0.11	34
	32.30	0.09	220
Medium	52.64	0.215	4
	47.20	0.18	9
	48.93	0.16	17
	44.58	0.15	18
	48.36	0.115	62
	47.20	0.095	210
Dense	69.59	0.25	5
	68.54	0.18	29
	74.04	0.15	135
	73.78	0.21	15
	73.52	0.135	472
	70.91	0.28	5

Table 5.1 - Summary of Soil Constants Determined by Bender Element Tests

Site	n	A	B
Chek Lap Kok (CLK)	0.24	459	431
Tung Chung (TC)	0.24	687	618
West Kowloon (CS1)	0.33	636	860
Tseung Kwan O (TKO)	0.22	501	434
Tin Shui Wai (TSW)	0.33	407	373

Table 6.1 - Summary of Constant p' Tests Conducted on the Five Marine Sands

Sand	Constant p' (kPa)	Initial Void Ratio e_o	Void Ratio at Steady State e_{ss}
Tung Chung (TC)	25	0.858	0.875
	50	0.867	0.902
	75	0.862	0.873
	450	0.777	0.765
	400	0.815	0.797
	300	0.790	0.803
	200	0.784	0.817
	199	0.812	0.828
	98	0.793	0.809
Chek Lap Kok (CLK)	50	0.61	0.617
	100	0.60	0.606
	150	0.565	0.605
West Kowloon (CS1)	50	0.538	0.546
	100	0.503	0.549
Tseung Kwan O (TKO)	153	0.705	0.775
	50	0.700	0.790
	247	0.757	0.777
Tin Shui Wai (TSW)	250	0.521	0.572
	330	0.485	0.550
	72	0.560	0.580

Table 6.2 - Index Properties of Additional Silica Sands

Index Properties	Erksak 330/0.7	Toyoura	Leighton Buzzard
Mineralogy			
Quartz : %	73	75	-
Feldspar : %	22	25	-
Other : %	5	0	-
Median Grain size D_{50} : mm	0.330	0.160	0.120
Effective grain size D_{10} : mm	0.190	0.120	0.095
Uniformity coefficient D_{60}/D_{10}	1.8	1.5	1.5
Passing 200 sieve : %	0.7	0	5
Specific gravity :	2.66	2.65	2.65
Maximum Void ratio e_{\max} :	0.753	0.981	1.023
Minimum void ratio e_{\min} :	0.527	0.608	0.665
Steady state void ratio at $p'=0, \Gamma$	0.7796	0.9247	0.9437
Slope of the steady state line, λ	0.387	0.4915	0.4553

Table 7.1 - Summary of Calibration Chamber Test Results for the TC Sand

Test	Relative Density D_r (%)	Void Ratio	Vertical effective confining stress, σ'_v (kPa)	Horizontal effective confining stress, σ'_h (kPa)	Cone tip resistance, q_c (kPa)	Shear Wave Velocity in vertical direction, V_s (m/sec)
1	39	0.845	48.2	25.6	1194.0	139.1
2	45	0.816	147.1	77.2	3625.0	199.1
3	52.6	0.783	100.5	50.6	3250.0	171.7
4	56.4	0.766	199.1	99.4	5685.0	214.6
5	48.7	0.801	49.8	30.7	1730.0	150.1
6	54	0.777	150.6	91.8	4760.0	215.5
7	61.9	0.741	52.5	35.3	4250.0	194.5
8	65.5	0.725	152.0	100.9	8050.0	234.0
9	64.5	0.729	101.2	64.6	6515.0	231.4
10	67.1	0.717	200.6	127.5	11500.0	280.7

Table 7.2 - Summary of Calibration Chamber Test Results for the CLK Sand

Test	Relative Density D_r (%)	Void Ratio	Vertical effective confining stress, σ'_v (kPa)	Horizontal effective confining stress, σ'_h (kPa)	Cone tip resistance, q_c (kPa)	Shear Wave Velocity in vertical direction, V_s (m/sec)
1	26.2	0.610	52.8	33.6	2320.0	154.1
2	29.7	0.601	150.9	96.5	4475.0	208.3
3	35.2	0.586	100.1	58.5	3050.0	179.4
4	37.6	0.579	199.8	116.8	6100.0	218.3
5	42.8	0.565	101.0	61.6	3400.0	183.3
6	45.1	0.559	200.6	122.4	6310.0	220.5
7	52.7	0.538	51.3	32.8	2920.0	159.6
8	55	0.532	150.8	96.7	7050.0	212.5
9	80.4	0.463	53.0	30.6	8925.0	187.4
10	81.4	0.460	151.8	87.5	16400.0	246.0

Table 7.3 - Summary of Computer Predicted Cone Penetration Resistance Values for TC Sand

Actual Chamber Test Data					Predicted Values		Corrected for free field
Test no.	Dr (%)	σ'_v (kPa)	σ'_h (kPa)	q_c (kPa)	q_{cp} (kPa)	q_{cfft}/q_{cp}	q_{cff} (kPa)
1	39	52.2	29.6	1194	1705.9	1.055	1259.2
2	45	148.2	78.1	3508	3762.1	1.041	3652.8
3	53	102.1	52.4	3231	3727.7	1.051	3396.6
4	56	198.6	99.4	5669	5810.0	1.039	5889.1
5	49	50.8	31.3	1778	2427.7	1.062	1888.4
6	54	148.7	89.3	4829	5130.8	1.038	5014.2
7	62	53.8	37.2	4241	3961.3	1.065	4518.0
8	66	152.0	100.9	7735	7382.9	1.041	8053.2
9	65	104.1	66.9	6341	5843.9	1.050	6657.7
19	67	199.9	125.8	10690	8495.0	1.038	11101.5
Remarks : $q_{cff} = q_c \times q_{cfft} / q_{cp}$							

Table 7.4 - Summary of Computer Predicted Cone Penetration Resistance Values for CLK Sand

Actual Chamber Test Data					Predicted Values		Corrected for free field
Test no.	Dr (%)	σ'_v (kPa)	σ'_h (kPa)	q_c (kPa)	q_{cp} (kPa)	q_{cpff}/q_{cp}	q_{cff} (kPa)
1	26	52.7	35.9	2311	1751.5	1.049	2424.9
2	30	148.2	93.2	4526	3919.1	1.036	4688.5
3	35	99.0	58.0	3102	3348.0	1.050	3256.9
4	38	197.8	115.5	5815	5758.9	1.040	6048.9
5	43	98.7	60.9	3389	4457.6	1.055	3574.4
6	45	196.8	118.7	6199	7121.8	1.044	6474.3
7	53	48.7	31.3	2977	4189.4	1.090	3245.3
8	55	148.5	94.7	6948	8217.8	1.055	7326.9
9	80.7	52.5	30.8	8906	10050.4	1.144	10189.3
10	81.4	149.8	86.5	15780	15898.8	1.081	17055.2
Remarks : $q_{cff} = q_c \times q_{cpff} / q_{cp}$							

Table 9.1 - Summary of Soil Parameters Used for the Proposed Correlations for the Five Hong Kong Sands

Sand	Steady State Line		e versus q_{cl} relationship (obtained from calibration chamber tests)		D_r versus q_{cl} relationship (obtained from calibration chamber tests)		e versus V_{sl} relationship (obtained from laboratory bender element tests)		
	Γ	λ	C_1	C_2	C_3	C_4	n	A	B
Tung Chung (TC)	0.9017	0.0491	1.1258	0.0425	-23.2	9.41	0.24	687	618
Chek Lap Kok (CLK)	0.6221	0.0191	0.8938	0.0391	-78.4	14.44	0.24	459	431
West Kowloon (CS1)	0.5591	0.0165	0.8247	0.0305	-56.7	12.61	0.33	636	860
Tseung Kwan O (TKO)	0.8181	0.0248	1.2550	0.0539	-86.5	14.67	0.22	501	434
Tin Shui Wai (TSW)	0.5946	0.0173	0.9563	0.0446	-96.3	15.67	0.33	407	373

LIST OF FIGURES

Figure No.		Page No.
1.1	Location of the New Airport at Chek Lap Kok	114
1.2	Location of the Tung Chung Reclamation Site	115
2.1	Location of Bulk Sampling at the Tung Chung (TC) Site (Scale 1:15,000)	116
2.2	Location of Bulk Sampling at the CLK Site	117
2.3	Location of Field Work at the TC Site	118
2.4(a)	Drillhole Log at the TC Site	119
2.4(b)	Drillhole Log at the TC Site	120
2.4(c)	Drillhole Log at the TC Site	121
2.5	Results of SPT-N Value Profile at the TC Site	122
2.6	Typical Details of Seismic Piezocone	123
2.7	Principle of the Vertical Seismic Profiling Method of Shear Wave Velocity Measurement Using the Seismic Piezocone	124
2.8(a)	Cone Resistance, Sleeve Friction versus Depth at the TC Site	125
2.8(b)	Effective Cone Tip Resistance and Pore Pressure versus Depth at the TC Site	126
2.8(c)	Effective Cone Tip Resistance, Sleeve Friction, and Soil Description versus Depth at the TC Site	127
2.9	Shear Wave Velocity versus Depth at the TC Site	128
2.10	Correlation between SPT - N Value and Cone Tip Resistance (q_c) for the Results Obtained from the TC Site	129
2.11	Relationship between Cone Penetration Test and Standard Penetration Test (from Burland and Burbidge, 1985)	130

Figure No.		Page No.
2.12	Relationship between Normalized Shear Wave Velocity (V_{sl}) and Normalized Cone Tip Resistance ($q_{cl}^{0.25}$) for the Results Obtained from the TC Site	131
2.13	Correlation between Normalized V_{sl} and (q_{cl}) ^{0.25} for CLK Sand	132
3.1(a)	Questionnaire Developed in this Study for the Survey of Hydraulic Fill Performance in Hong Kong	133
3.1(b)	Questionnaire Developed in this Study for the Survey of Hydraulic Fill Performance in Hong Kong	134
3.1(c)	Questionnaire Developed in this Study for the Survey of Hydraulic Fill Performance in Hong Kong	135
3.1(d)	Questionnaire Developed in this Study for the Survey of Hydraulic Fill Performance in Hong Kong	136
3.2	Airport Location Plan Including Hong Kong's Geology and Reclamation (after Newman et al, 1996)	137
3.3	Plan of Reclamation at the CLK Site (after Newman et al, 1996)	138
3.4	Ground Treatment Layout Plan at the CLK Site	139
3.5	Locations of Extraction Areas of Marine Sands Used in the Five Reclamation Sites Examined in this Study (Modified from Whiteside, 1991)	140
3.6	Classification of Operation Difficulty on the Process of Winning of Marine Sands	141
3.7	Typical CPT Results Observed at the Tseung Kwan O Reclamation Site	142
3.8	Summary of Cone Tip Resistance at Area 1 - CLK Site (after Newman et al, 1996)	143
3.9	Summary of Cone Tip Resistance at Area 2 - CLK Site (after Newman et al, 1996)	144

Figure No.		Page No.
3.10	Final Equilibrium Shape of Sand Mass after Bottom Dumping	145
3.11	Random Layered Distribution of Bottom Dumped Soil Berms	146
3.12(a)	Total Bottom Dumped Fill Thickness of 14 m Indicates “GOOD” Improvement in q_c Profile	147
3.12(b)	Total Bottom Dumped Fill Thickness of 10 m Indicates “GOOD” Improvement in q_c Profile	148
3.13(a)	Total Bottom Dumped Fill Thickness of 8 m Indicates “FAIR” Improvement in q_c Profile	149
3.13(b)	Total Bottom Dumped Fill Thickness of 9 m Indicates “FAIR” Improvement in q_c Profile	150
3.14(a)	Total Bottom Dumped Fill Thickness of 4.5 m Indicates “POOR” Improvement in q_c Profile	151
3.14(b)	Total Bottom Dumped Fill Thickness of 4 m Indicates “POOR” Improvement in q_c Profile	152
3.15	Distribution of Sand Particles in Subaerial Beaching by Pipeline Discharge Method	153
3.16	CPT Profile at CS1 Showing Low q_c Value above Sea Level without any Compaction Work by Bullozers	154
3.17	Situation at the End of a Subaerial Hydraulic Sand Fill (after Verkerke and Volbeda, 1991)	155
4.1	Grain Size Distribution Curves of the Well Mixed TC and CLK Bulk Samples	156
4.2	Compaction Test Results of CLK Sand	157
4.3	Compaction Test Results of TC Sand	158
4.4	Coefficient of Permeability of CLK Sand	159
4.5	Coefficient of Permeability of TC Sand	160
4.6	Results of Triaxial Undrained Tests on the Tung Chung Sand with Relative Density 31.9% to 38.9%	161

Figure No.		Page No.
4.7	Results of Triaxial Undrained Tests on the Tung Chung Sand with Relative Density 47.3% to 53.0%	162
4.8	Results of Triaxial Undrained Tests on the Tung Chung Sand with Relative Density 67.1% to 69.5%	163
4.9	Liquefaction Potential Curves for the Tung Chung Sand	164
4.10(a)	Typical Cyclic Test Results on TC Sand ($D_r = 30.8\%$, S.R. = 0.145)	165
4.10(b)	Typical Cyclic Test Results on TC Sand ($D_r = 30.8\%$, S.R. = 0.145)	166
4.11	Liquefaction Potential Curves for the CLK Sand	167
5.1	Setup of Bender Element (Shear Wave Velocity Measurement)	168
5.2	Shear Wave Velocity (V_s) versus Confining Pressure (σ'_c) Chek Lap Kok Sand	169
5.3	Shear Wave Velocity (V_s) versus Confining Pressure (σ'_c) Tung Chung Sand	170
5.4	Shear Wave Velocity (V_s) versus Confining Pressure (σ'_c) West Kowloon Sand	171
5.5	Shear Wave Velocity (V_s) versus Confining Pressure (σ'_c) Tseung Kwan O Sand	172
5.6	Shear Wave Velocity (V_s) versus Confining Pressure (σ'_c) Tin Shui Wai Sand	173
5.7	Shear Wave Velocity (V_s) versus Void Ratio (e) Chek Lap Kok Sand	174
5.8	Shear Wave Velocity (V_s) versus Void Ratio (e) Tung Chung Sand	175
5.9	Shear Wave Velocity (V_s) versus Void Ratio (e) West Kowloon Sand	176
5.10	Shear Wave Velocity (V_s) versus Void Ratio (e) Tseung Kwan O Sand	177

Figure No.		Page No.
5.11	Shear Wave Velocity (V_s) versus Void Ratio (e) Tin Shui Wai Sand	178
5.12	Normalized Shear Wave Velocity (V_{sl}) versus Void Ratio (e) Chek Lap Kok Sand	179
5.13	Normalized Shear Wave Velocity (V_{sl}) versus Void Ratio (e) Tung Chung Sand	180
5.14	Normalized Shear Wave Velocity (V_{sl}) versus Void Ratio (e) West Kowloon Sand	181
5.15	Normalized Shear Wave Velocity (V_{sl}) versus Void Ratio (e) Tseung Kwan O Sand	182
5.16	Normalized Shear Wave Velocity (V_{sl}) versus Void Ratio (e) Tin Shui Wai Sand	183
6.1	Definition of State Parameter (after Been & Jefferies, 1985)	184
6.2	Typical Test Showing a Quasi-Steady State Condition (after Been et al, 1991)	185
6.3	Steady State Line for Undrained Triaxial Compression Tests on Tung Chung (TC) Sand	186
6.4	Steady State Line for Undrained Triaxial Compression Tests on Chek Lap Kok (CLK) Sand	187
6.5	Steady State Line for Undrained Triaxial Compression Tests on West Kowloon (CS1) Sand	188
6.6	Steady State Line for Undrained Triaxial Compression Tests on Tseung Kwan O (TKO) Sand	189
6.7	Steady State Line for Undrained Triaxial Compression Tests on Tin Shui Wai (TSW) Sand	190
6.8	Steady State Line for Leighton Buzzard Sand Showing Curvature Similar to That of Line for Erksak 330/0.7 Sand (Initial State of All Samples Was above the Steady State Line; All Tests Triaxial Compression) (after Been et al, 1991)	191

Figure No.		Page No.
6.9	Steady State Line for Undrained Compression Tests on Contractive Samples of Erksak 330/0.7 Sand with Initial States above the Steady State Line (after Been et al, 1991)	192
6.10	Typical Test Results of Undrained Test on Loose Sample Showing Strain Softening Behaviour (Loose Sample; $e = 0.771$, $\sigma_{3c}' = 500$ kPa on Erksak 330/0.7 Sand) (after Been et al, 1991)	193
6.11	Interpretation of Steady State Line by Undrained Triaxial Test on Loose Contractive Soil Sample	194
6.12	Results of Constant p' Test on Tung Chung Sand with $e_o = 0.858$ and $p' = 25$ kPa	195
6.13	Steady State Boundary in e -log p' Space for the TC Sand	196
6.14	Steady State Boundary in e -log p' Space for the CLK Sand	196
6.15	Steady State Boundary in e -log p' Space for the CS1 Sand	197
6.16	Steady State Boundary in e -log p' Space for the TKO Sand	197
6.17	Steady State Boundary in e -log p' Space for the TSW Sand	198
6.18	Search for the Optimized (α) Value for the TC Sand	198
6.19	Steady State Line in $e - p'^{\alpha}$ Space for the TC Sand	199
6.20	Steady State Line in $e - p'^{\alpha}$ Space for the CLK Sand	199
6.21	Steady State Line in $e - p'^{\alpha}$ Space for the CS1 Sand	200
6.22	Steady State Line in $e - p'^{\alpha}$ Space for the TKO Sand	200
6.23	Steady State Line in $e - p'^{\alpha}$ Space for the TSW Sand	201
6.24	Steady State Line in $e - (p'/p_a)^{0.75}$ Space for the TC Sand	201

Figure No.		Page No.
6.25	Steady State Line in $e - (p'/p_a)^{0.75}$ Space for the CLK Sand	202
6.26	Steady State Line in $e - (p'/p_a)^{0.75}$ Space for the CS1 Sand	202
6.27	Steady State Line in $e - (p'/p_a)^{0.75}$ Space for the TKO Sand	203
6.28	Steady State Line in $e - (p'/p_a)^{0.75}$ Space for the TSW Sand	203
6.29	CIU Test on Tung Chung Sand with $e_o = 0.905$, $\sigma_{3c}' = 200$ kPa	204
6.30	Steady State Boundary Represented in e -log p' and $e - (p'/p_a)^{0.75}$ Spaces for the Erksak 330/0.7 Sand Tested by Been et al (1991)	205
6.31	Steady State Boundary Represented in e -log p' and $e - (p'/p_a)^{0.75}$ Spaces for the Leighton Buzzard Sand Tested by Been et al (1991)	206
6.32	Steady State Boundary Represented in e -log p' and $e - (p'/p_a)^{0.75}$ Spaces for the Toyoura Sand Tested by Verdugo and Ishihara (1991)	207
6.33	Steady State Boundary Represented in e -log p' and $e - (p'/p_a)^{0.75}$ Spaces for the CLK Sand Test by Robertson (1994)	208
7.1	Scheme of the Funnel Method for Specimen Preparation (after Frelti et al, 1995)	209
7.2	Schematic of Bender Elements Location in Calibration Chamber	210
7.3	Comparison between q_c Predicted by the Computer Code and the Actual Chamber Test Results for TC Sand	211
7.4	Comparison between q_c Predicted by the Computer Code and the Actual Chamber Test Results for CLK Sand	211
7.5	Relationship between q_c Obtained from Calibration Chamber Tests and Corrected Free Field Penetration Resistance (q_{cff}) for TC Sand	212

Figure No.		Page No.
7.6	Relationship between q_c Obtained from Calibration Chamber Tests and Corrected Free Field Penetration Resistance (q_{cfr}) for CLK Sand	212
7.7	Correlation between Void Ratio (e) with the Normalized Cone Tip Resistance ($q_{cl}^{0.25}$) for the TC Sand	213
7.8	Correlation between Void Ratio (e) with the Normalized Cone Tip Resistance ($q_{cl}^{0.25}$) for the CLK Sand	213
7.9	Correlation between Void Ratio (e) with the Normalized Cone Tip Resistance ($q_{cl}^{0.25}$) for the CS1 Sand	214
7.10	Correlation between Void Ratio (e) with the Normalized Cone Tip Resistance ($q_{cl}^{0.25}$) for the TKO Sand	214
7.11	Correlation between Void Ratio (e) with the Normalized Cone Tip Resistance ($q_{cl}^{0.25}$) for the TSW Sand	215
7.12	Correlation between Relative Density (D_r) with the Normalized Cone Tip Resistance ($q_{cl}^{0.25}$) for the TC Sand	215
7.13	Correlation between Relative Density (D_r) with the Normalized Cone Tip Resistance ($q_{cl}^{0.25}$) for the CLK Sand	216
7.14	Correlation between Relative Density (D_r) with the Normalized Cone Tip Resistance ($q_{cl}^{0.25}$) for the CS1 Sand	216
7.15	Correlation between Relative Density (D_r) with the Normalized Cone Tip Resistance ($q_{cl}^{0.25}$) for the TKO Sand	217
7.16	Correlation between Relative Density (D_r) with the Normalized Cone Tip Resistance ($q_{cl}^{0.25}$) for the TSW Sand	217

Figure No.		Page No.
7.17	Effective Mean Normal Stress (p') versus Cone Tip Resistance (q_c) with Contours of Relative Density (D_r) and Typical Calibration Test Results (Marked with Laboratory Measured D_r Values in Percentage) for the TC Sand	218
7.18	Effective Mean Normal Stress (p') versus Cone Tip Resistance (q_c) with Contours of Relative Density (D_r) and Typical Calibration Test Results (Marked with Laboratory Measured D_r Values in Percentage) for the CLK Sand	219
7.19	Effective Mean Normal Stress (p') versus Cone Tip Resistance (q_c) with Contours of Relative Density (D_r) and Typical Calibration Test Results (Marked with Laboratory Measured D_r Values in Percentage) for the CS1 Sand	220
7.20	Effective Mean Normal Stress (p') versus Cone Tip Resistance (q_c) with Contours of Relative Density (D_r) and Typical Calibration Test Results (Marked with Laboratory Measured D_r Values in Percentage) for the TKO Sand	221
7.21	Effective Mean Normal Stress (p') versus Cone Tip Resistance (q_c) with Contours of Relative Density (D_r) and Typical Calibration Test Results (Marked with Laboratory Measured D_r Values in Percentage) for the TSW Sand	222
7.22	Comparison between Relative Density Obtained in Calibration Chamber Test and That Predicted by Eq. (7.10) for the TC Sand	223
7.23	Comparison between Relative Density Obtained in Calibration Chamber Test and That Predicted by Eq. (7.10) for the CLK Sand	224
7.24	Comparison between Relative Density Obtained in Calibration Chamber Test and That Predicted by Eq. (7.10) for the CS1 Sand	225
7.25	Comparison between Relative Density Obtained in Calibration Chamber Test and That Predicted by Eq. (7.10) for the TKO Sand	226

Figure No.		Page No.
7.26	Comparison between Relative Density Obtained in Calibration Chamber Test and That Predicted by Eq. (7.10) for the TSW Sand	227
7.27	Correlation between Void Ratio and Normalized Shear Wave Velocity for the TC Sand	228
7.28	Correlation between Void Ratio and Normalized Shear Wave Velocity for the CLK Sand	228
7.29	Correlation between Normalized Cone Tip Resistance ($q_{cl}^{0.25}$) and Normalized Shear Wave Velocity (V_{sl}) for the TC Sand	229
7.30	Correlation between Normalized Cone Tip Resistance ($q_{cl}^{0.25}$) and Normalized Shear Wave Velocity (V_{sl}) for the CLK Sand	229
8.1	Assumed Soil Profile for Site Response Analysis in the Tung Chung (TC) Site	230
8.2	Assumed Soil Profile for Site Response Analysis in the Chek Lap Kok (CLK) Site	231
8.3	Predicted Effective Mean Normal Stress and Excess Pore Pressure at a Depth of 5.5 m (Tung Chung Site)	232
8.4	Predicted Effective Mean Normal Stress and Excess Pore Pressure at a Depth of 6.5 m (Tung Chung Site)	233
8.5	Predicted Effective Mean Normal Stress and Excess Pore Pressure at a Depth of 7.5 m (Tung Chung Site)	234
8.6	Predicted Effective Mean Normal Stress and Excess Pore Pressure at a Depth of 7.5 m (Chek Lap Kok Site)	235
8.7	Predicted Effective Mean Normal Stress and Excess Pore Pressure at a Depth of 9.5 m (Chek Lap Kok Site)	236
8.8	Predicted Effective Mean Normal Stress and Excess Pore Pressure at a Depth of 11.5 m (Chek Lap Kok Site)	237
8.9	Predicted Effective Mean Normal Stress and Excess Pore Pressure at a Depth of 13.5 m (Chek Lap Kok Site)	238

Figure No.		Page No.
8.10	Predicted Effective Mean Normal Stress and Excess Pore Pressure at a Depth of 15.5 m (Chek Lap Kok Site)	239
8.11	Predicted Effective Mean Normal Stress and Excess Pore Pressure at a Depth of 17.5 m (Chek Lap Kok Site)	240
8.12	Predicted Effective Mean Normal Stress and Excess Pore Pressure at a Depth of 20.5 m (Chek Lap Kok Site)	241
8.13	Prediction of Earthquake Induced Surface Settlement in the Tung Chung Site	242
8.14	Prediction of Earthquake Induced Surface Settlement in the Chek Lap Kok Site	243
8.15	Ground Surface Response Spectra in Tung Chung Site	244
8.16	Ground Surface Response Spectra in Chek Lap Kok Site	245
9.1	Comparison of the Calibration Chamber Test Results for the Five Hong Kong Marine Sands with the Other Uniformly Graded Quartz Sands (Modified from Jamiolkowski et al, 1985)	246
9.2	p' versus q_c with Contours of State Parameter (Ψ) Varied from $\Psi = 0.1$ to $\Psi = -0.1$ for the TC Sand	247
9.3	p' versus q_c with Contours of State Parameter (Ψ) Varied from $\Psi = 0.1$ to $\Psi = -0.1$ for the CLK Sand	248
9.4	Variation of $\Psi = 0$ Profiles (Contractive/Dilative Boundary) for the Five Hong Kong Marine Sands	249
9.5	Variation of $\Psi = 0$ Profiles for the TC Sand with $K_0 = 0.4$ to $K_0 = 1.0$	250
9.6	Variation of $\Psi = 0$ Profiles for the CLK Sand with $K_0 = 0.4$ to $K_0 = 1.0$	251
9.7	Effects of $\Psi_{FS} = -0.05$ and -0.1 on the $q_{c(min)}$ for the TC Sand	252
9.8	Effects of $\Psi_{FS} = -0.05$ and -0.1 on the $q_{c(min)}$ for the CLK Sand	253

Figure No.		Page No.
9.9	Predicted p' versus q_c Profiles (with Relative Density, D_r of 40%) for the Five Hong Kong Marine Sands	254
9.10	Comparison between $\Psi = 0$ Profiles Based on V_s Correlation for the Five Hong Kong Marine Sands	255
9.11	Comparison of the Tung Chung Field CPT Data with $q_{c(min)}$ Defining the Contractive/Dilative Boundary	256
9.12	Comparison of the CLK Field CPT Data with $q_{c(min)}$ Defining the Contractive/Dilative Boundary	257
9.13	Comparison of the Shear Wave Velocity Profile Determined by SCPT at the Tung Chung Site with the $V_{s(min)}$ Defining the Contractive/Dilative Boundary	258
9.14	Comparison of the Shear Wave Velocity Profile Determined by SCPT at the CLK Site with the $V_{s(min)}$ Defining the Contractive/Dilative Boundary (cc-results Obtained by Calibration Chamber Tests; Be-results Obtained by Bender Elements Measurement in Triaxial Specimen)	259

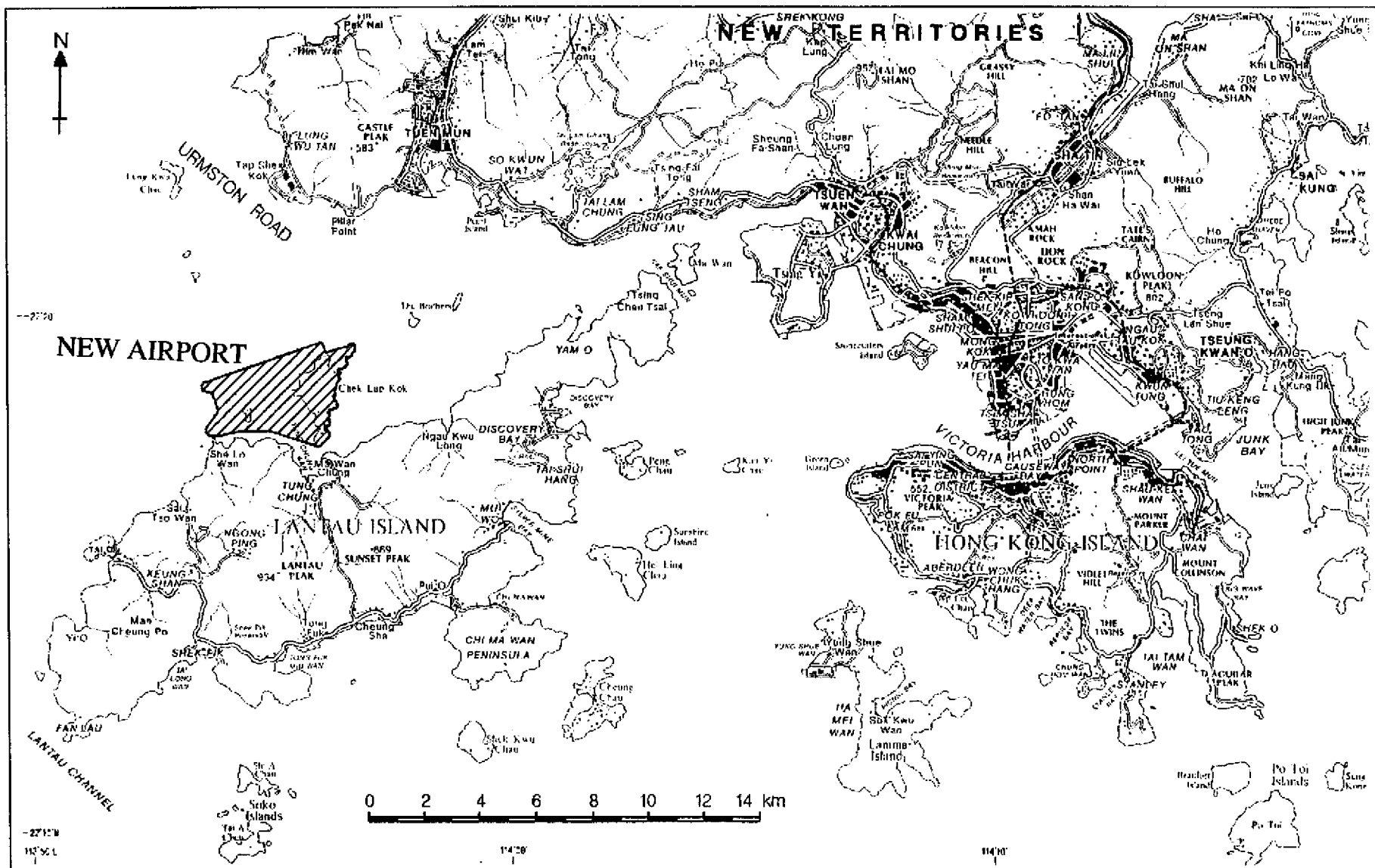


Figure 1.1 - Location of the New Airport at Chek Lap Kok

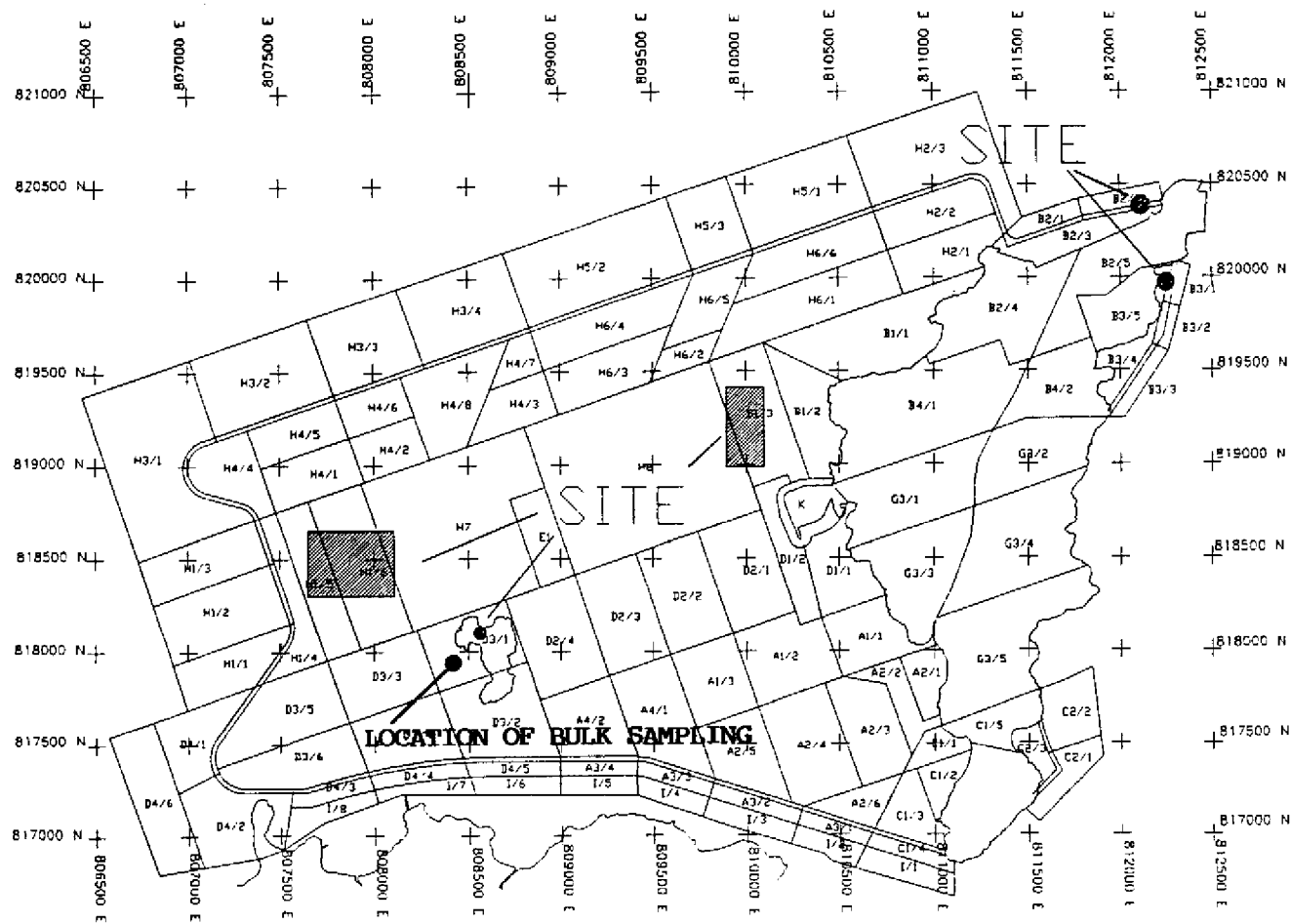


Figure 2.2 - Location of Bulk Sampling at the CLK Site

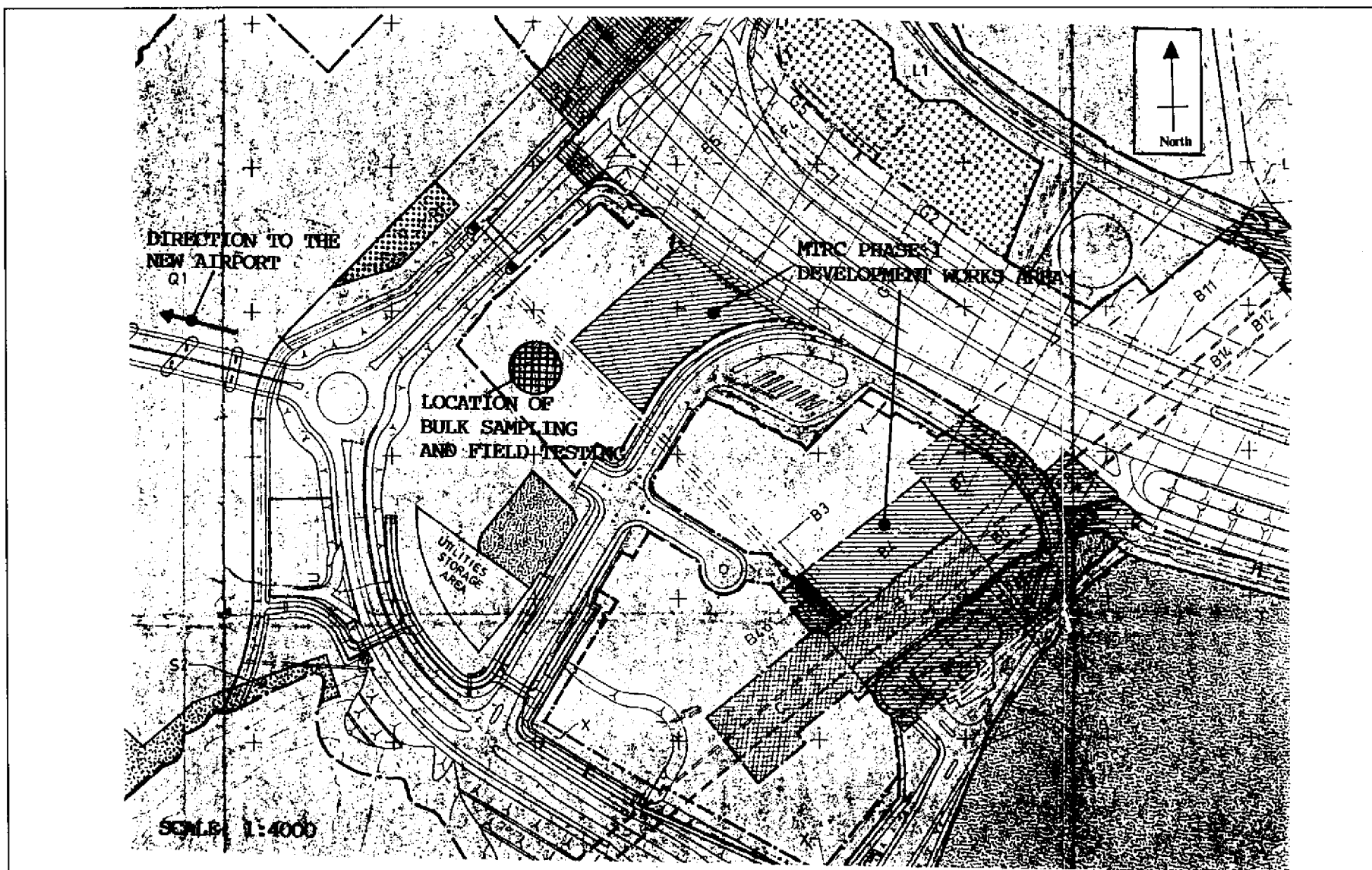



Figure 2.3 - Location of Field Work at the TC Site

		DRILLHOLE RECORD				HOLE NO. DH1	
		CONTRACT NO. GE/93/08		LG21518/52		SHEET 1 of 3	
PROJECT Study of Hydraulic Fill Performance for Marine Reclamation Tung Chung New Town Development Phase 1							
METHOD Rotary				CO-ORDINATES E 811693.38 N 816853.39		WORKS ORDER No. GE/93/08.57	
MACHINE & No. D10 Diamont Boart						DATE from 24/12/94 to 29/12/94	
FLUSHING MEDIUM Polymer Mud				ORIENTATION Vertical		GROUND-LEVEL 6.02 mPD	

Drilling Progress	Casing depth/size	Water level/time/date	Total core Recovery %	Solid core Recovery %	R.Q.D.	Fracture Index	Tests	Samples	Reduced Level	Depth (m)	Legend	Grade	Description
24/12/94	Sx												
1			70					1		1.00			Medium dense becoming loose, dark grey silty fine to medium, occasionally coarse SAND with some shell fragments (FILL)
2							(0,0, 2,5,5,5) N=17	2		2.00			
3			50					3		2.60			
4							(1,3, 5,5,5,6) N=21	4		3.60			From 3.70m-6.80m slightly silty and fine to coarse in grain size
5			20					5		4.20			
6							(1,1, 1,3,3,4) N=11	6		5.20			
7			85					7		5.80			
8							(1,1, 1,2,3,3) N=9	8		6.80			
9	Px	3.20m	80					9		7.40			
28/12/94							(2,2, 2,2,2,1) N=7	10		8.40			
10			100					11		9.00			Loose, dark grey, silty very clayey fine, occasionally medium to coarse SAND with some shell fragments and occasional thin lenses (<10mm) of clayey sandy silt (MARINE DEPOSIT/FILL?)
								12		10.00			

• SMALL DISTURBED SAMPLE □ LARGE DISTURBED SAMPLE ▨ SPT LINER SAMPLE ▩ U75 UNDISTURBED SAMPLE ▩ U100 UNDISTURBED SAMPLE ▨ MAZIER SAMPLE ▩ PITON SAMPLE	△ WATER SAMPLE ▨ PIEZOMETER TIP □ STANDPIPE ↓ STANDARD PENETRATION TEST ⊥ PERMEABILITY TEST ∇ IN-SITU VANE SHEAR TEST	LOGGED <u>S.P.Su</u> DATE <u>30/12/94</u> CHECKED <u>T.F.</u> DATE <u>6/4/94</u>	REMARKS
--	--	---	---------

Figure 2.4(a) - Drillhole Log at the TC Site

		DRILLHOLE RECORD				HOLE NO. DH1	
		CONTRACT NO. GE/93/08 LG21518/52				SHEET 2 of 3	
PROJECT Study of Hydraulic Fill Performance for Marine Reclamation Tung Chung New Town Development Phase 1							
METHOD Rotary			CO-ORDINATES			WORKS ORDER No. GE/93/08.57	
MACHINE & No. D10 Diamont Boart			E 811693.38 N 816853.39			DATE from 24/12/94 to 29/12/94	
FLUSHING MEDIUM Polymer Mud			ORIENTATION Vertical			GROUND-LEVEL 6.02 mPD	

Drilling Progress	Casing depth/size	Water level/time/date	Total core Recovery %	Solid core Recovery %	R.Q.D.	Fracture Index	Tests	Samples	Reduced Level	Depth (m)	Legend	Grade	Description
							(2.2, 2.2, 2.2) N=8	17		5.10			As sheet 1 of 3
11			100					18	-4.58	10.60			Medium dense, dark grey silty fine to medium, occasionally coarse SAND with some shell fragments (MARINE DEPOSIT/FILL?)
								19					
12			100				(1.2, 3.3, 3.4) N=13	20		11.60			Very soft, dark grey, clayey sandy SILT with occasional shell fragments (MARINE DEPOSIT)
								21	-6.18	12.20			
13								22					
								23		13.20			
14			100				(1.0, 0.0, 1.0) N=1	24		13.80			Medium dense, dark grey, clayey silty fine to medium, occasionally coarse SAND with some shell fragments and occasional lenses (< 10mm) of clayey sandy silt (MARINE DEPOSIT)
								25					
15			100				(1.2, 5.4, 5.2) N=15	26	-8.88	14.80			
								27		15.40			
16								28					
								29		16.40			
17			100				(7.2, 3.3, 3.4) N=13	30		17.00			
								31					
18		2.80m						32		18.00			
								33		18.40			
19			100				(3.4, 4.5, 5.6) N=20	34	-12.58	18.60			Medium dense, light reddish yellow mottled whitish grey, slightly clayey silty medium to coarse SAND with some subangular to subrounded fine to medium gravel sized quartz and moderately strong to strong rock fragments (ALLUVIUM)
								35		19.65			
20							(3.4, 4.5, 5.6) N=20						

<div style="display: flex; justify-content: space-between;"> <div style="width: 45%;"> <p> SMALL DISTURBED SAMPLE</p> <p> LARGE DISTURBED SAMPLE</p> <p> SPT LINER SAMPLE</p> <p> U78 UNDISTURBED SAMPLE</p> <p> U100 UNDISTURBED SAMPLE</p> <p> MAZIER SAMPLE</p> <p> PISTON SAMPLE</p> </div> <div style="width: 45%;"> <p> WATER SAMPLE</p> <p> PIEZOMETER TIP</p> <p> STANDPIPE</p> <p> STANDARD PENETRATION TEST</p> <p> PERMEABILITY TEST</p> <p> IN-SITU VANE SHEAR TEST</p> </div> </div>	LOGGED <u>S.P.Su</u> DATE <u>30/12/94</u> CHECKED <u>T.F.</u> DATE <u>6/4/94</u>	REMARKS
---	---	---------

Figure 2.4(b) - Drillhole Log at the TC Site

		DRILLHOLE RECORD				HOLE NO. DH1	
		CONTRACT NO. GE/93/08 LG21518/52				SHEET 3 of 3	
PROJECT Study of Hydraulic Fill Performance for Marine Reclamation Tung Chung New Town Development Phase 1							
METHOD Rotary				CO-ORDINATES E 811693.38 N 816853.39		WORKS ORDER No. GE/93/08.57	
MACHINE & No. D10 Diamont Boart						DATE from 24/12/94 to 29/12/94	
FLUSHING MEDIUM Polymer Mud				ORIENTATION Vertical		GROUND-LEVEL 6.02 mPD	

Drilling Progress	Casing depth/size	Water level/ time/ date	Total core Recovery %	Solid core Recovery %	R.Q.D.	Fracture Index	Tests	Samples	Reduced Level	Depth (m)	Legend	Grade	Description
							5, 7, 7, 9) N = 28	• 7/36	14.13	20.15			End of investigation hole at 20.10m
21													
22													
23													
24													
25													
26													
27													
28													
29													
30													

<div style="display: flex; justify-content: space-between;"> <div style="width: 45%;"> <p>▲ SMALL DISTURBED SAMPLE</p> <p>■ LARGE DISTURBED SAMPLE</p> <p>▨ SPT LINER SAMPLE</p> <p>▨ U76 UNDISTURBED SAMPLE</p> <p>▨ U100 UNDISTURBED SAMPLE</p> <p>▨ MAZIER SAMPLE</p> <p>▨ PISTON SAMPLE</p> </div> <div style="width: 45%;"> <p>△ WATER SAMPLE</p> <p>■ PIEZOMETER TIP</p> <p>▨ STANDPIPE</p> <p>⊥ STANDARD PENETRATION TEST</p> <p>⊥ PERMEABILITY TEST</p> <p>✓ IN-SITU VANE SHEAR TEST</p> </div> </div>	<p>LOGGED <u>S.P.Su</u></p> <p>DATE <u>30/12/94</u></p> <p>CHECKED <u>T.F.</u></p> <p>DATE <u>6/4/94</u></p>	<p>REMARKS</p>
--	--	----------------

Figure 2.4(c) - Drillhole Log at the TC Site

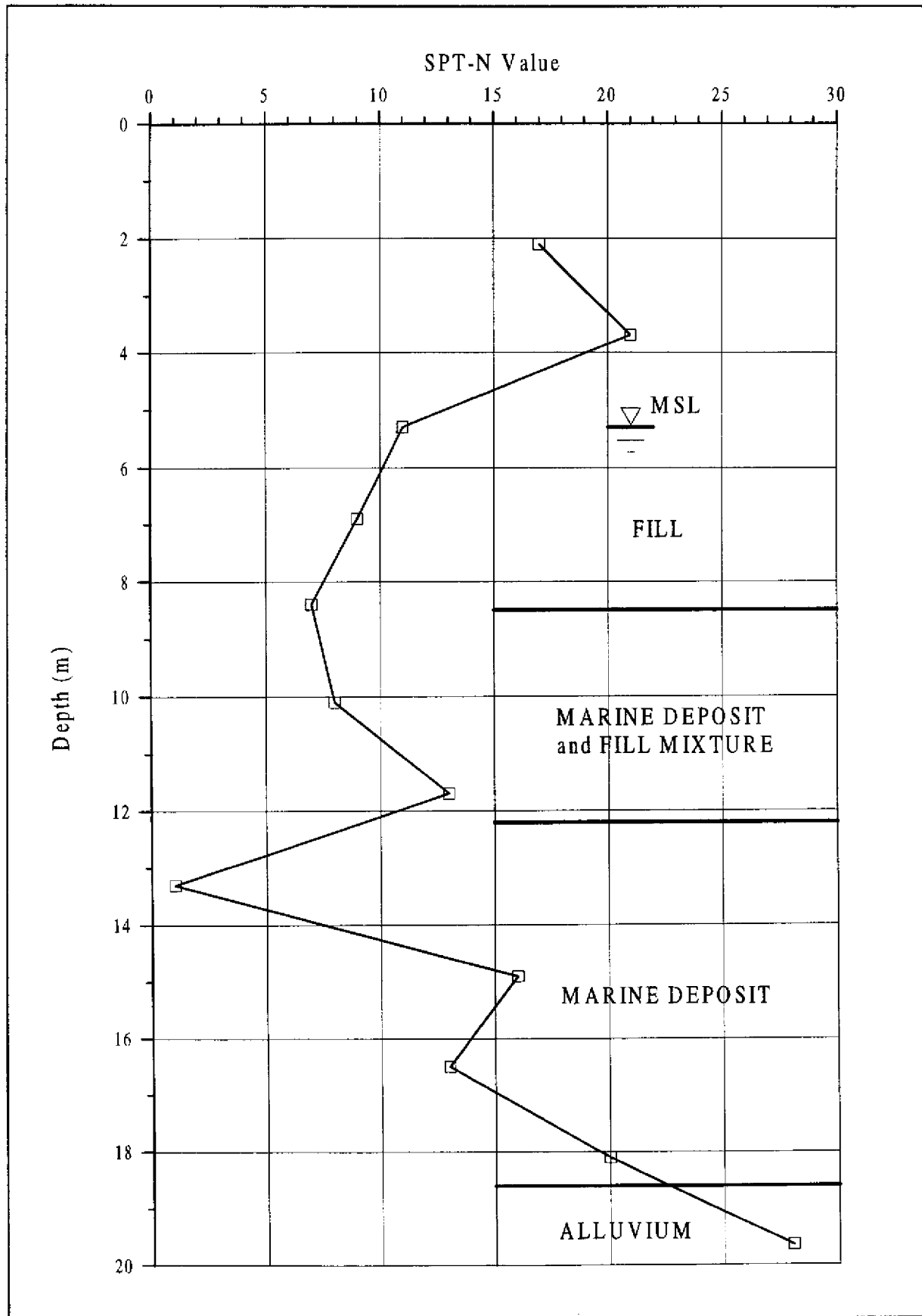


Figure 2.5 - Results of SPT-N Value Profile at the TC Site

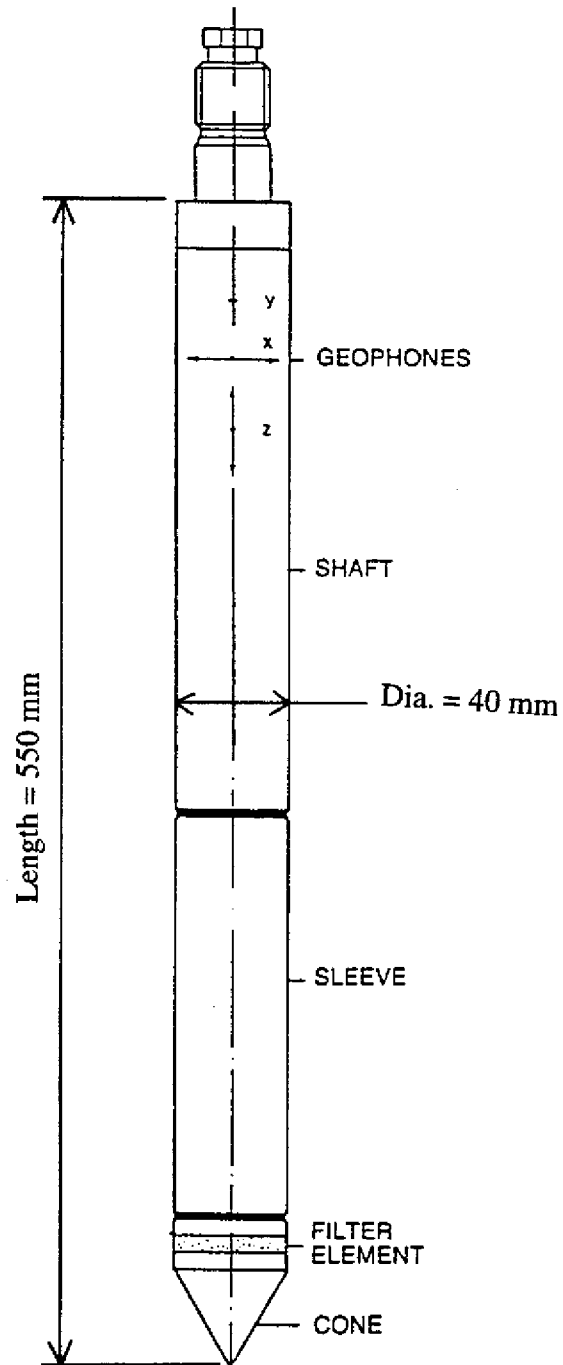


Figure 2.6 - Typical Details of Seismic Piezocone

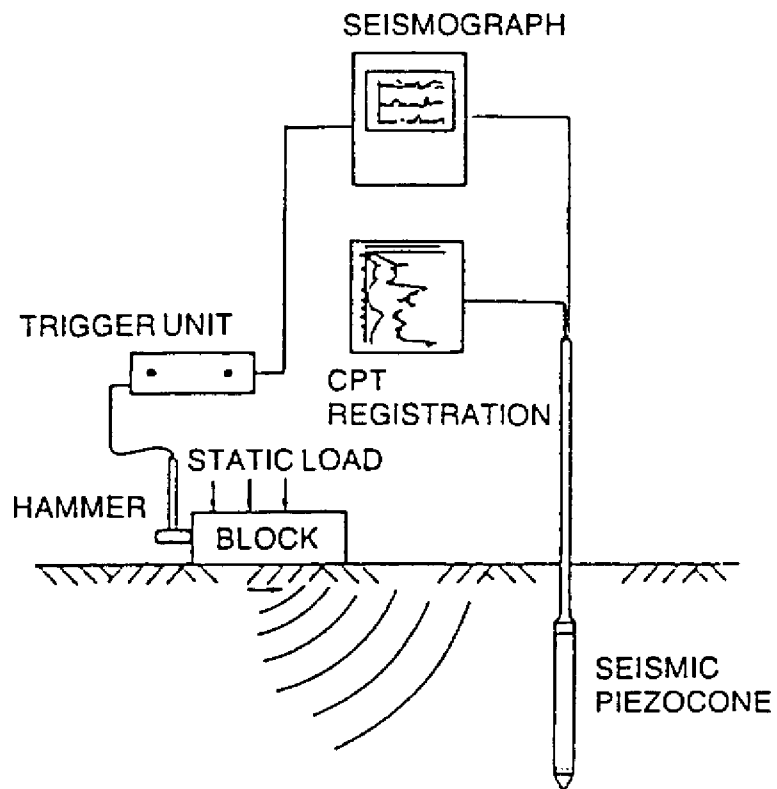


Figure 2.7 - Principle of the Vertical Seismic Profiling Method of Shear Wave Velocity Measurement Using the Seismic Piezocone

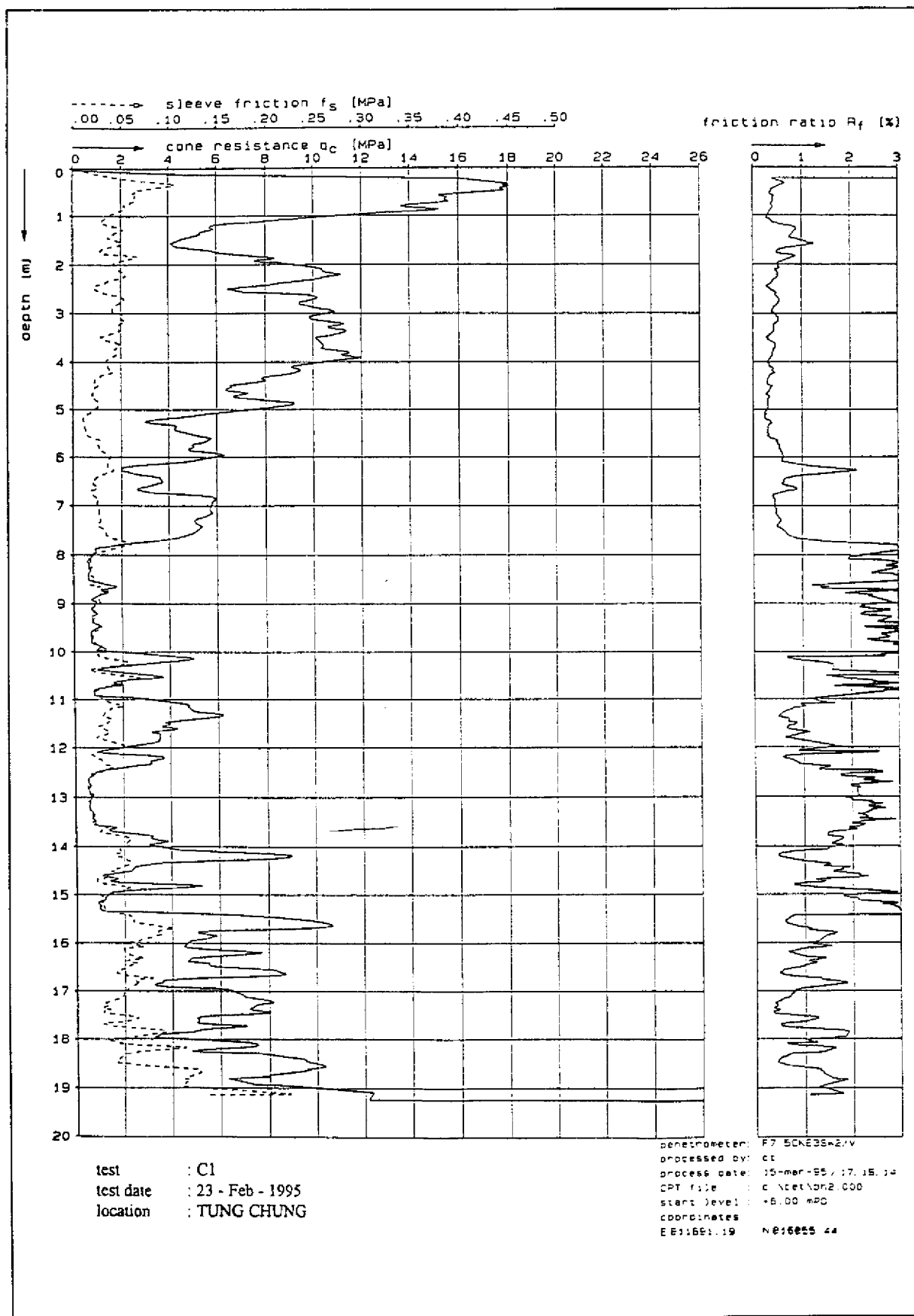


Figure 2.8(a) - Cone Resistance, Sleeve Friction versus Depth at the TC Site

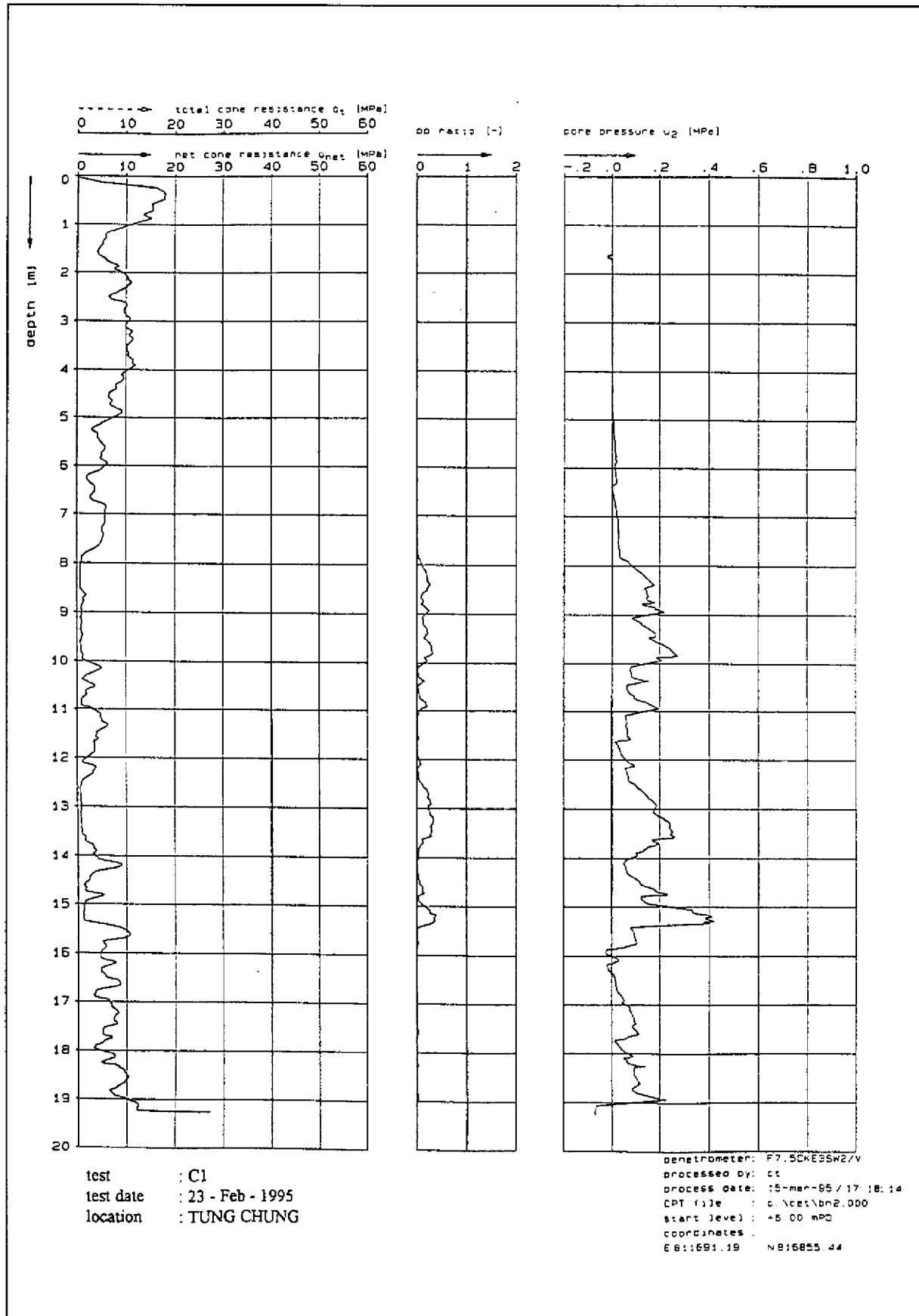


Figure 2.8(b) - Effective Cone Tip Resistance and Pore Pressure versus Depth at the TC Site

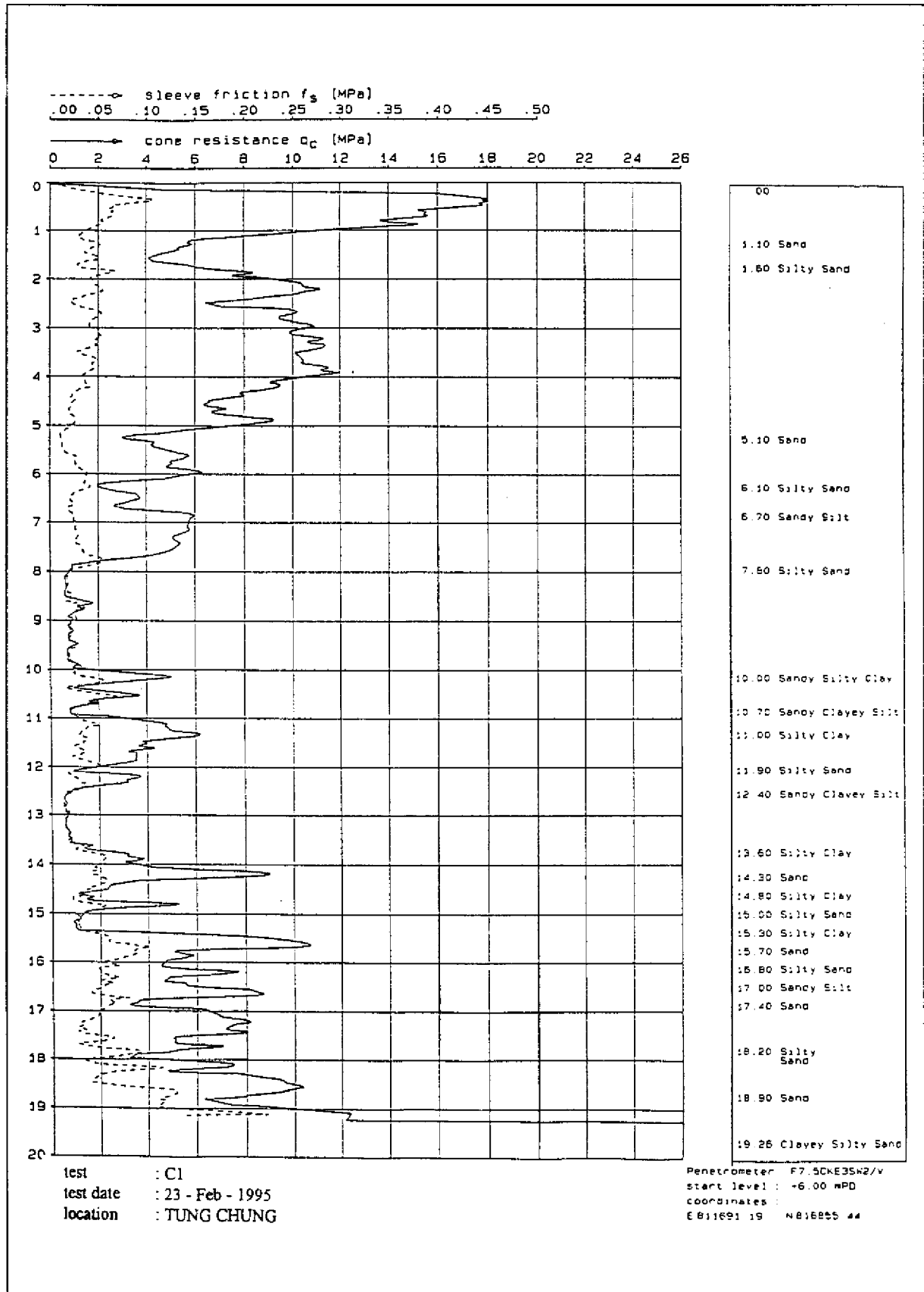


Figure 2.8(c) - Effective Cone Tip Resistance, Sleeve Friction, and Soil Description versus Depth at the TC Site

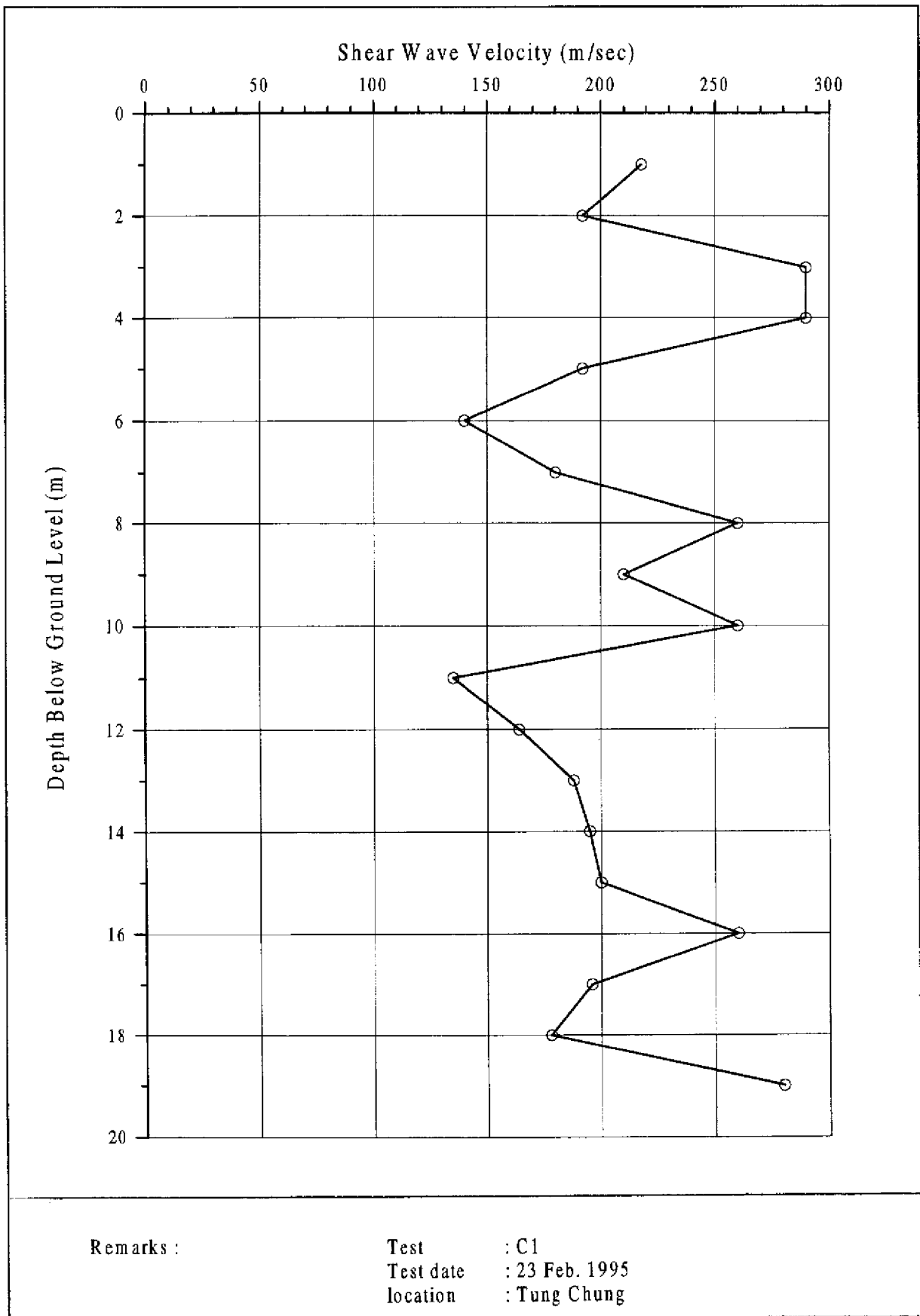


Figure 2.9 - Shear Wave Velocity versus Depth at the TC Site

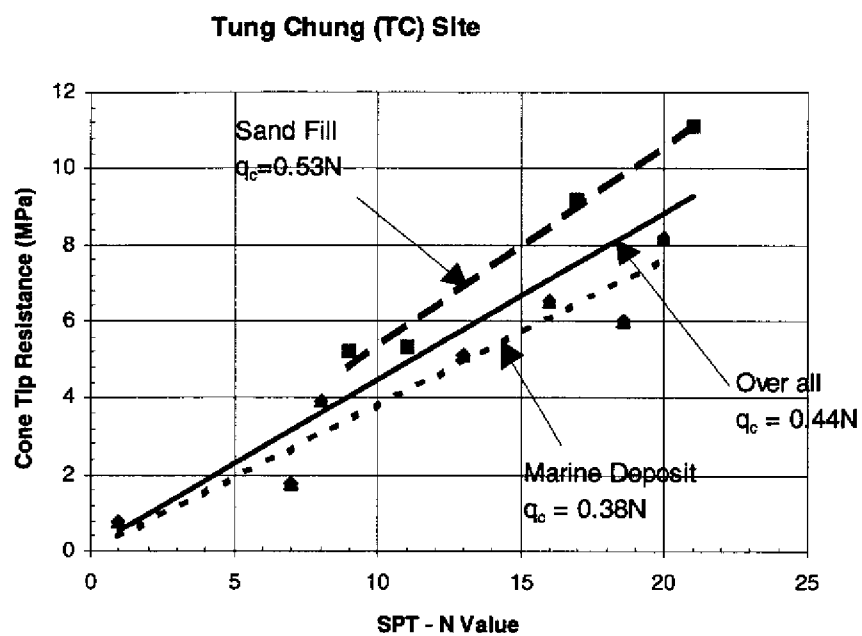
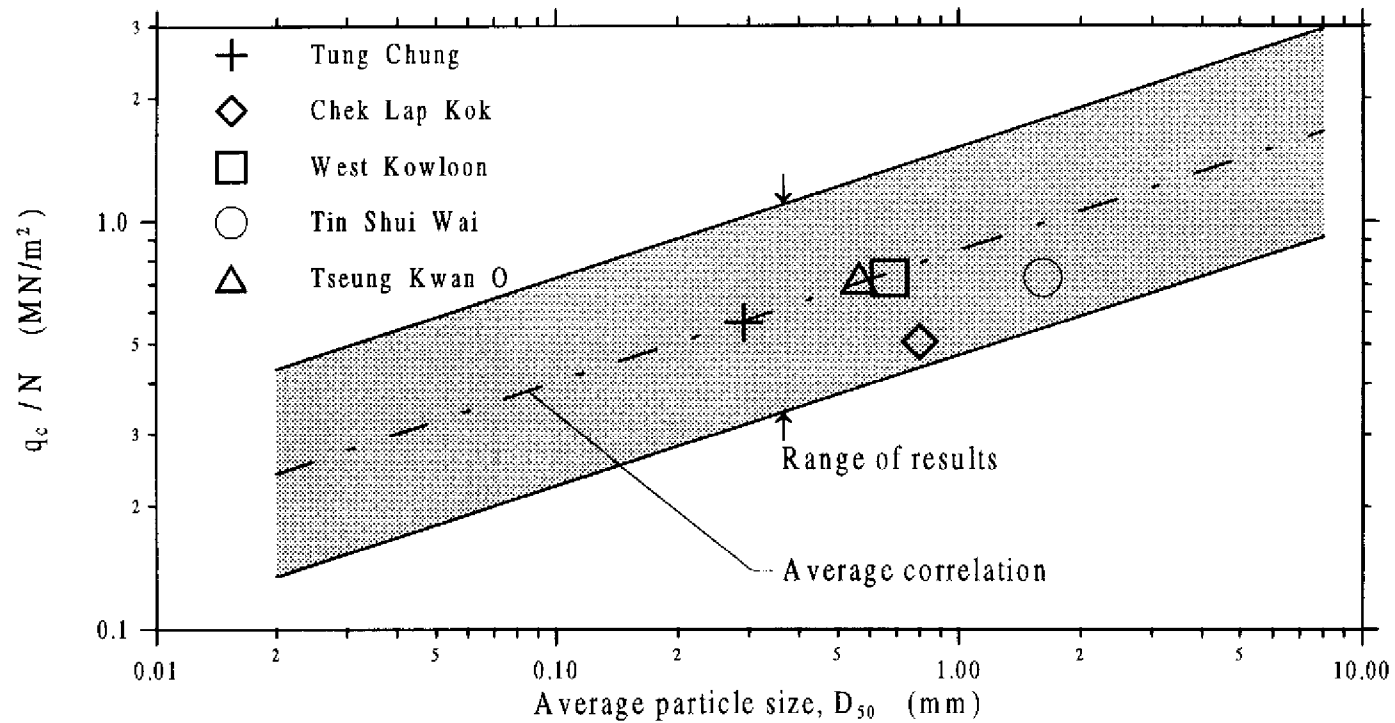


Figure 2.10 - Correlation between SPT - N Value and Cone Tip Resistance (q_c) for the Results Obtained from the TC Site



Medium	Coarse	Fine	Medium	Coarse	Fine	Medium
SILT		SAND			GRAVEL	

Figure 2.11 - Relationship between Cone Penetration Test and Standard Penetration Test (from Burland and Burbidge, 1985)

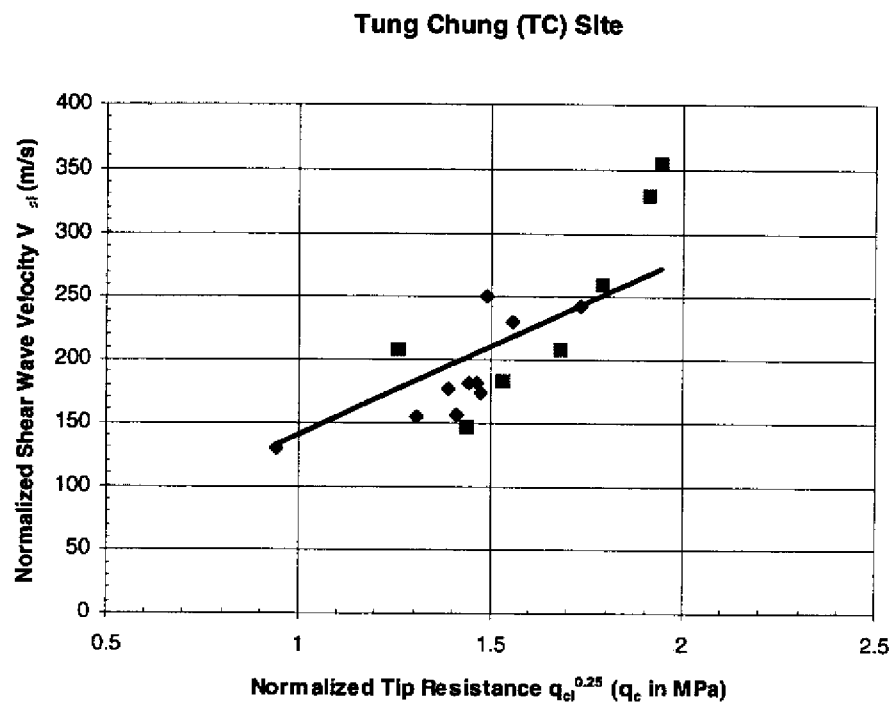


Figure 2.12 - Relationship between Normalized Shear Wave Velocity (V_{si}) and Normalized Cone Tip Resistance ($q_{cl}^{0.25}$) for the Results Obtained from the TC Site

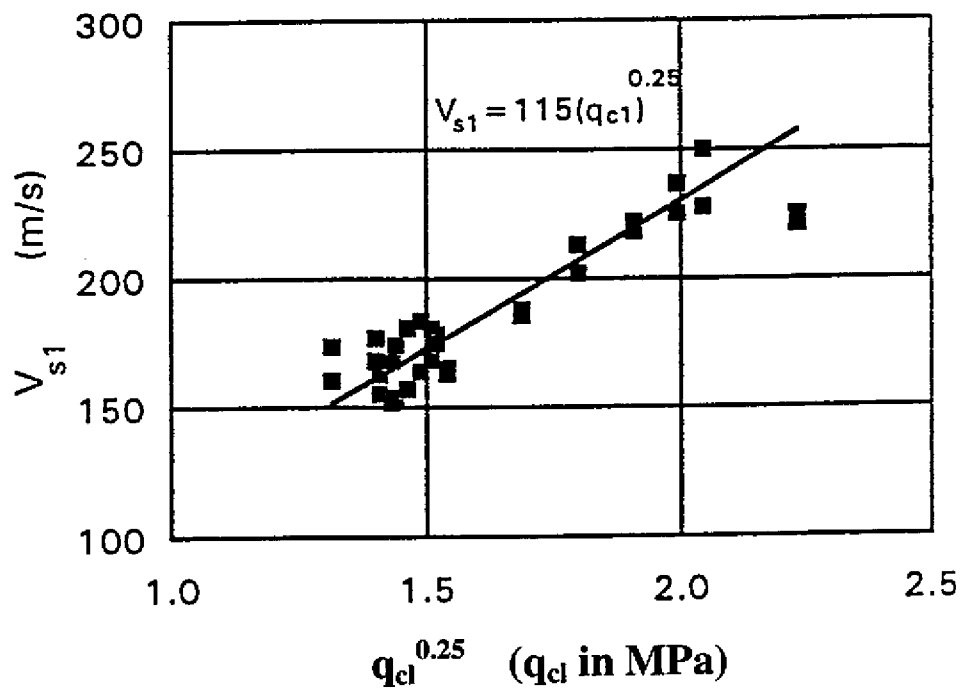


Figure 2.13 - Correlation between Normalized V_{s1} and $(q_{cl})^{0.25}$ for CLK Sand

1.0 Location of site:

2.0 Soil Stratigraphy:

Please provide the following information:

- general soil stratigraphy at the site
- location of ground water table or sea level

3.0 Extraction and Rehandling of Fill Material:

In this section, please provide detail information about sources and types of fill materials used for the reclamation work at the site, extraction technique employed, and mode of transportation of filling materials to the site. You may wish to consider the following points in response to the question:

- sources and types of borrow materials
- geologic origin of borrow materials (e.g. marine deposit, alluvial, reworked alluvium)
- extraction and dredging technique
- mixing and upgrading of dredged materials on location
- quality control to ensure the quality of borrow materials
- mode of transportation of fill materials to the site
- storage area, rehandling basin or stockpile of the fill material before reclamation work

Figure 3.1(a) - Questionnaire Developed in this Study for the Survey of Hydraulic Fill Performance in Hong Kong

4.0 Site Preparation work:

In this section, please provide detail information about the site preparation work employed before the actual filling process. You may wish to consider the following points in response to the question:

- removal and dredging of marine mud
- pre-drainage or ground improvement work
- leveling or sand blanket layer
- use of geotextile
- partial dredging of marine mud to form channel for passage of vessels or utilities

5.0 Reclamation and Filling Methods:

The following sections characterized some common methods of land reclamation and filling deposition in Hong Kong. As not all methods of deposition are employed at a particular site, please only fill in the sections relevant to the construction methods employed at the subject site location.

5.1 Bottom-dump Method:

If bottom-dump method was employed at the site, please provide detail information about the process. You may wish to consider the following points in response to the question:

- deposition level (in mPD)
- type and size (in cubic meter per load) of vessel used
- type and operation of discharge valves or doors located on the underside of the vessel
- discharge rate and stationary of vessel
- any specification of sub-aqueous side slopes.
- any construction of low bunds at seabed to control distribution of bottom dumped material.

Figure 3.1(b) - Questionnaire Developed in this Study for the Survey of Hydraulic Fill Performance in Hong Kong

5.2 High-velocity (spigotting or rainbow) discharge:

If high-velocity discharge method was employed at the site, please provide detail information about the process. You may wish to consider the following points in response to the question:

- deposition level (in mPD)
- discharging technique - floating pipeline, rainbow, or spigotting
- location of discharge point relative to the water level
- sand-water mixture ratio
- discharge rate, velocity, and size of discharge outlet
- any specification of sub-aqueous side slopes.
- any construction of low bunds at seabed to control distribution of discharged material.

5.3 Low-velocity pipe-line (pump-out) discharge:

If low-velocity pump-out discharge method was employed at the site, please provide detail information about the process. You may wish to consider the following points in response to the question:

- deposition level (in mPD)
- location of discharge point to sand body and water level
- sand-water mixture ratio
- discharge rate, velocity, and size of discharge pipe
- use of bulldozers in leveling
- construction of perimeter containment bunds (low dikes) and resulting temporary water level

Figure 3.1(c) - Questionnaire Developed in this Study for the Survey of Hydraulic Fill Performance in Hong Kong

6.0 Subsequent Ground Improvement Work:

Please provide information in regards to the ground improvement work adopted at the site after the filling process completed. You may wish to consider the following points in response to the question:

- surcharge level, surcharging material, and period of surcharge pre-loading
- installation of wick drains, type, depth, spacing and pattern
- deep compaction and/or vibro-compaction, type, spacing and compaction efforts
- final reclamation level and land use

7.0 Remarks:

Please provide additional remarks in particular to the overall reclamation process at the site, if any.

Figure 3.1(d) - Questionnaire Developed in this Study for the Survey of Hydraulic Fill Performance in Hong Kong

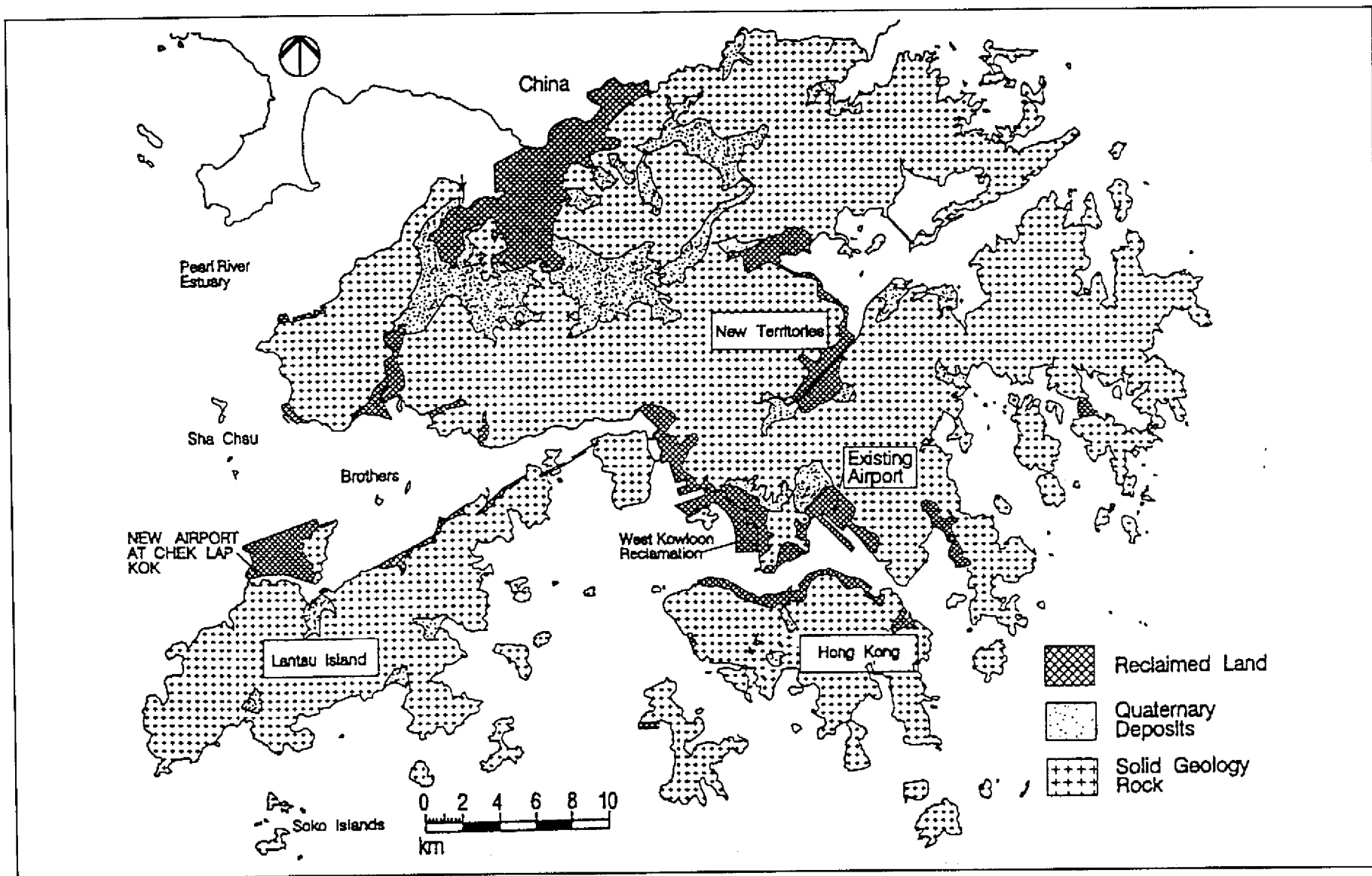


Figure 3.2 - Airport Location Plan Including Hong Kong's Geology and Reclamation (after Newman et al, 1996)

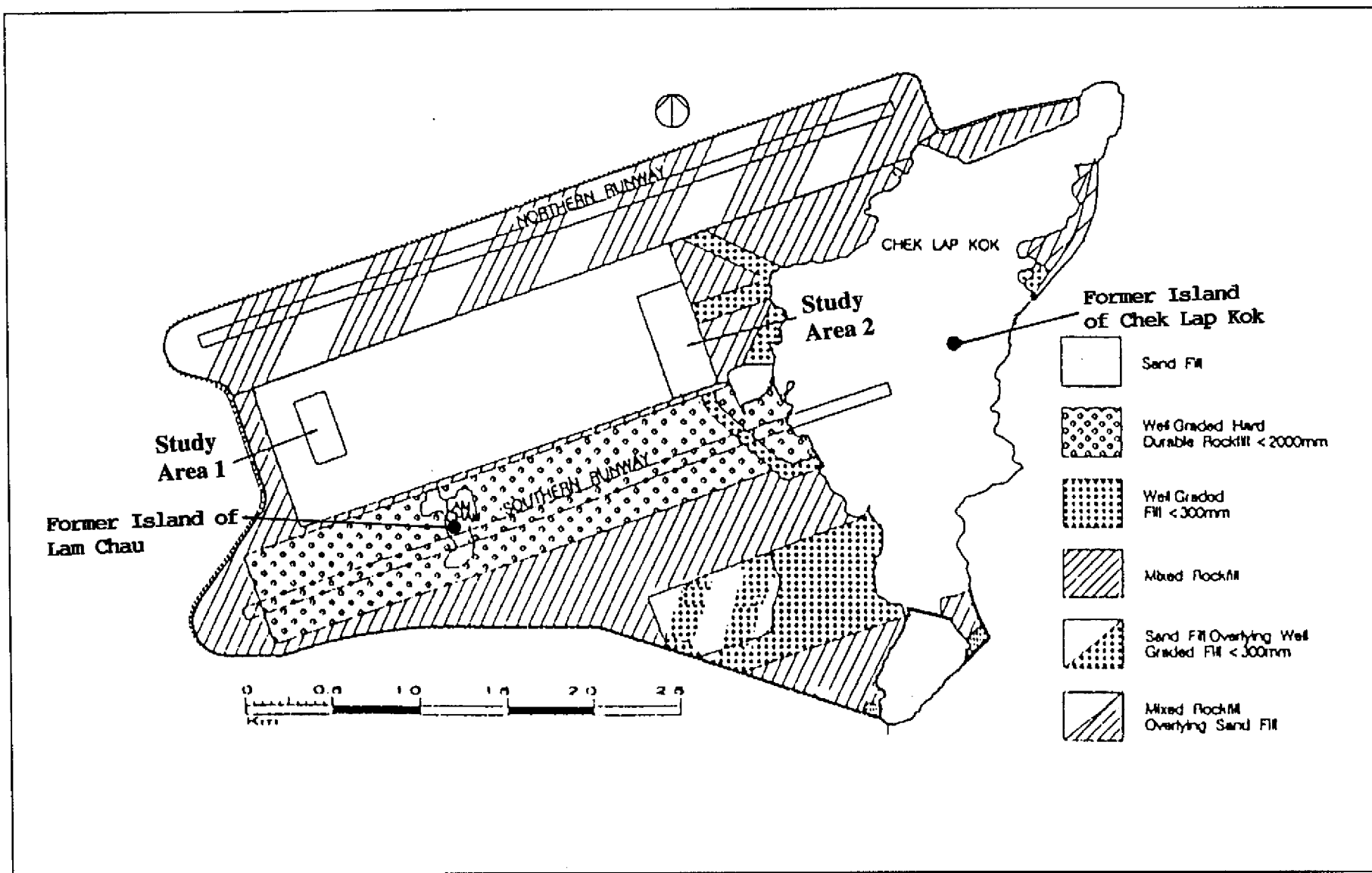


Figure 3.3 - Plan of Reclamation at the CLK Site (after Newman et al, 1996)

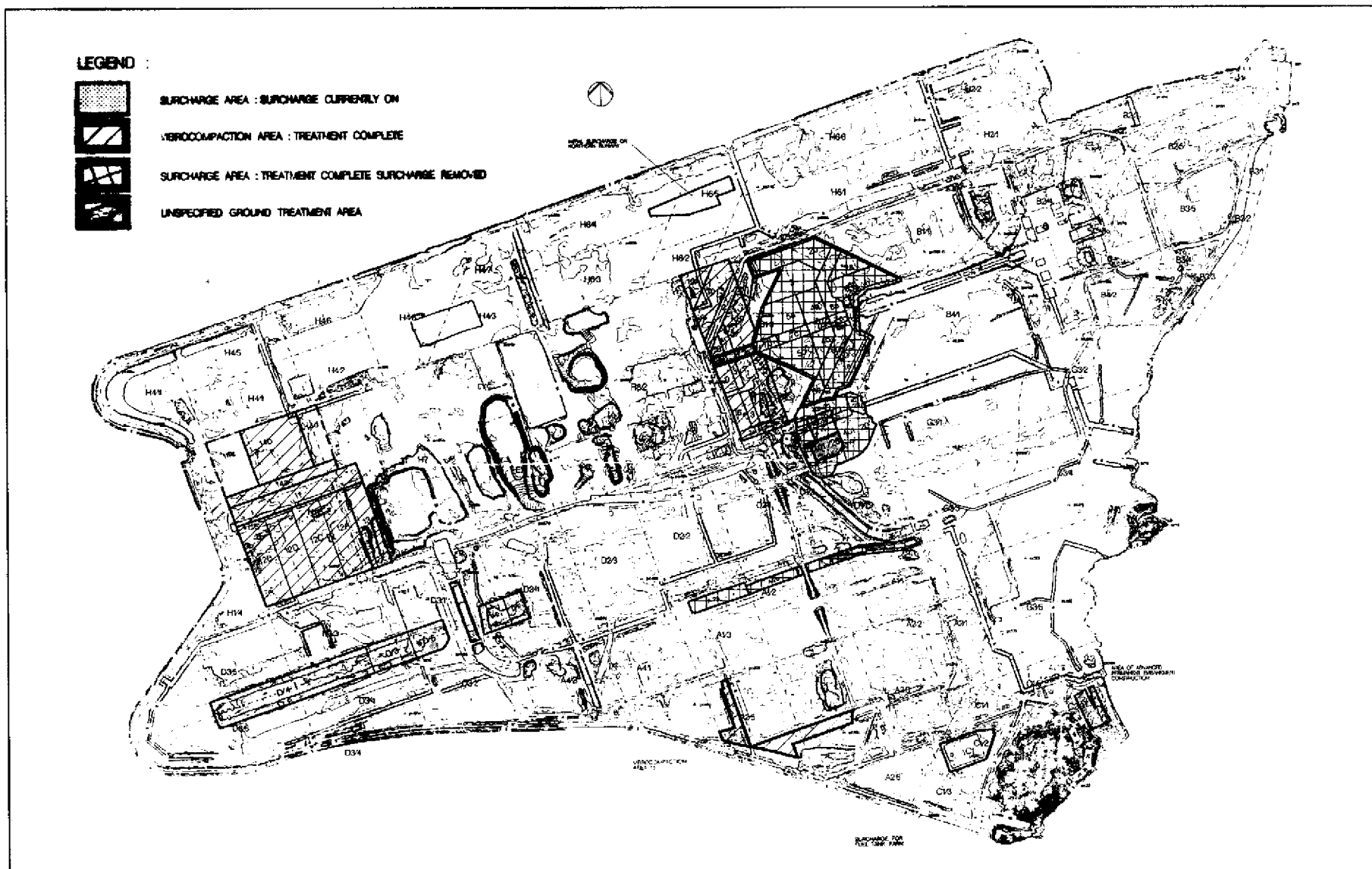


Figure 3.4 - Ground Treatment Layout Plan at the CLK Site

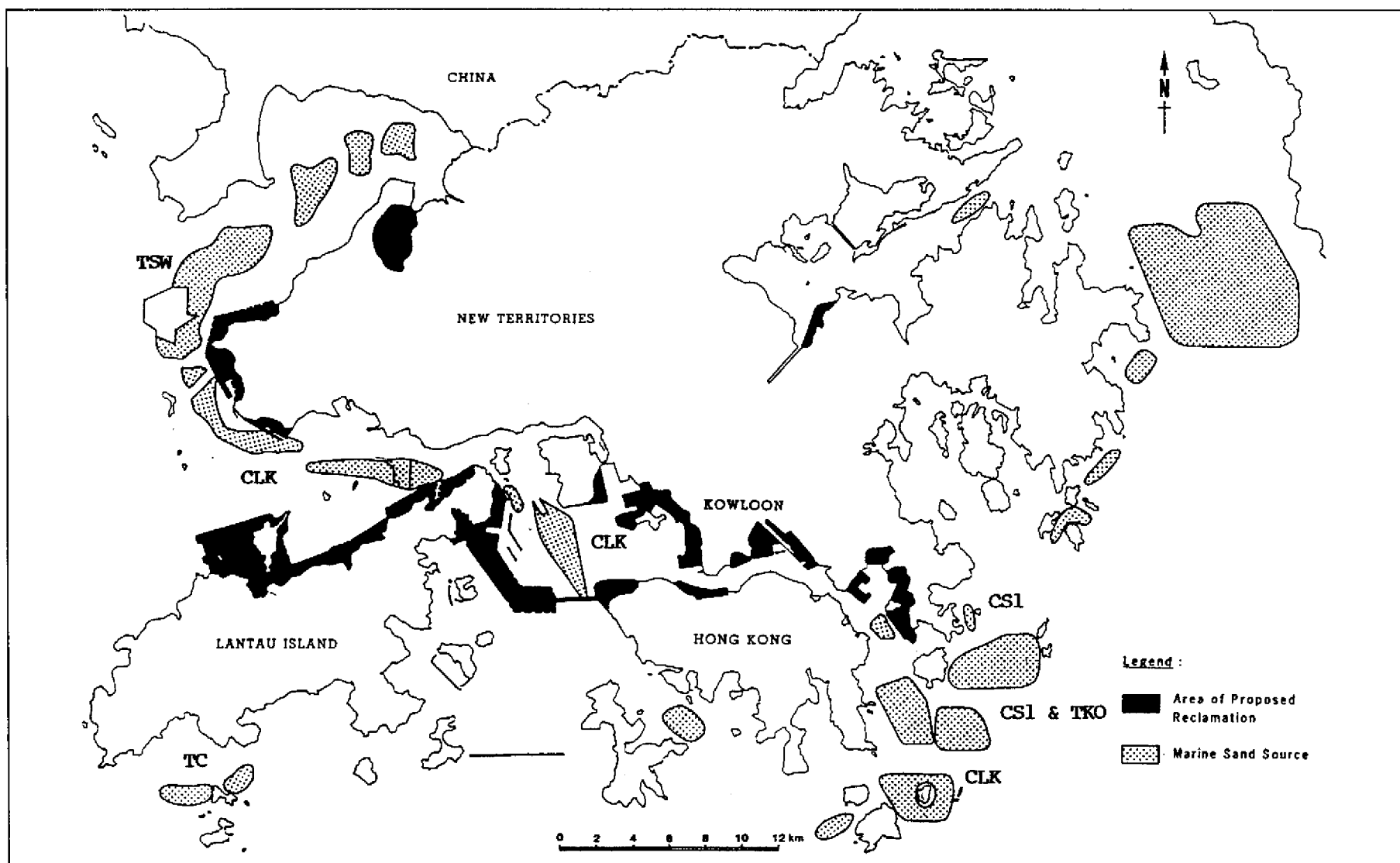


Figure 3.5 - Locations of Extraction Areas of Marine Sands Used in the Five Reclamation Sites Examined in this Study
(Modified from Whiteside, 1991)

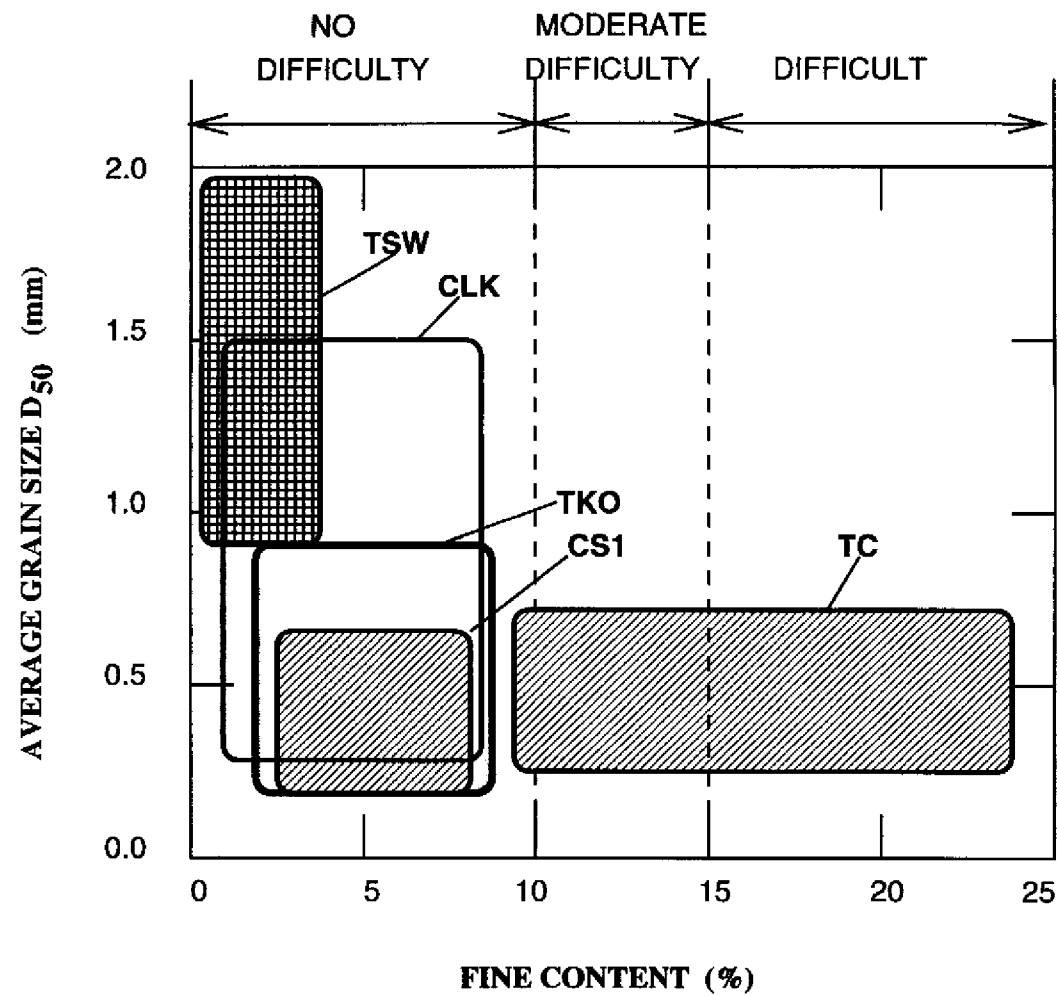


Figure 3.6 - Classification of Operation Difficulty on the Process of Winning of Marine Sands

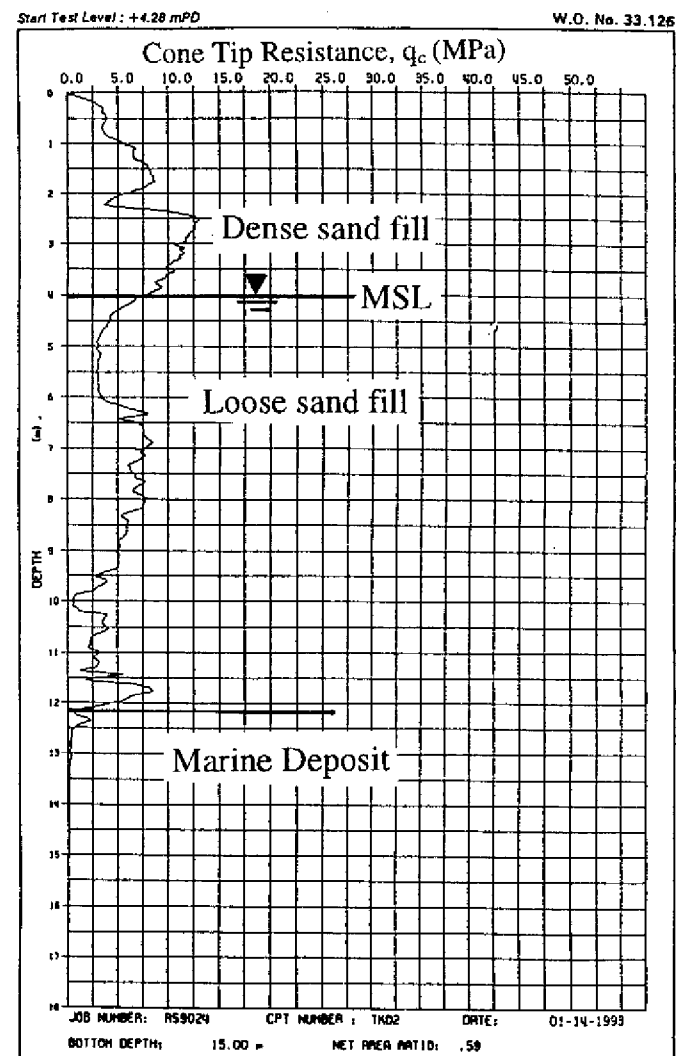
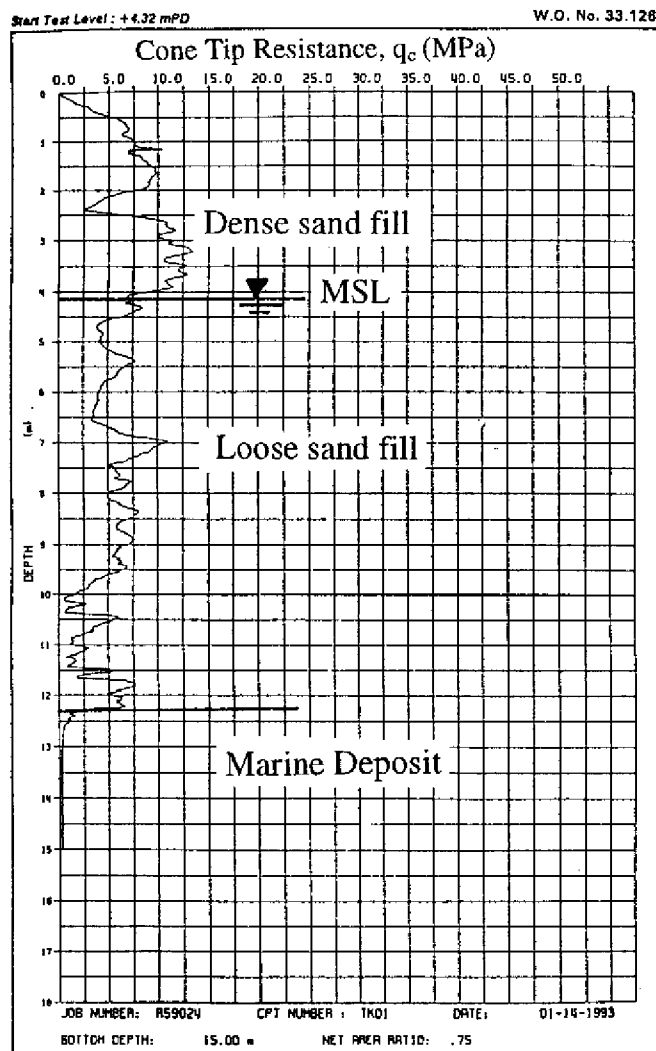


Figure 3.7 - Typical CPT Results Observed at the Tseung Kwan O Reclamation Site

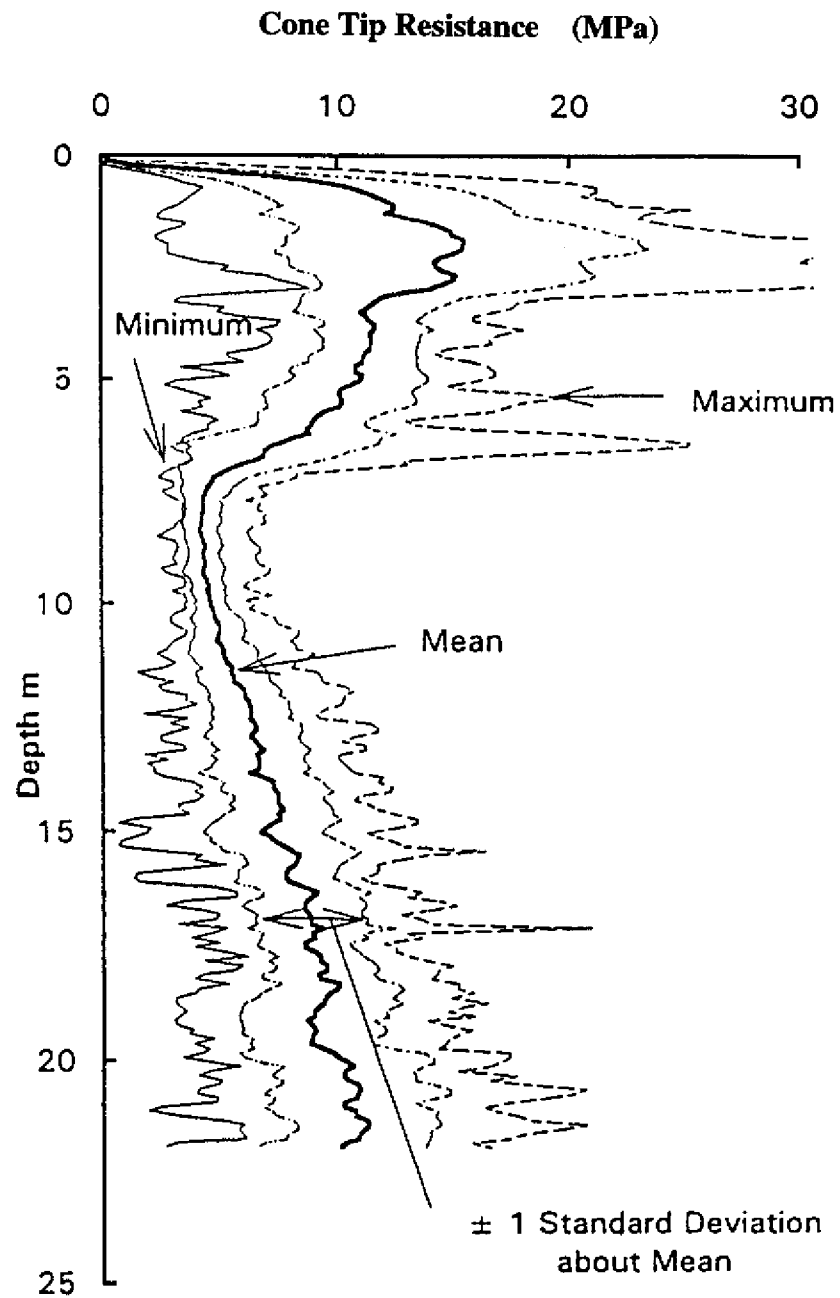


Figure 3.8 - Summary of Cone Tip Resistance at Area 1 - CLK Site
(after Newman et al, 1996)

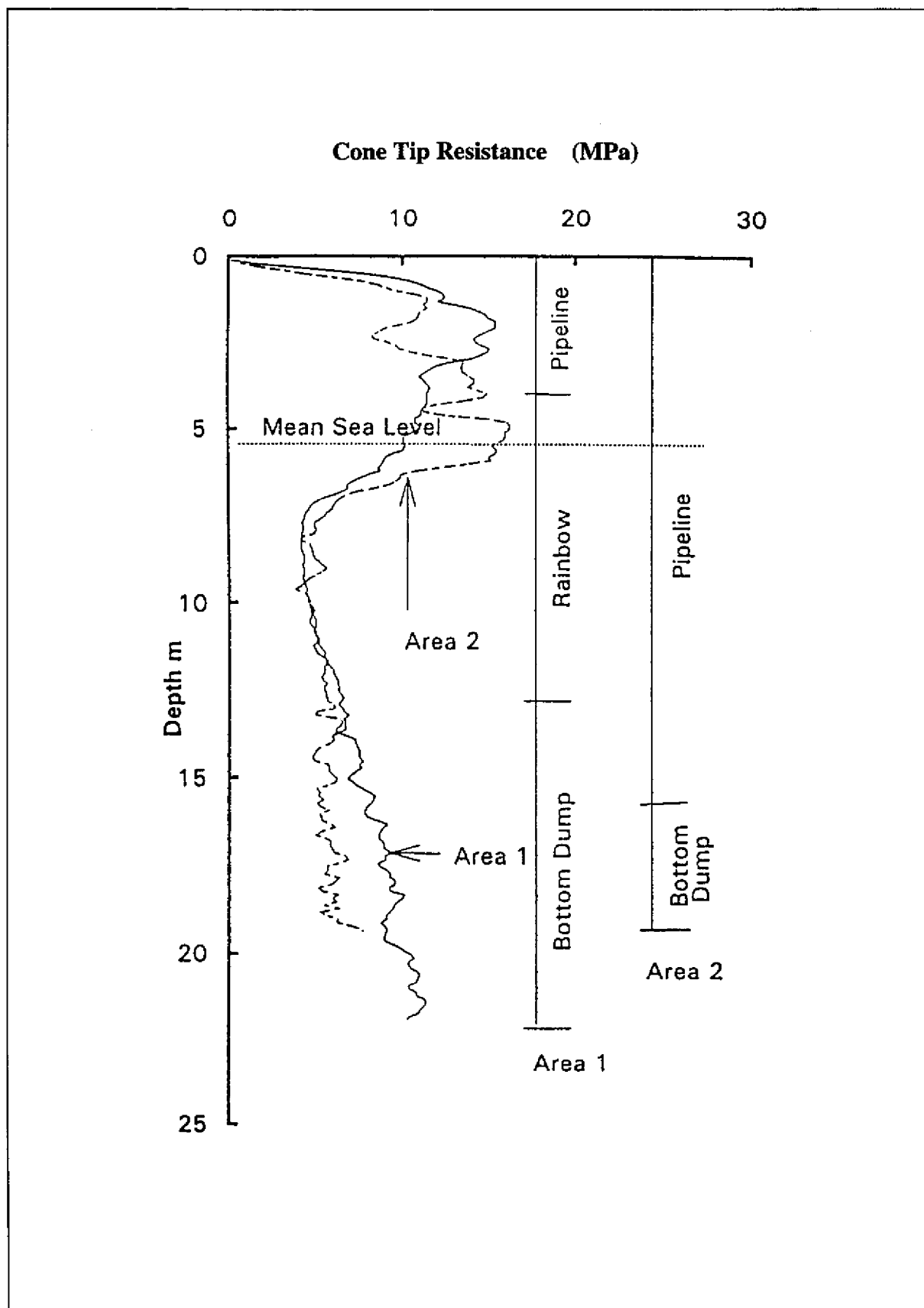


Figure 3.9 - Summary of Cone Tip Resistance at Area 2 - CLK Site
(after Newman et al, 1996)

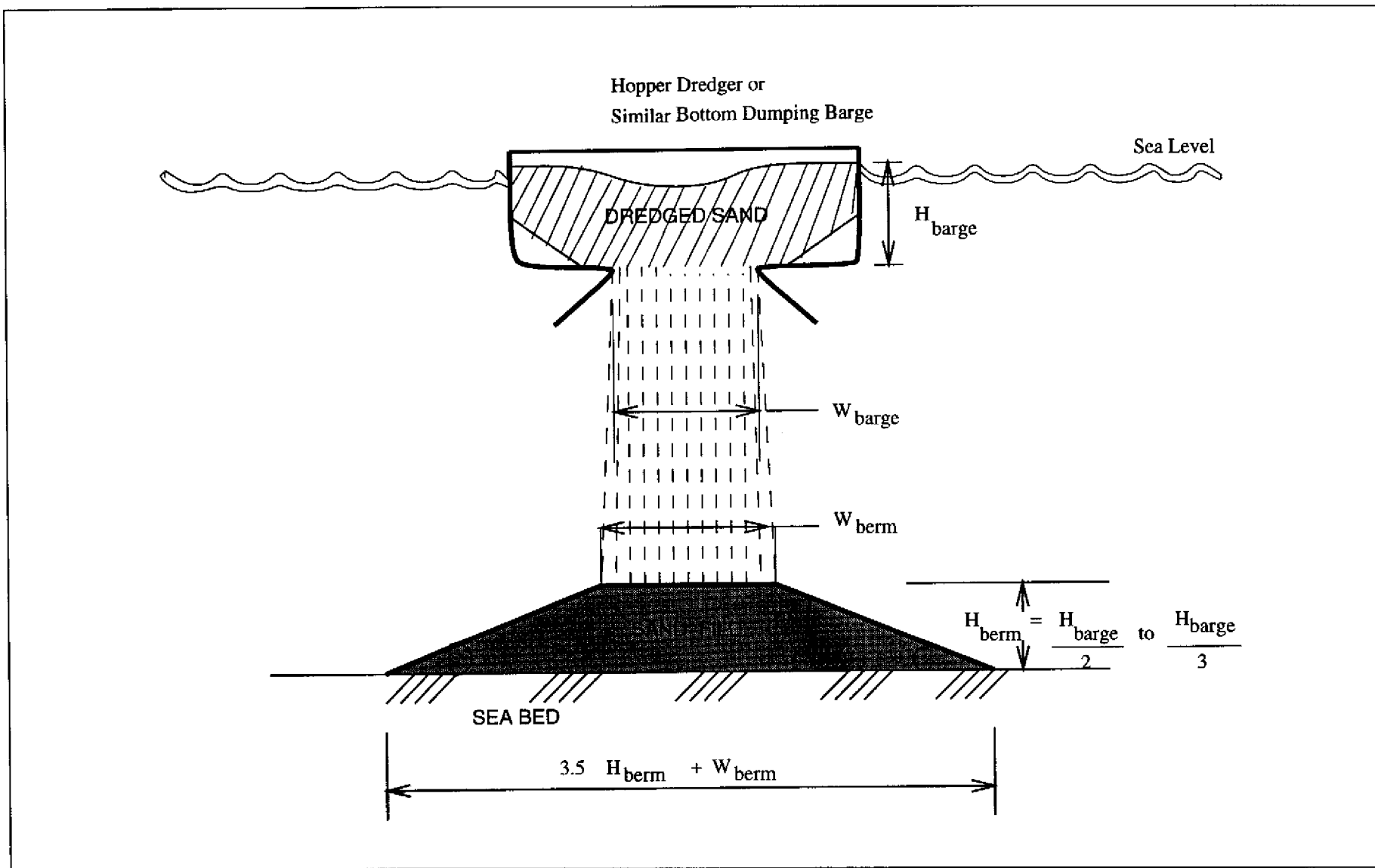


Figure 3.10 - Final Equilibrium Shape of Sand Mass after Bottom Dumping

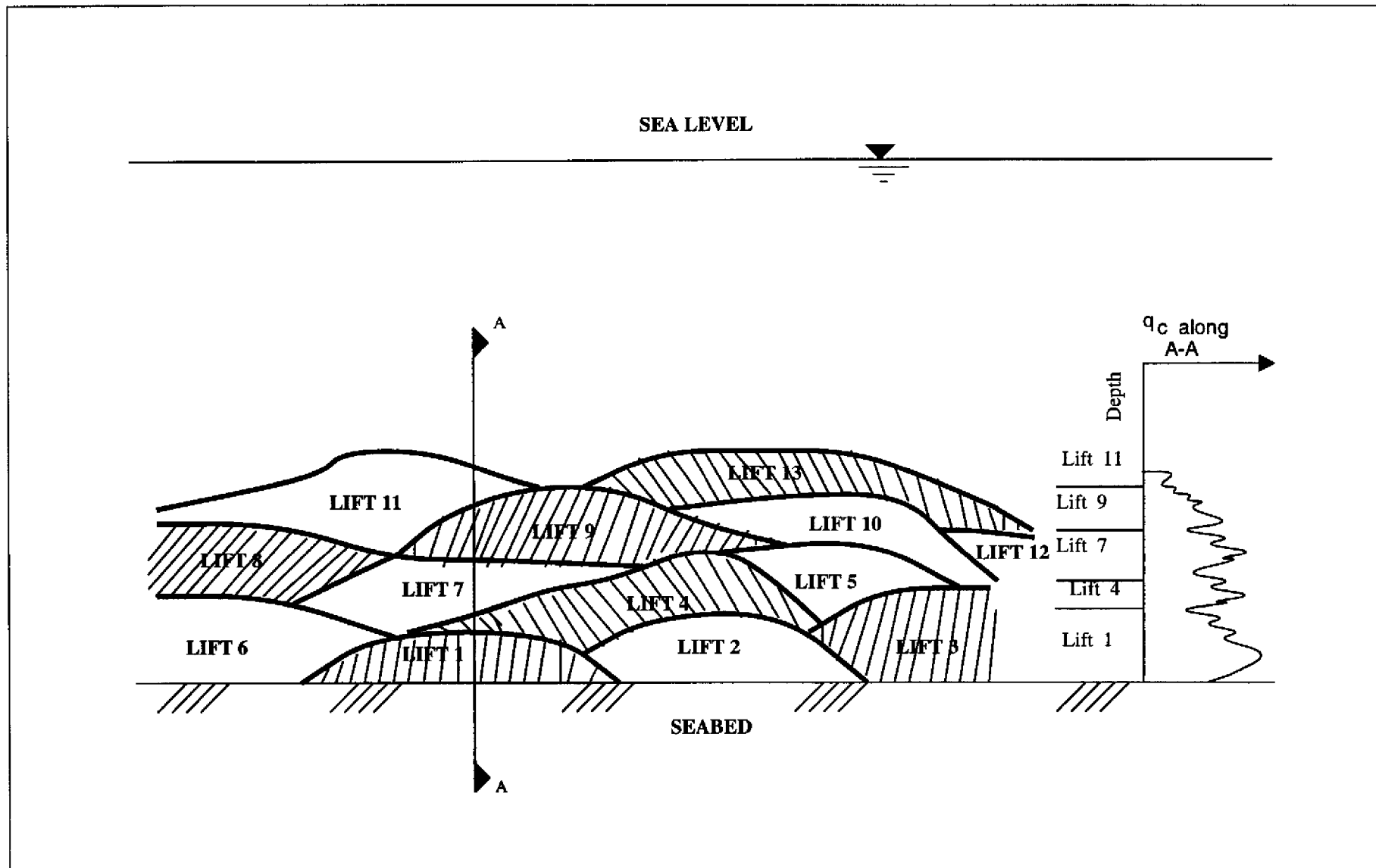


Figure 3.11 - Random Layered Distribution of Bottom Dumped Soil Berms

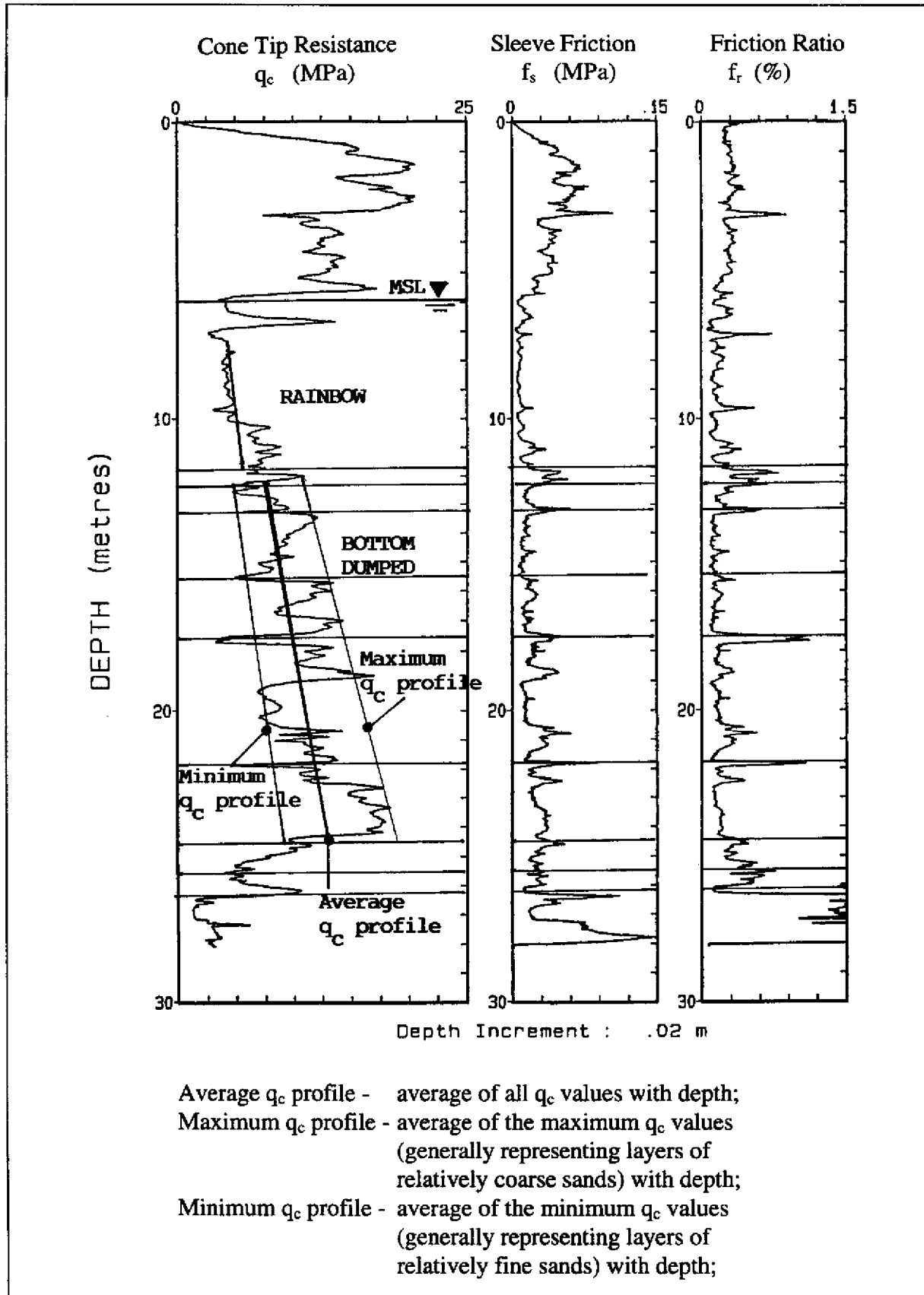
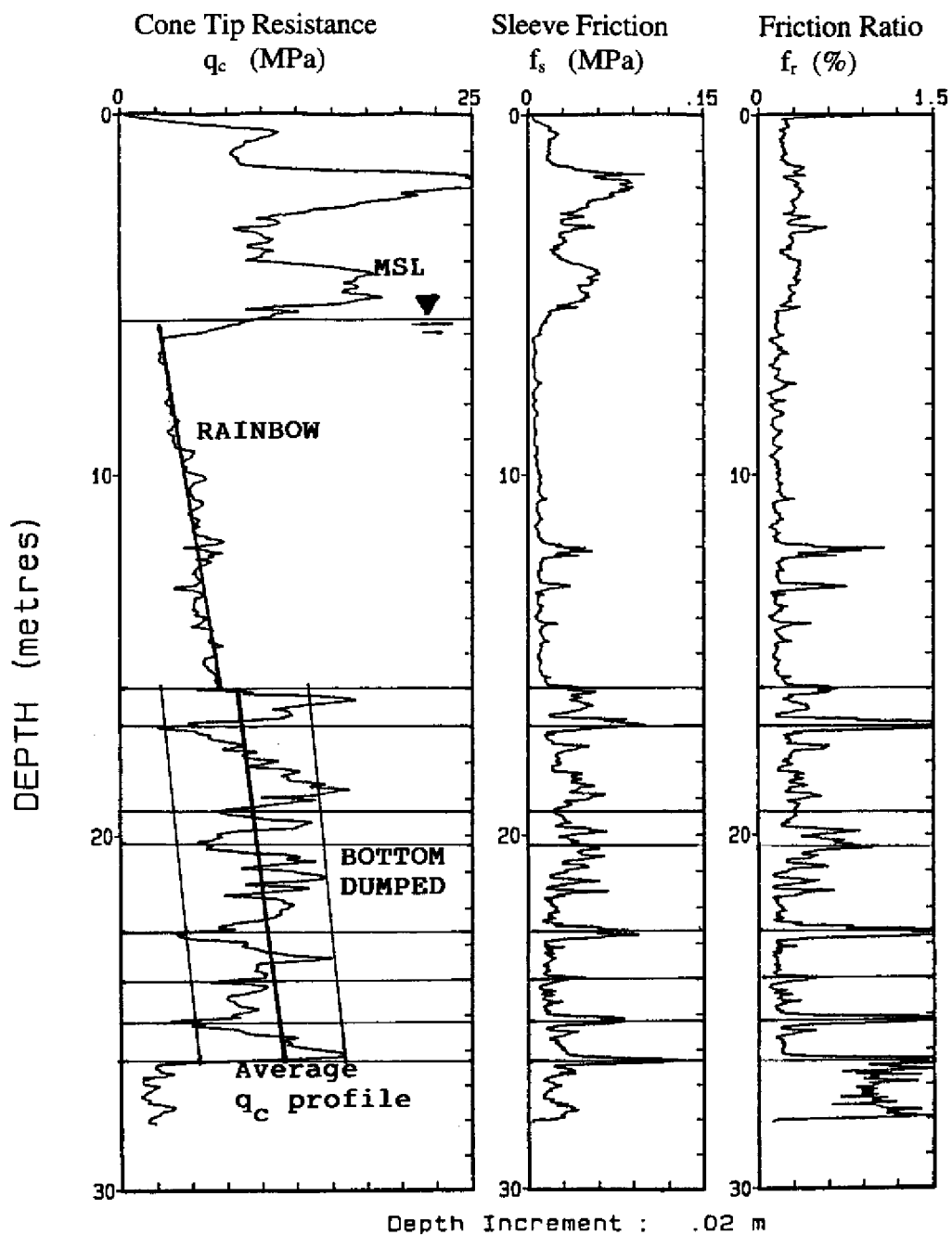
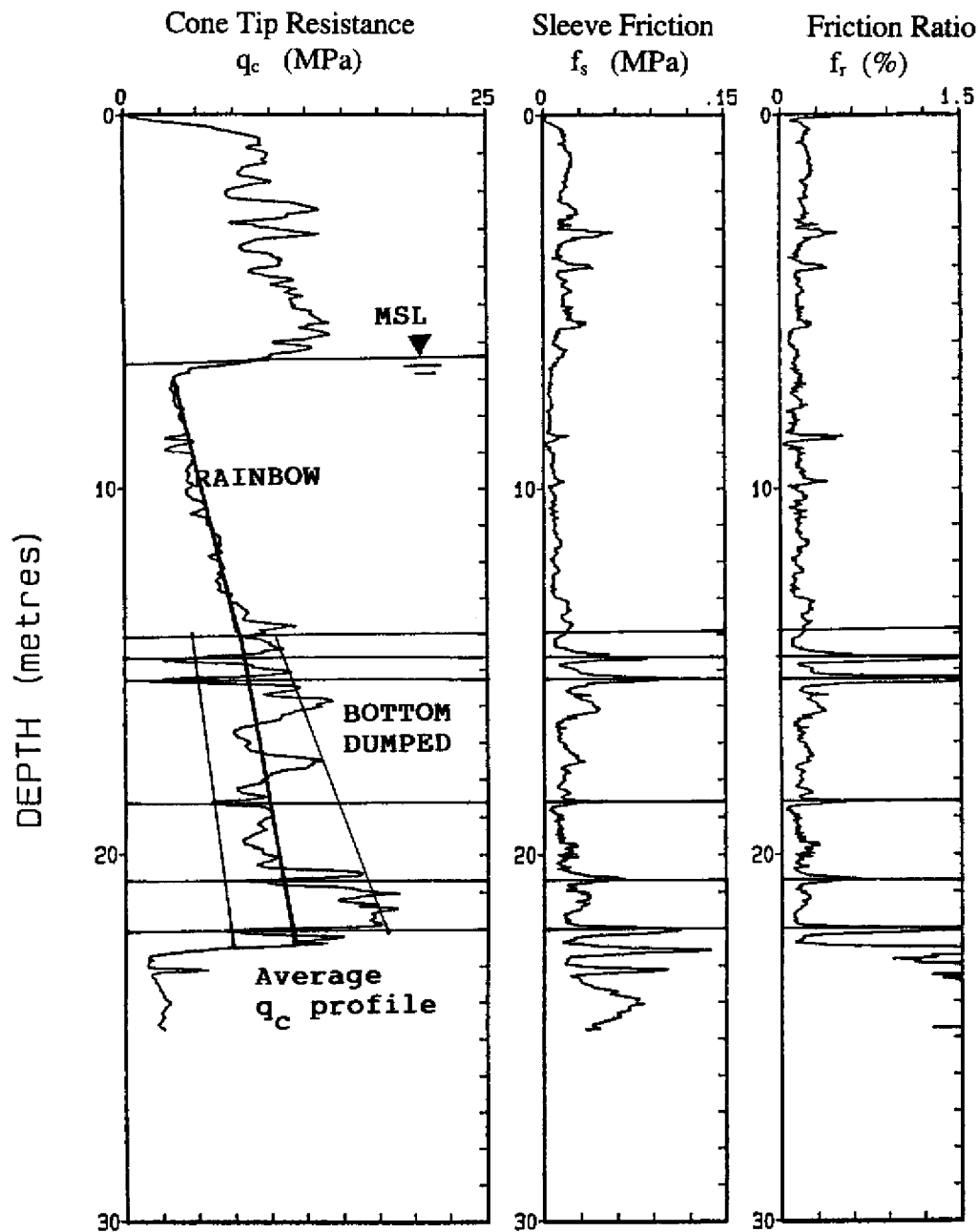


Figure 3.12(a) - Total Bottom Dumped Fill Thickness of 14 m Indicates "GOOD" Improvement in q_c Profile



Average q_c profile - average of all q_c values with depth;
 Maximum q_c profile - average of the maximum q_c values
 (generally representing layers of
 relatively coarse sands) with depth;
 Minimum q_c profile - average of the minimum q_c values
 (generally representing layers of
 relatively fine sands) with depth;

Figure 3.12(b) - Total Bottom Dumped Fill Thickness of 10 m Indicates
 "GOOD" Improvement in q_c Profile



Average q_c profile - average of all q_c values with depth;
Maximum q_c profile - average of the maximum q_c values
(generally representing layers of
relatively coarse sands) with depth;
Minimum q_c profile - average of the minimum q_c values
(generally representing layers of
relatively fine sands) with depth;

Figure 3.13(a) - Total Bottom Dumped Fill Thickness of 8 m Indicates
"FAIR" Improvement in q_c Profile

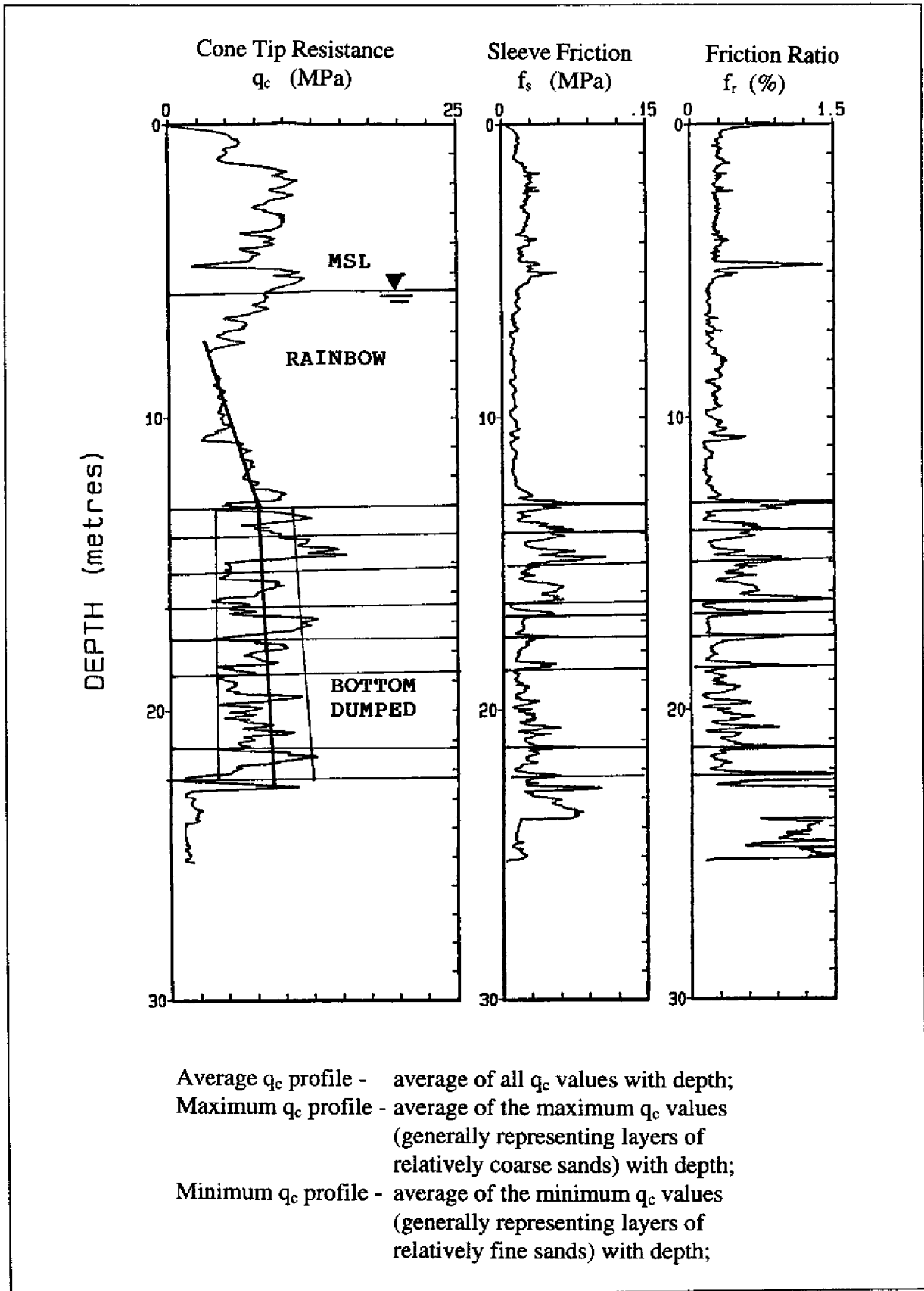


Figure 3.13(b) - Total Bottom Dumped Fill Thickness of 9 m Indicates
“FAIR” Improvement in q_c Profile

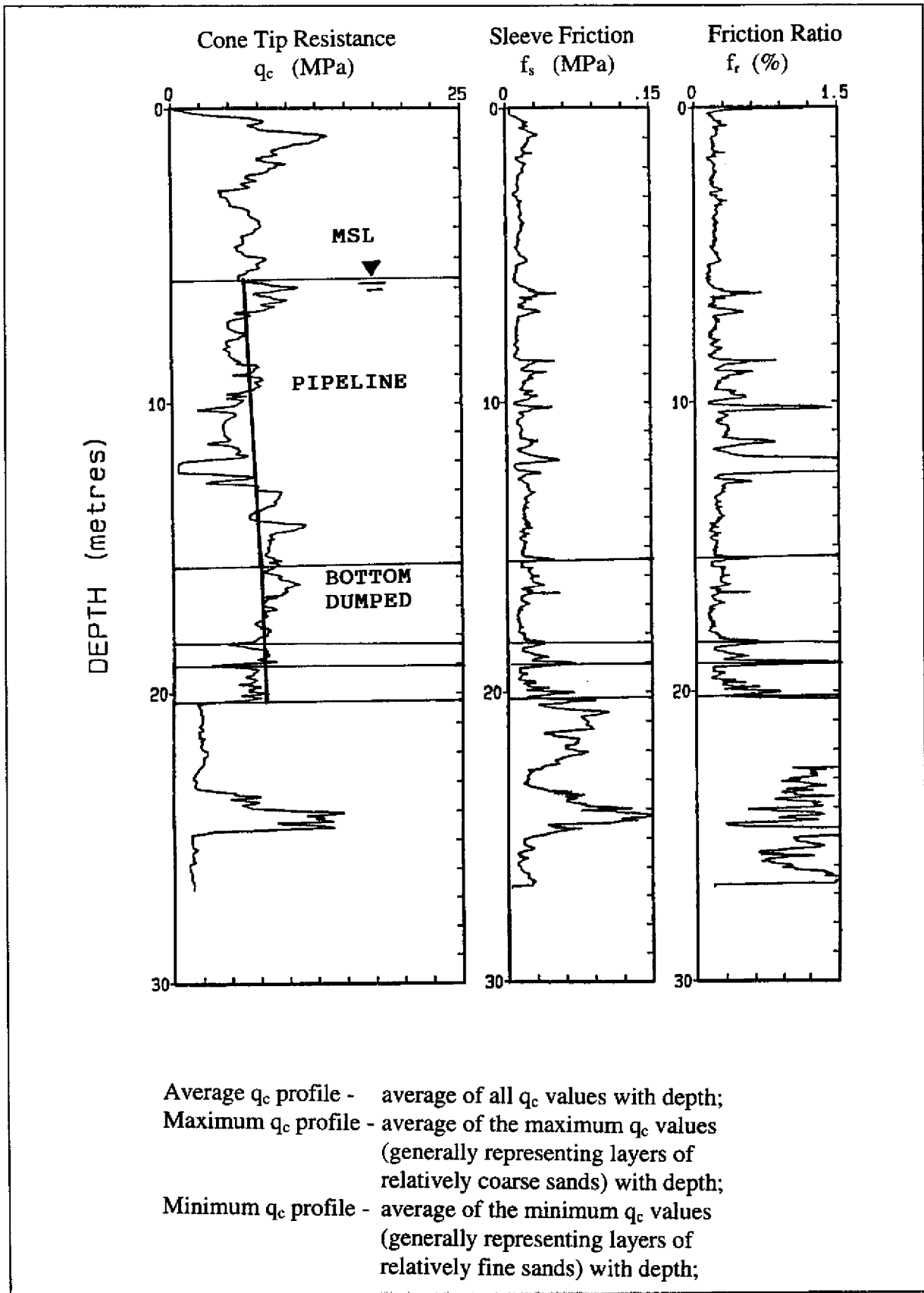
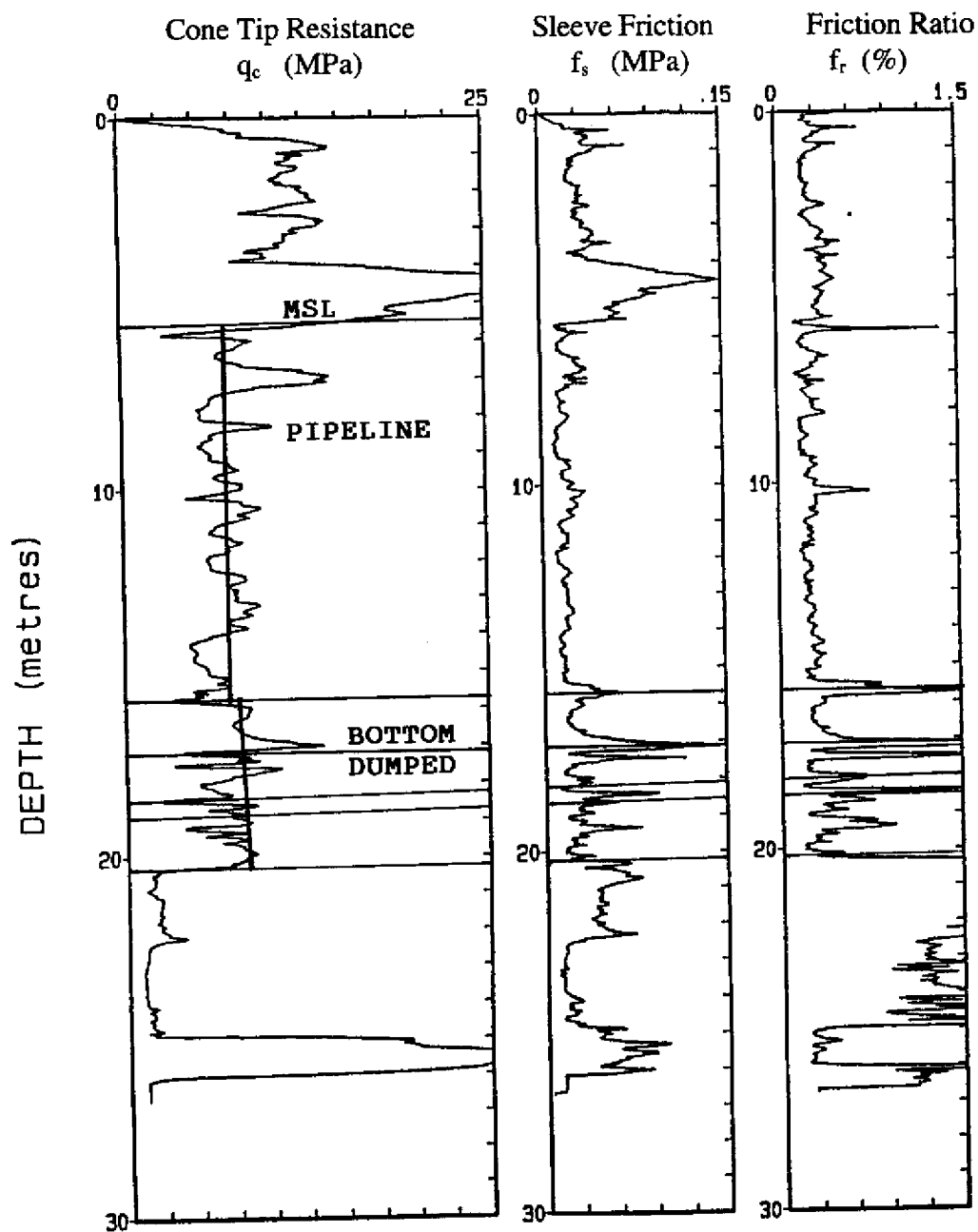


Figure 3.14(a) - Total Bottom Dumped Fill Thickness of 4.5 m Indicates
"POOR" Improvement in q_c Profile



Average q_c profile - average of all q_c values with depth;
Maximum q_c profile - average of the maximum q_c values
(generally representing layers of
relatively coarse sands) with depth;
Minimum q_c profile - average of the minimum q_c values
(generally representing layers of
relatively fine sands) with depth;

Figure 3.14(b) - Total Bottom Dumped Fill Thickness of 4 m Indicates
"POOR" Improvement in q_c Profile

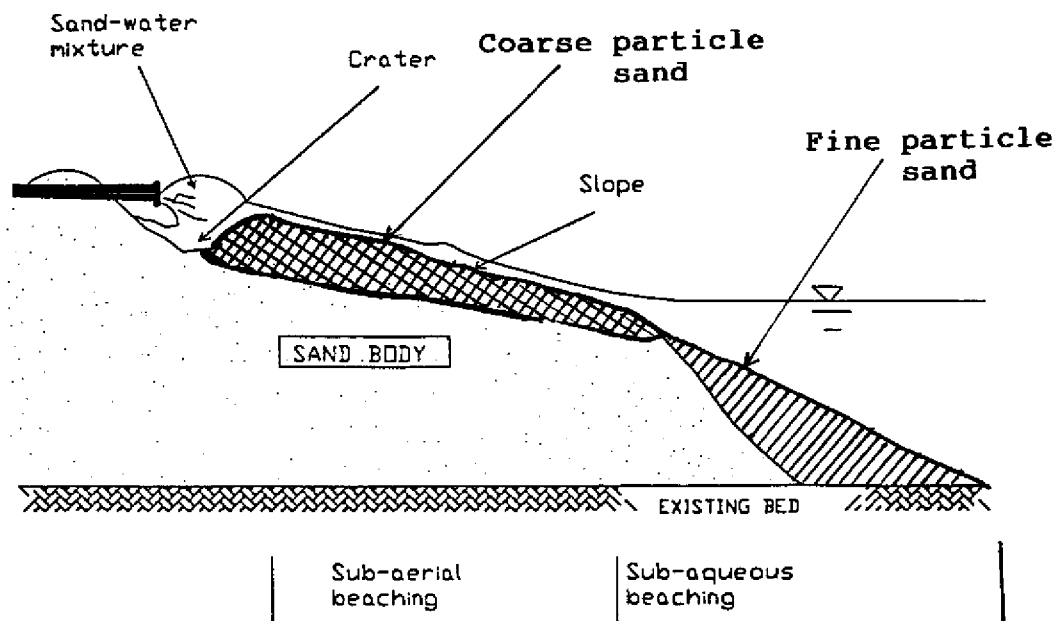


Figure 3.15 - Distribution of Sand Particles in Subaerial Beaching by Pipeline Discharge Method

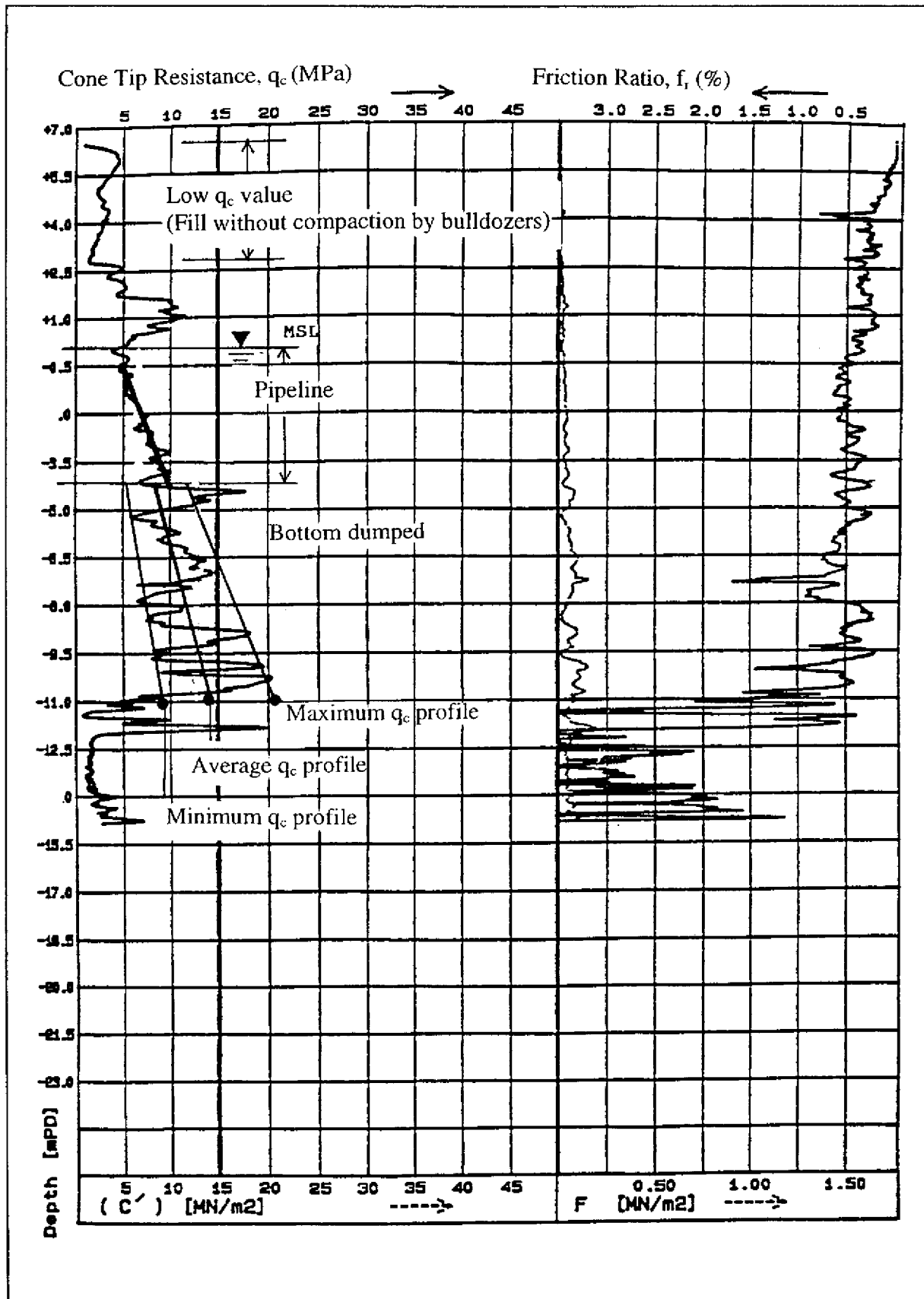


Figure 3.16 - CPT Profile at CS1 Showing Low q_c Value above Sea Level without any Compaction Work by Bulldozers

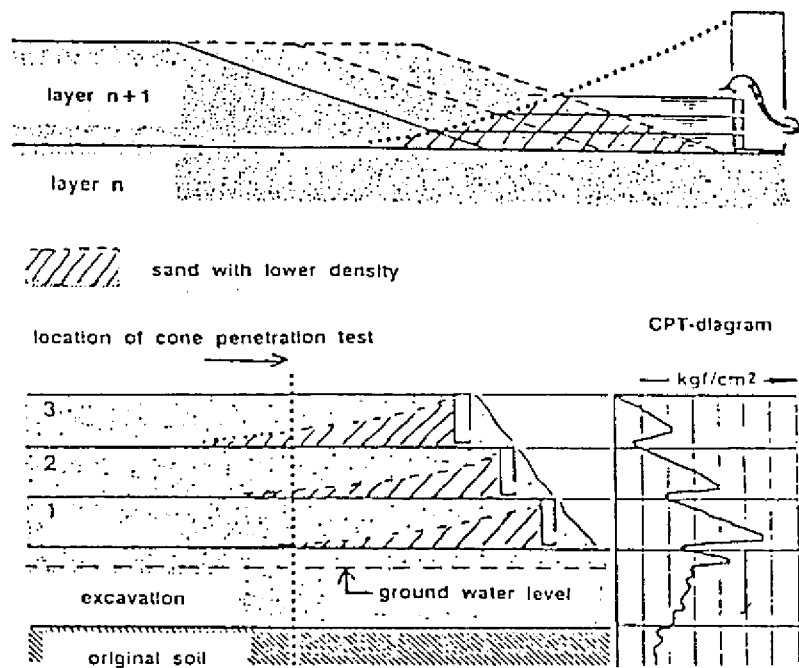


Figure 3.17 - Situation at the End of a Subaerial Hydraulic Sand Fill
(after Verkerke and Volbeda, 1991)

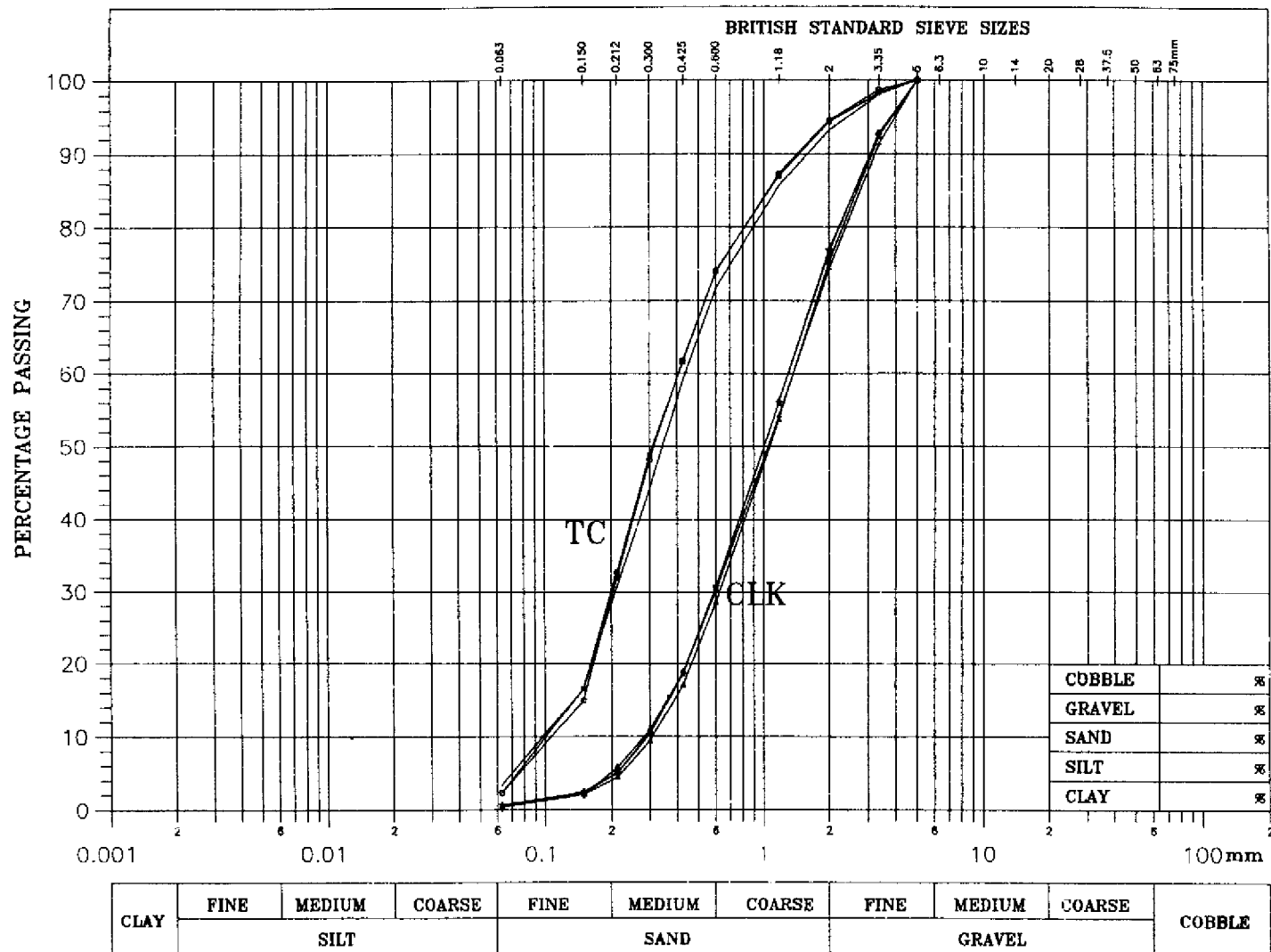


Figure 4.1 - Grain Size Distribution Curves of the Well Mixed TC and CLK Bulk Samples

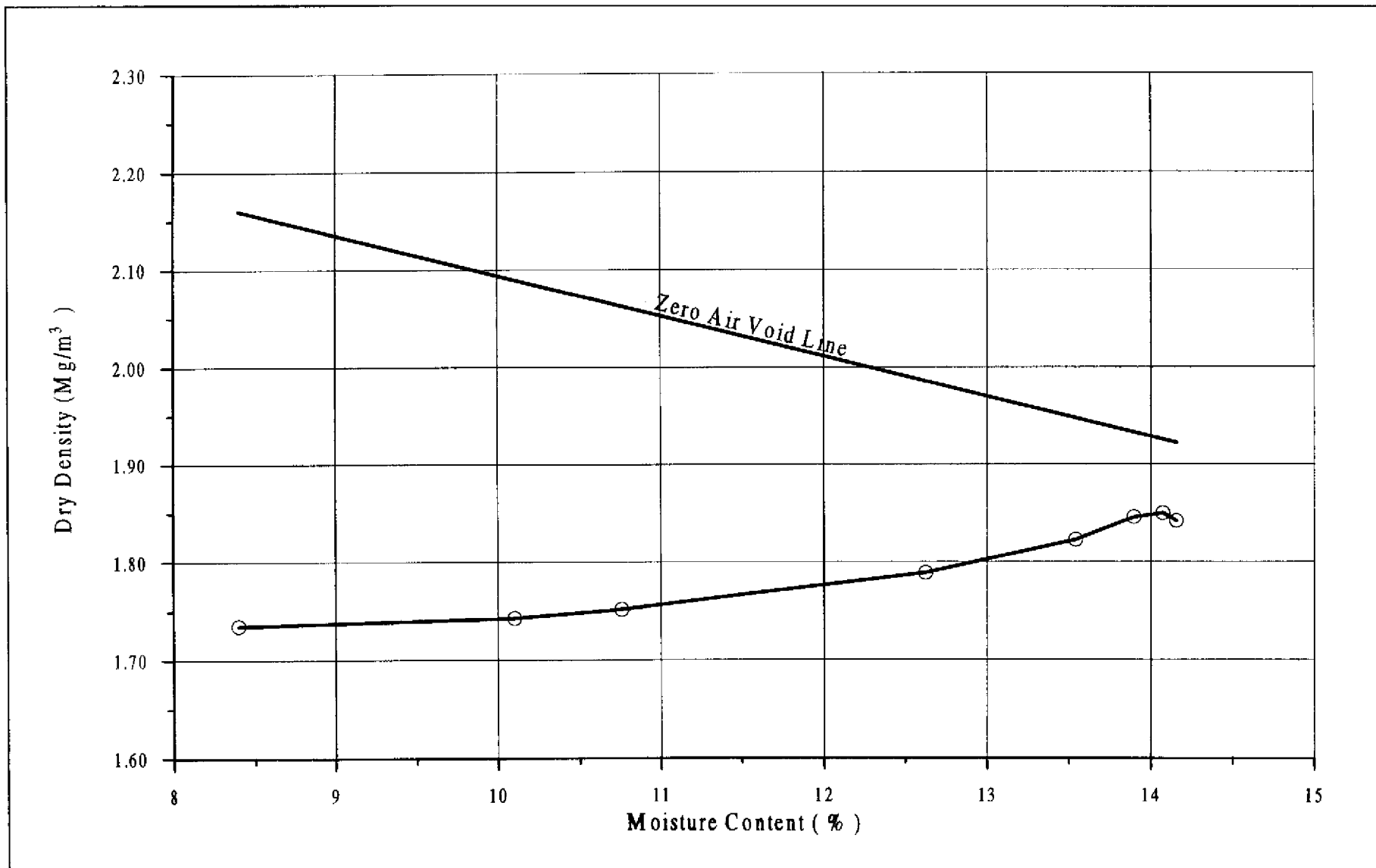


Figure 4.2 - Compaction Test Results of CLK Sand

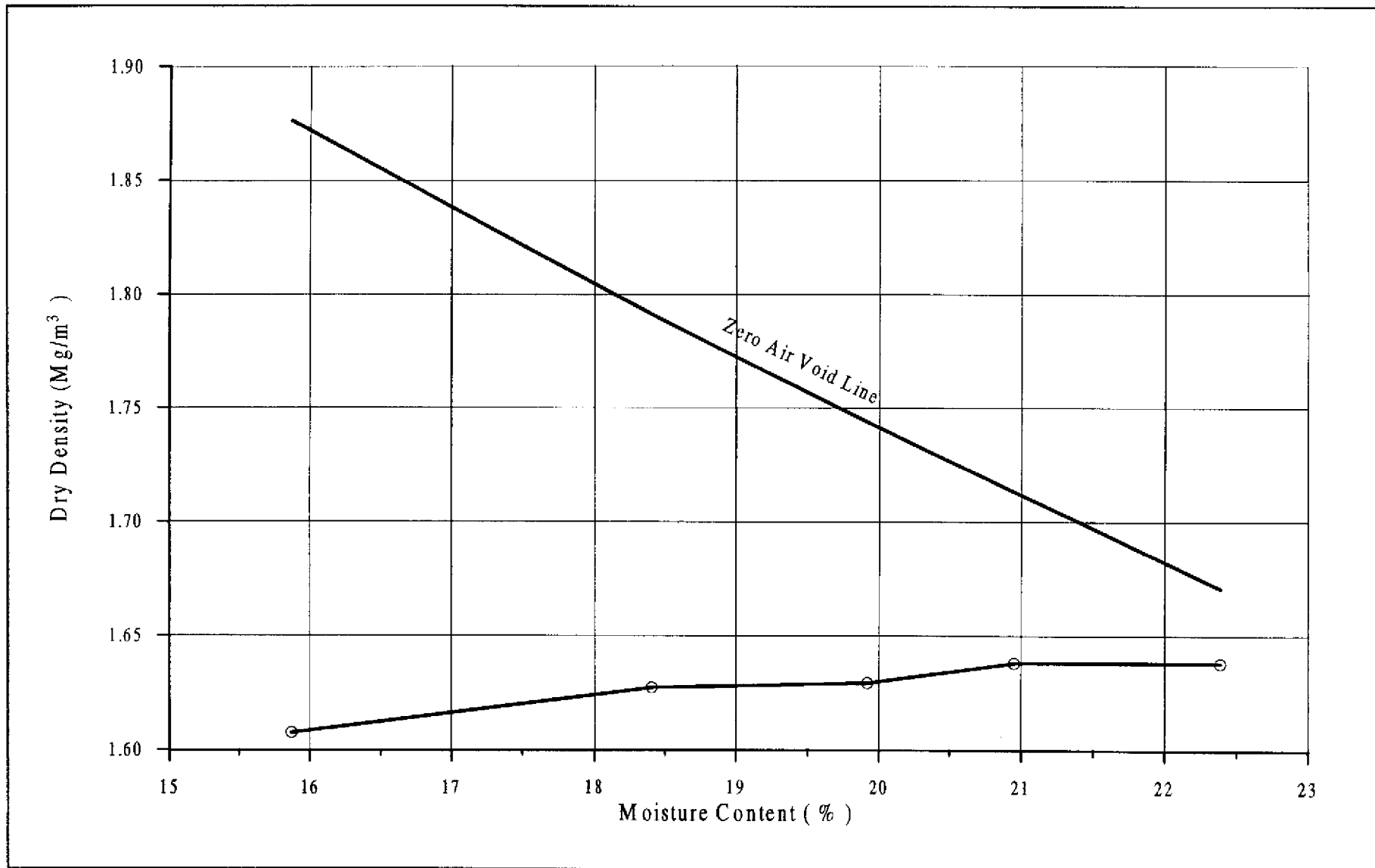


Figure 4.3 - Compaction Test Results of TC Sand

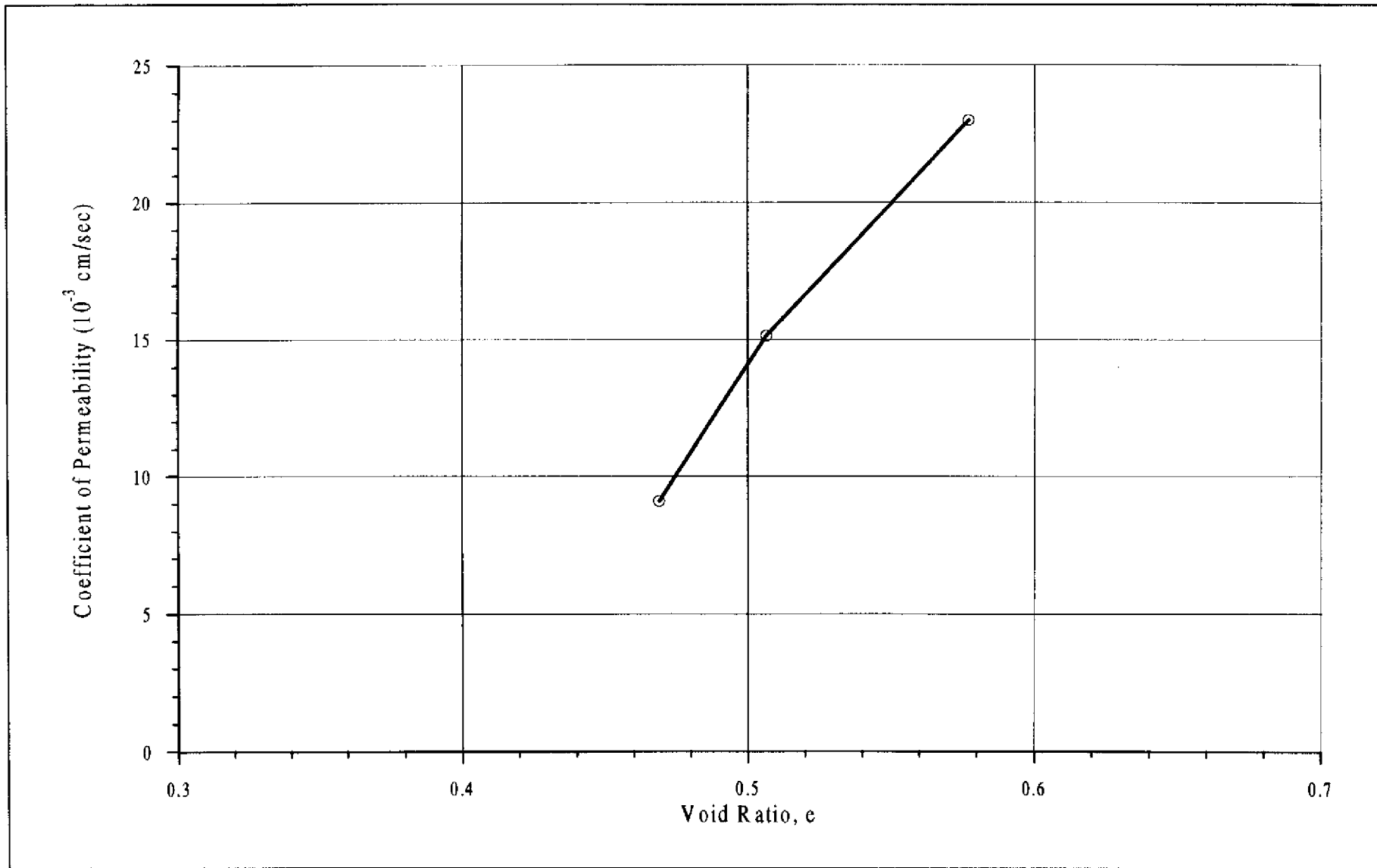


Figure 4.4 - Coefficient of Permeability of CLK Sand

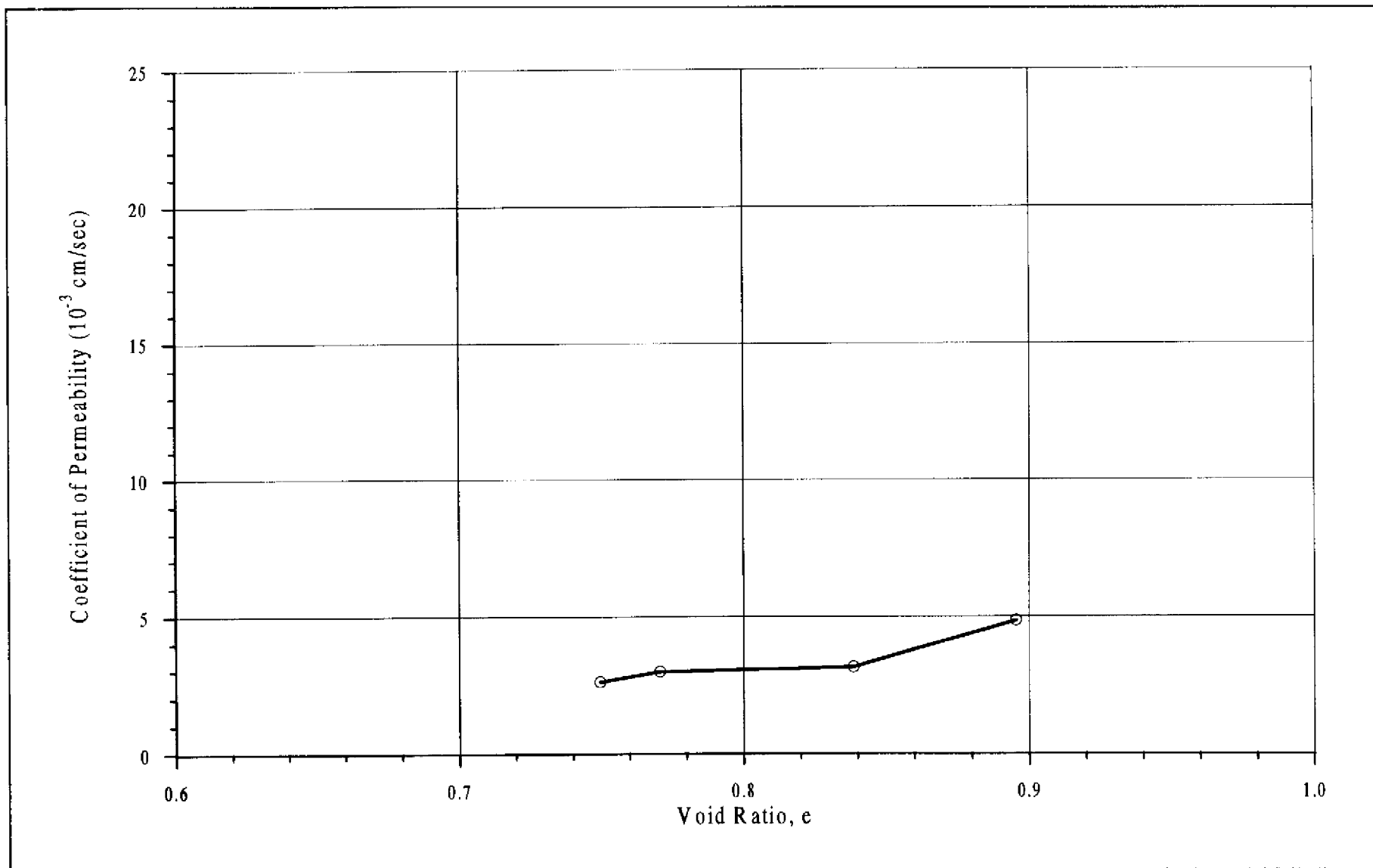
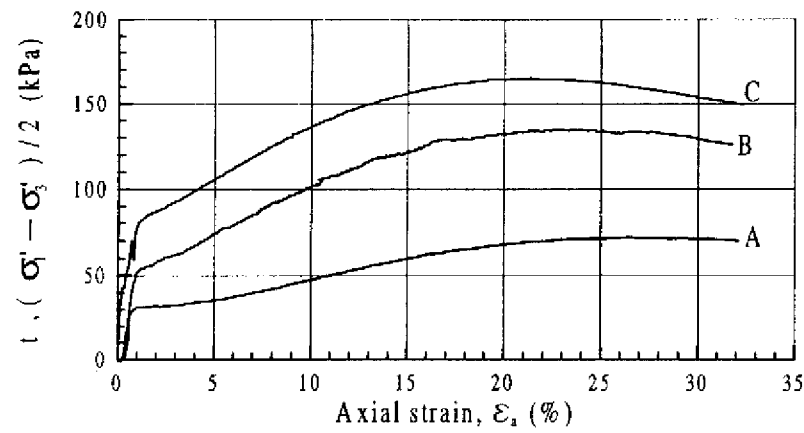
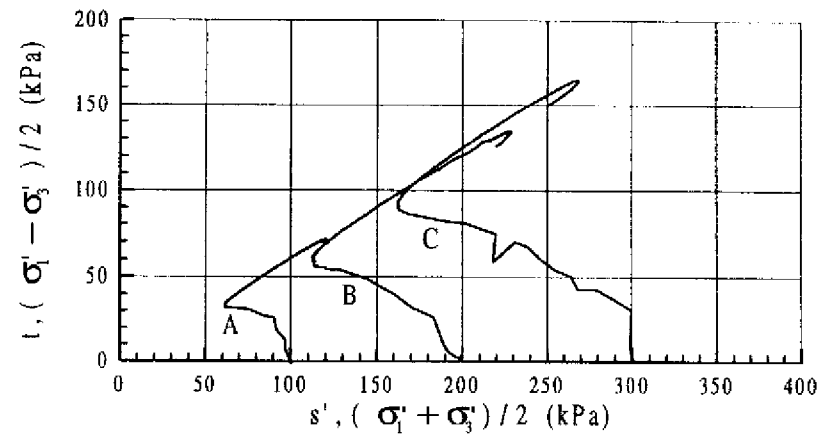


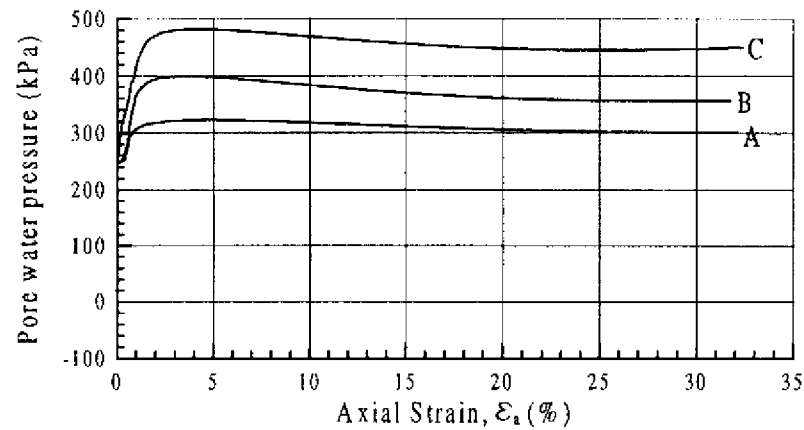
Figure 4.5 - Coefficient of Permeability of TC Sand



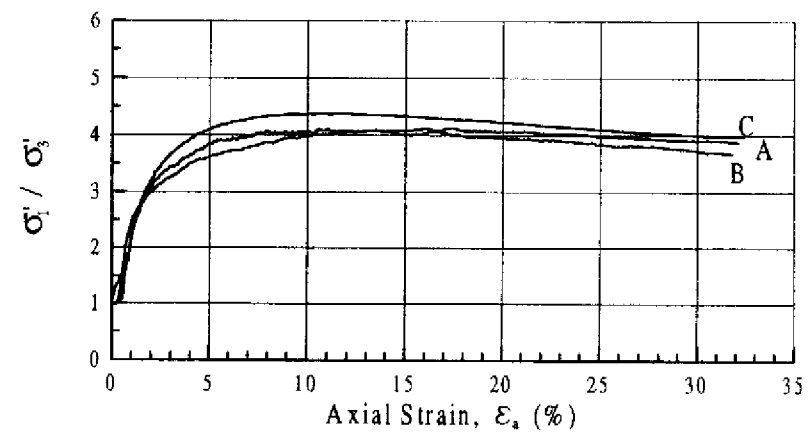
(a) t Vs. Axial Strain



(b) t Vs. s'



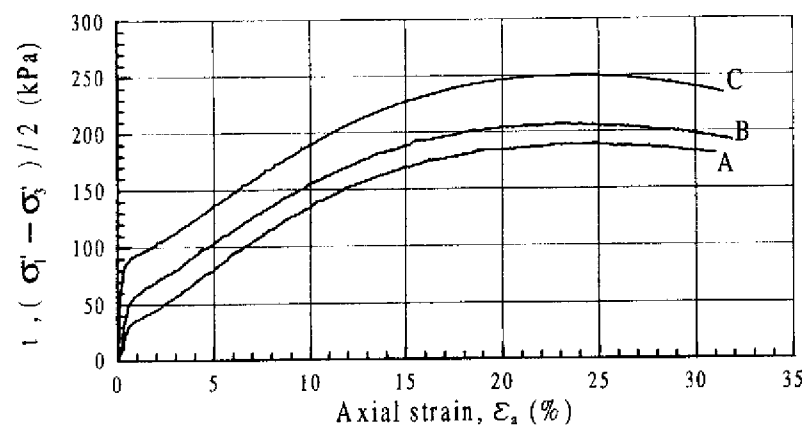
(c) Pore Water Pressure Vs. Axial Strain



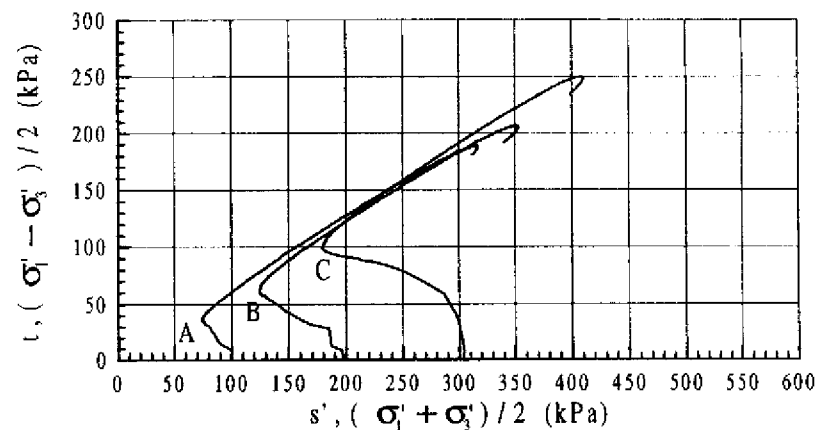
(d) σ_1' / σ_3' Vs. Axial Strain

File name : TCUS2CX	Dr = 36.50%	Consolidation stress = 100 kPa	Legend : A
File name : TCUS2A	Dr = 36.20%	Consolidation stress = 200 kPa	B
File name : TCUS2B	Dr = 38.90%	Consolidation stress = 300 kPa	C

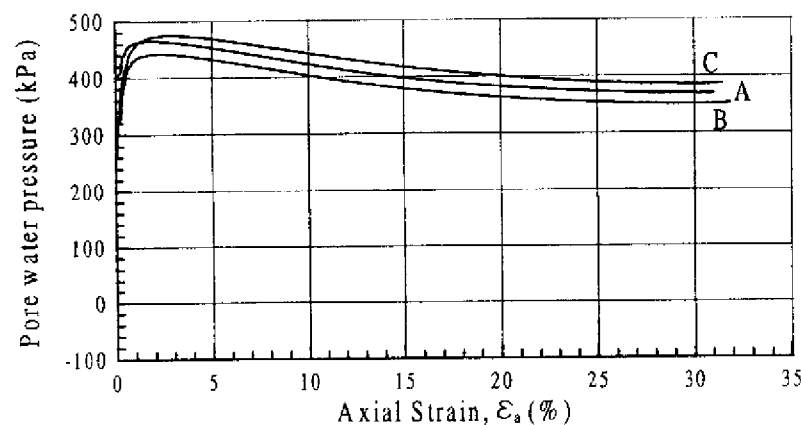
Figure 4.6 - Results of Triaxial Undrained Tests on the Tung Chung Sand with Relative Density 31.9% to 38.9%



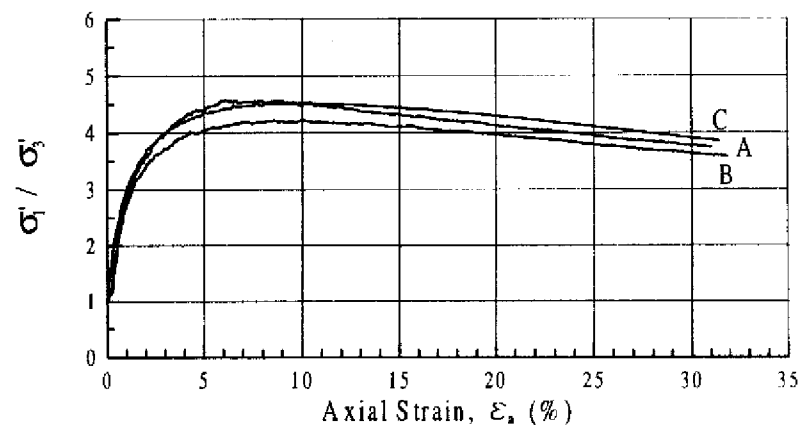
(a) t Vs. Axial Strain



(b) t Vs. s'



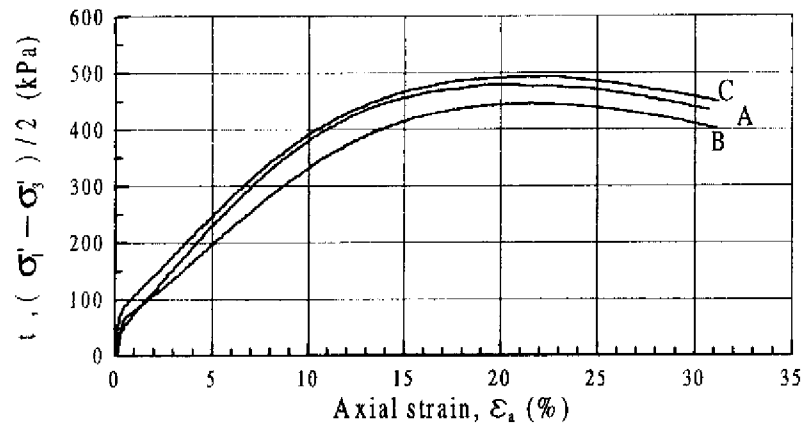
(c) Pore Water Pressure Vs. Axial Strain



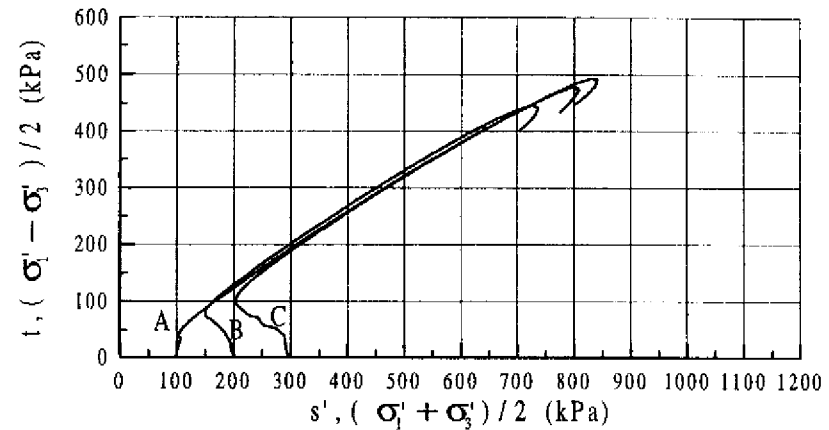
(d) σ'_1 / σ'_3 Vs. Axial Strain

File name : TCUS1F	Dr = 47.30%	Consolidation stress = 100 kPa	Legend : A
File name : TCUS1D	Dr = 49.70%	Consolidation stress = 200 kPa	B
File name : TCUS1E	Dr = 53.00%	Consolidation stress = 300 kPa	C

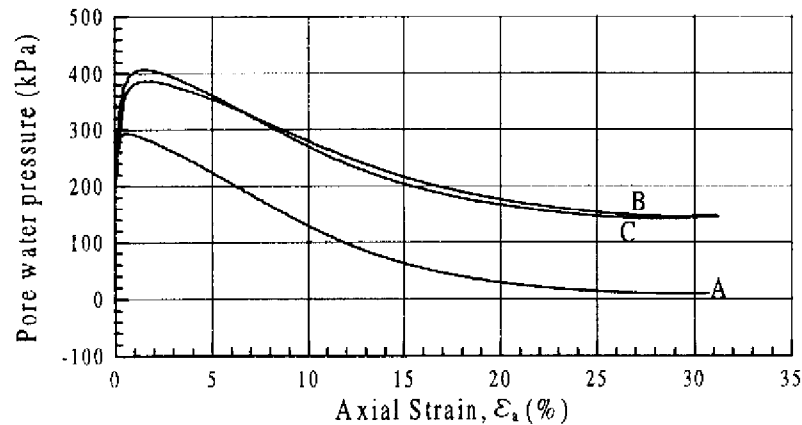
Figure 4.7 - Results of Triaxial Undrained Tests on the Tung Chung Sand with Relative Density 47.3% to 53.0%



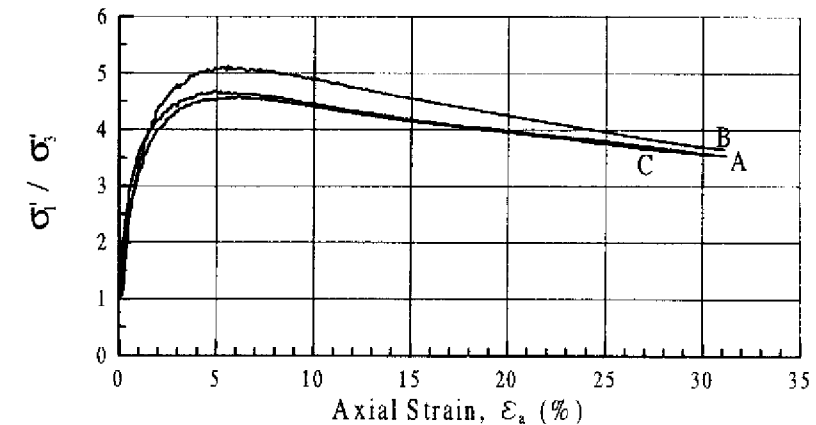
(a) t Vs. Axial Strain



(b) t Vs. s'



(c) Pore Water Pressure Vs. Axial Strain



(d) σ'_1 / σ'_3 Vs. Axial Strain

File name : TCUS3C	Dr = 69.50%	Consolidation stress = 100 kPa	Legend : A
File name : TCUS3B	Dr = 67.10%	Consolidation stress = 200 kPa	B
File name : TCUS3A	Dr = 69.30%	Consolidation stress = 300 kPa	C

Figure 4.8 - Results of Triaxial Undrained Tests on the Tung Chung Sand with Relative Density 67.1% to 69.5%

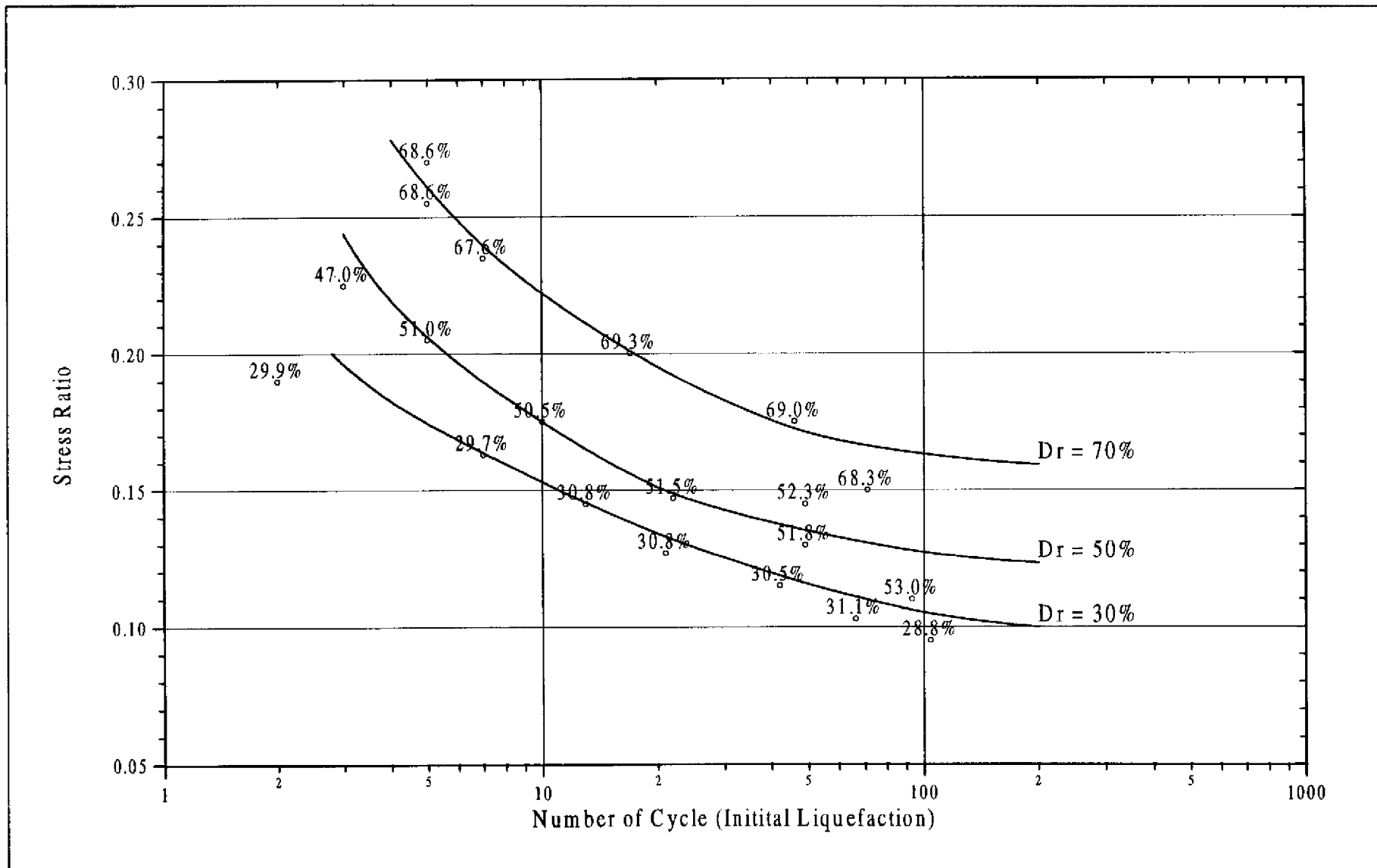


Figure 4.9 - Liquefaction Potential Curves for the Tung Chung Sand

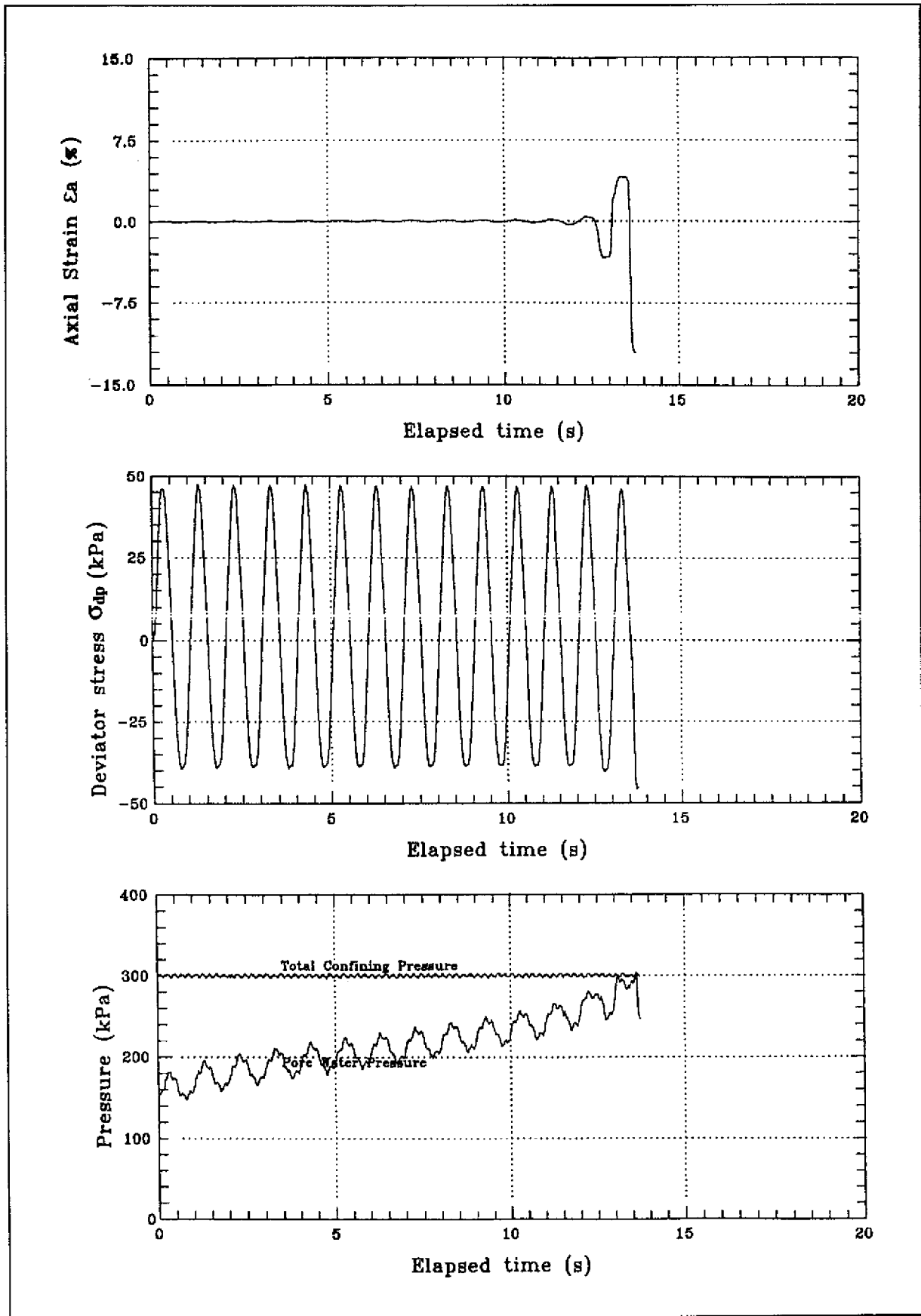


Figure 4.10(a) - Typical Cyclic Test Results on TC Sand ($D_r = 30.8\%$, $S.R. = 0.145$)

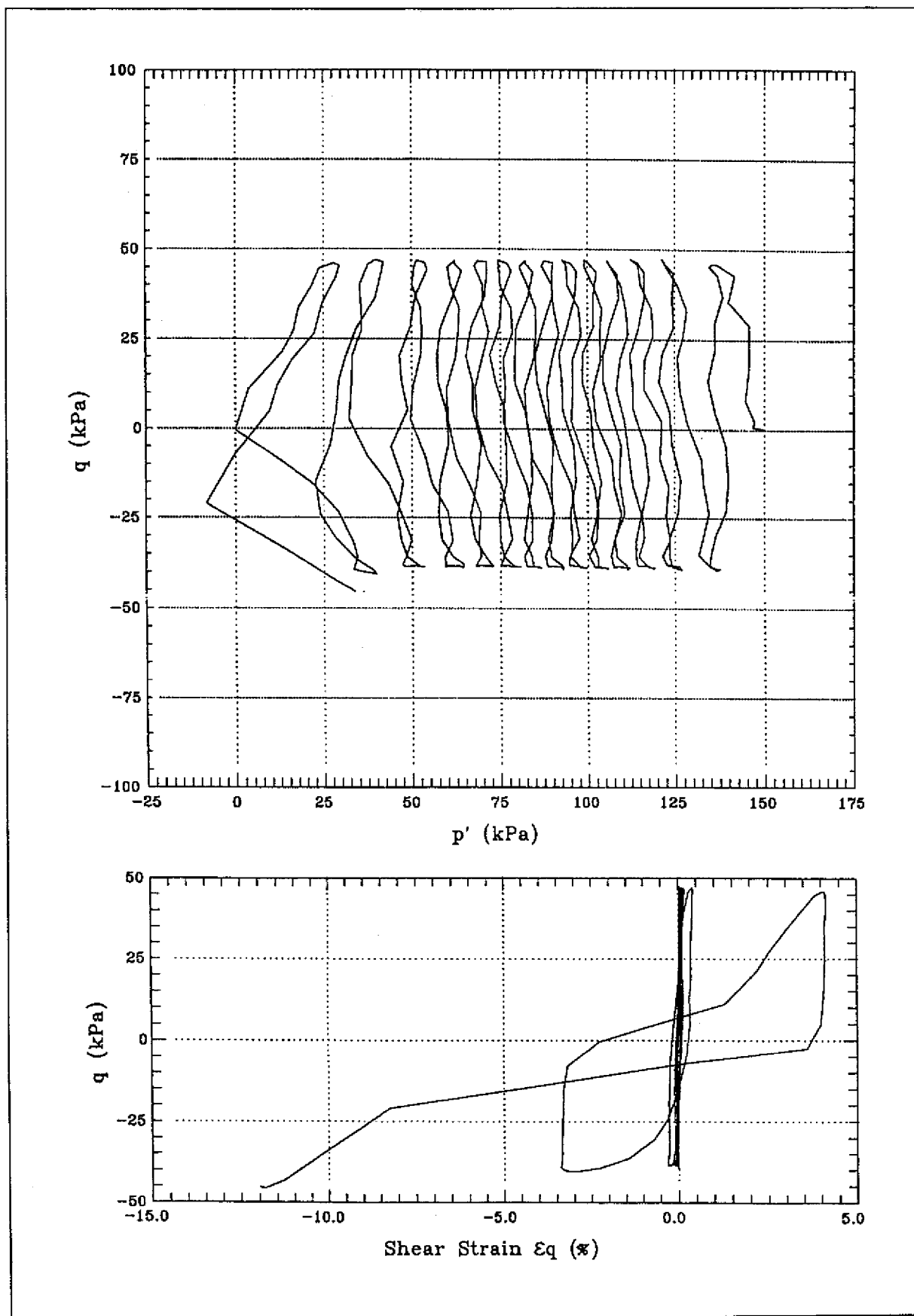


Figure 4.10(b) - Typical Cyclic Test Results on TC Sand ($D_r = 30.8\%$, $S.R. = 0.145$)

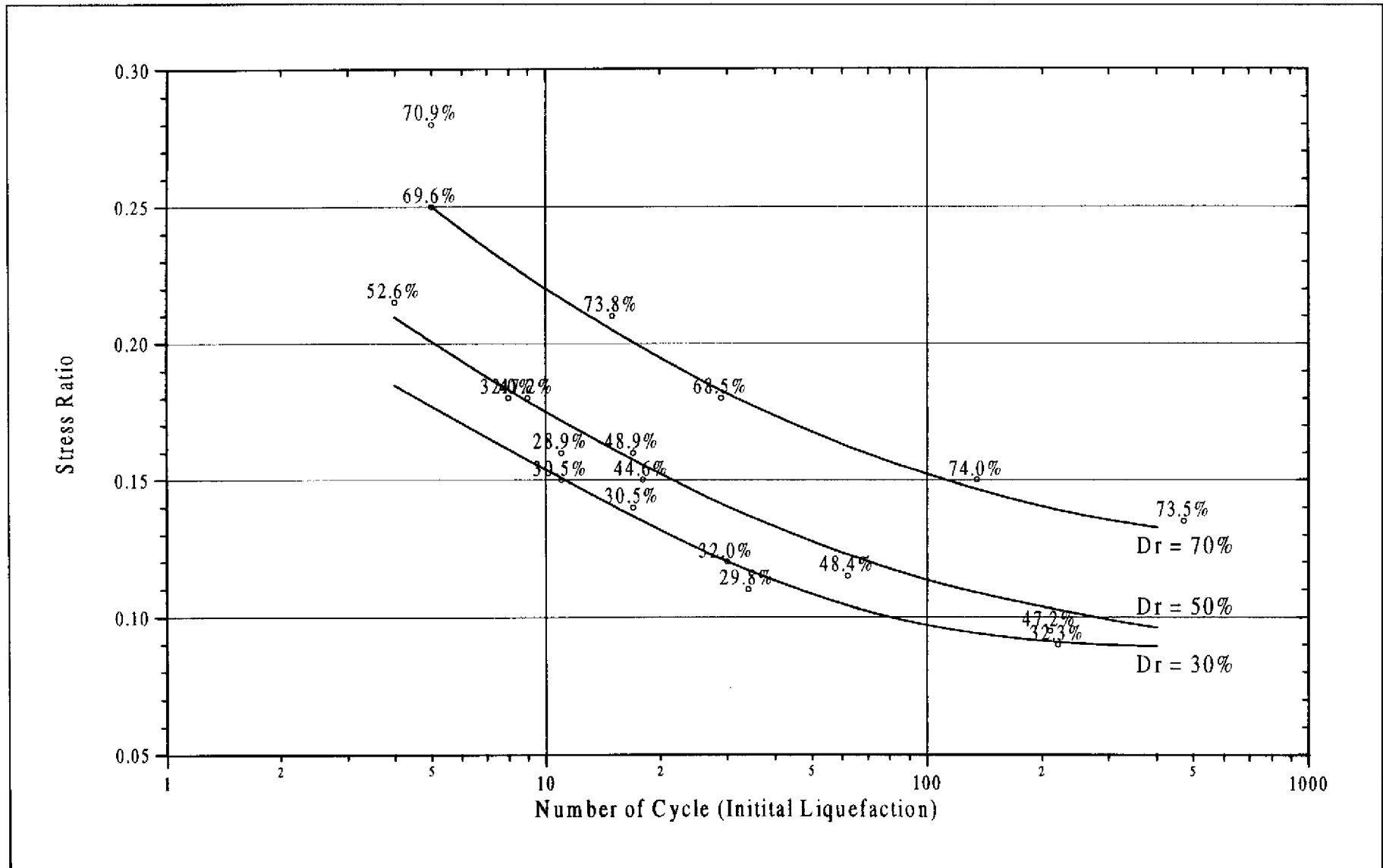


Figure 4.11 - Liquefaction Potential Curves for the CLK Sand

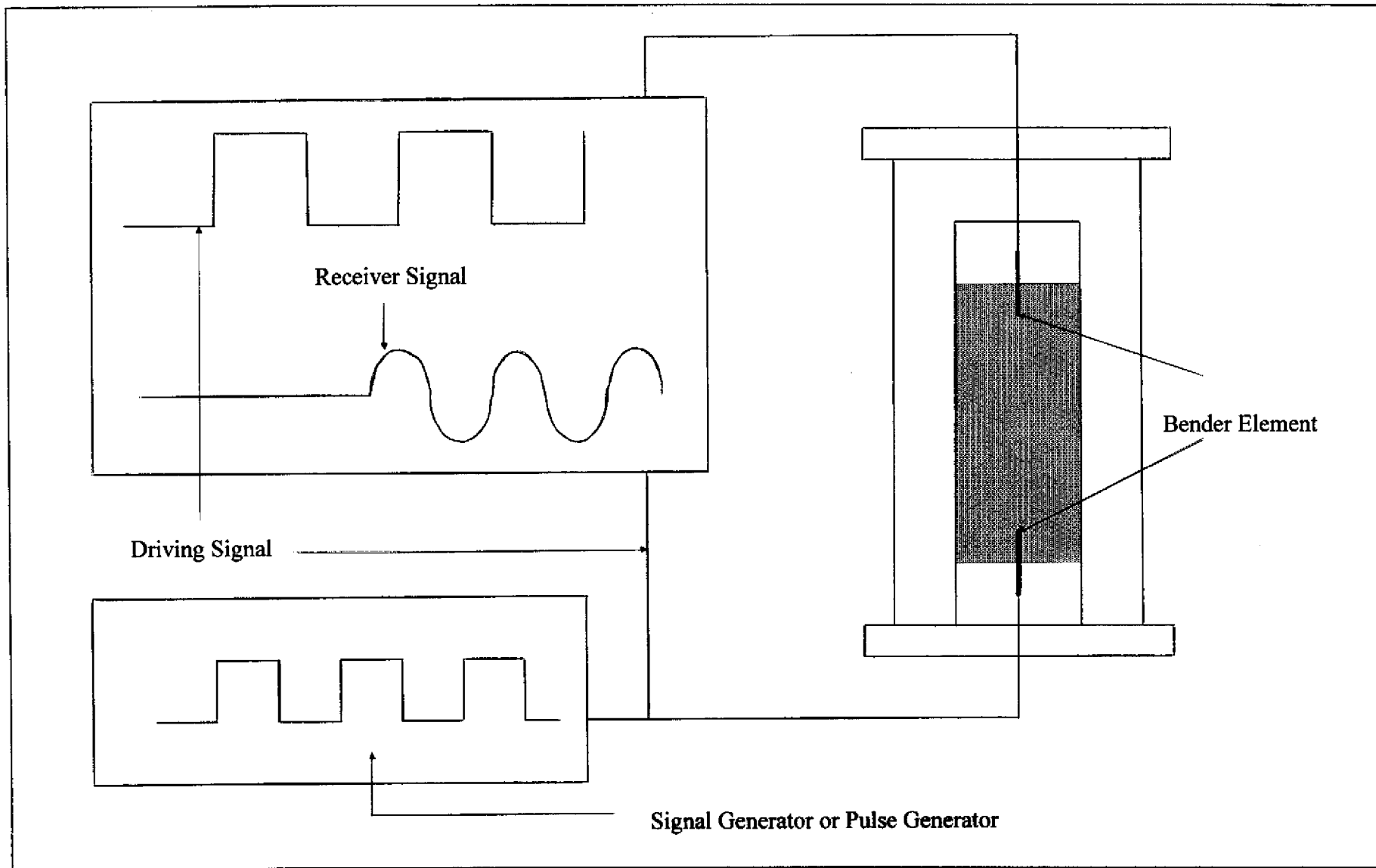


Figure 5.1 - Setup of Bender Element (Shear Wave Velocity Measurement)

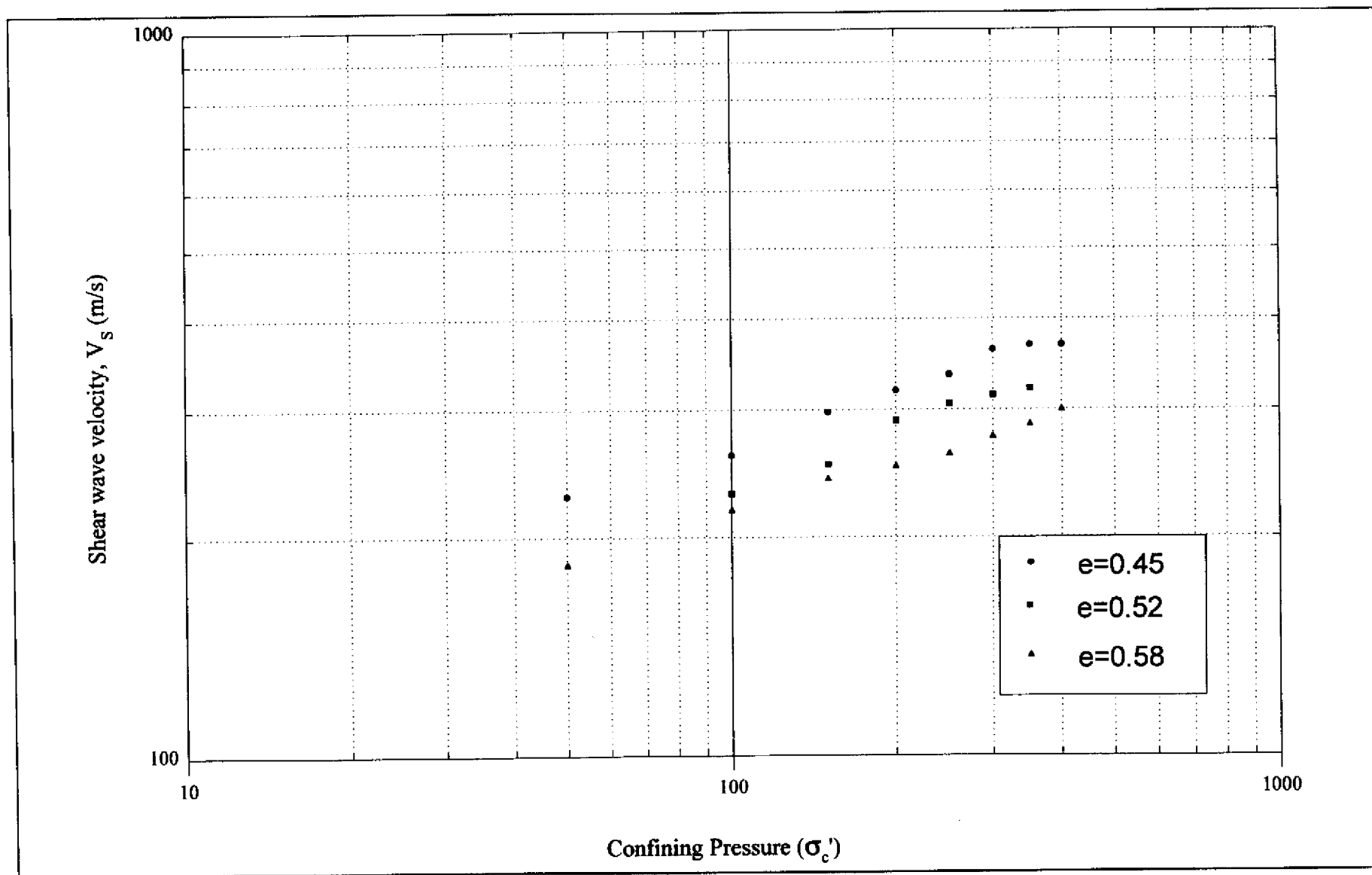


Figure 5.2 - Shear Wave Velocity (V_s) versus Confining Pressure (σ'_c) Chek Lap Kok Sand

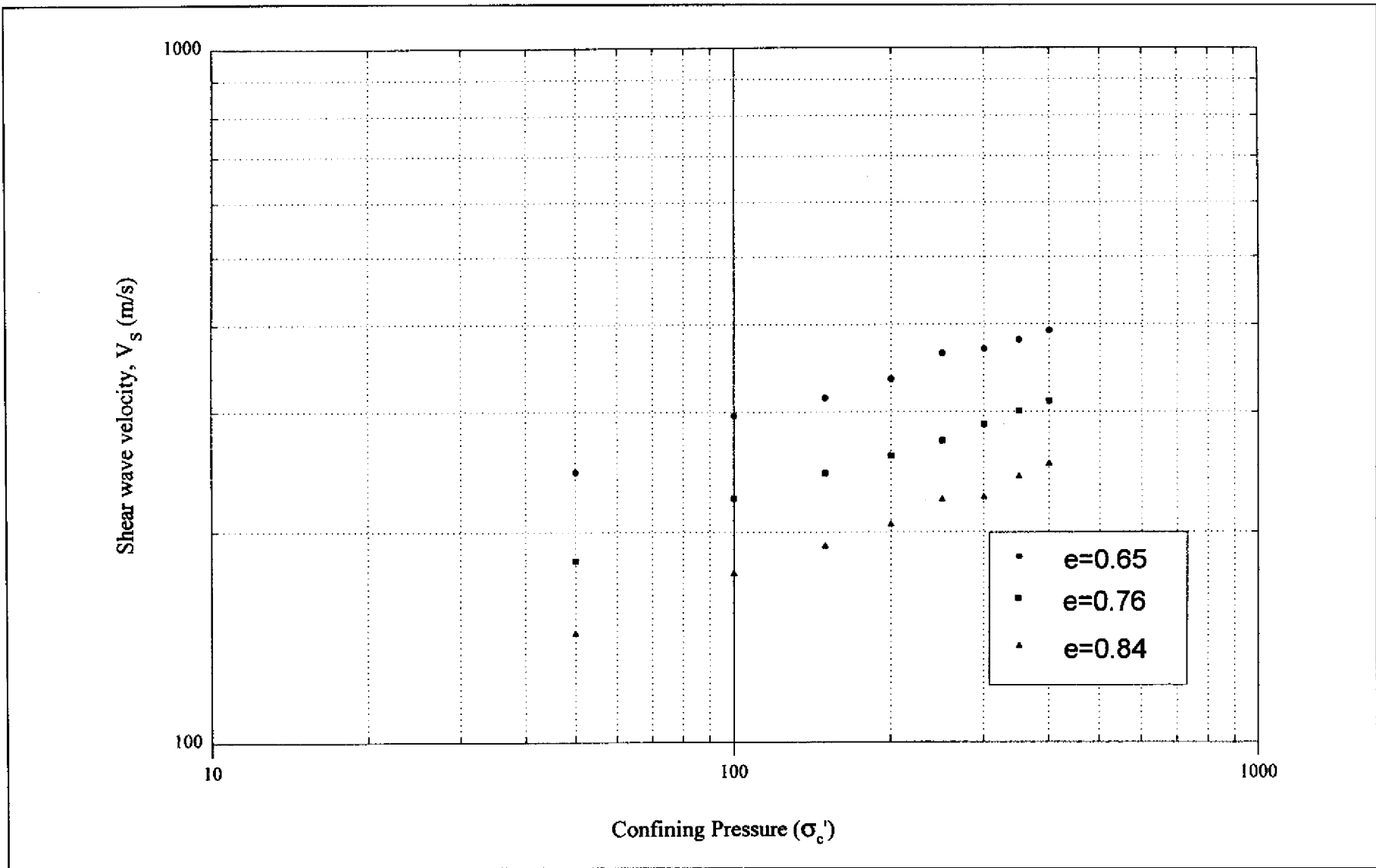


Figure 5.3 - Shear Wave Velocity (V_s) versus Confining Pressure (σ'_c) Tung Chung Sand

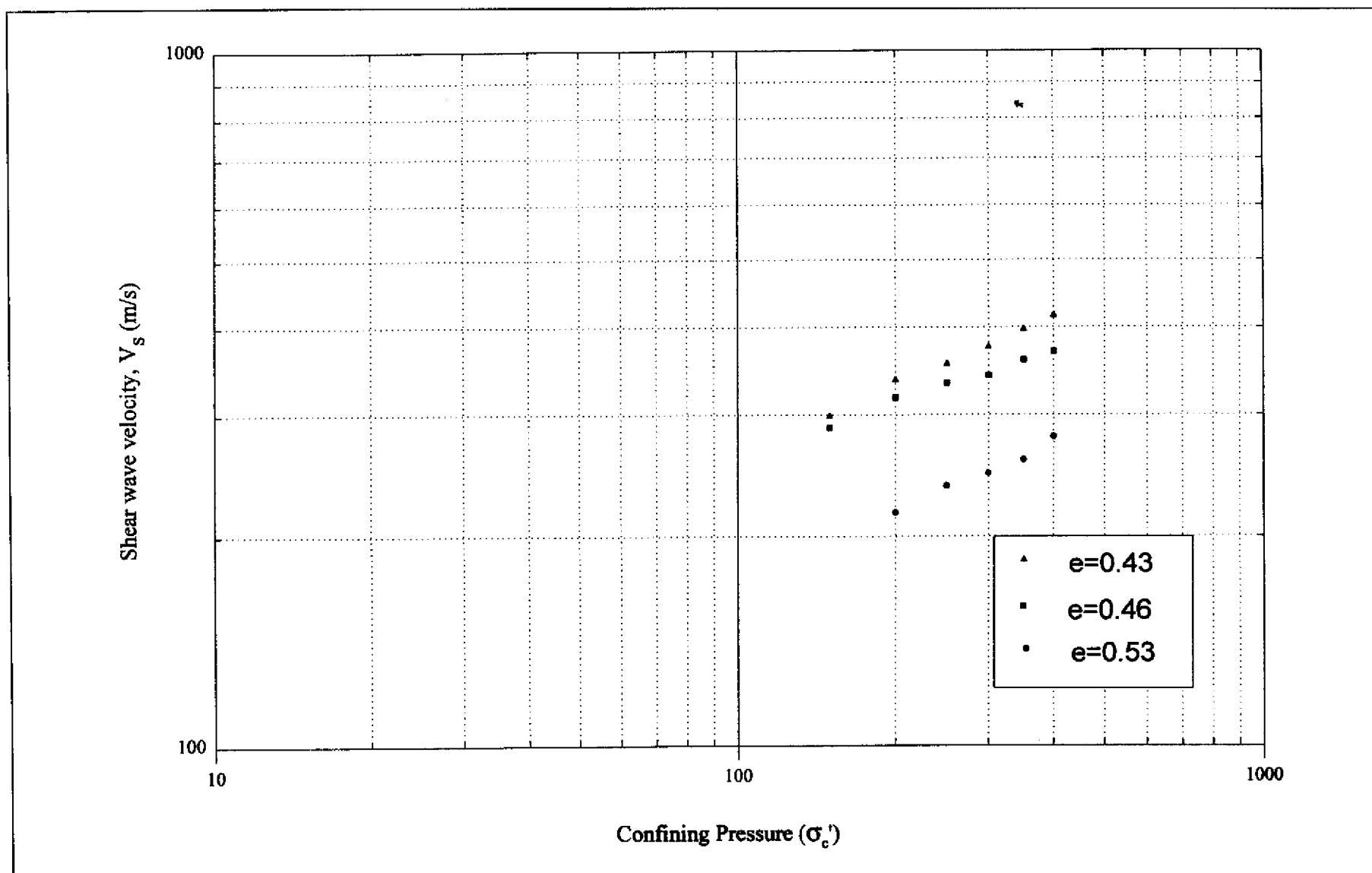


Figure 5.4 - Shear Wave Velocity (V_s) versus Confining Pressure (σ'_c) West Kowloon Sand

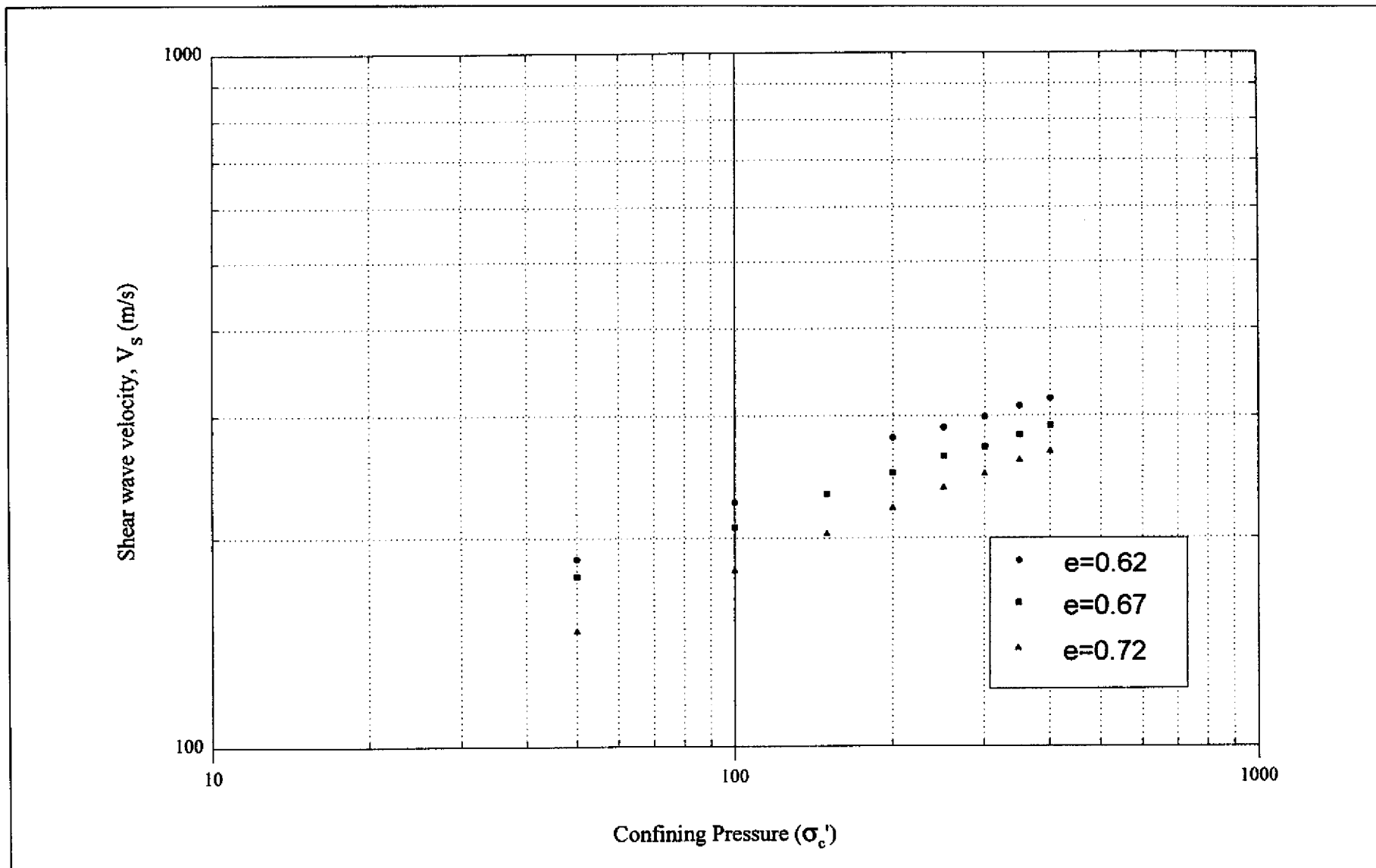


Figure 5.5 - Shear Wave Velocity (V_s) versus Confining Pressure (σ'_c) Tseung Kwan O Sand

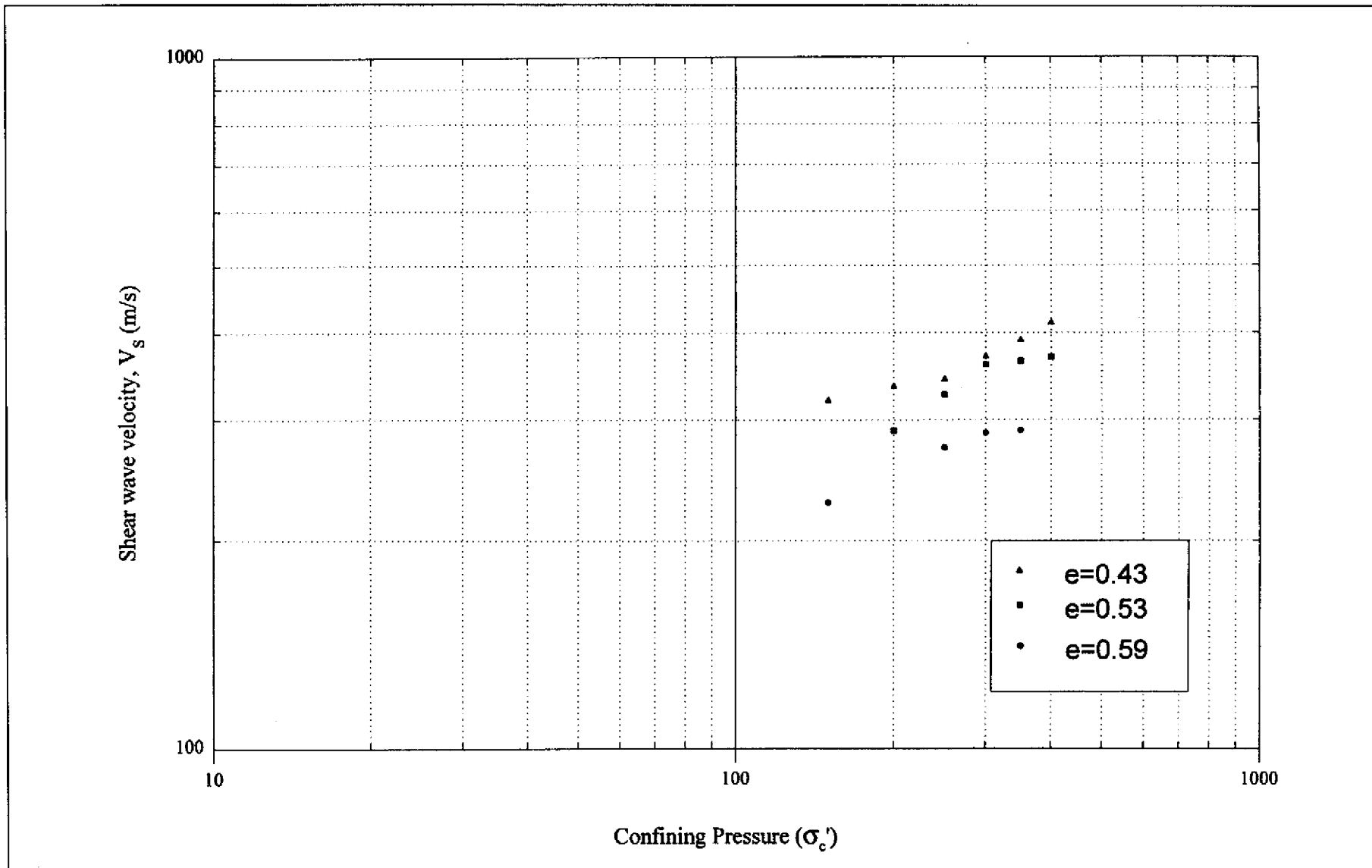


Figure 5.6 - Shear Wave Velocity (V_s) versus Confining Pressure (σ'_c) Tin Shui Wai Sand

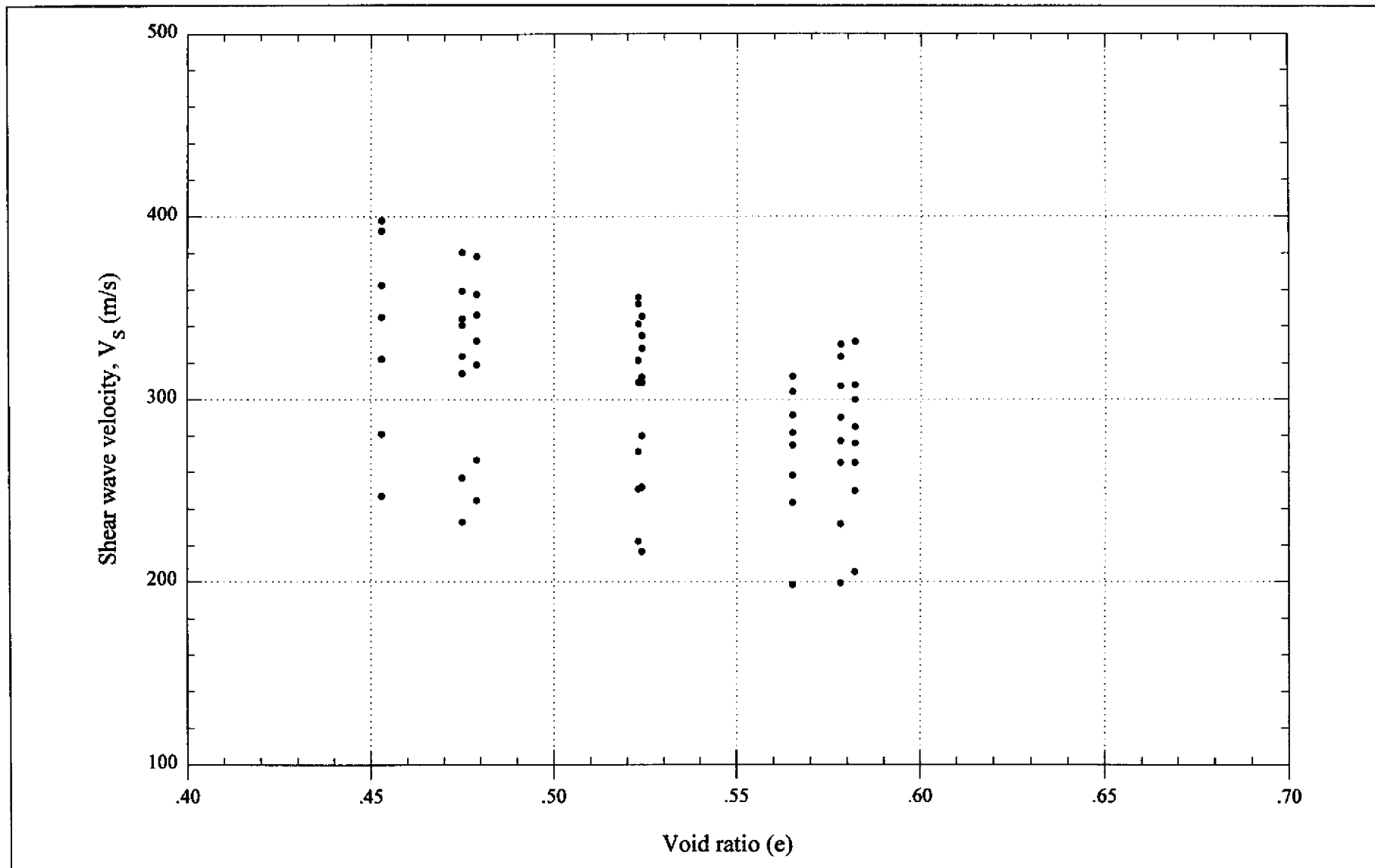


Figure 5.7 - Shear Wave Velocity (V_s) versus Void Ratio (e) Chek Lap Kok Sand

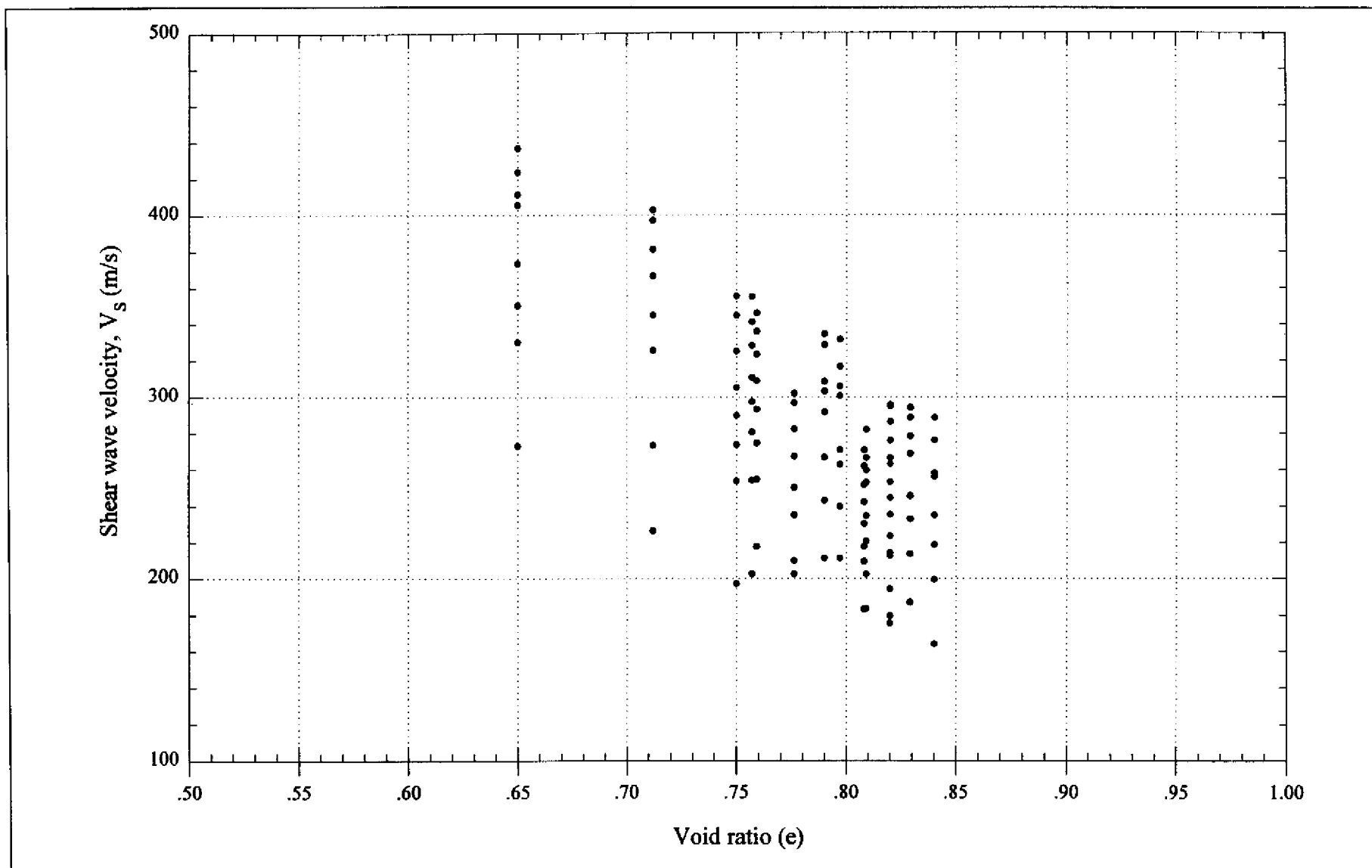


Figure 5.8 - Shear Wave Velocity (V_s) versus Void Ratio (e) Tung Chung Sand

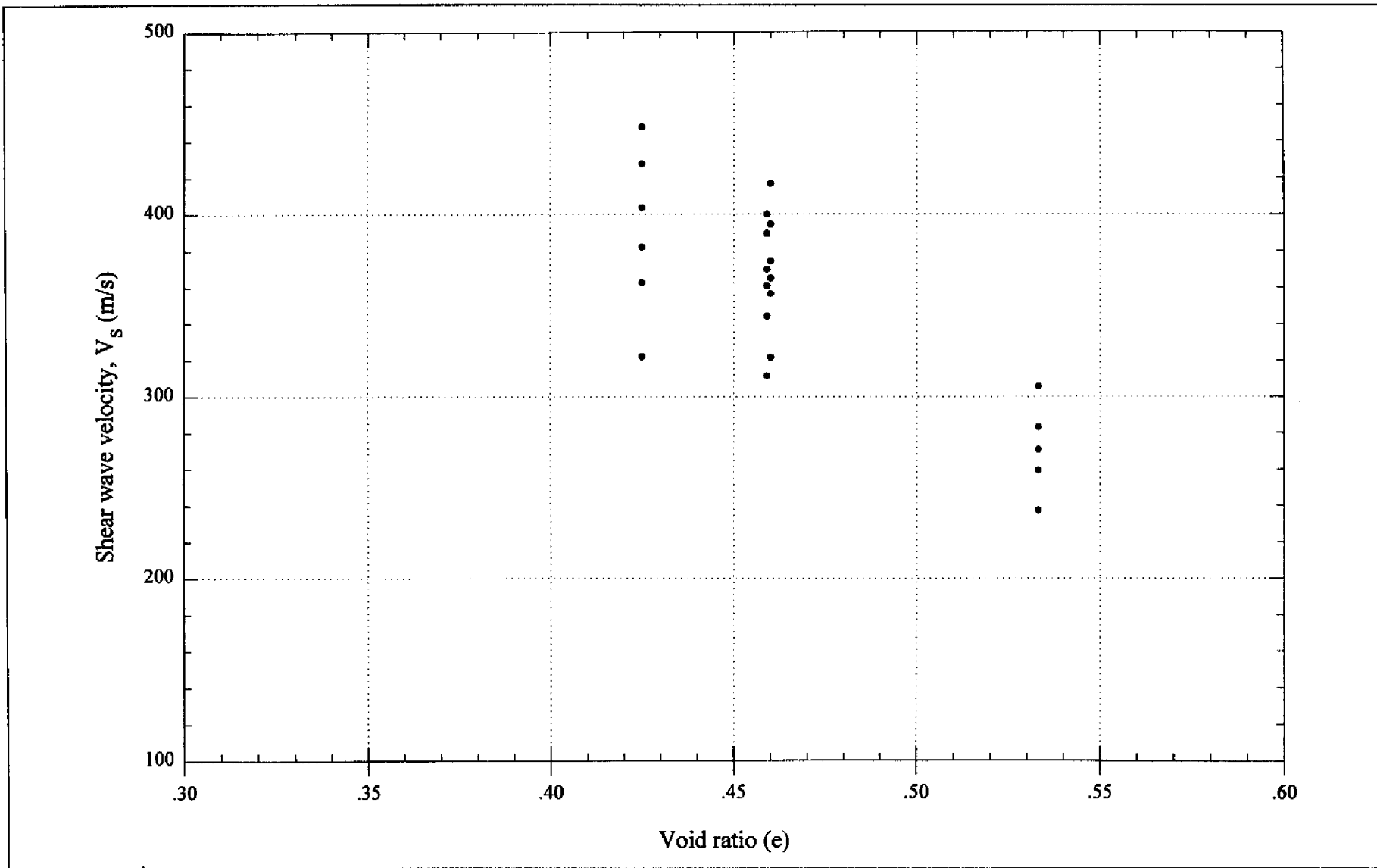


Figure 5.9 - Shear Wave Velocity (V_s) versus Void Ratio (e) West Kowloon Sand

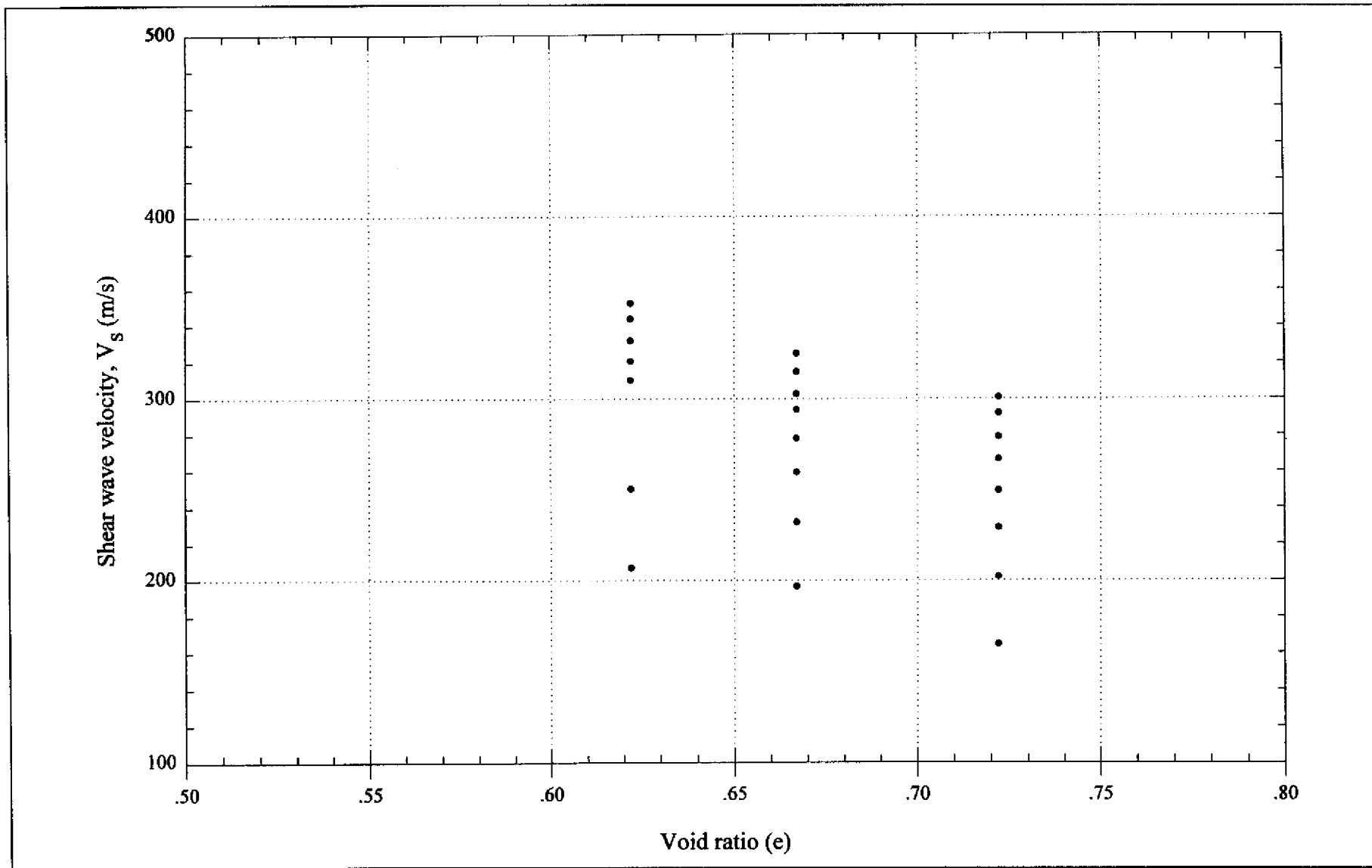


Figure 5.10 - Shear Wave Velocity (V_s) versus Void Ratio (e) Tseung Kwan O Sand

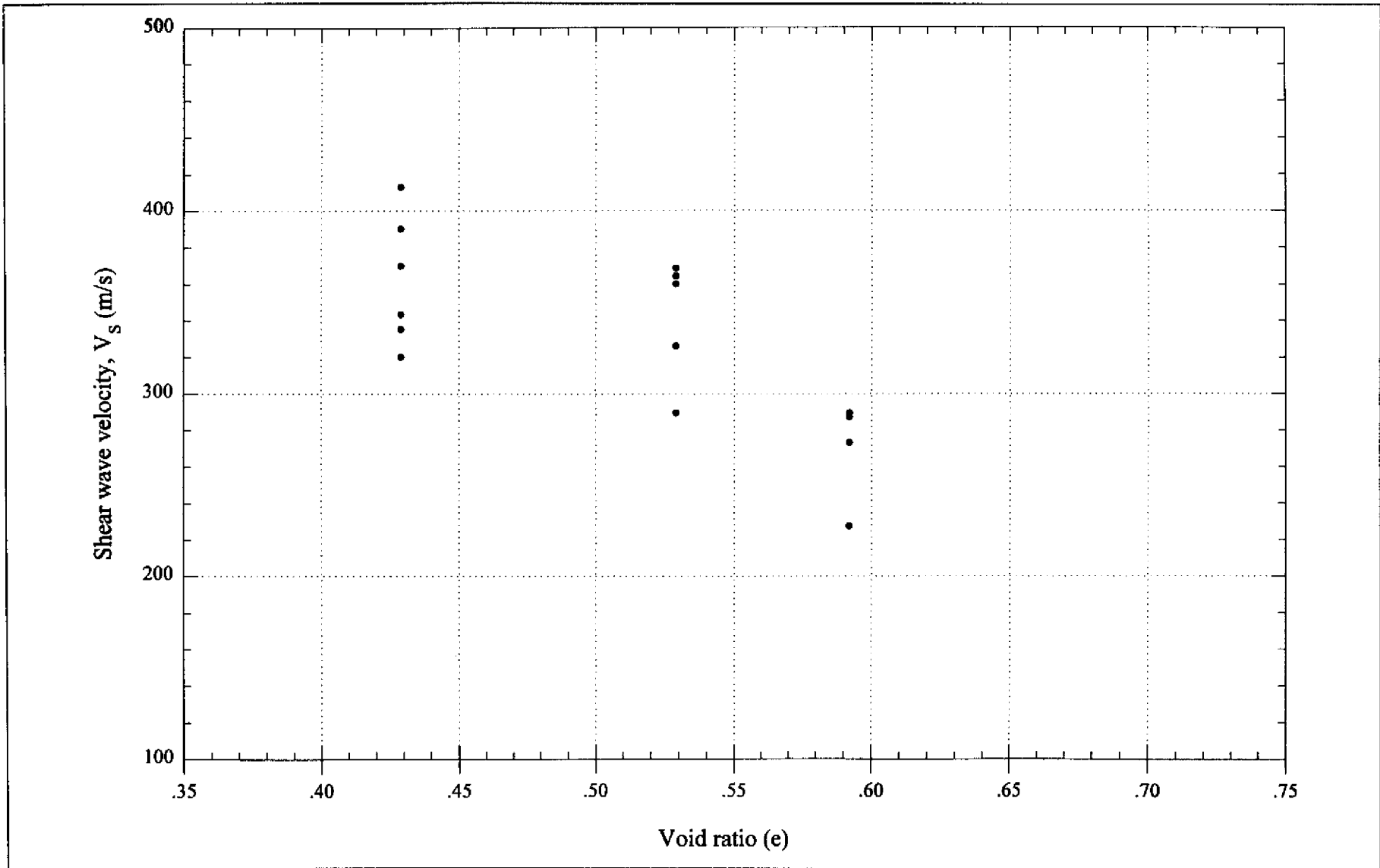


Figure 5.11 - Shear Wave Velocity (V_s) versus Void Ratio (e) Tin Shui Wai Sand

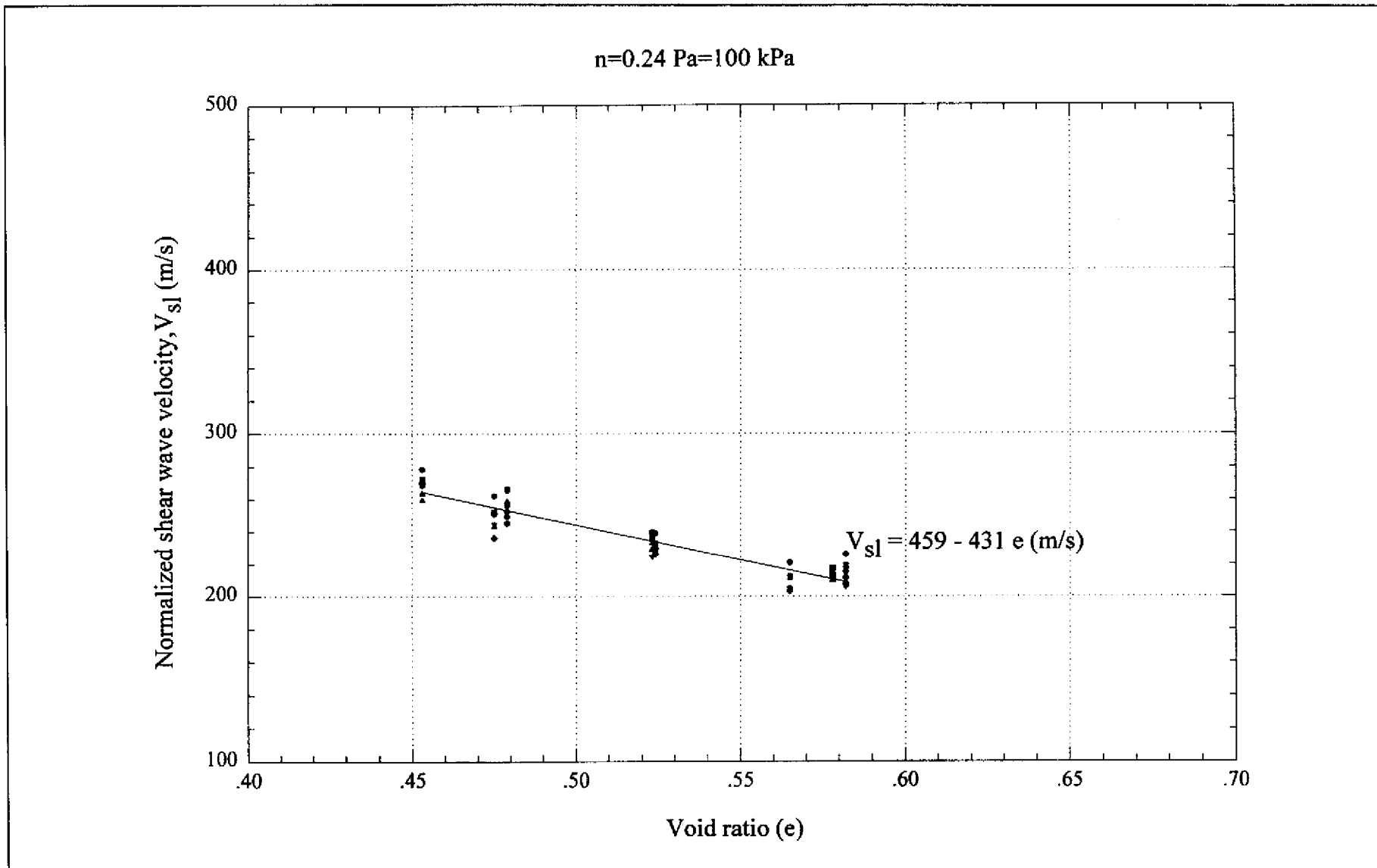


Figure 5.12 - Normalized Shear Wave Velocity (V_{sl}) versus Void Ratio (e) Chek Lap Kok Sand

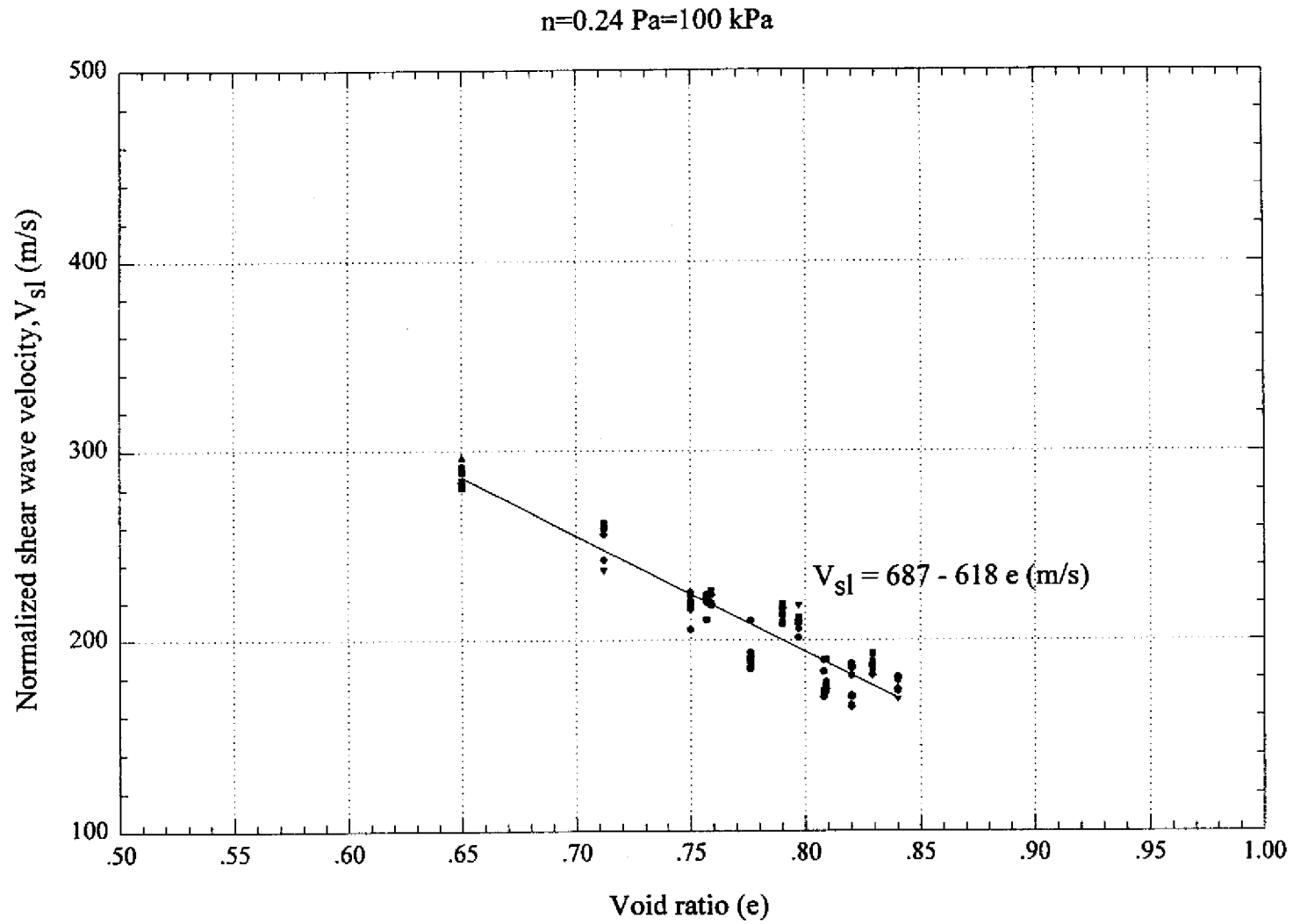


Figure 5.13 - Normalized Shear Wave Velocity (V_{sl}) versus Void Ratio (e) Tung Chung Sand

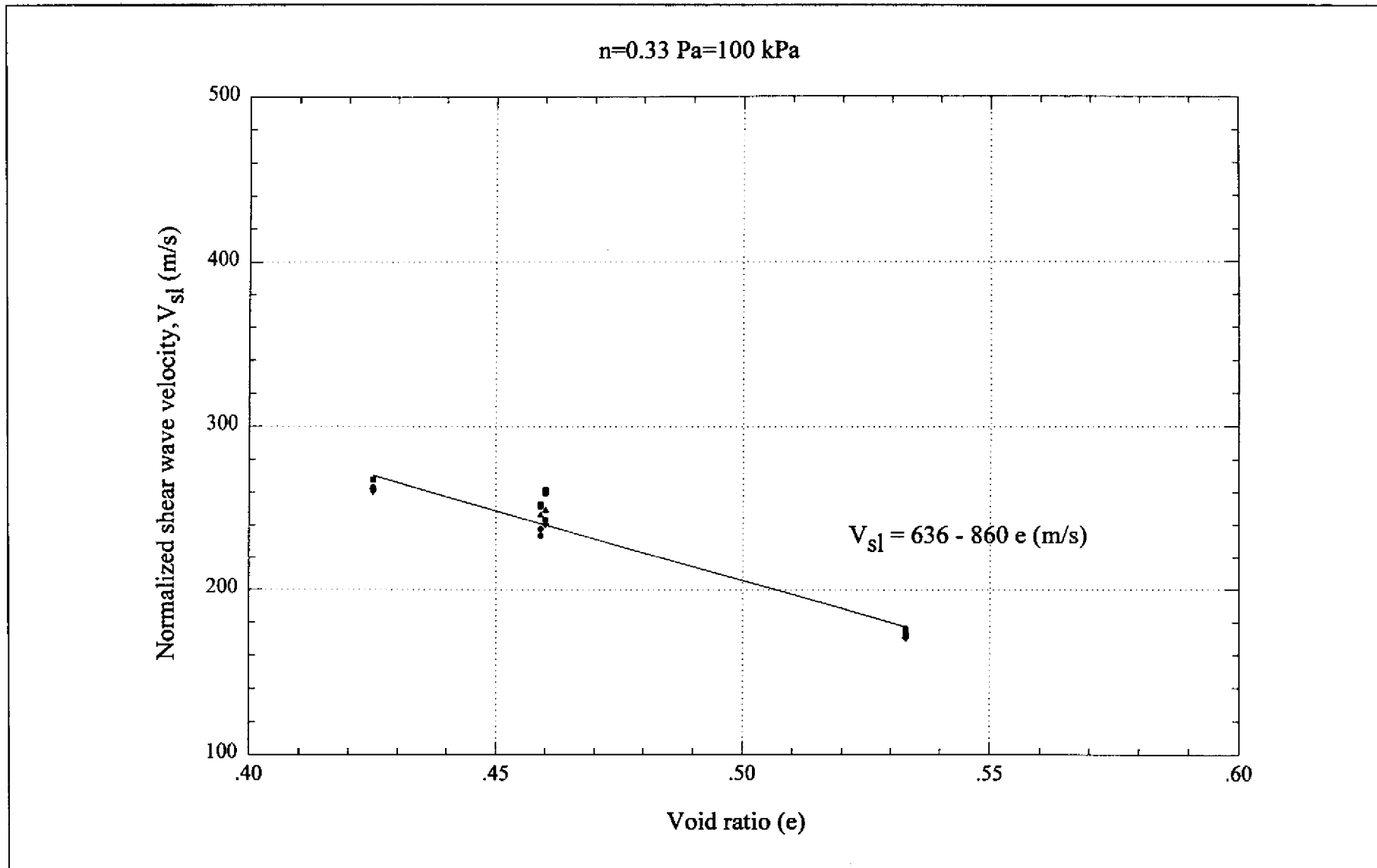


Figure 5.14 - Normalized Shear Wave Velocity (V_{sl}) versus Void Ratio (e) West Kowloon Sand

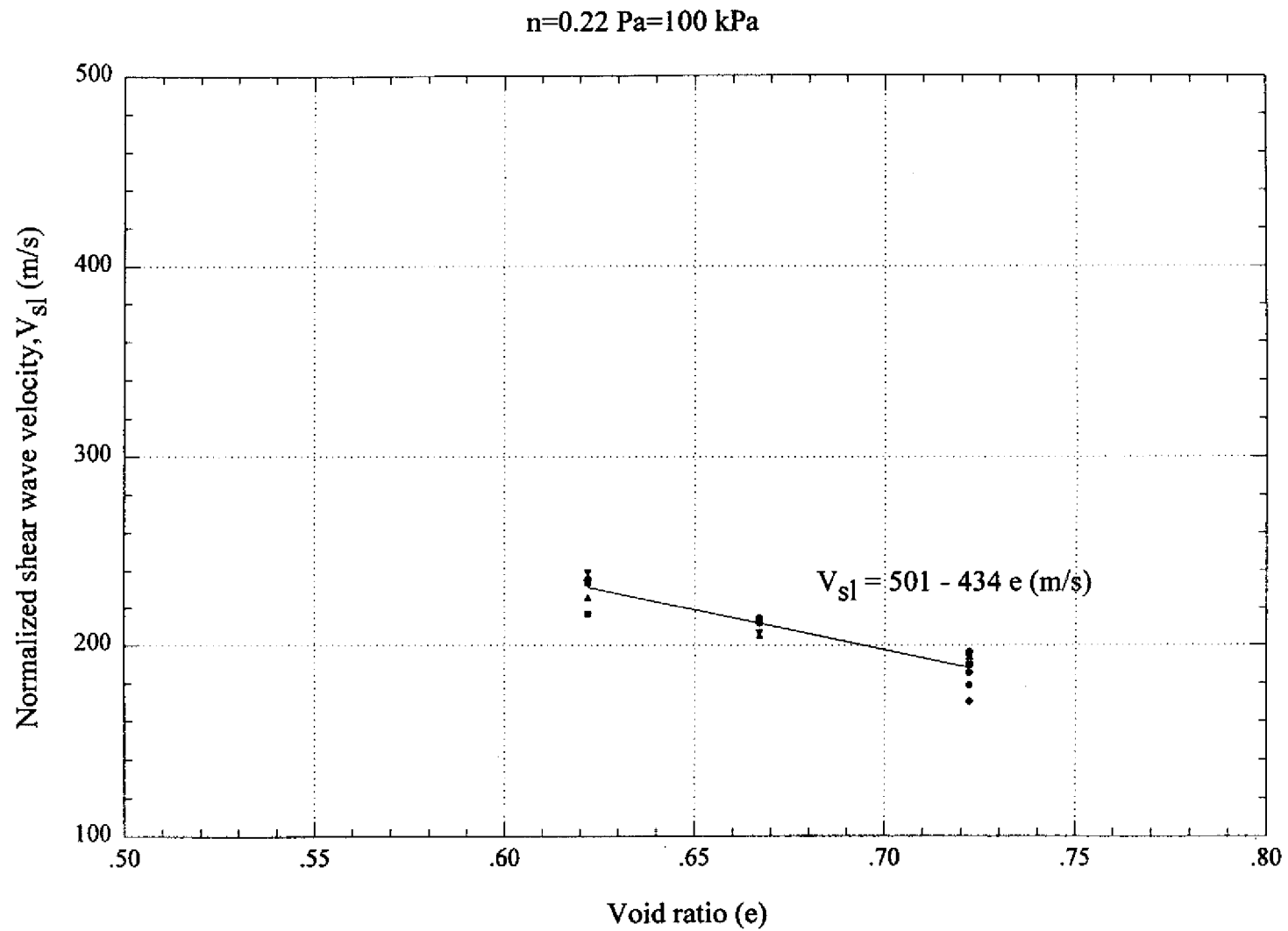


Figure 5.15 - Normalized Shear Wave Velocity (V_{sl}) versus Void Ratio (e) Tseung Kwan O Sand

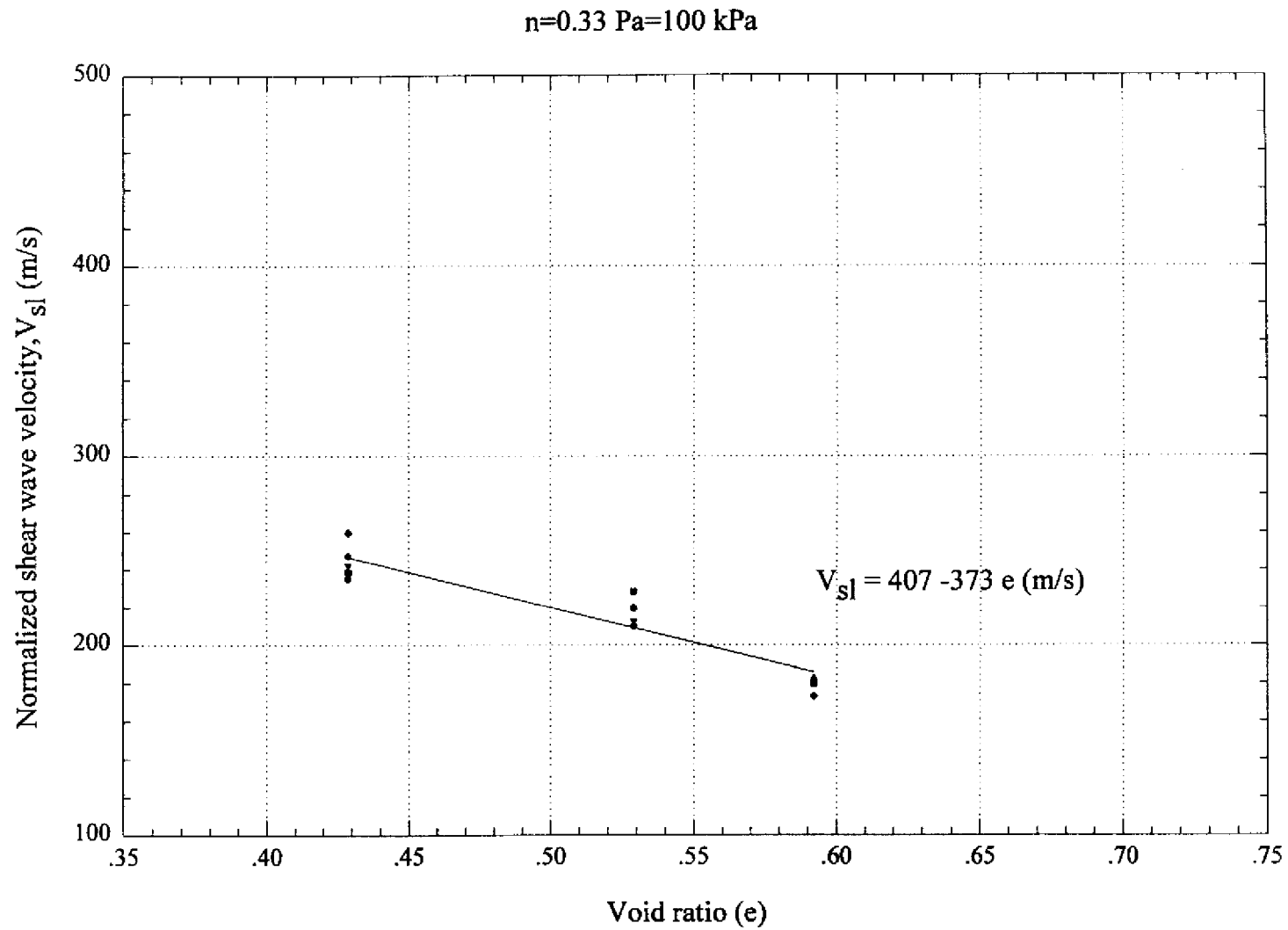


Figure 5.16 - Normalized Shear Wave Velocity (V_{sl}) versus Void Ratio (e) Tin Shui Wai Sand

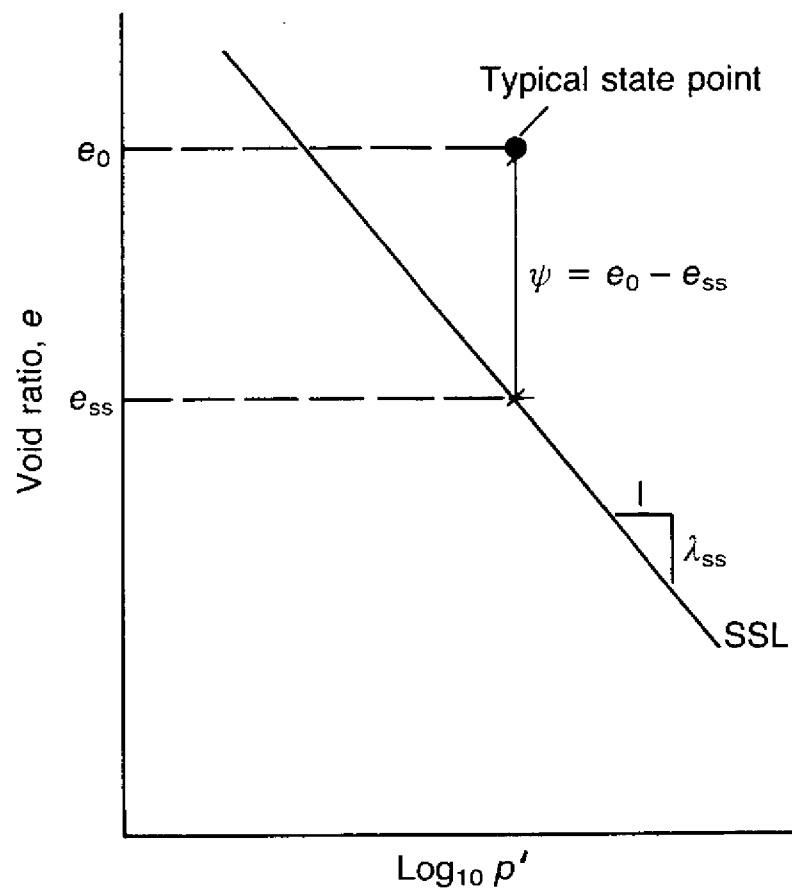


Figure 6.1 - Definition of State Parameter (after Been & Jefferies, 1985)

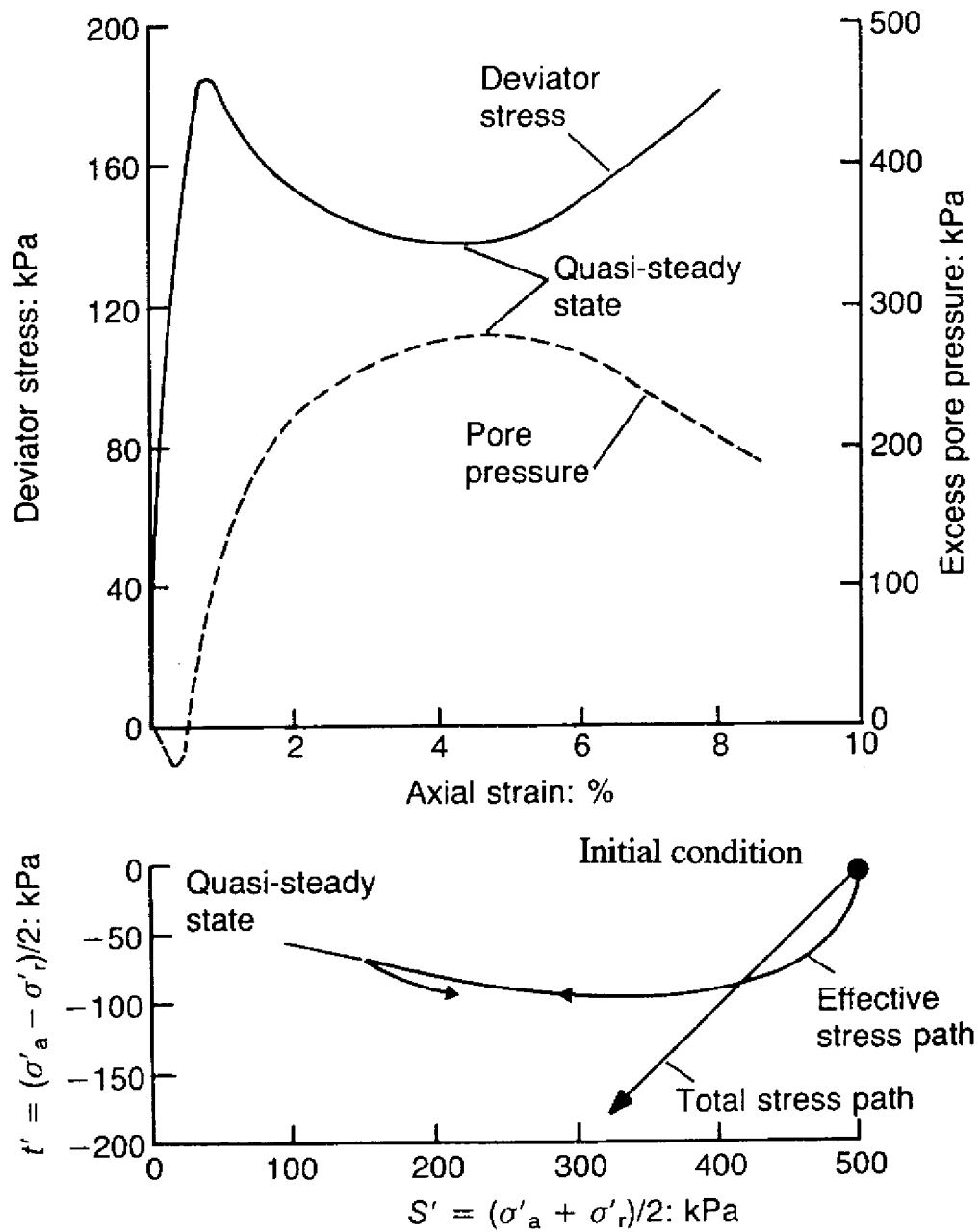


Figure 6.2 - Typical Test Showing a Quasi-Steady State Condition (after Been et al, 1991)

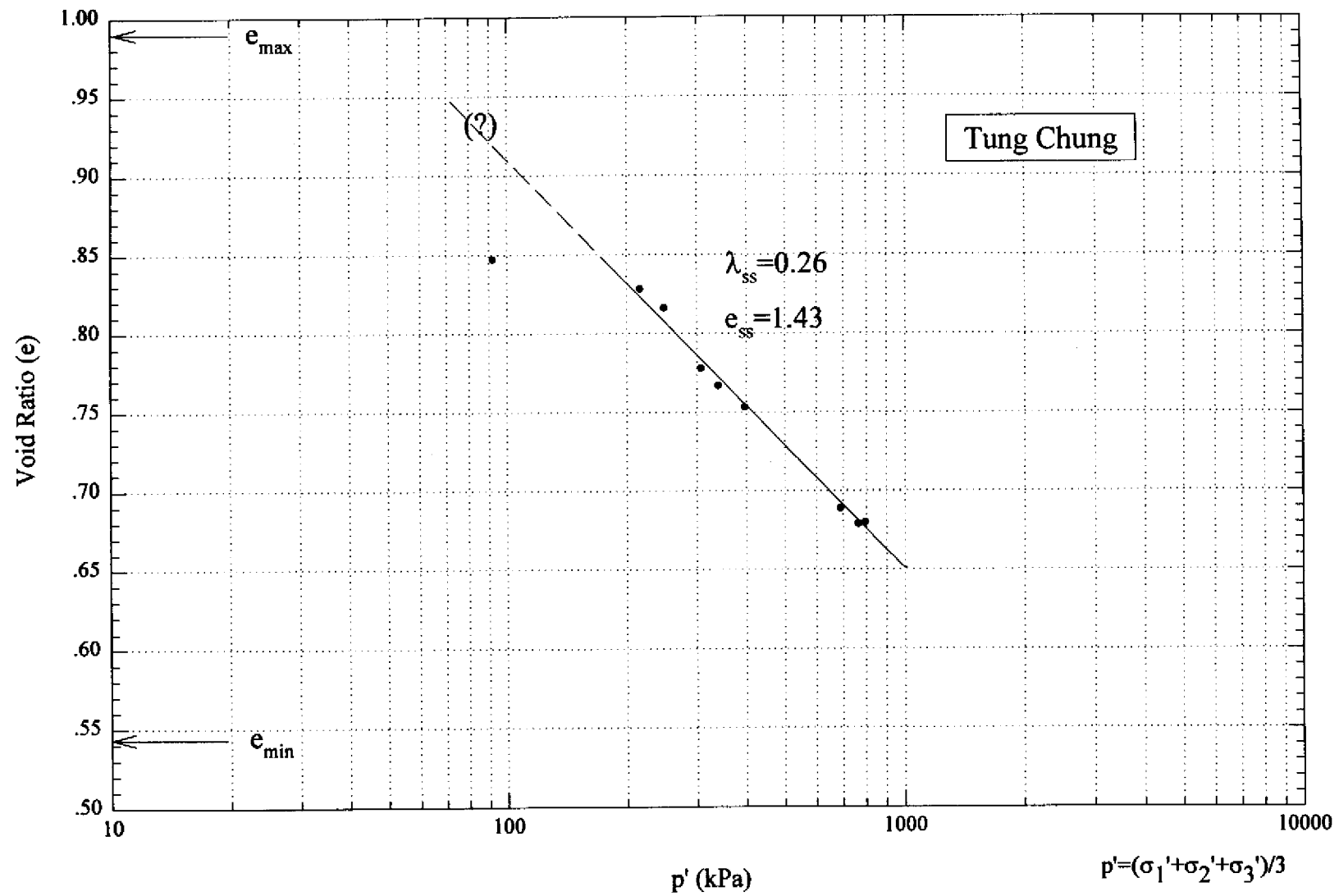


Figure 6.3 - Steady State Line for Undrained Triaxial Compression Tests on Tung Chung (TC) Sand

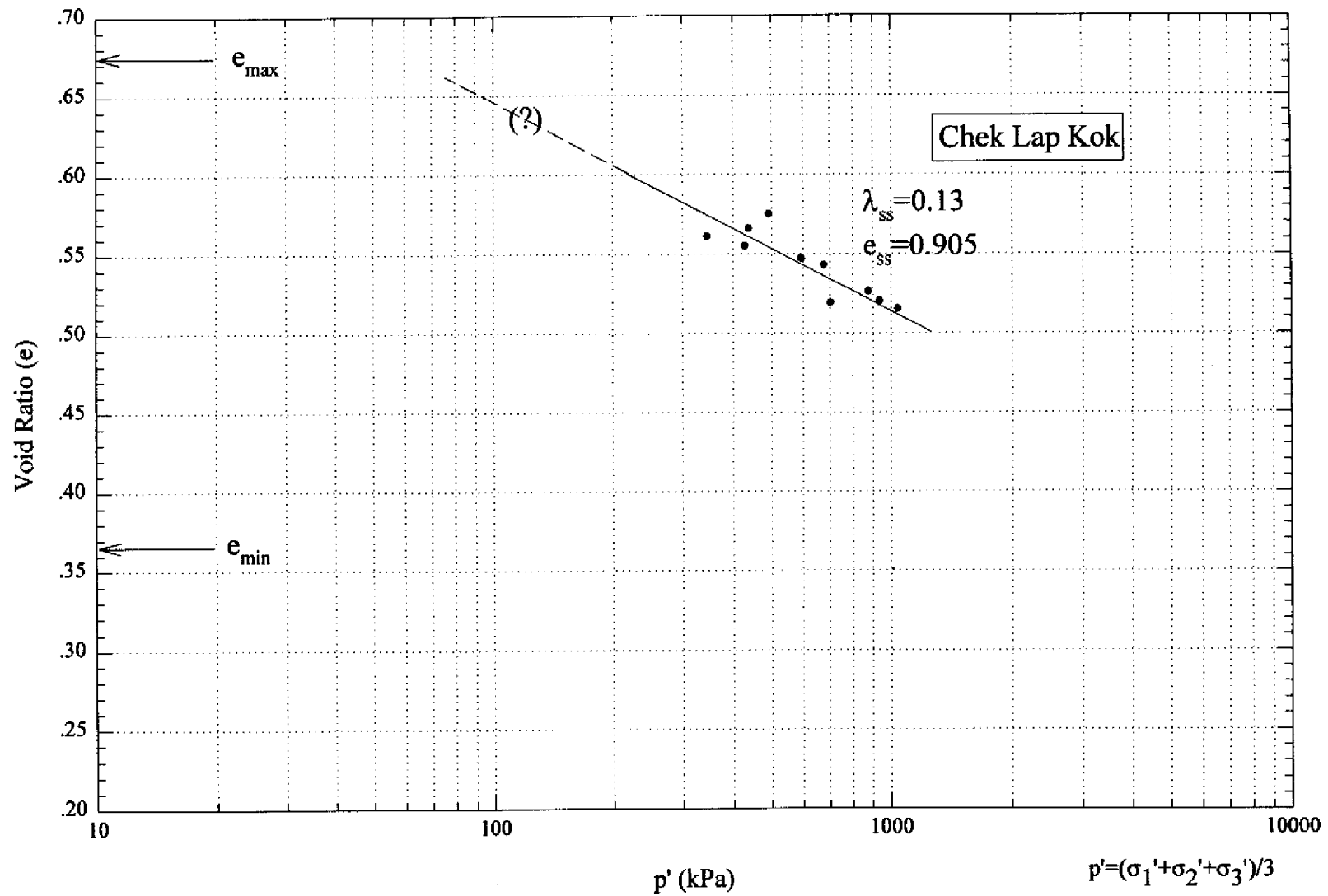


Figure 6.4 - Steady State Line for Undrained Triaxial Compression Tests on Chek Lap Kok (CLK) Sand

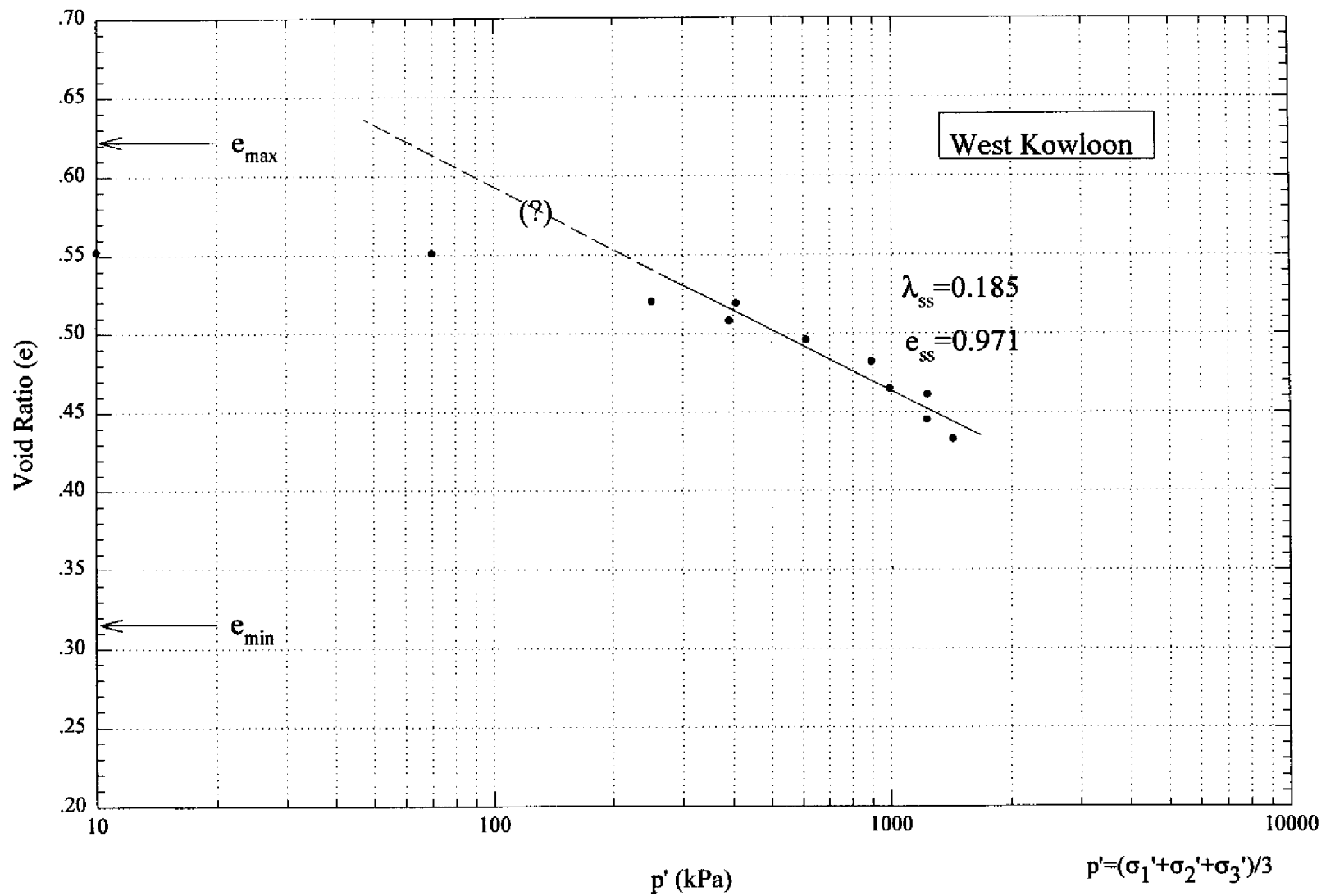


Figure 6.5 - Steady State Line for Undrained Triaxial Compression Tests on West Kowloon (CS1) Sand

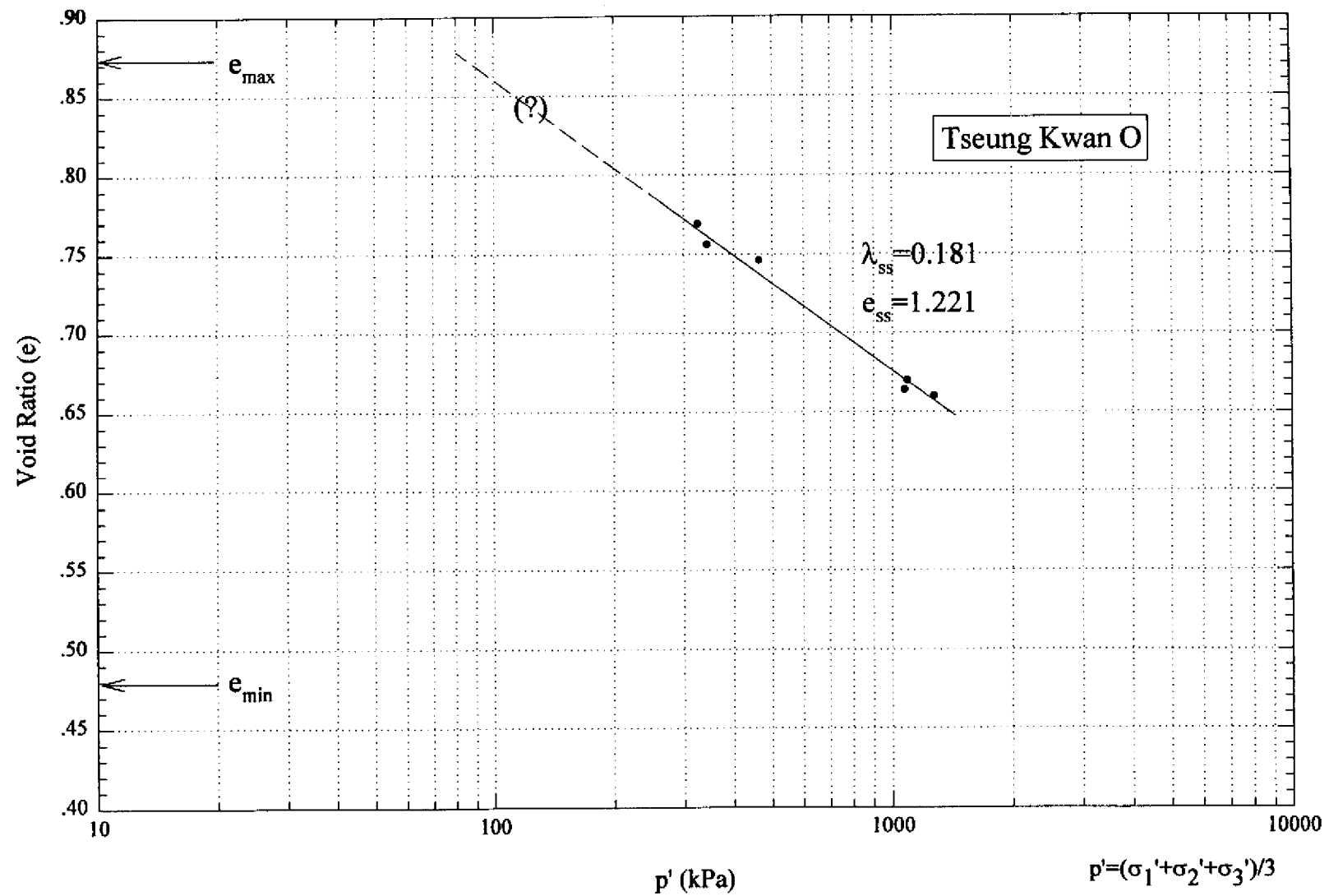


Figure 6.6 - Steady State Line for Undrained Triaxial Compression Tests on Tseung Kwan O (TKO) Sand

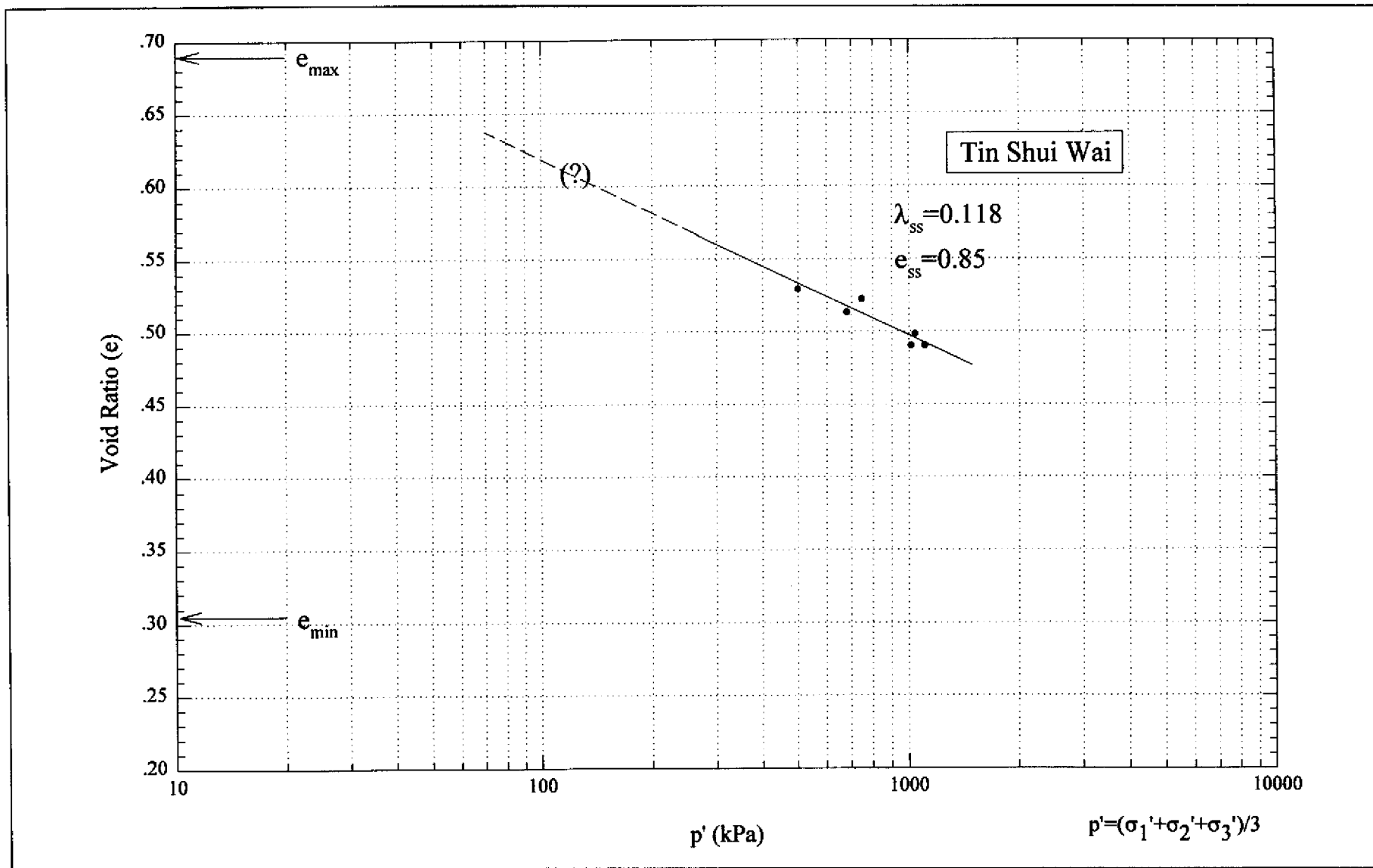


Figure 6.7 - Steady State Line for Undrained Triaxial Compression Tests on Tin Shui Wai (TSW) Sand

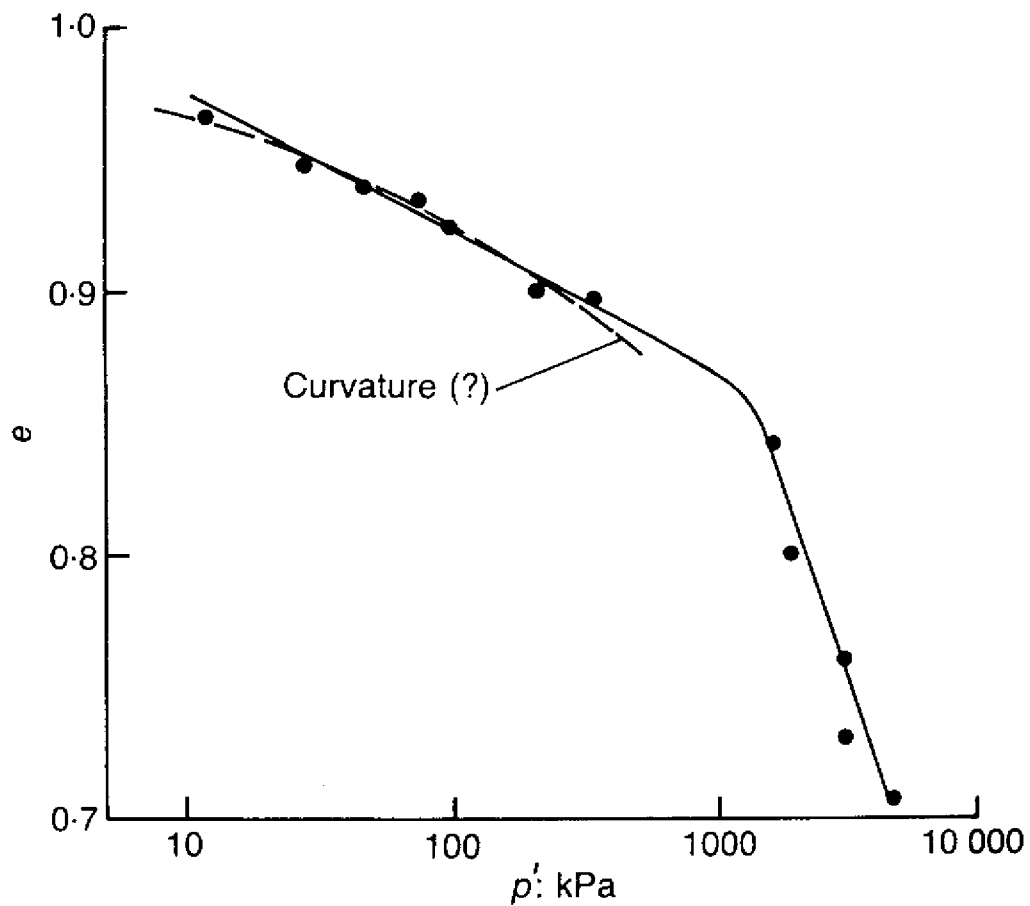


Figure 6.8 - Steady State Line for Leighton Buzzard Sand Showing Curvature Similar to That of Line for Erksak 330/0.7 Sand (Initial State of All Samples Was above the Steady State Line; All Tests Triaxial Compression) (after Been et al, 1991)

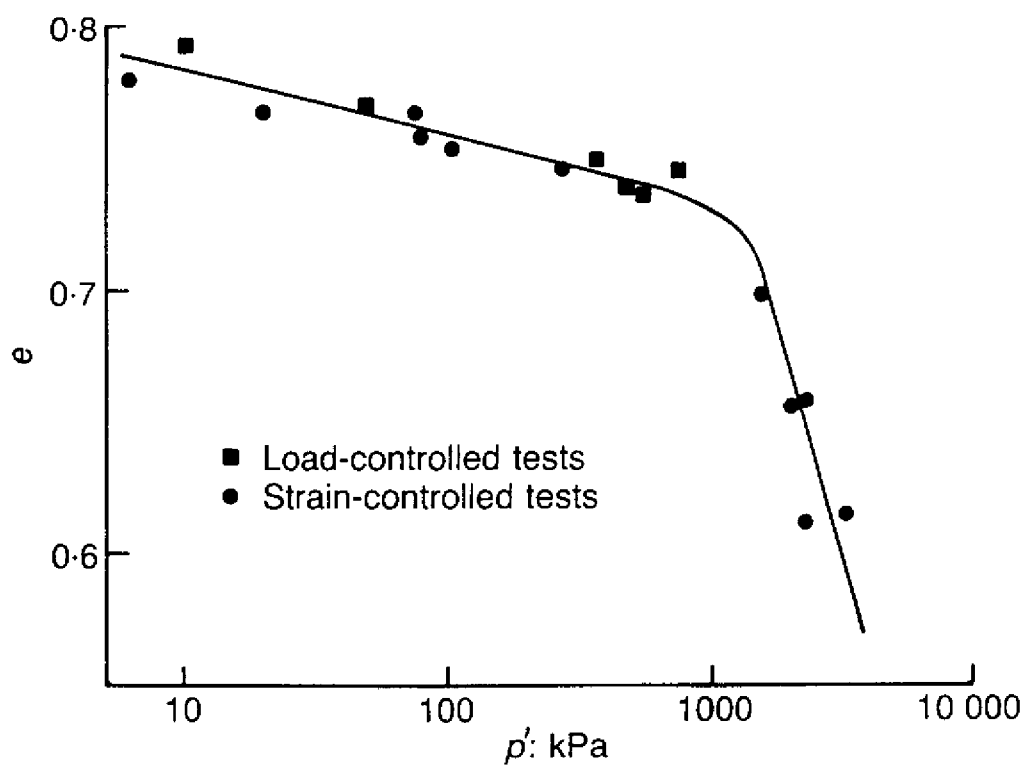


Figure 6.9 - Steady State Line for Undrained Compression Tests on Contractive Samples of Erksak 330/0.7 Sand with Initial States above the Steady State Line (after Been et al, 1991)

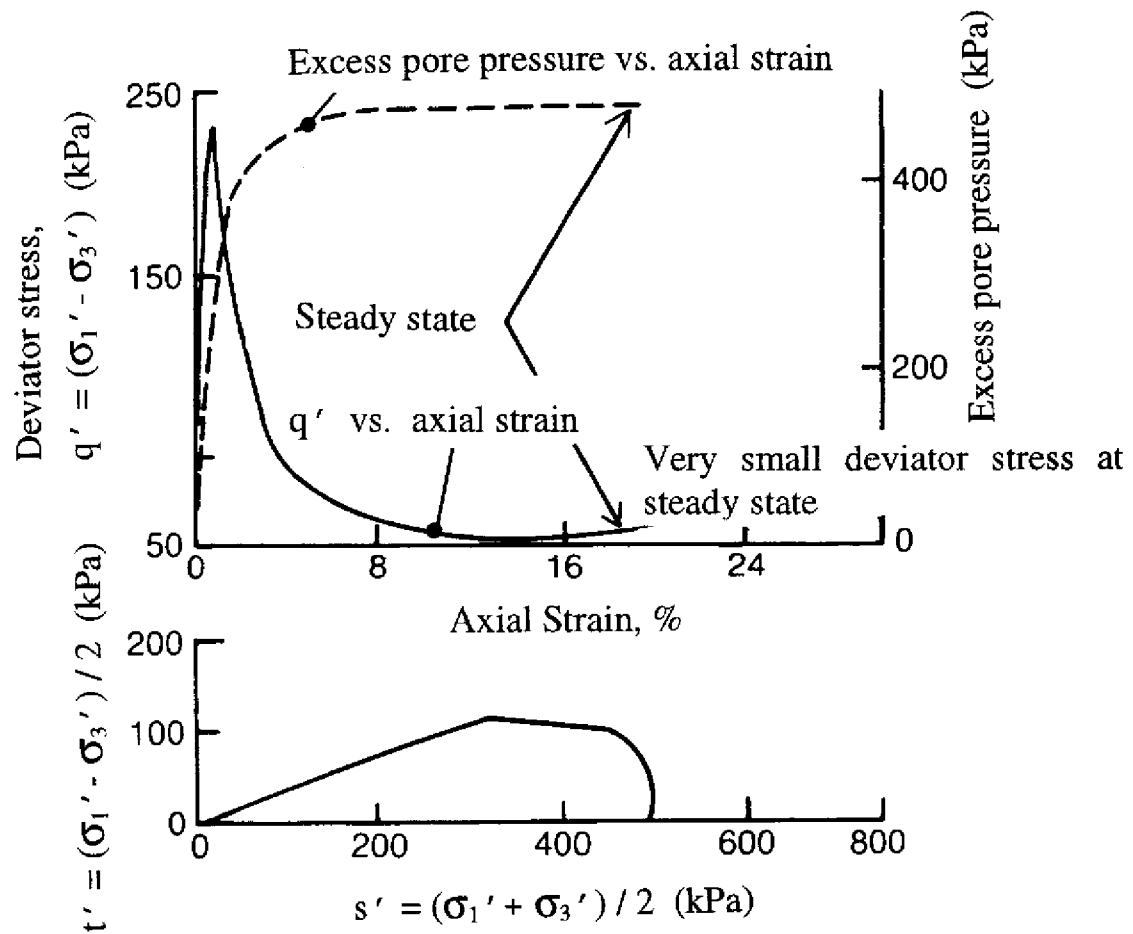


Figure 6.10 - Typical Test Results of Undrained Test on Loose Sample Showing Strain Softening Behaviour (Loose Sample; $e = 0.771$, $\sigma_{3c}' = 500$ kPa on Erksak 330/0.7 Sand) (after Been et al, 1991)

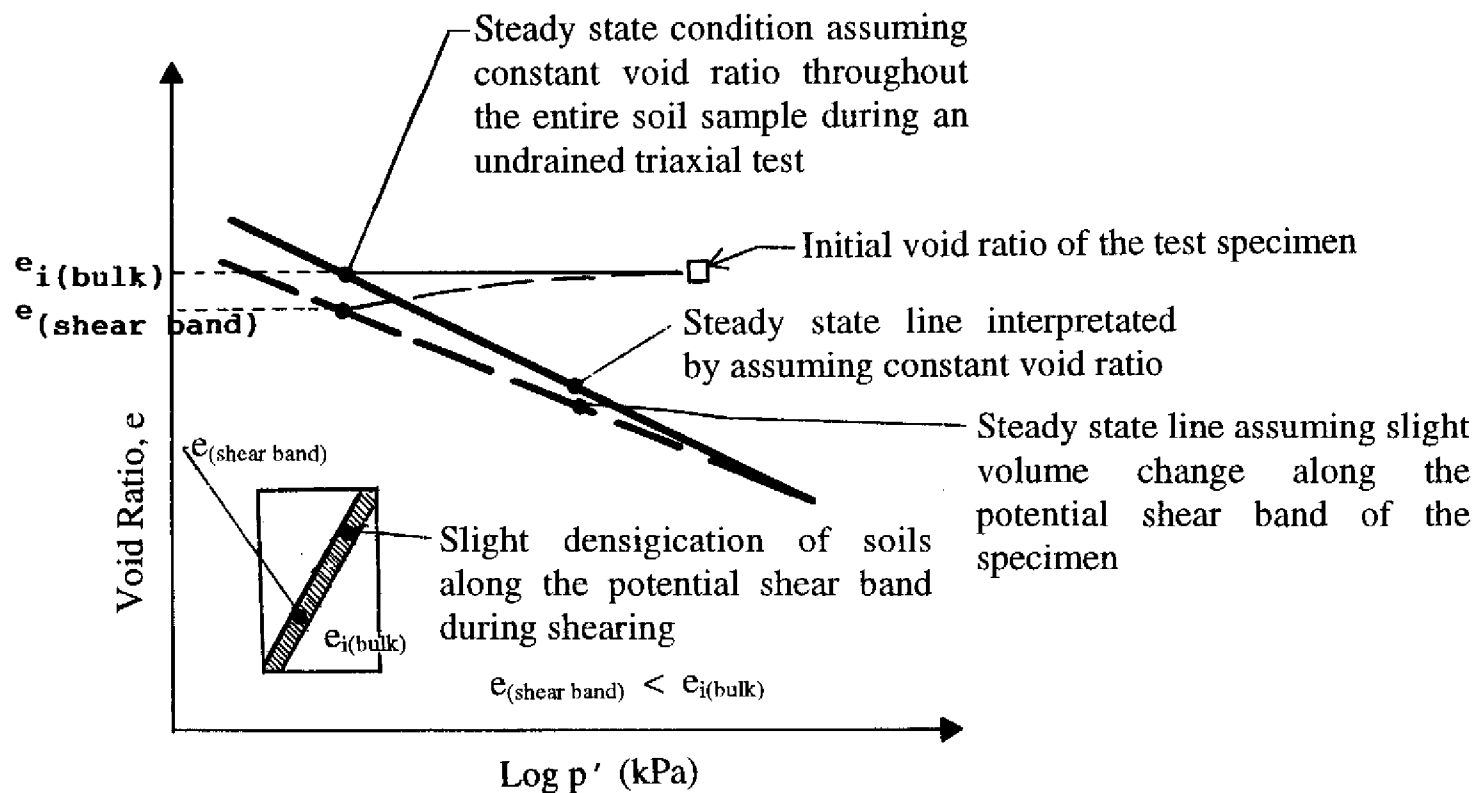
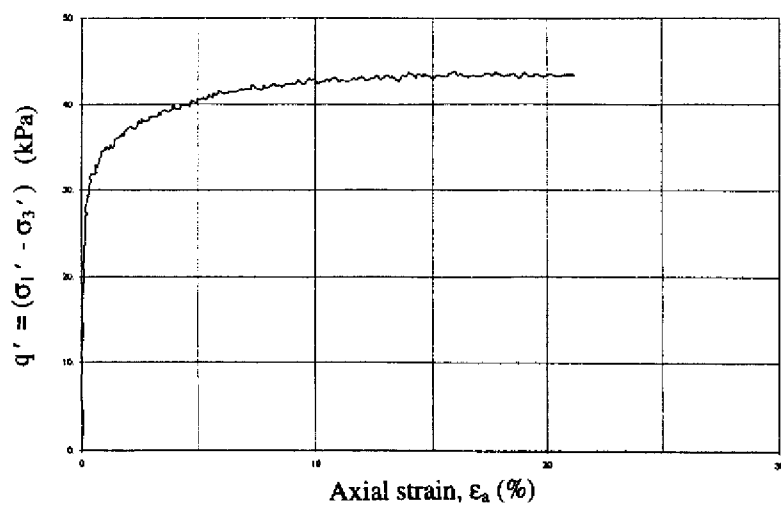
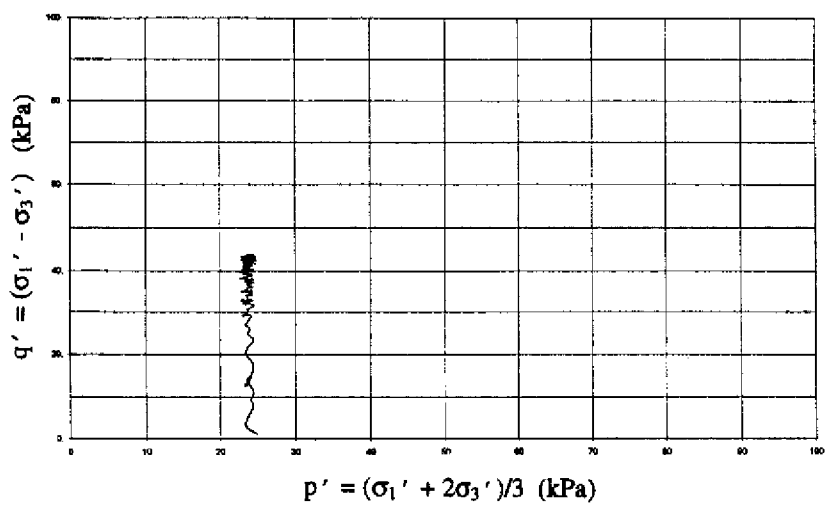


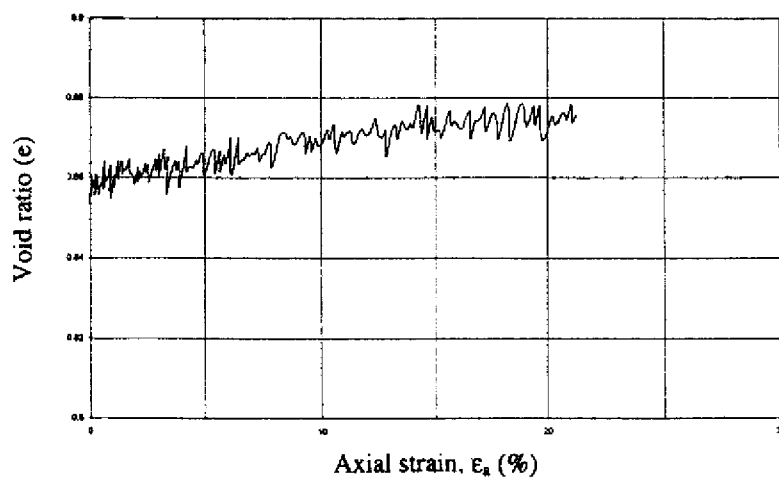
Figure 6.11 - Interpretation of Steady State Line by Undrained Triaxial Test on Loose Contractive Soil Sample



(a)



(b)



(c)

Figure 6.12 - Results of Constant p' Test on Tung Chung Sand with $e_o = 0.858$ and $p' = 25 \text{ kPa}$

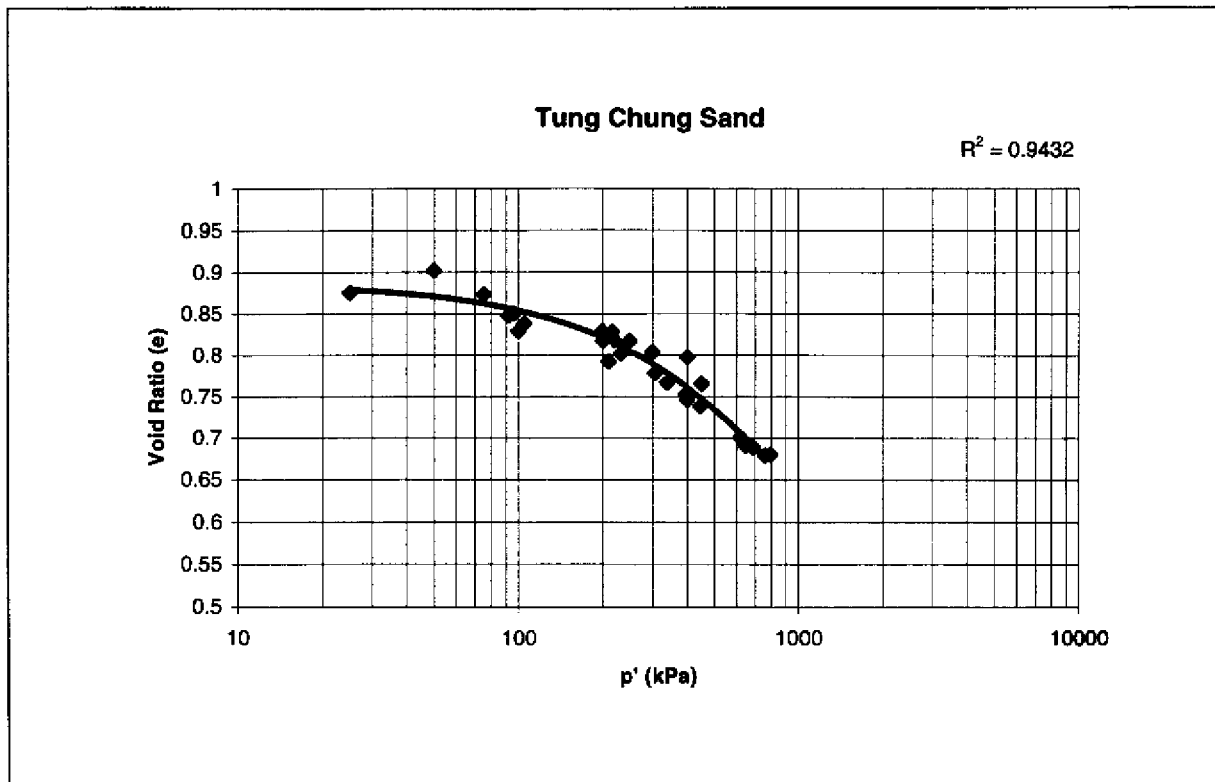


Figure 6.13 - Steady State Boundary in e -log p' Space for the TC Sand

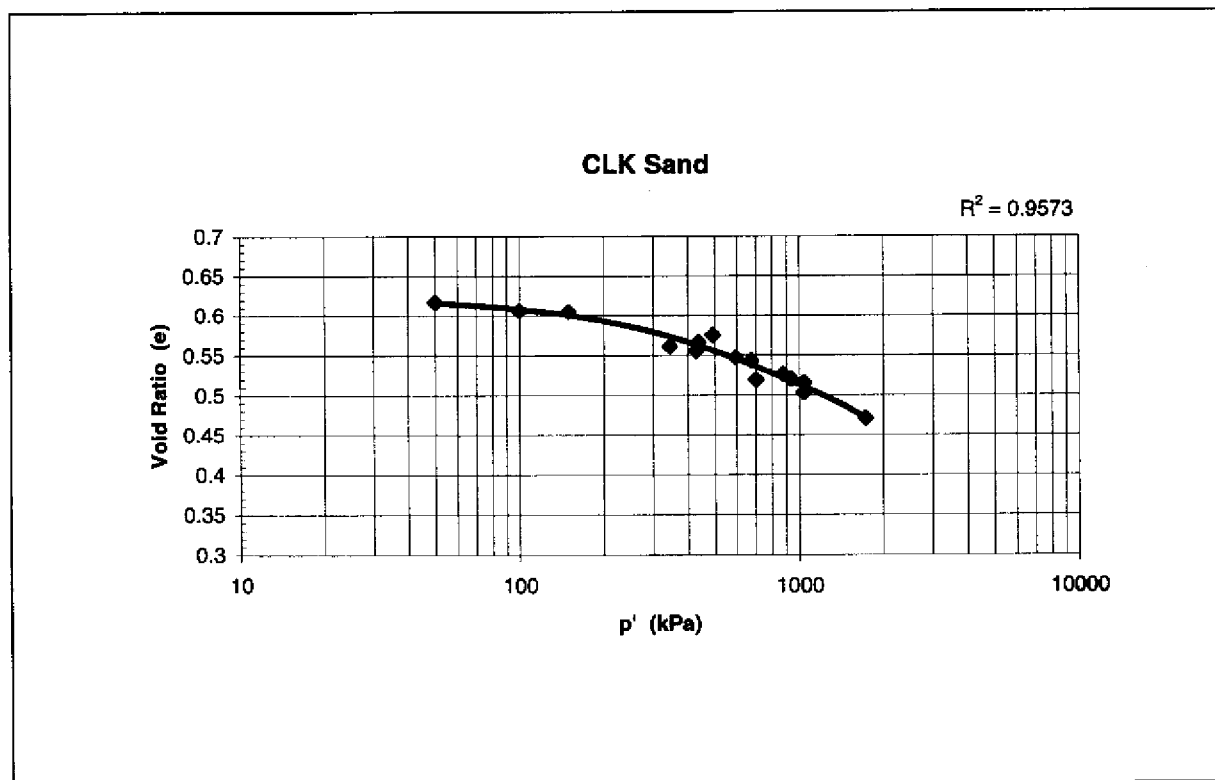


Figure 6.14 - Steady State Boundary in e -log p' Space for the CLK Sand

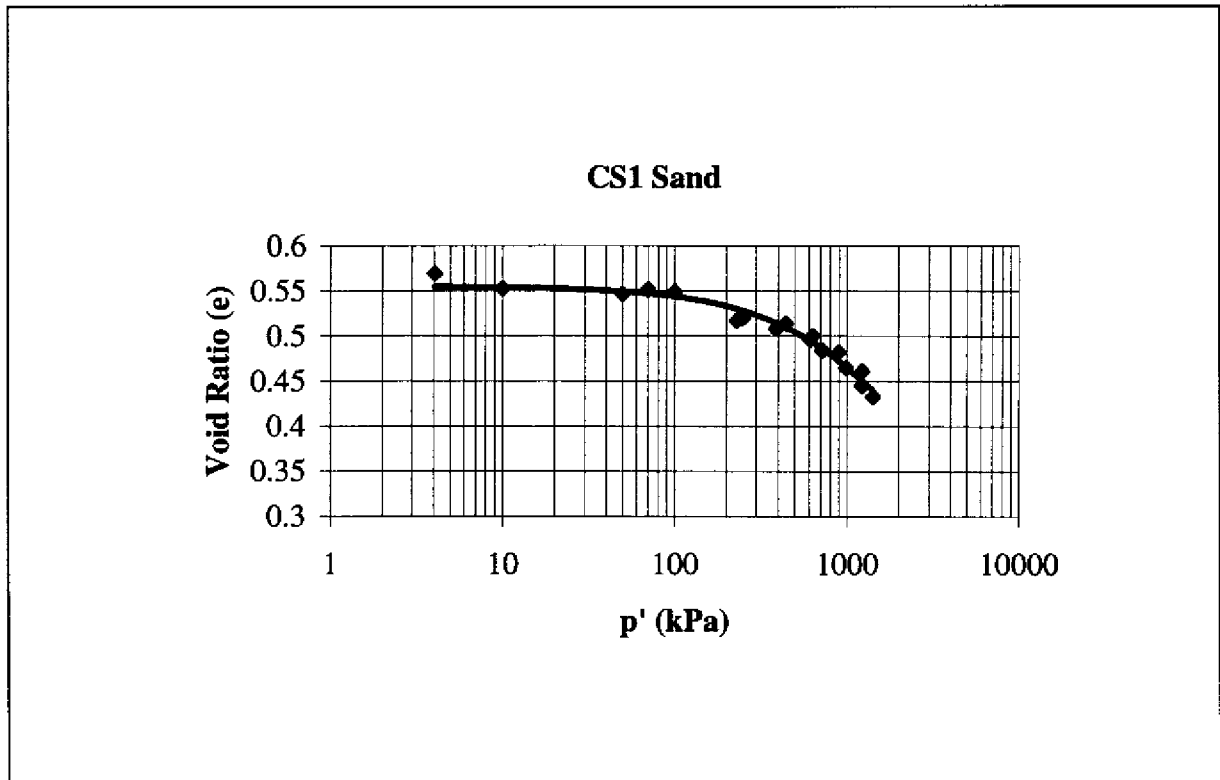


Figure 6.15 - Steady State Boundary in e-log p' Space for the CS1 Sand

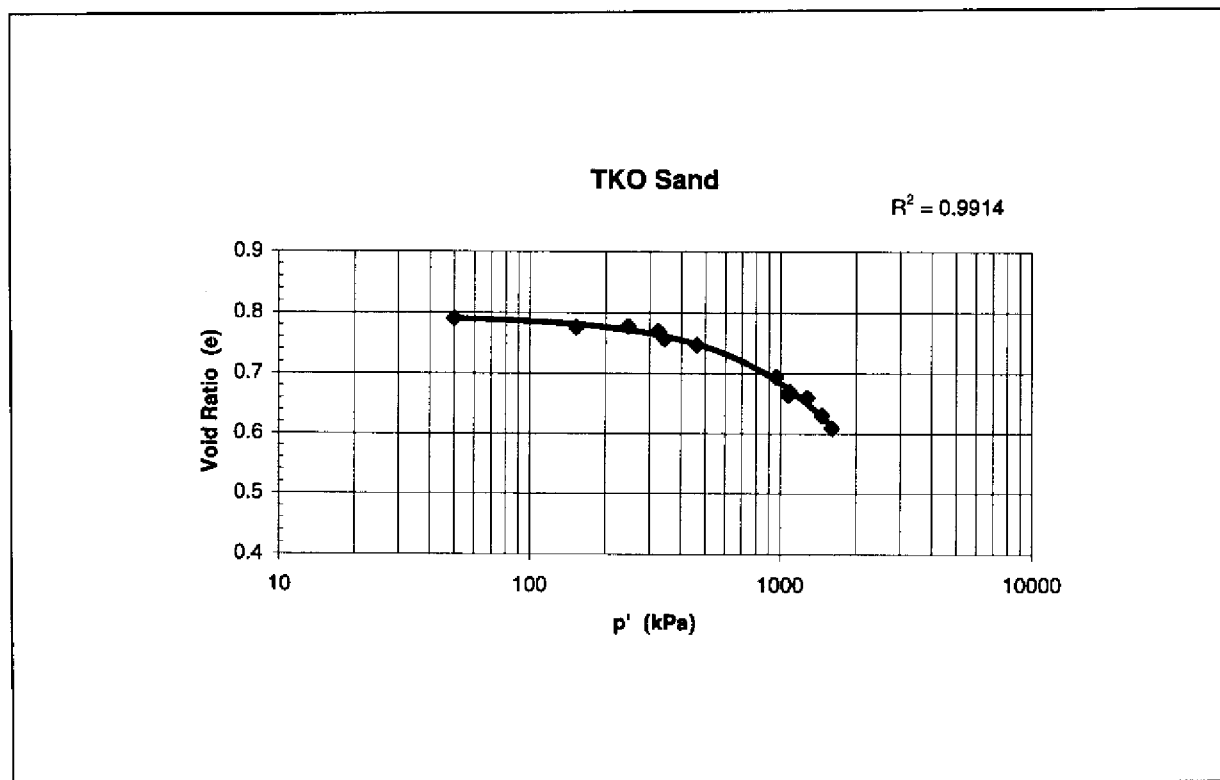


Figure 6.16 - Steady State Boundary in e-log p' Space for the TKO Sand

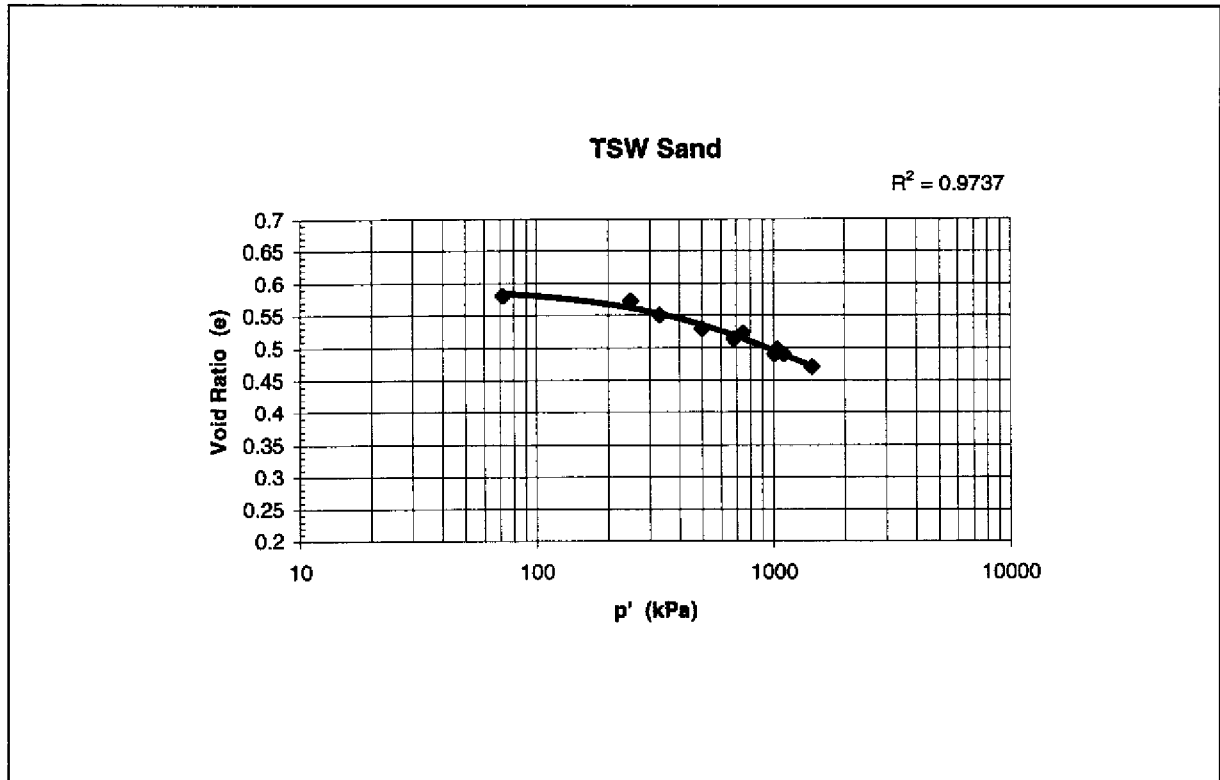


Figure 6.17 - Steady State Boundary in e -log p' Space for the TSW Sand

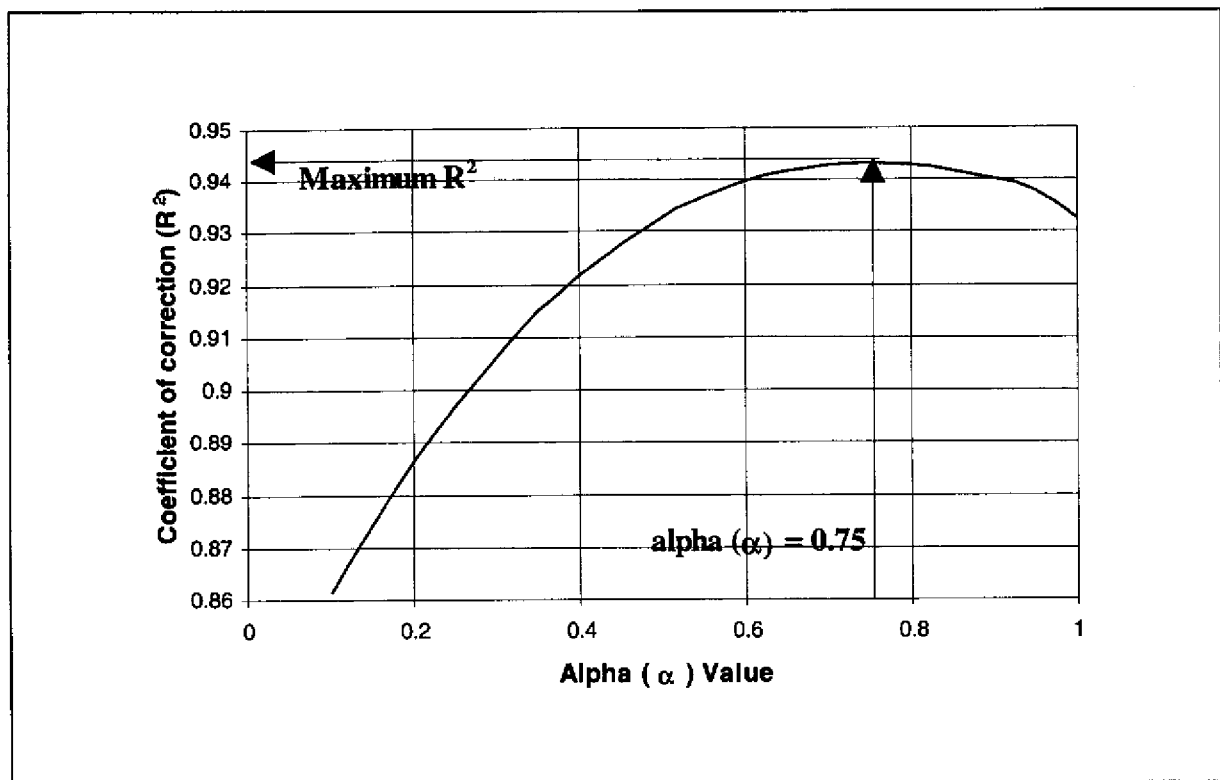


Figure 6.18 - Search for the Optimized (α) Value for the TC Sand

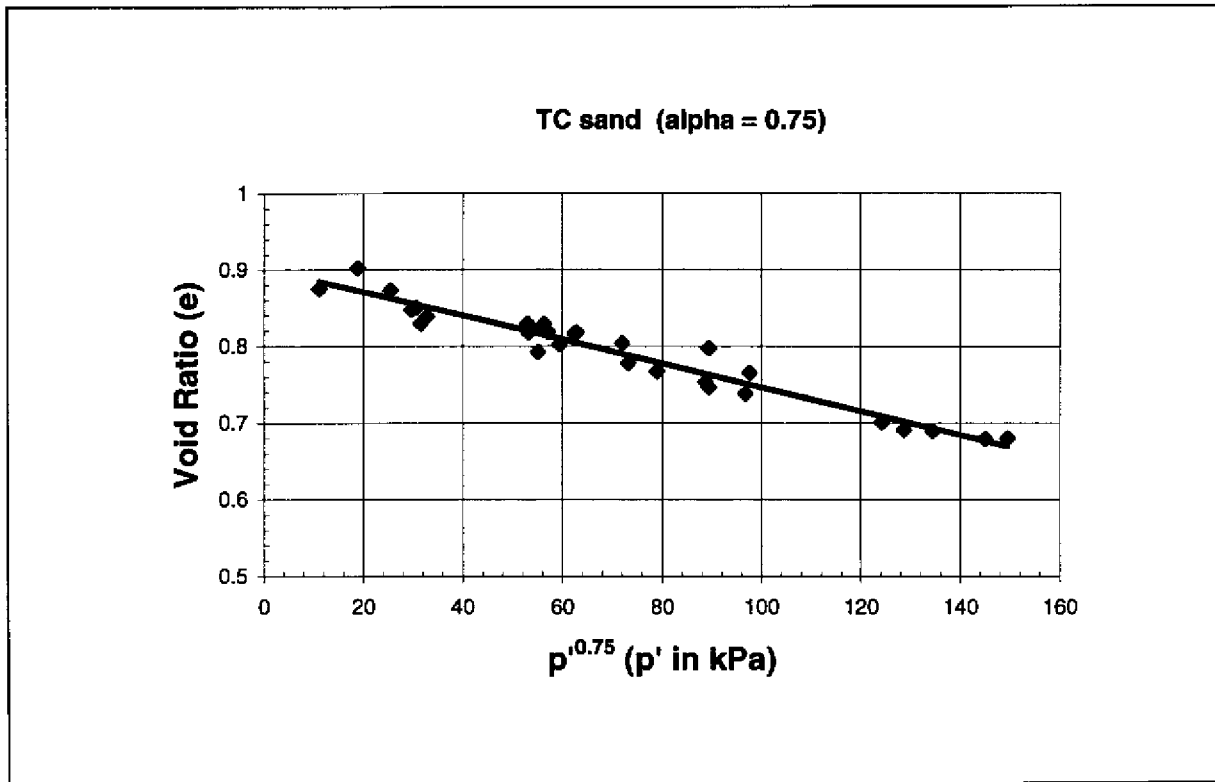


Figure 6.19 - Steady State Line in $e - p'^{\alpha}$ Space for the TC Sand

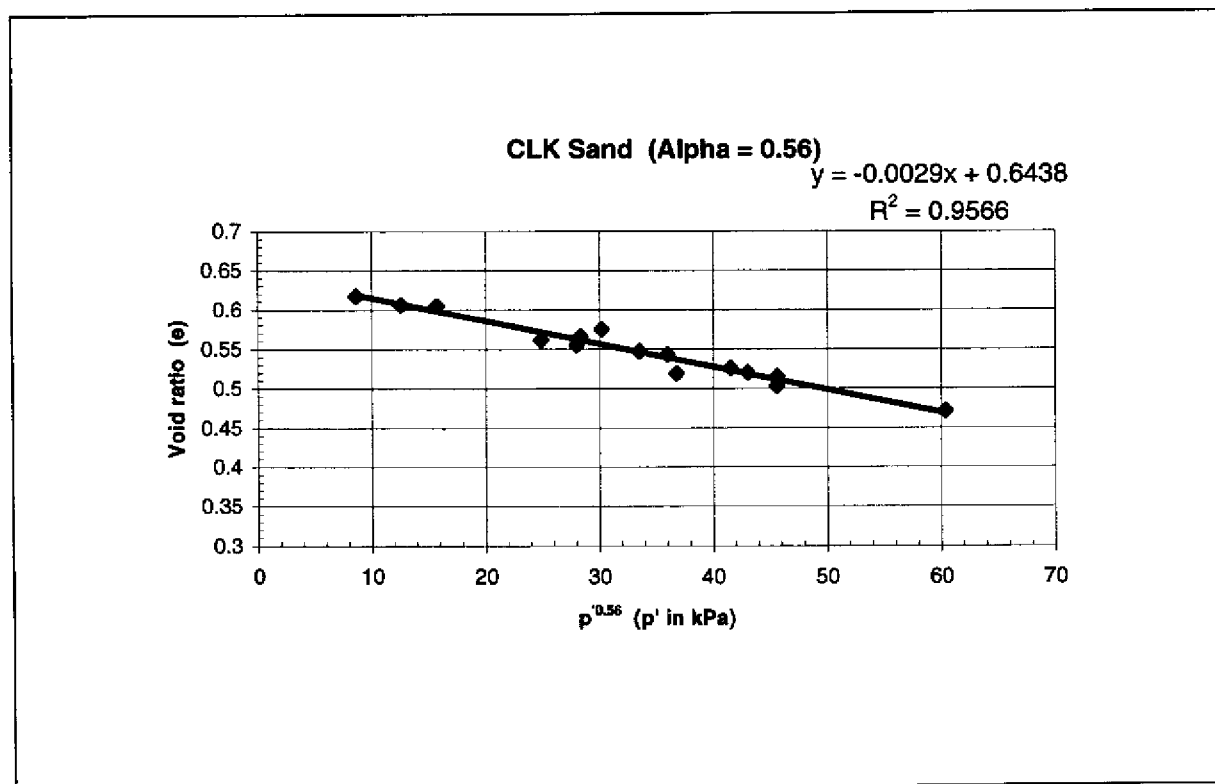


Figure 6.20 - Steady State Line in $e - p'^{\alpha}$ Space for the CLK Sand

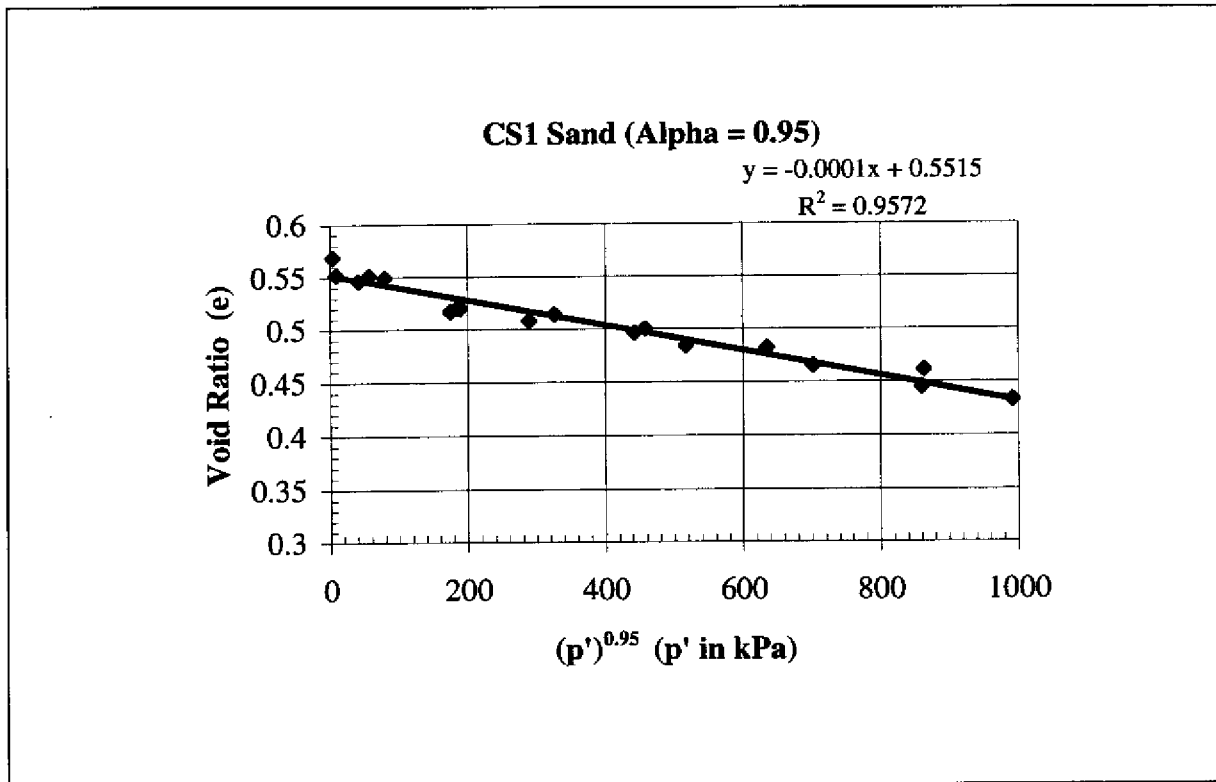


Figure 6.21 - Steady State Line in $e - p'^{\alpha}$ Space for the CS1 Sand

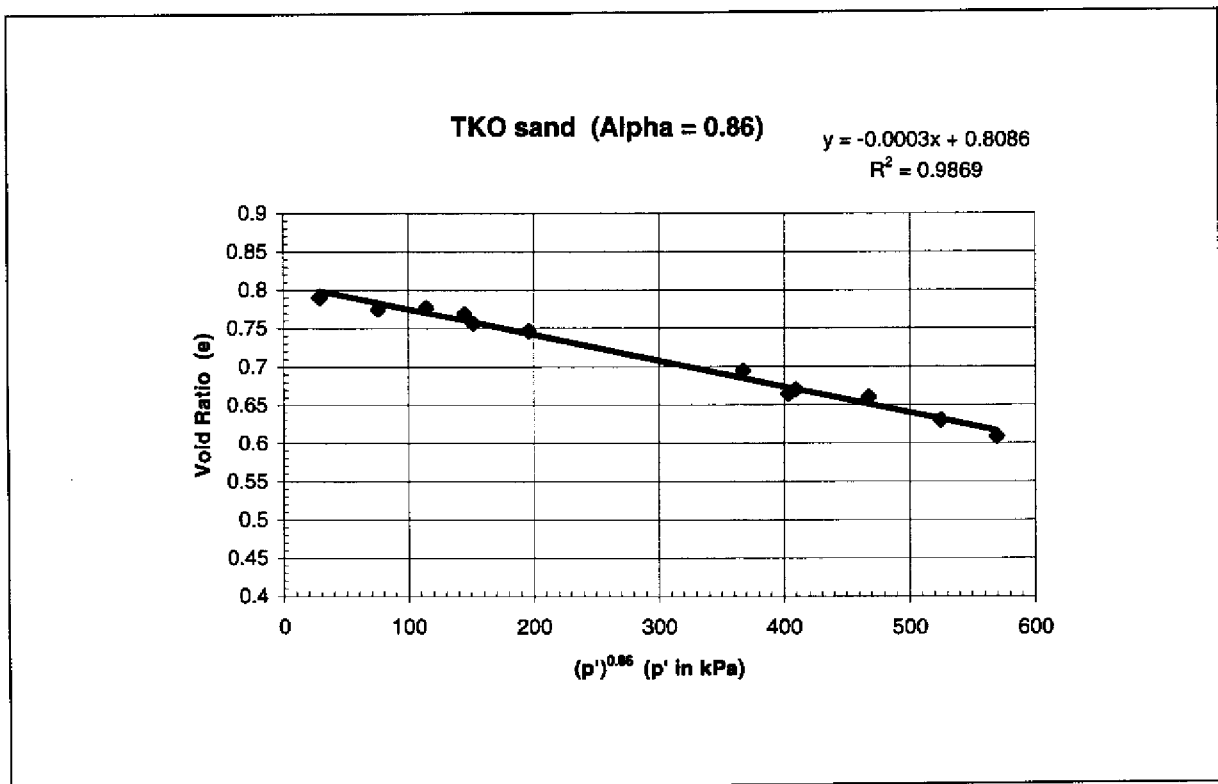


Figure 6.22 - Steady State Line in $e - p'^{\alpha}$ Space for the TKO Sand

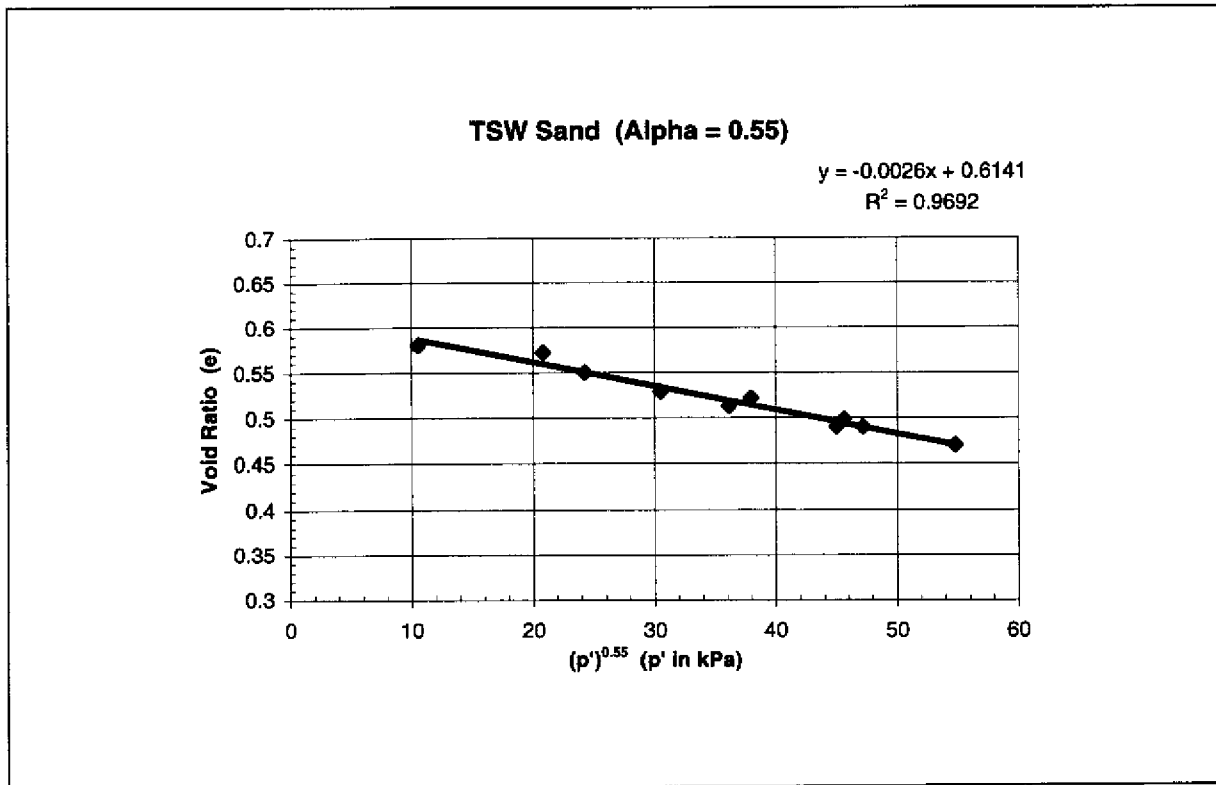


Figure 6.23 - Steady State Line in $e - p'^{\alpha}$ Space for the TSW Sand

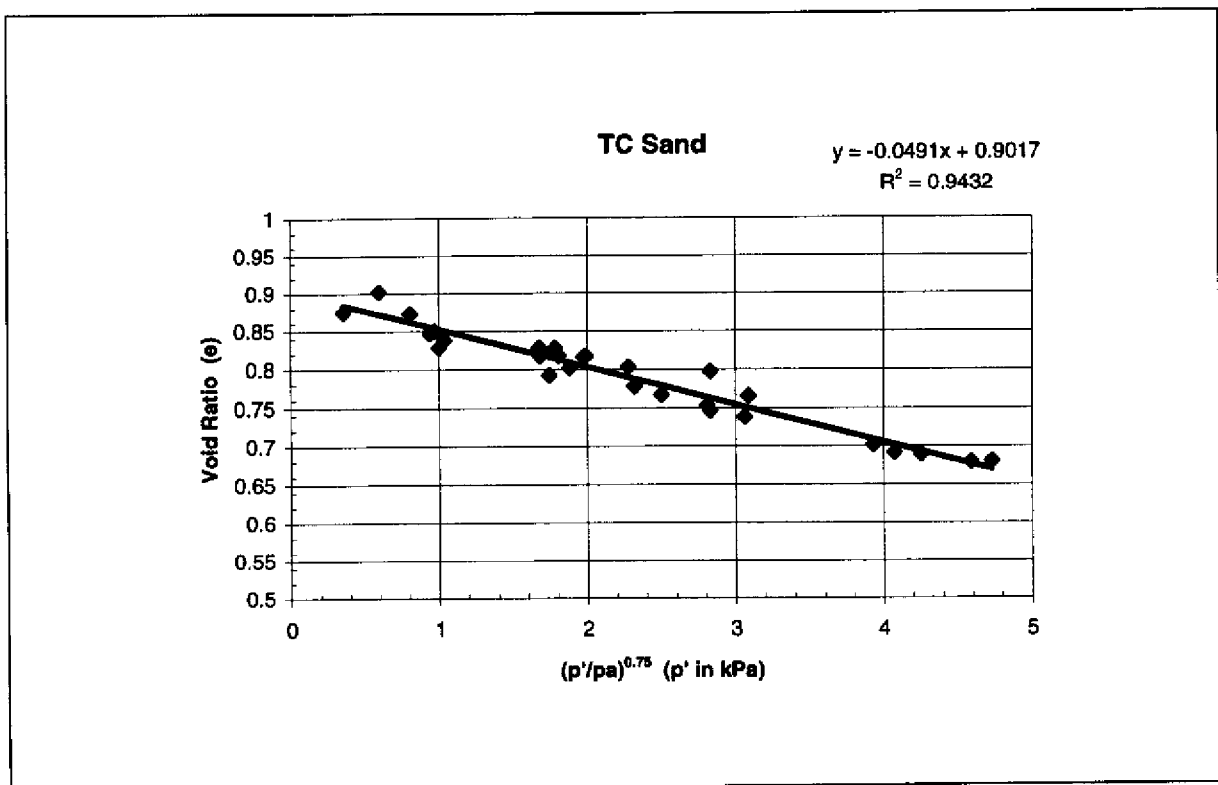


Figure 6.24 - Steady State Line in $e - (p'/p_a)^{0.75}$ Space for the TC Sand

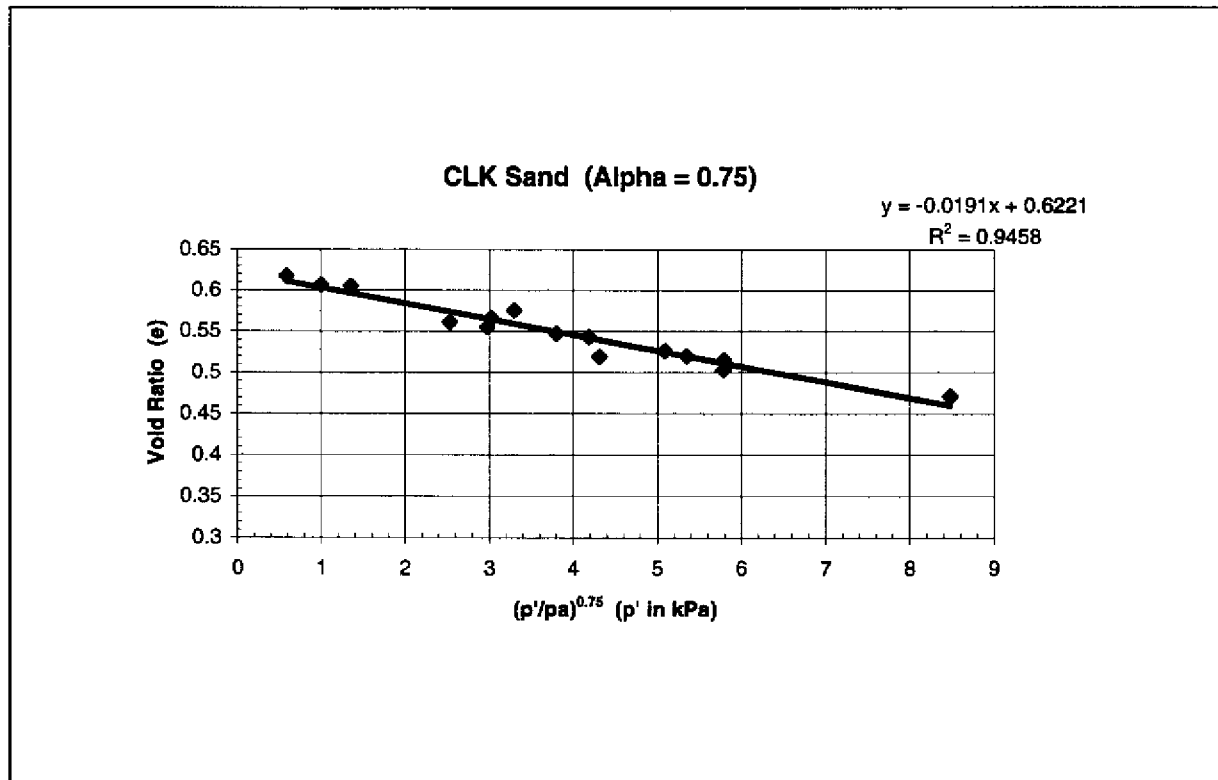


Figure 6.25 - Steady State Line in $e - (p'/p_a)^{0.75}$ Space for the CLK Sand

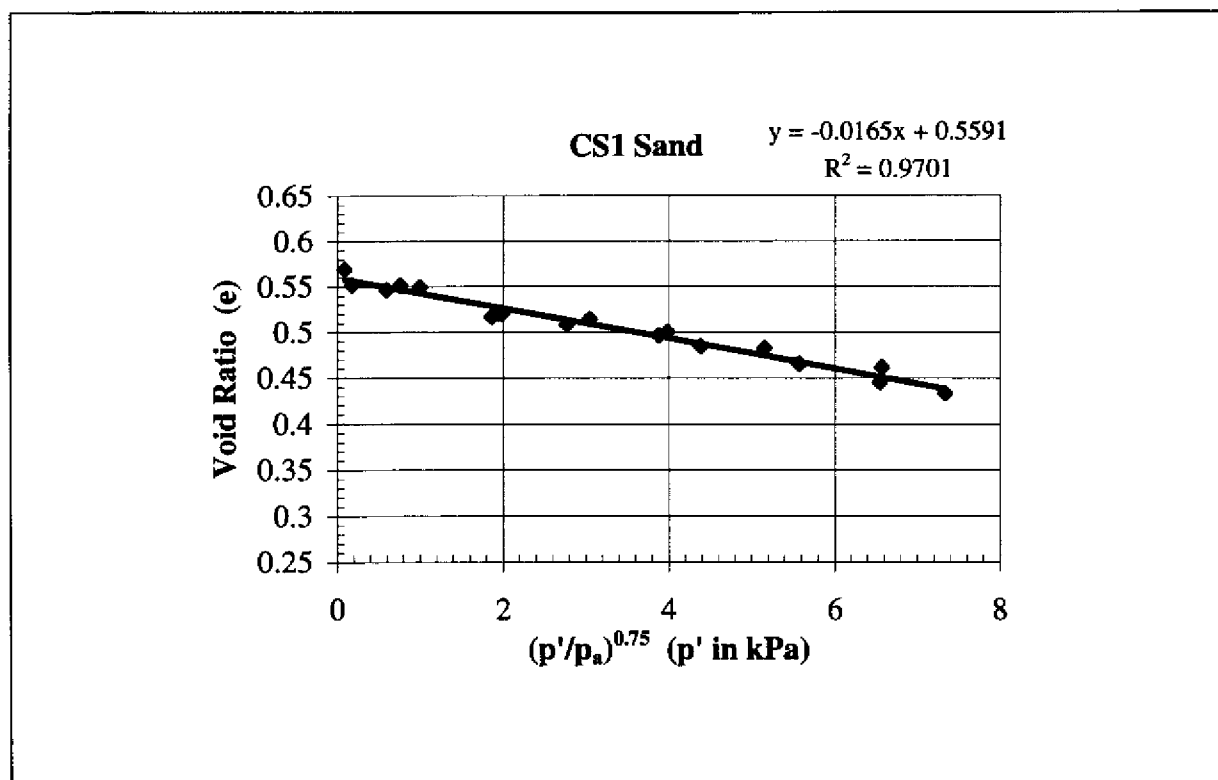


Figure 6.26 - Steady State Line in $e - (p'/p_a)^{0.75}$ Space for the CS1 Sand

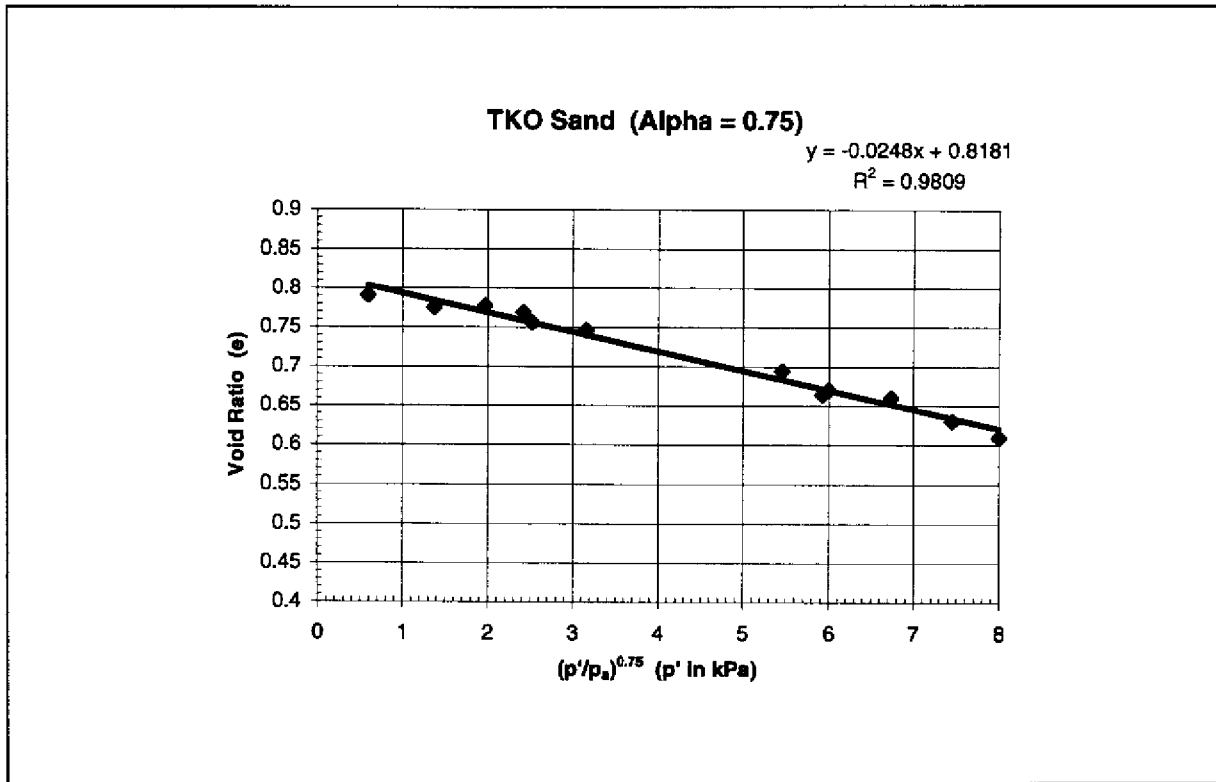


Figure 6.27 - Steady State Line in $e - (p'/p_a)^{0.75}$ Space for the TKO Sand

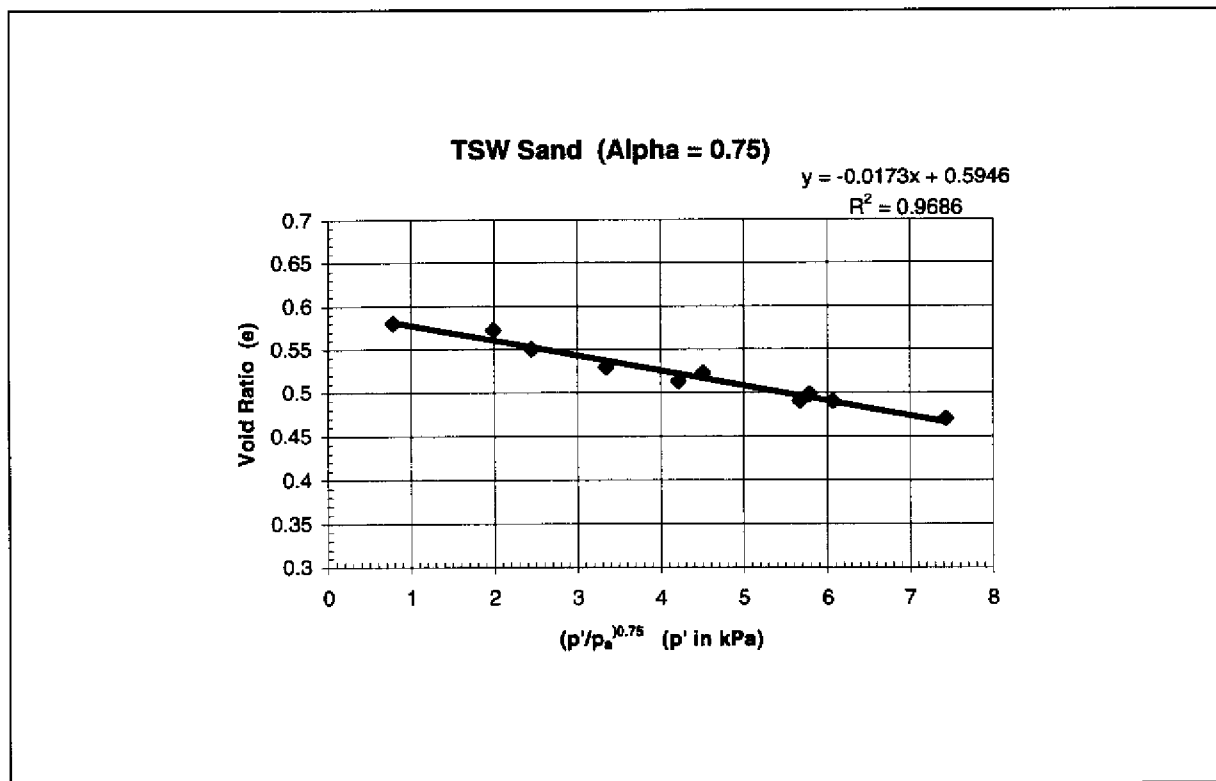


Figure 6.28 - Steady State Line in $e - (p'/p_a)^{0.75}$ Space for the TSW Sand

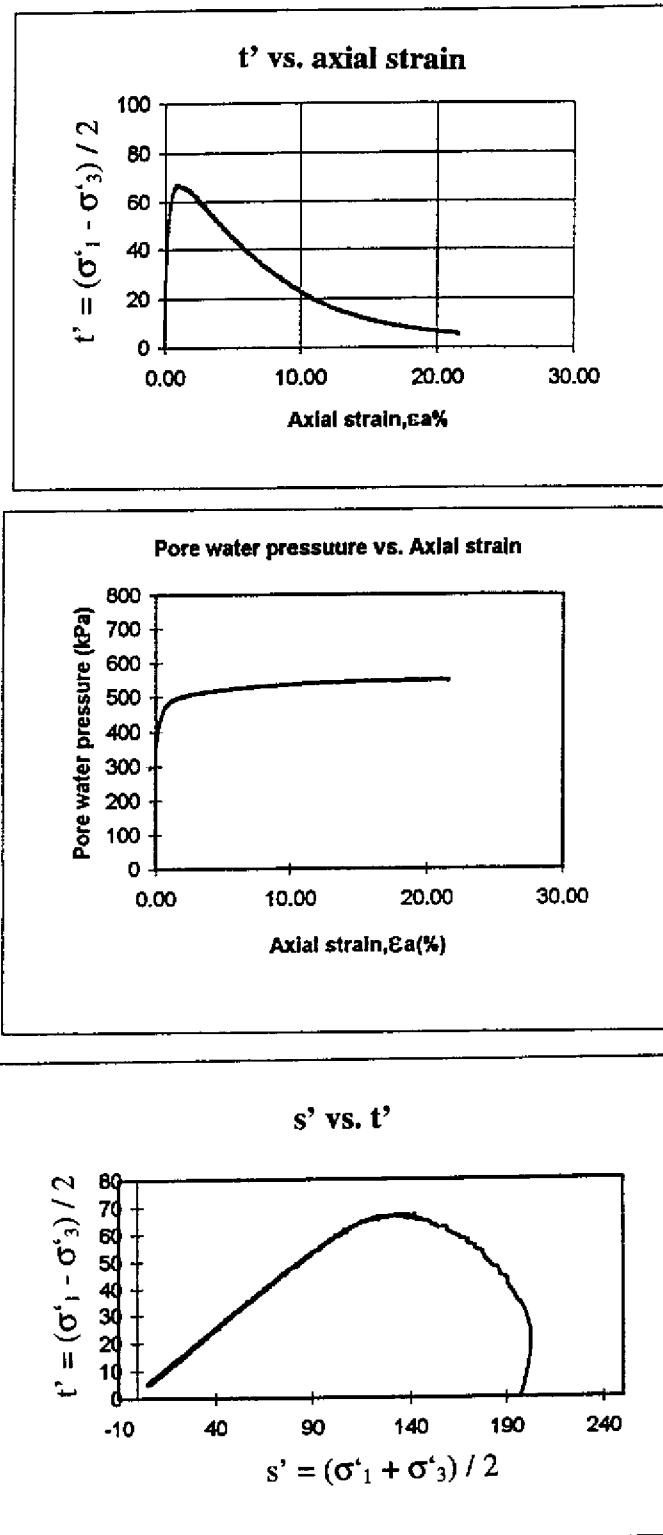


Figure 6.29 - CIU Test on Tung Chung Sand with $e_0 = 0.905$, $\sigma'_{3c} = 200$ kPa

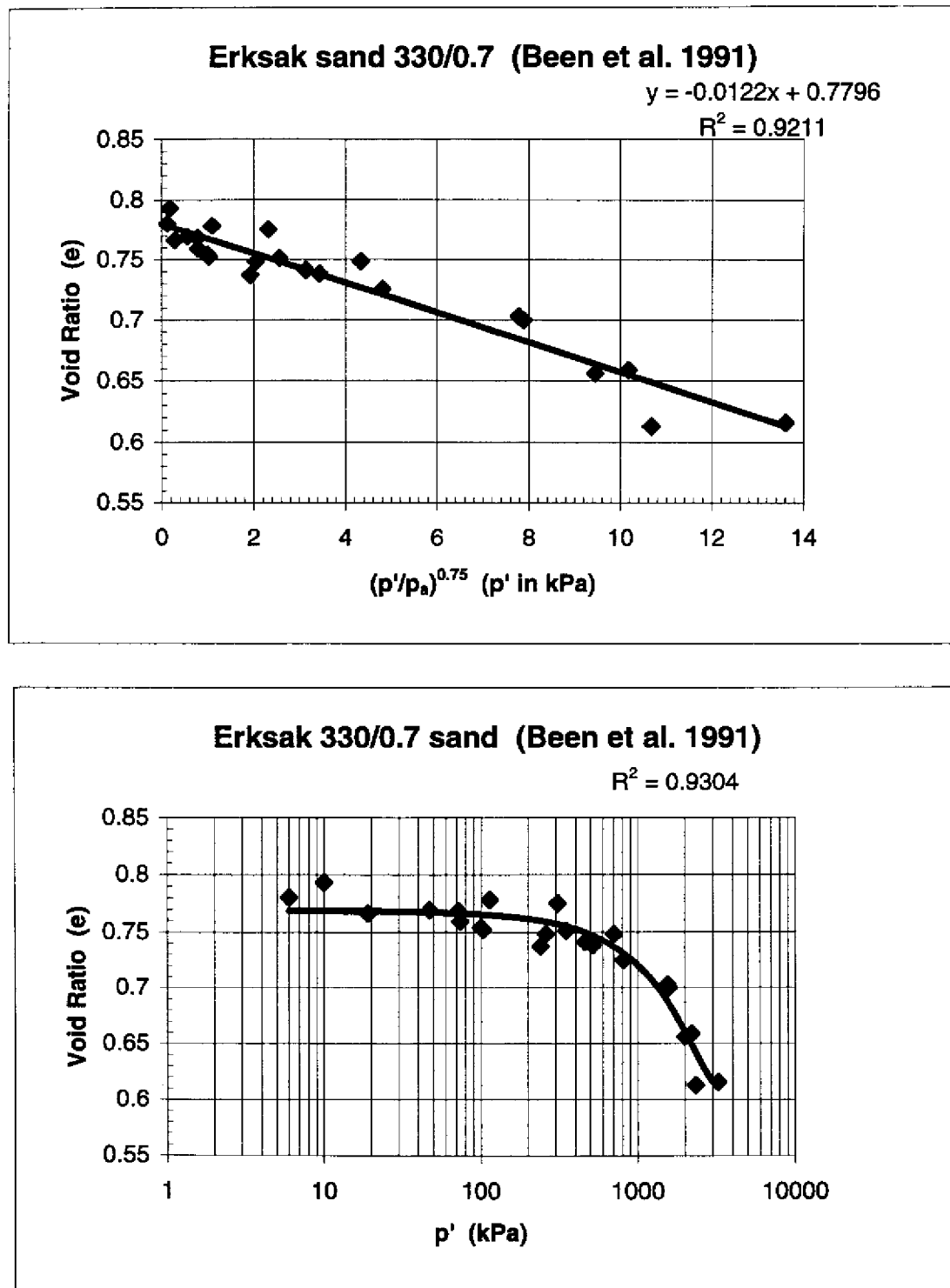


Figure 6.30 - Steady State Boundary Represented in e - $\log p'$ and e - $(p'/p_a)^{0.75}$ Spaces for the Erksak 330/0.7 Sand Tested by Been et al (1991)

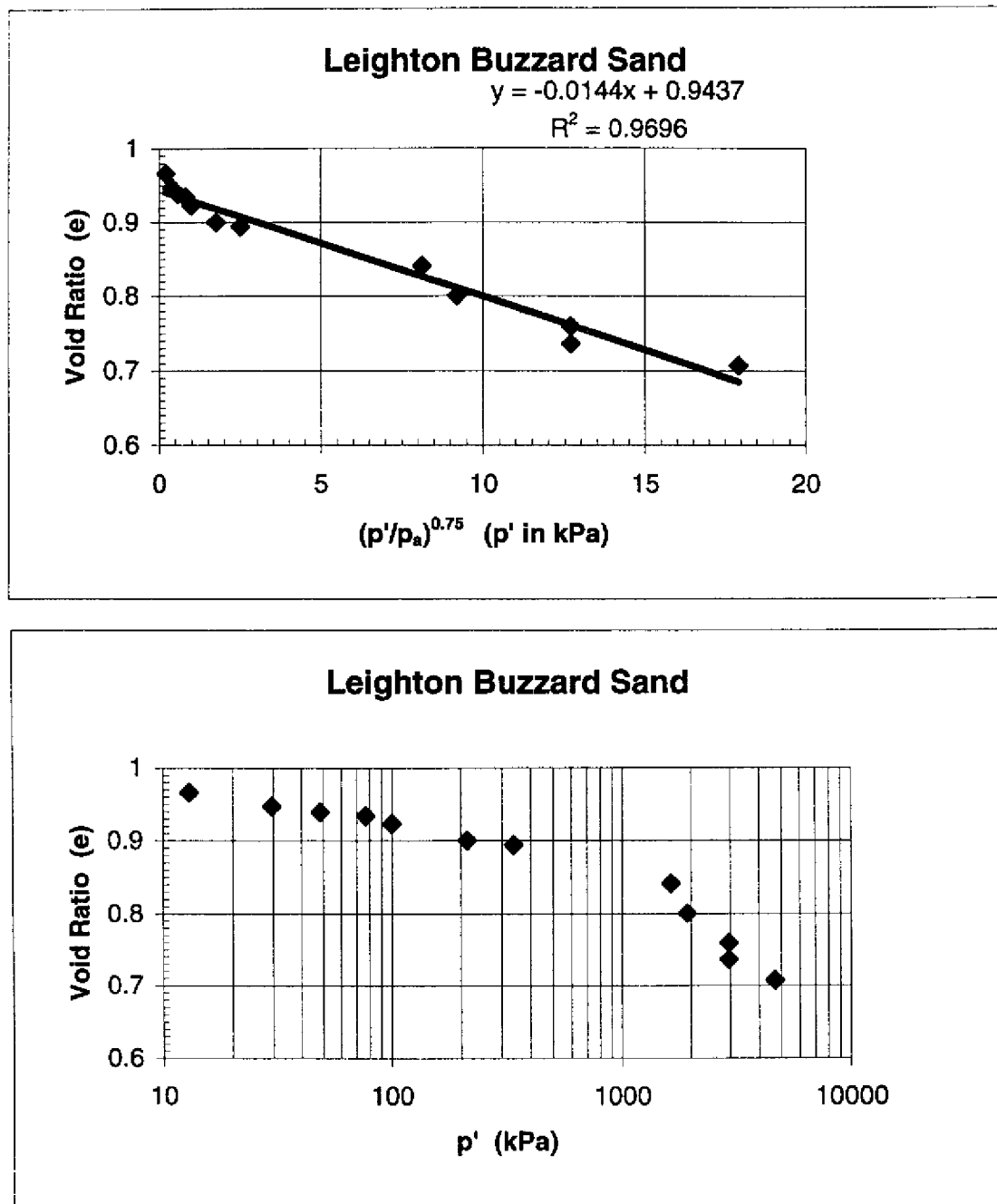


Figure 6.31 - Steady State Boundary Represented in e - $\log p'$ and e - $(p'/p_a)^{0.75}$ Spaces for the Leighton Buzzard Sand Tested by Been et al (1991)

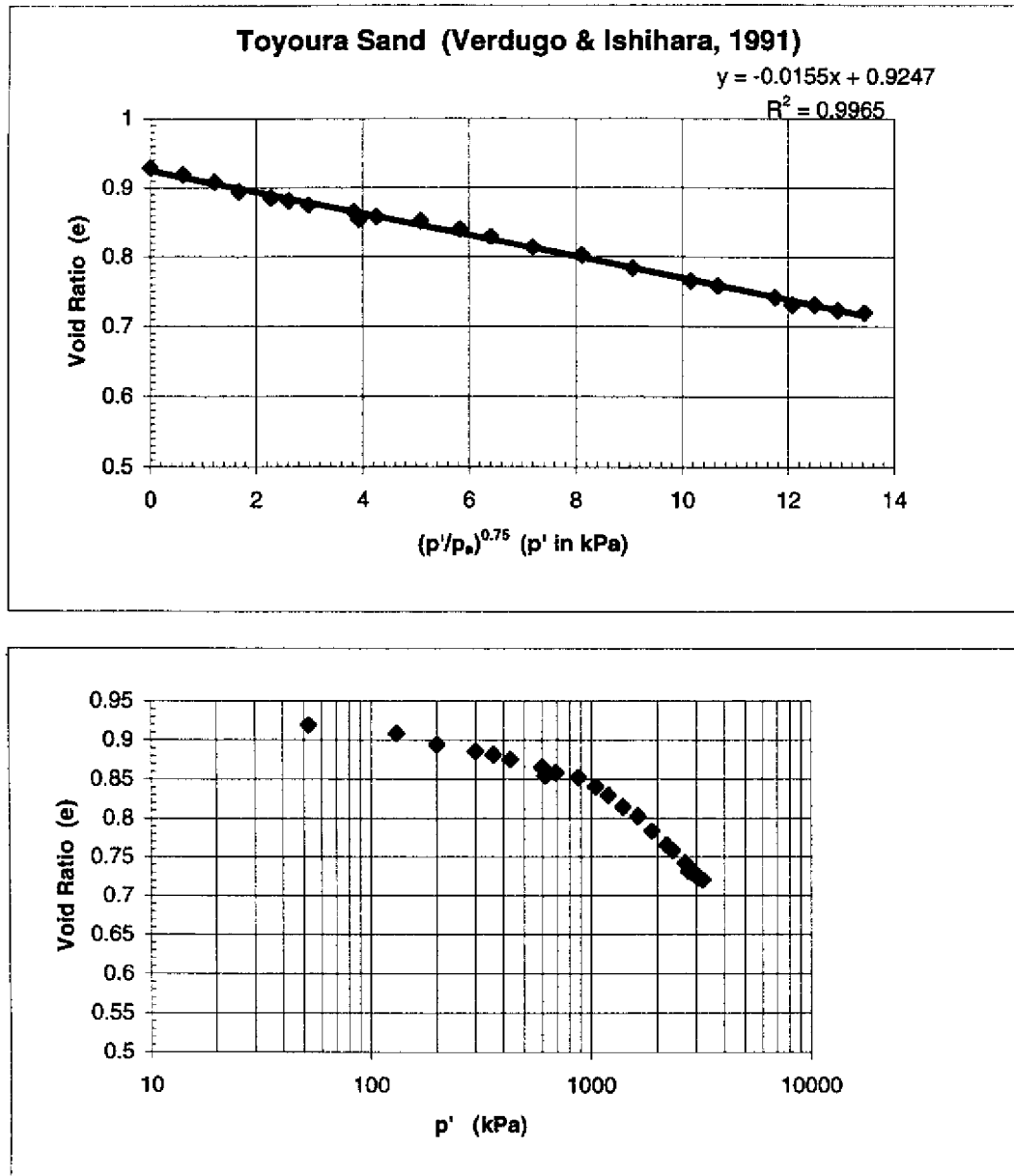


Figure 6.32 - Steady State Boundary Represented in e - $\log p'$ and e - $(p'/p_a)^{0.75}$ Spaces for the Toyoura Sand Tested by Verdugo and Ishihara (1991)

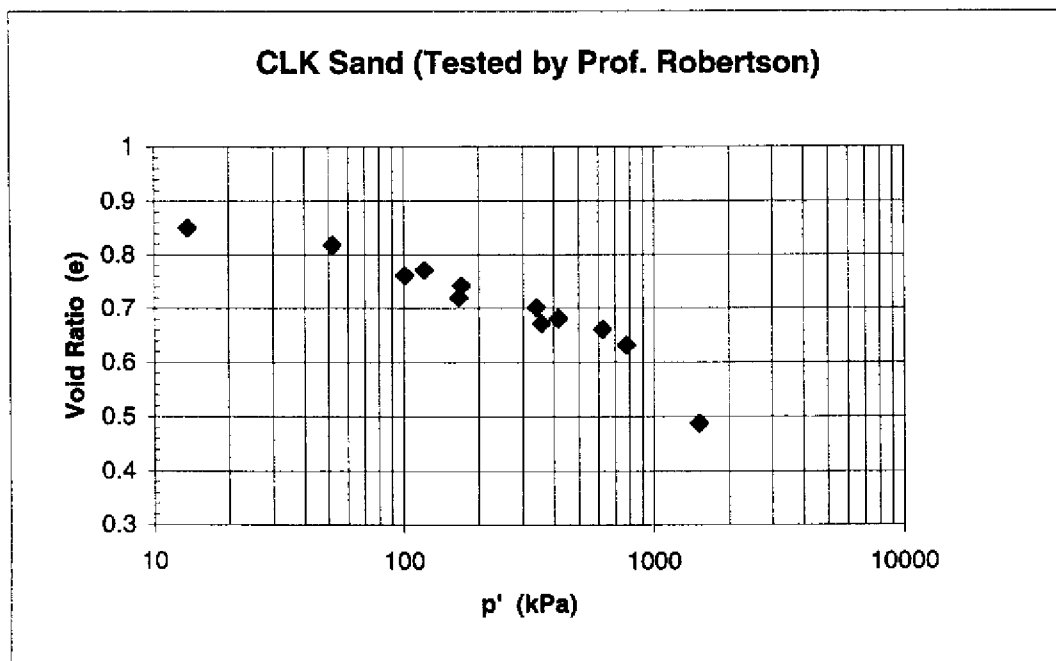
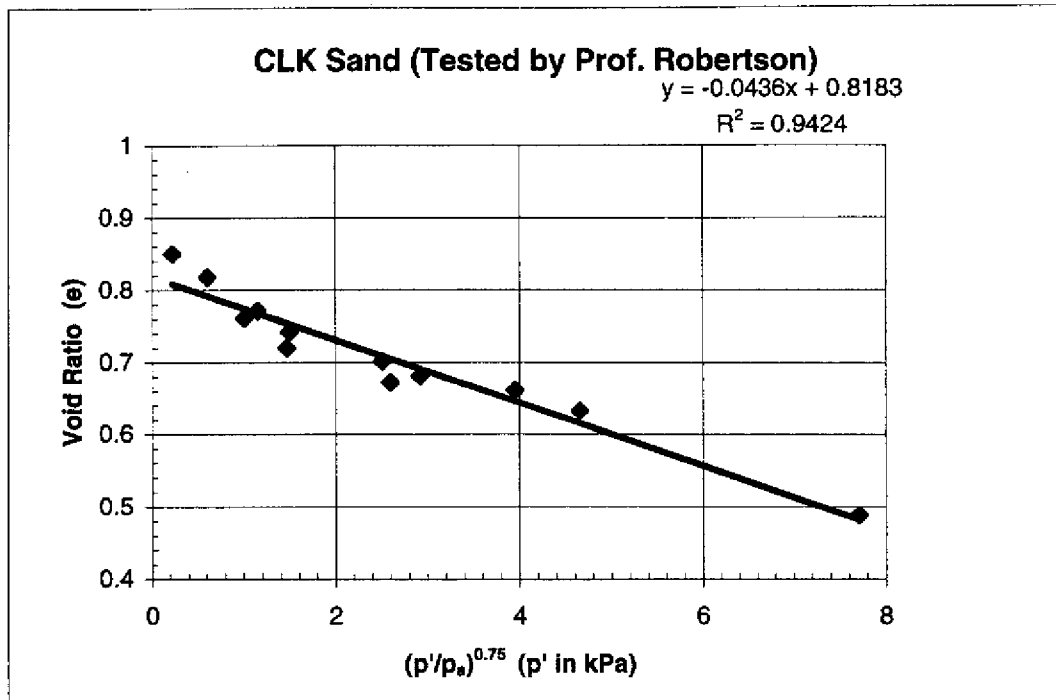


Figure 6.33 - Steady State Boundary Represented in $e - \log p'$ and $e - (p'/p_a)^{0.75}$ Spaces for the CLK Sand Test by Robertson (1994)

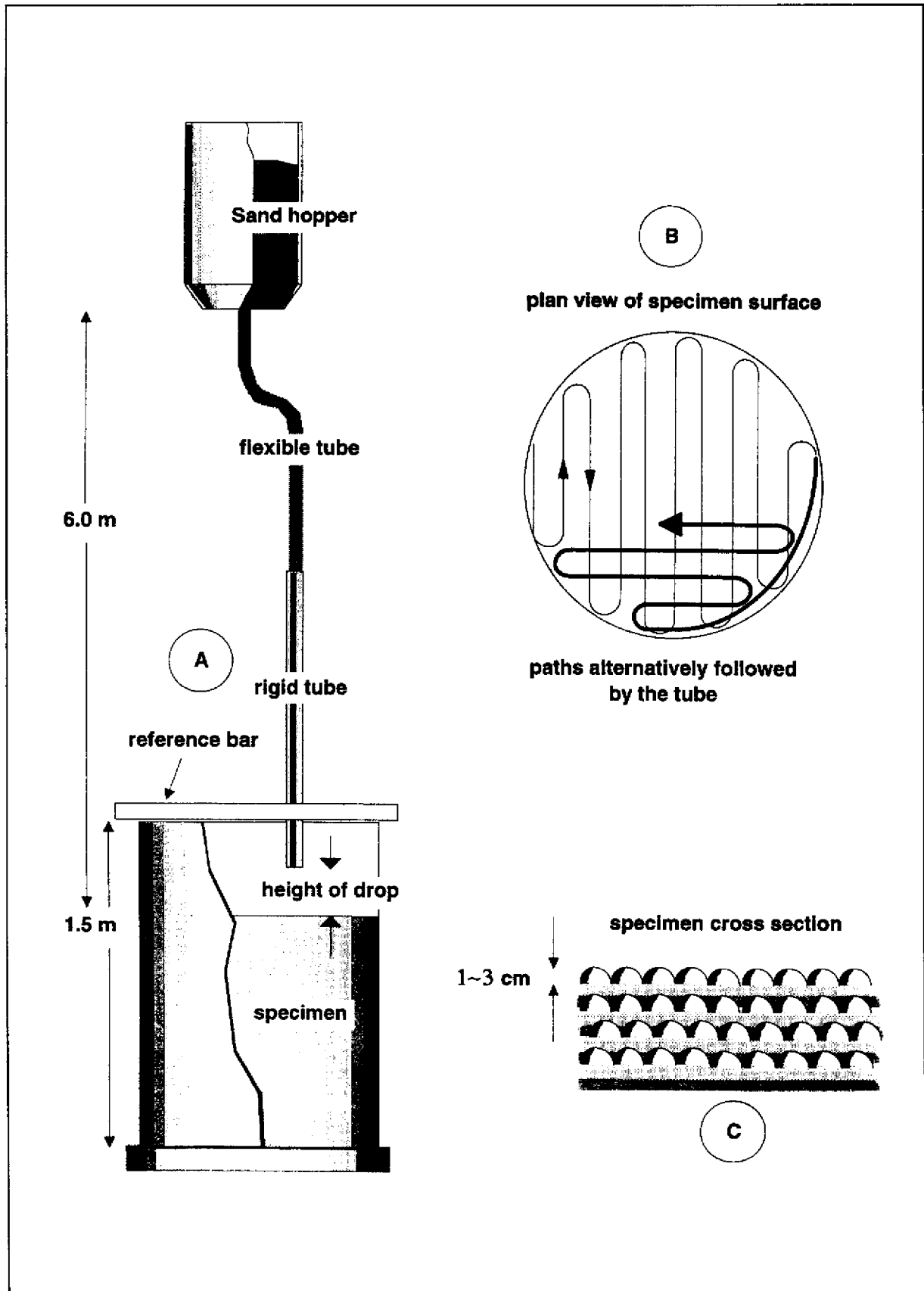


Figure 7.1 - Scheme of the Funnel Method for Specimen Preparation
(after Frelti et al, 1995)

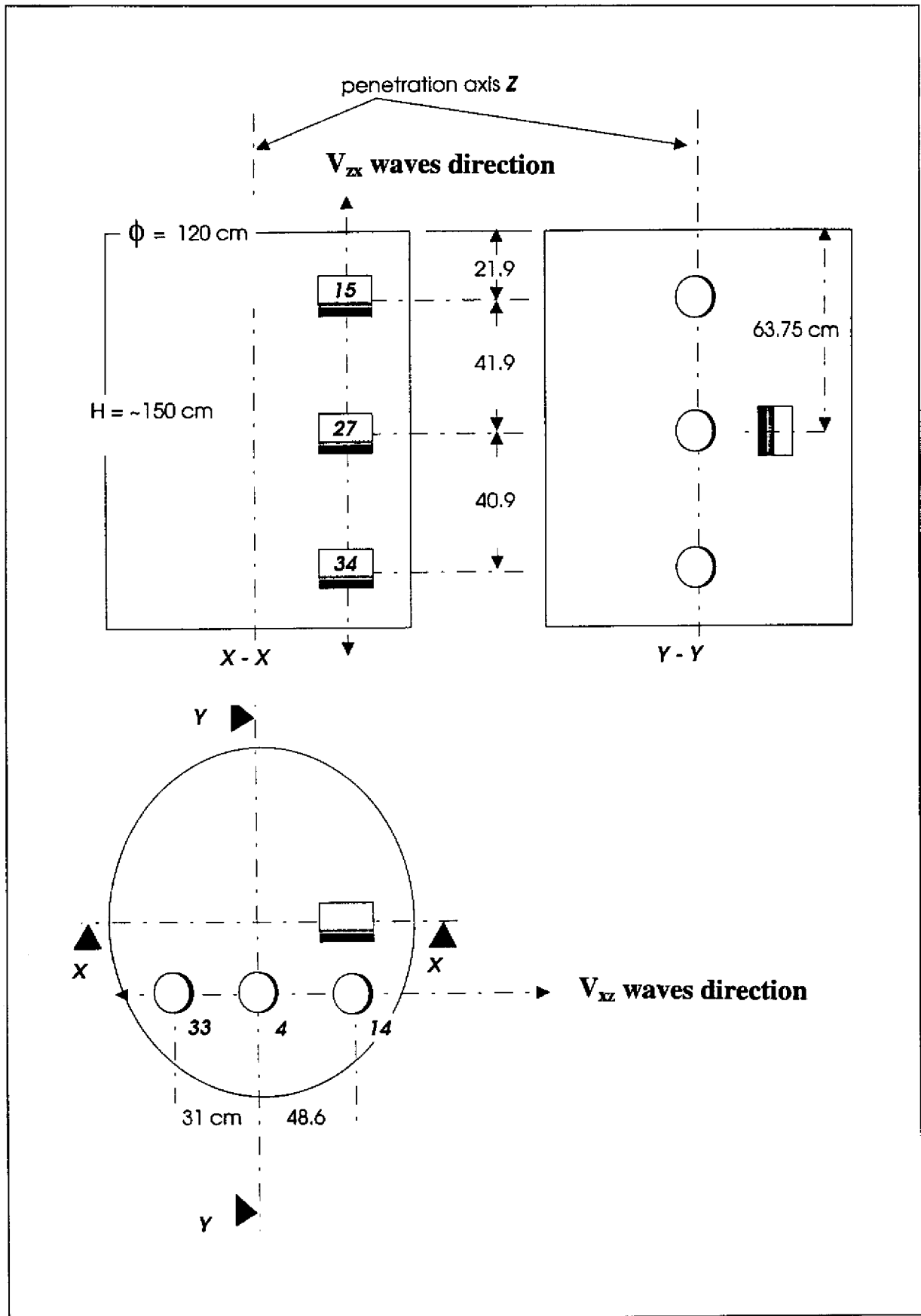


Figure 7.2 - Schematic of Bender Elements Location in Calibration Chamber

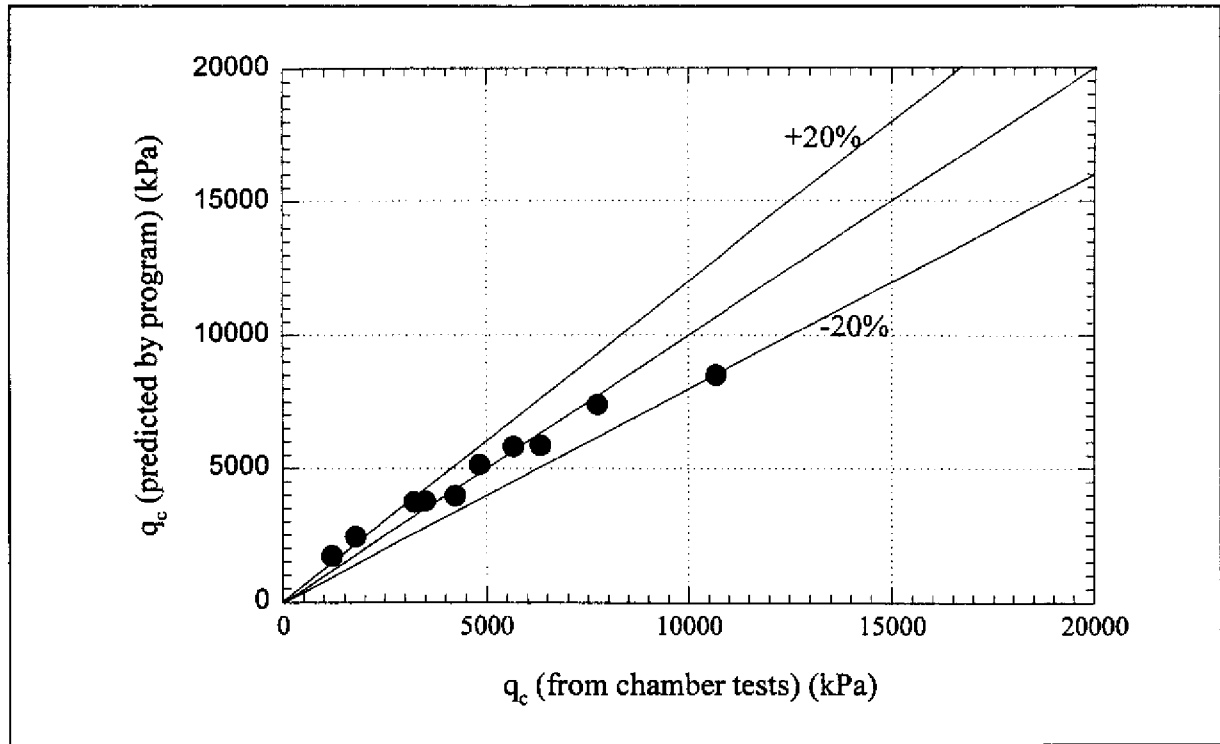


Figure 7.3 - Comparison between q_c Predicted by the Computer Code and the Actual Chamber Test Results for TC Sand

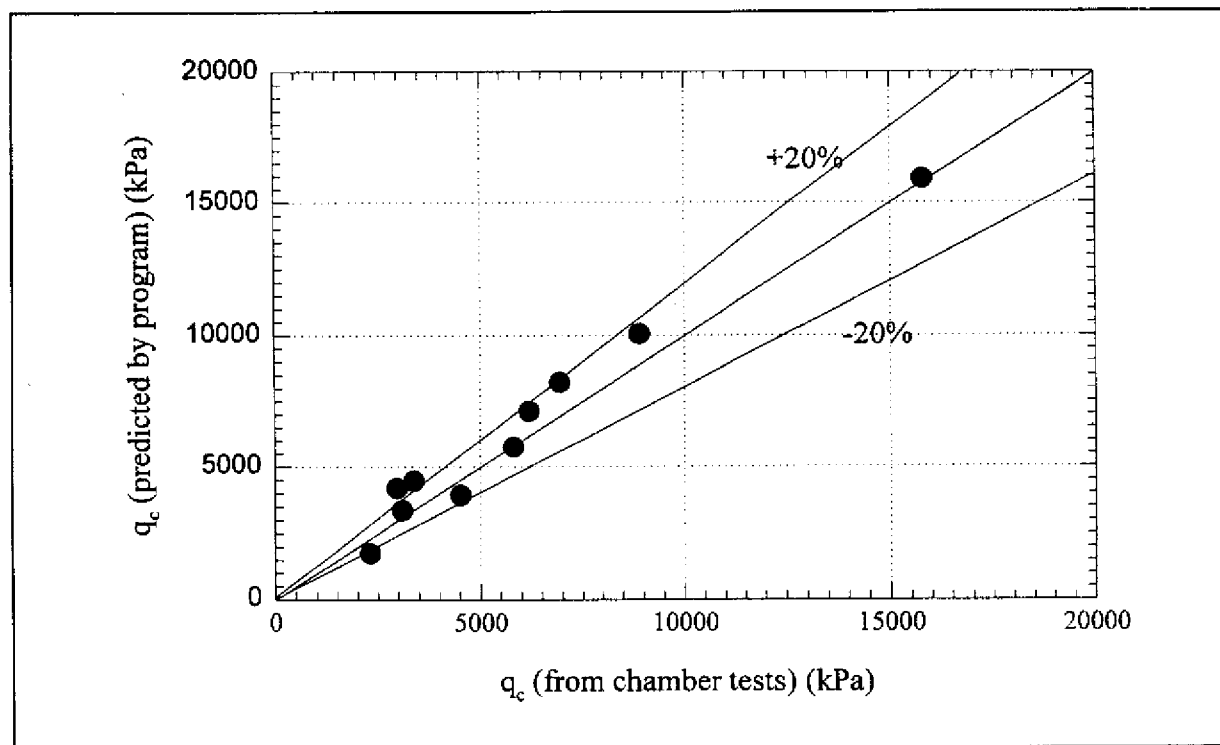


Figure 7.4 - Comparison between q_c Predicted by the Computer Code and the Actual Chamber Test Results for CLK Sand

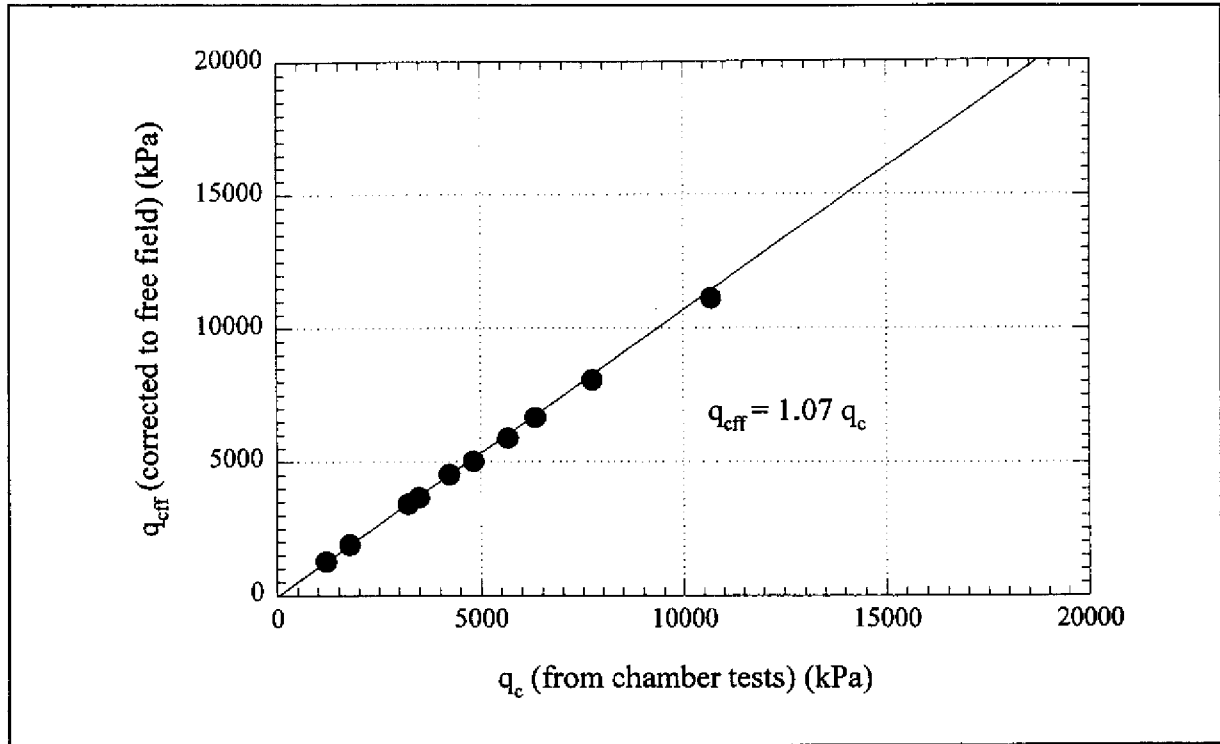


Figure 7.5 - Relationship between q_c Obtained from Calibration Chamber Tests and Corrected Free Field Penetration Resistance ($q_{c,ff}$) for TC Sand

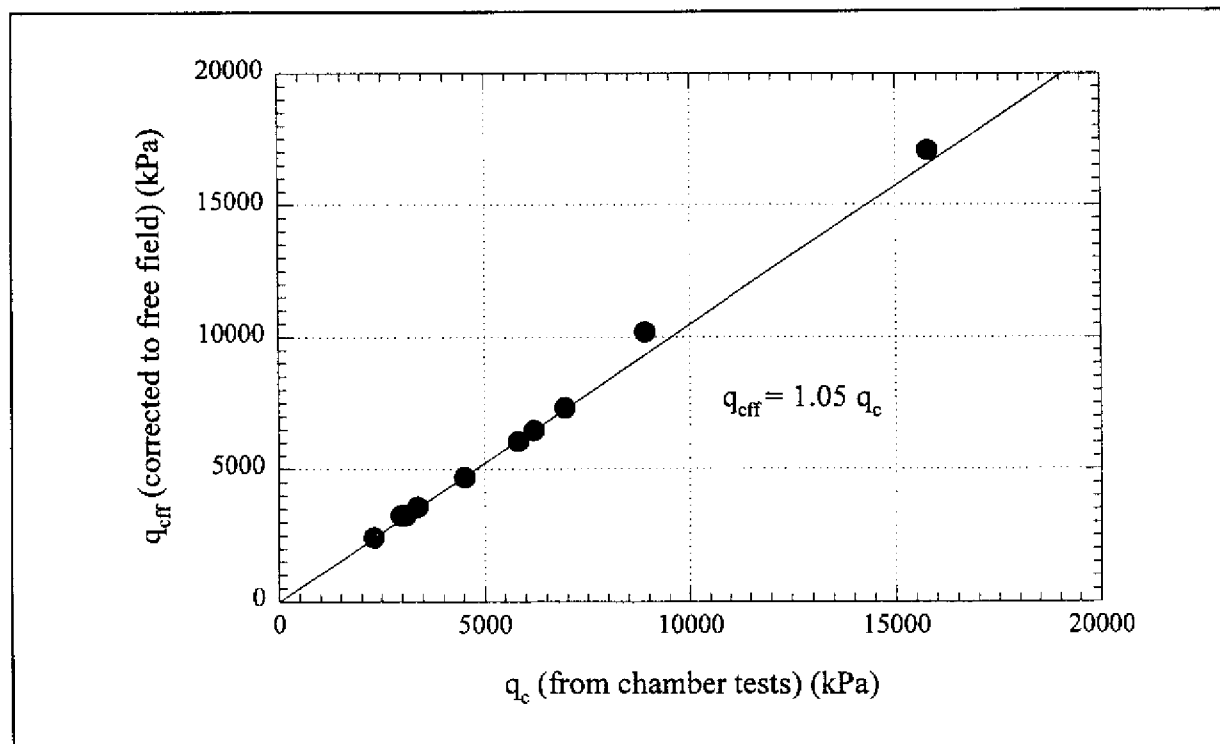


Figure 7.6 - Relationship between q_c Obtained from Calibration Chamber Tests and Corrected Free Field Penetration Resistance ($q_{c,ff}$) for CLK Sand

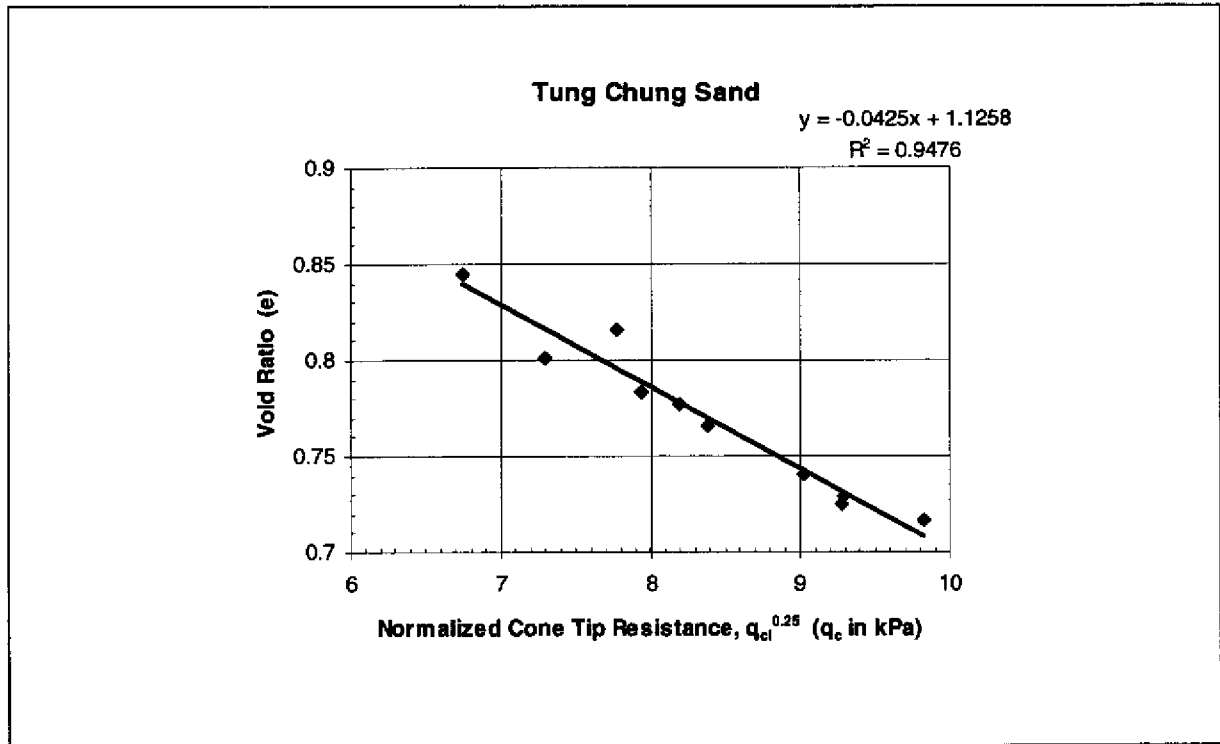


Figure 7.7 - Correlation between Void Ratio (e) with the Normalized Cone Tip Resistance ($q_{cl}^{0.25}$) for the TC Sand

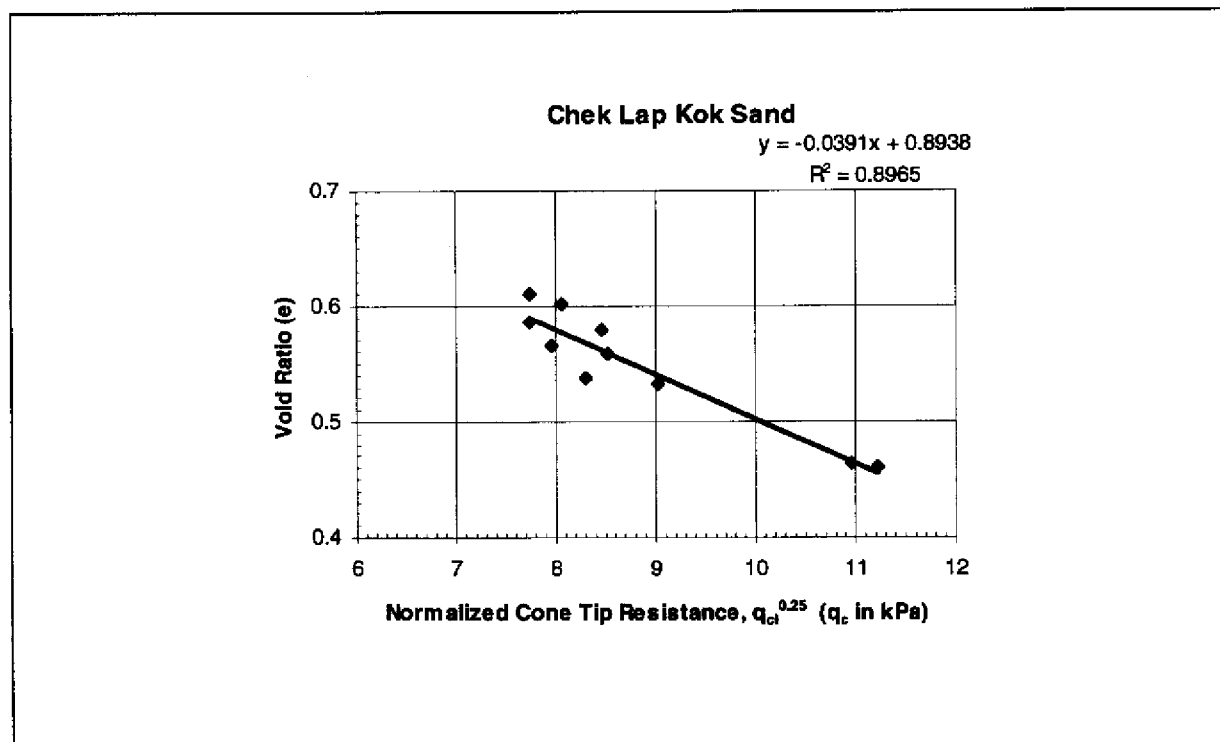


Figure 7.8 - Correlation between Void Ratio (e) with the Normalized Cone Tip Resistance ($q_{cl}^{0.25}$) for the CLK Sand

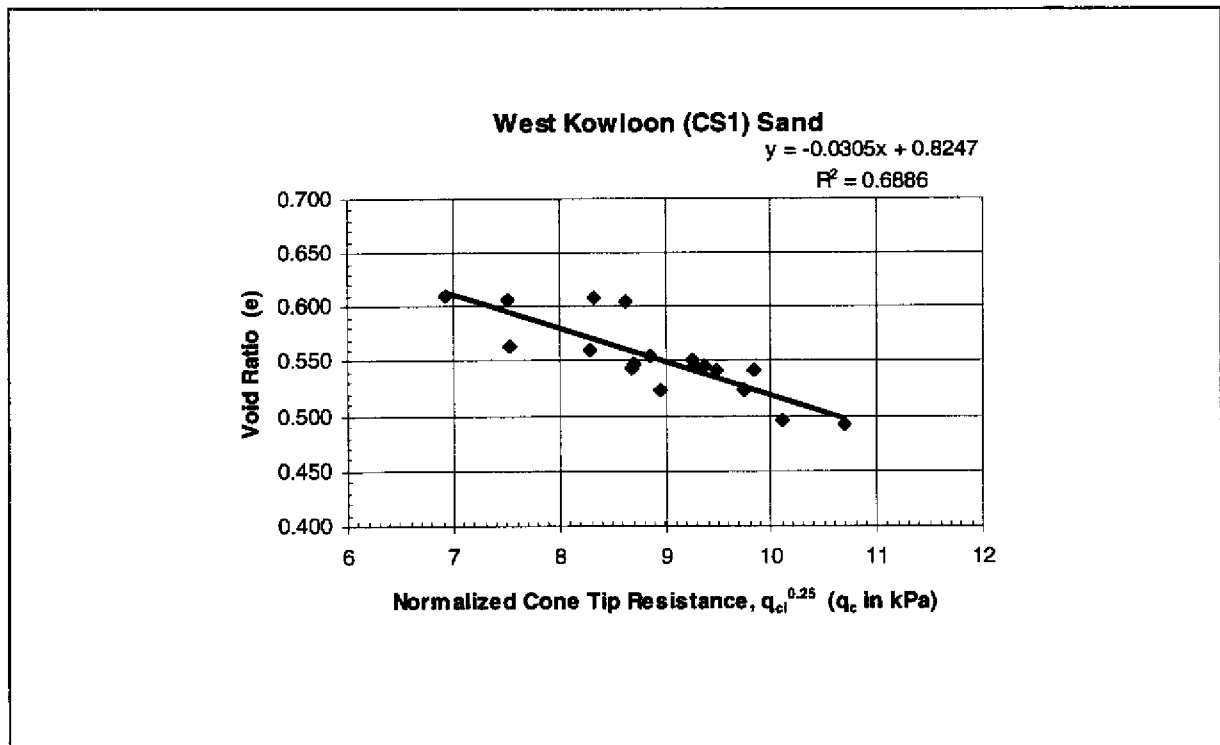


Figure 7.9 - Correlation between Void Ratio (e) with the Normalized Cone Tip Resistance ($q_{cl}^{0.25}$) for the CS1 Sand

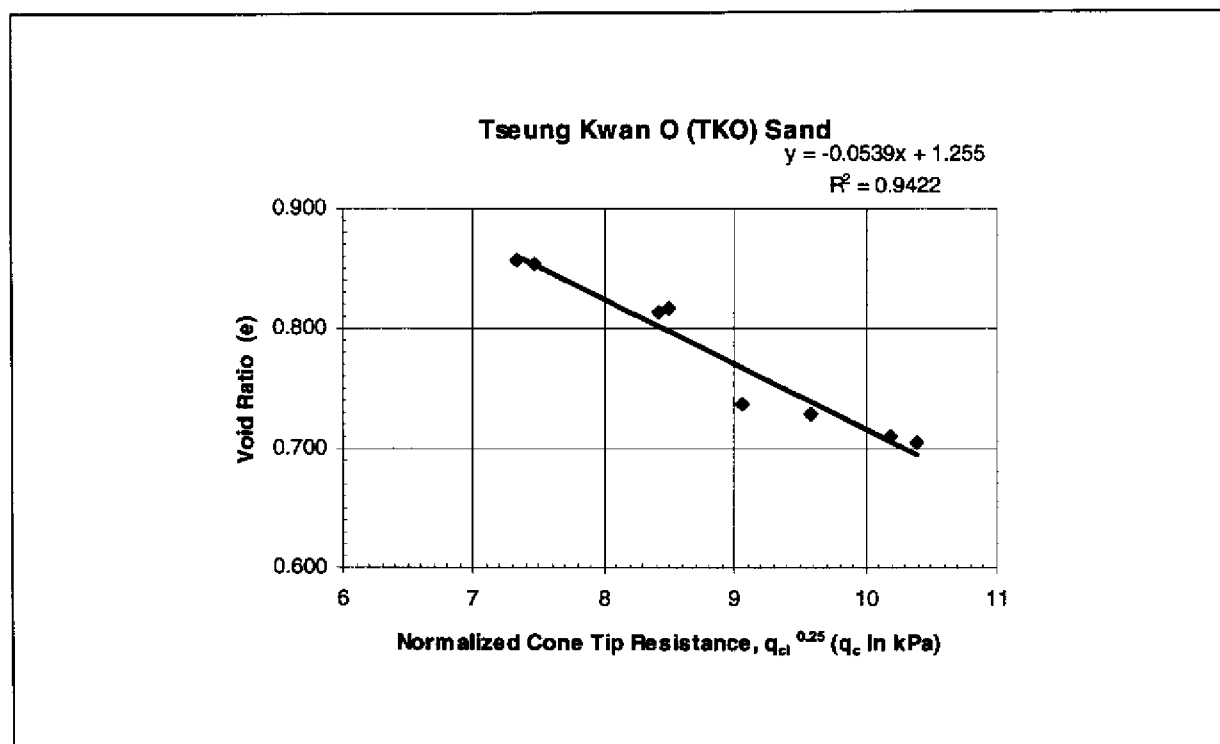


Figure 7.10 - Correlation between Void Ratio (e) with the Normalized Cone Tip Resistance ($q_{cl}^{0.25}$) for the TKO Sand

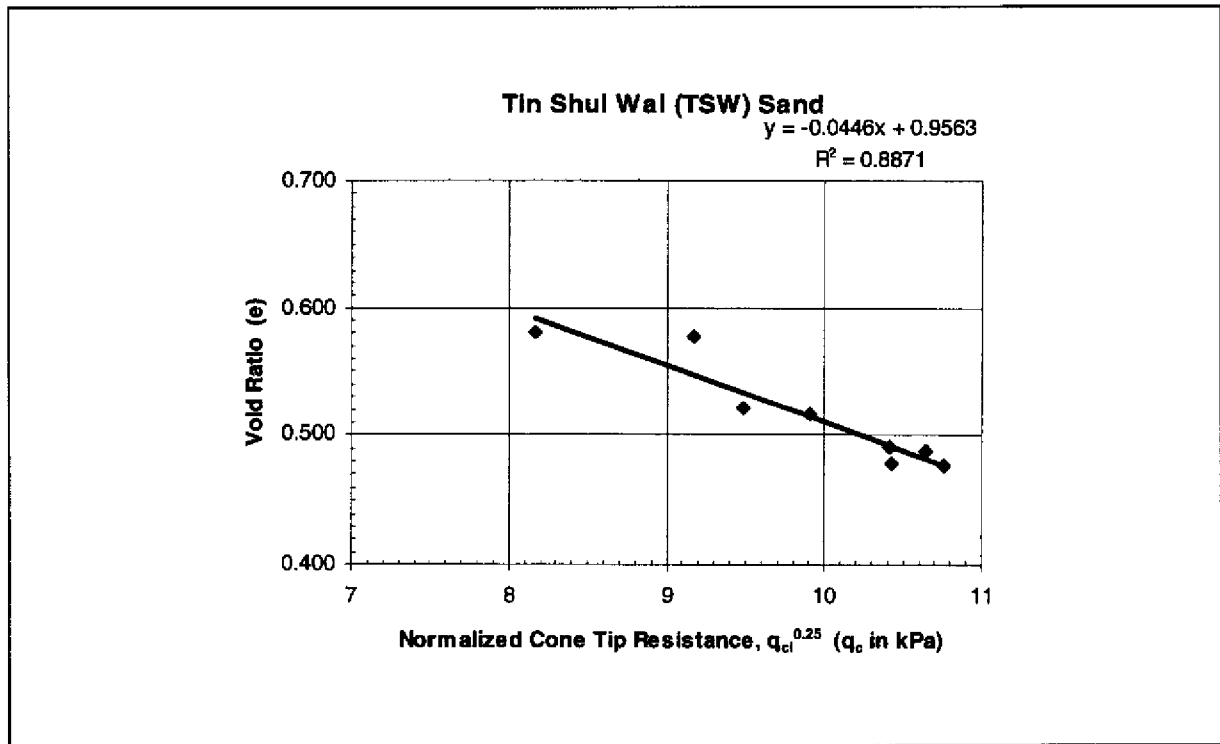


Figure 7.11 - Correlation between Vold Ratio (e) with the Normalized Cone Tip Resistance ($q_{cl}^{0.25}$) for the TSW Sand

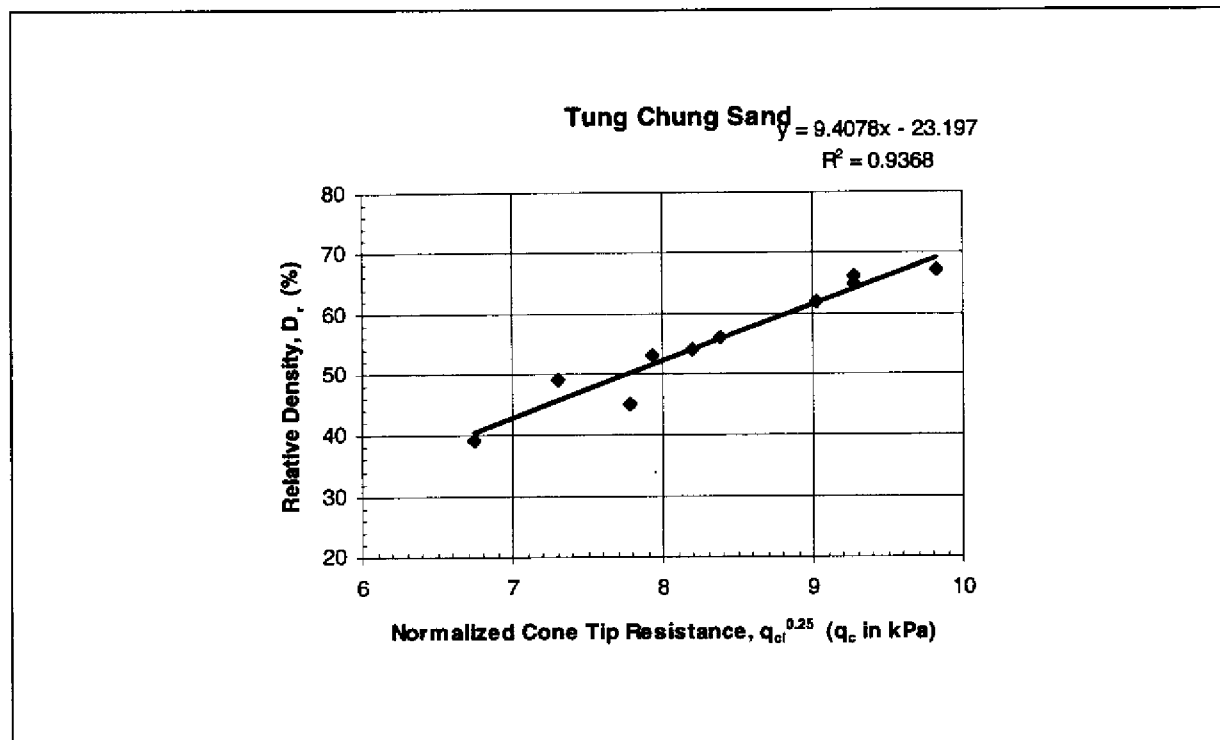


Figure 7.12 - Correlation between Relative Density (D_r) with the Normalized Cone Tip Resistance ($q_{cl}^{0.25}$) for the TC Sand

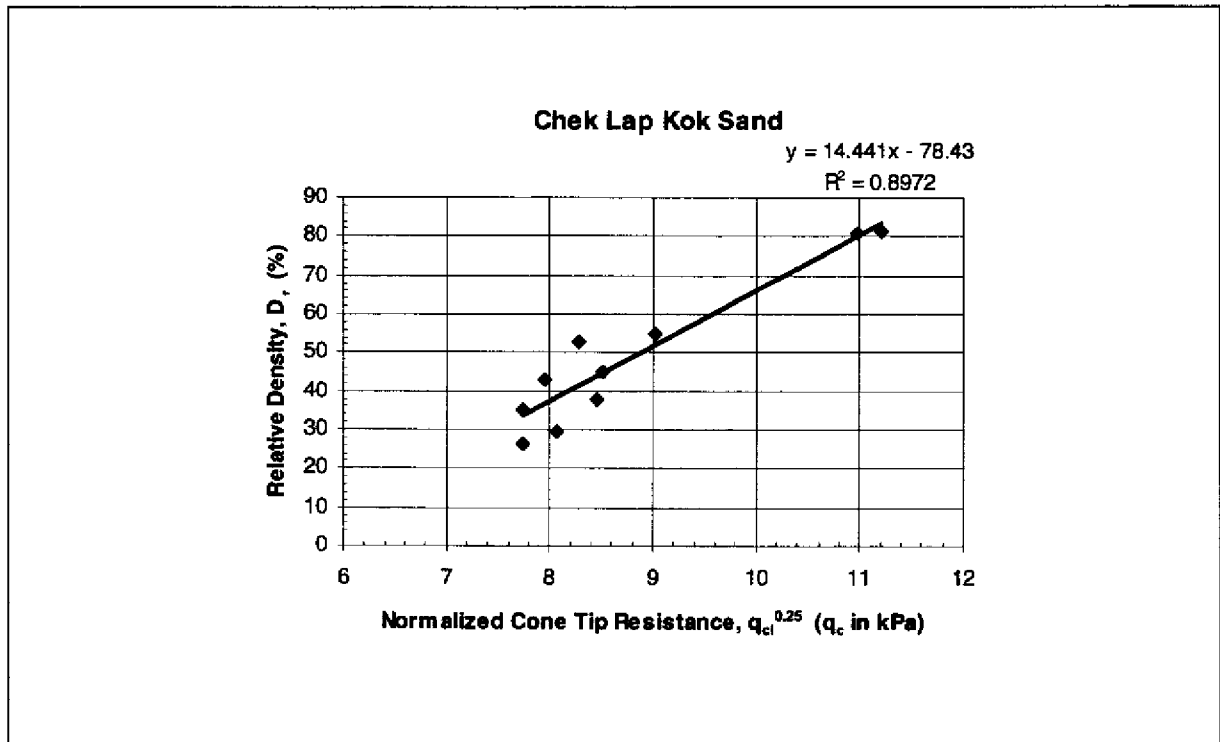


Figure 7.13 - Correlation between Relative Density (D_r) with the Normalized Cone Tip Resistance ($q_{cl}^{0.25}$) for the CLK Sand

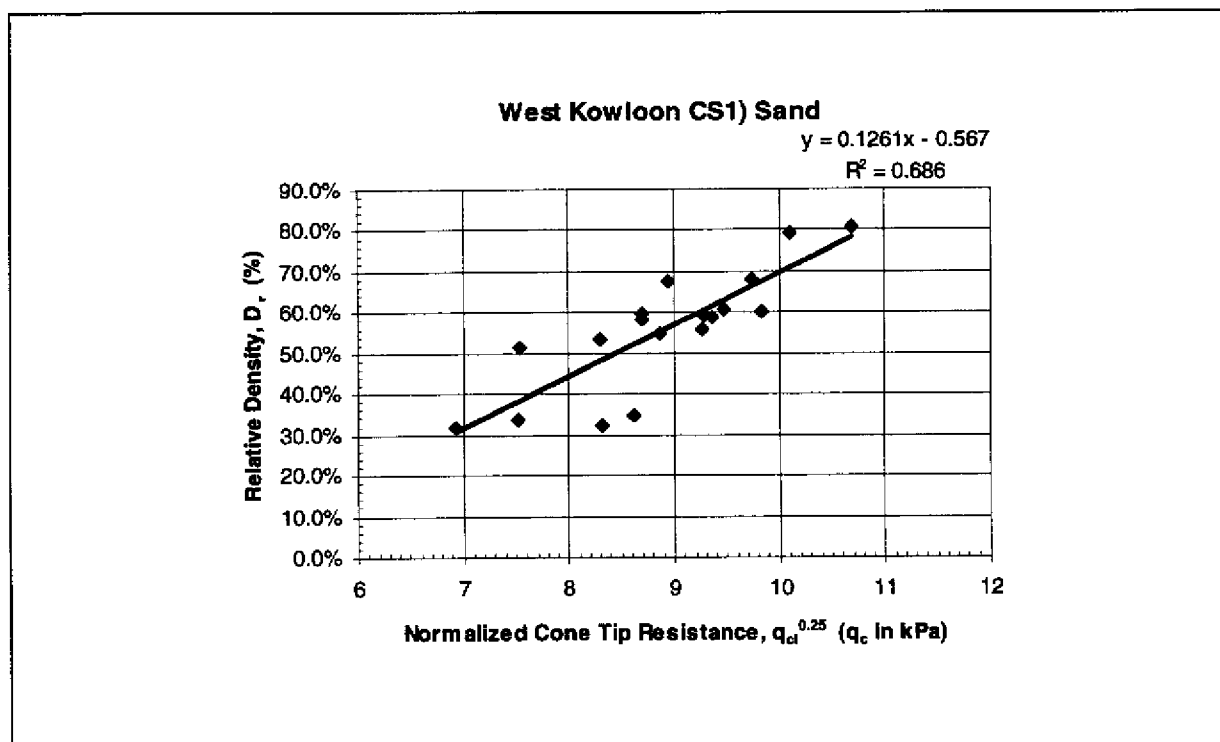


Figure 7.14 - Correlation between Relative Density (D_r) with the Normalized Cone Tip Resistance ($q_{cl}^{0.25}$) for the CS1 Sand

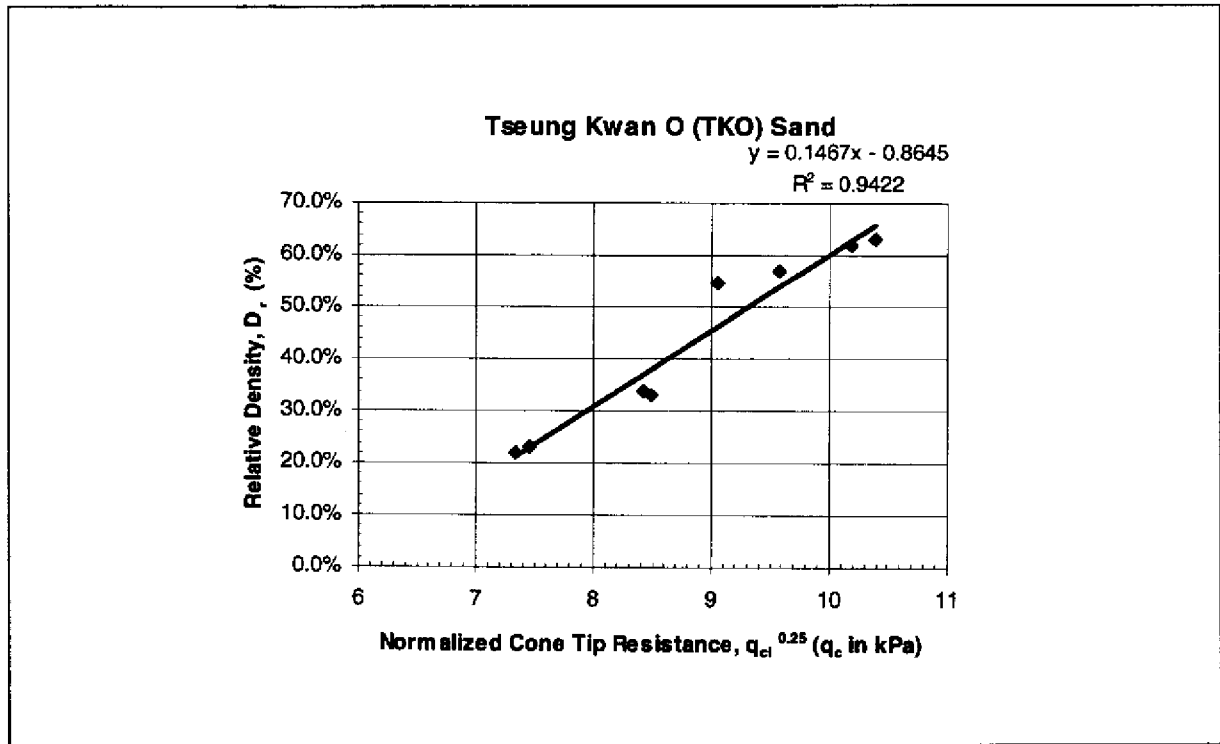


Figure 7.15 - Correlation between Relative Density (D_r) with the Normalized Cone Tip Resistance ($q_{cl}^{0.25}$) for the TKO Sand

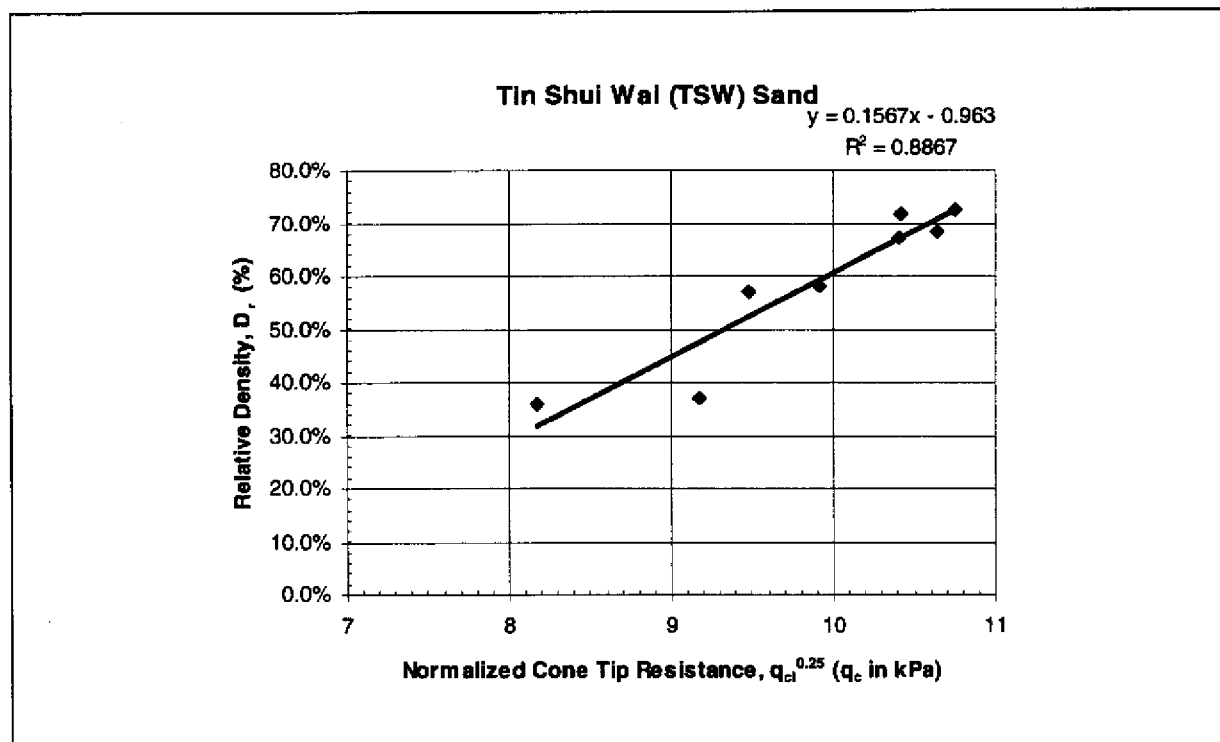


Figure 7.16 - Correlation between Relative Density (D_r) with the Normalized Cone Tip Resistance ($q_{cl}^{0.25}$) for the TSW Sand

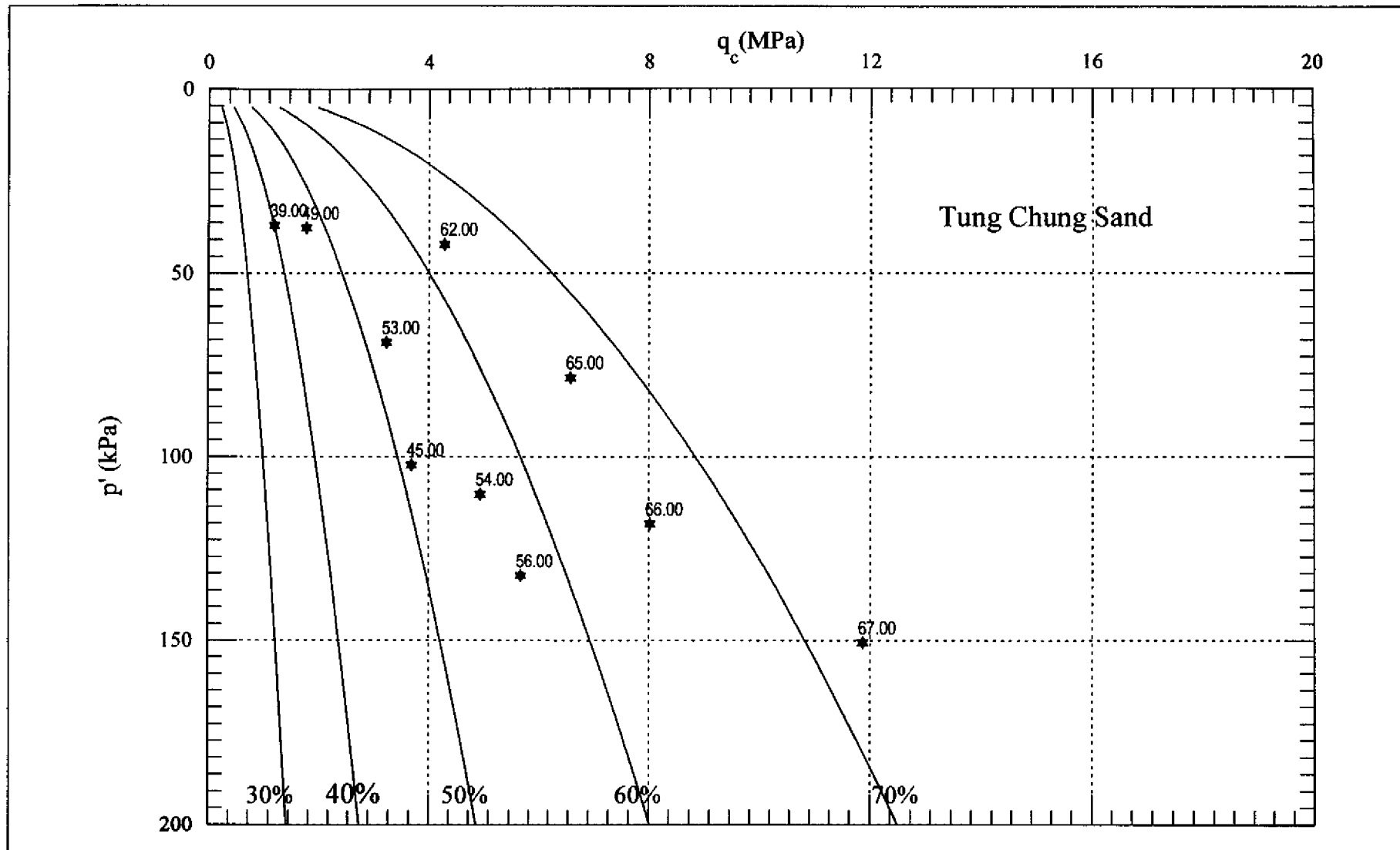


Figure 7.17 - Effective Mean Normal Stress (p') versus Cone Tip Resistance (q_c) with Contours of Relative Density (D_r) and Typical Calibration Test Results (Marked with Laboratory Measured D_r Values in Percentage) for the TC Sand

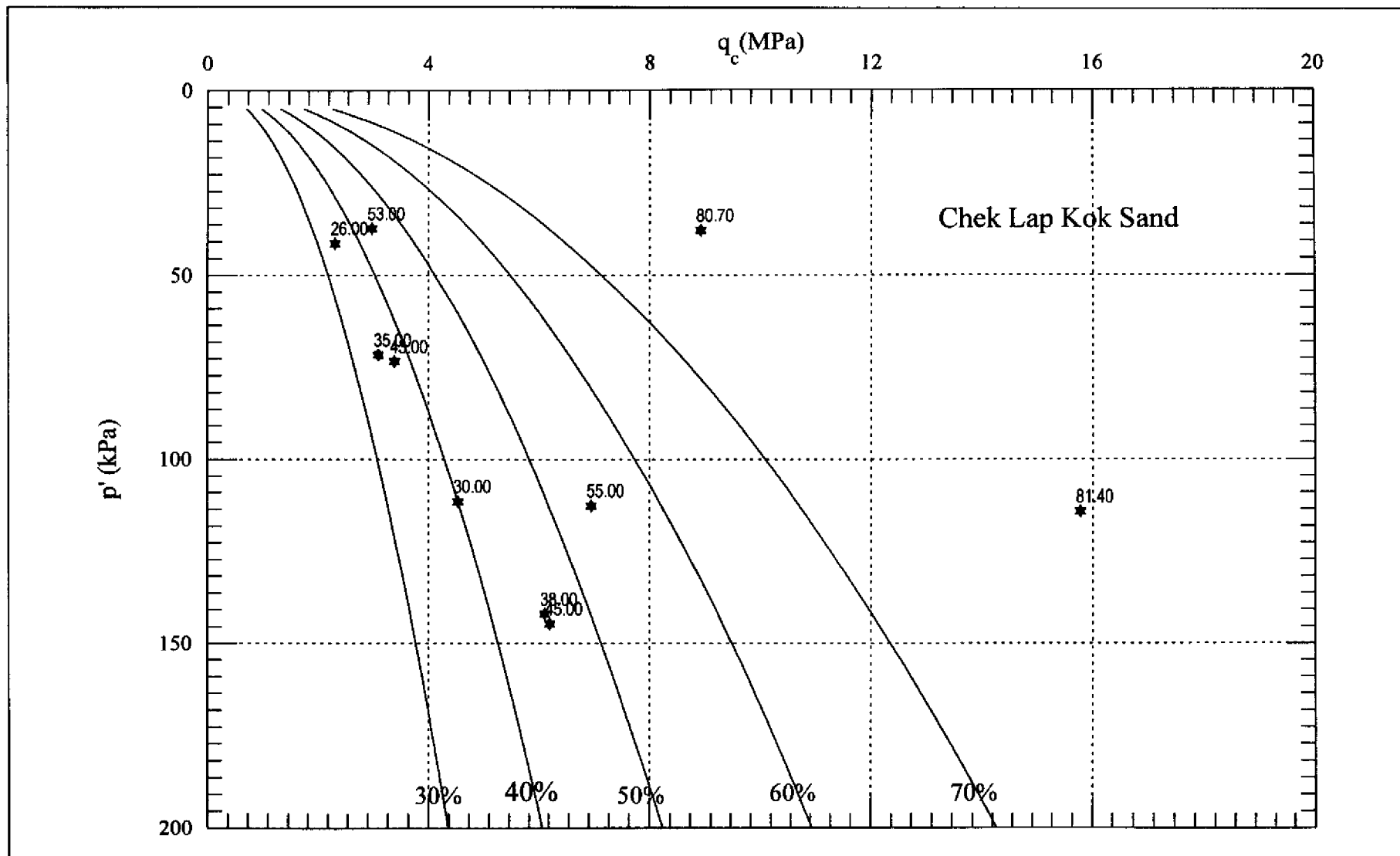


Figure 7.18 - Effective Mean Normal Stress (p') versus Cone Tip Resistance (q_c) with Contours of Relative Density (D_r) and Typical Calibration Test Results (Marked with Laboratory Measured D_r Values in Percentage) for the CLK Sand

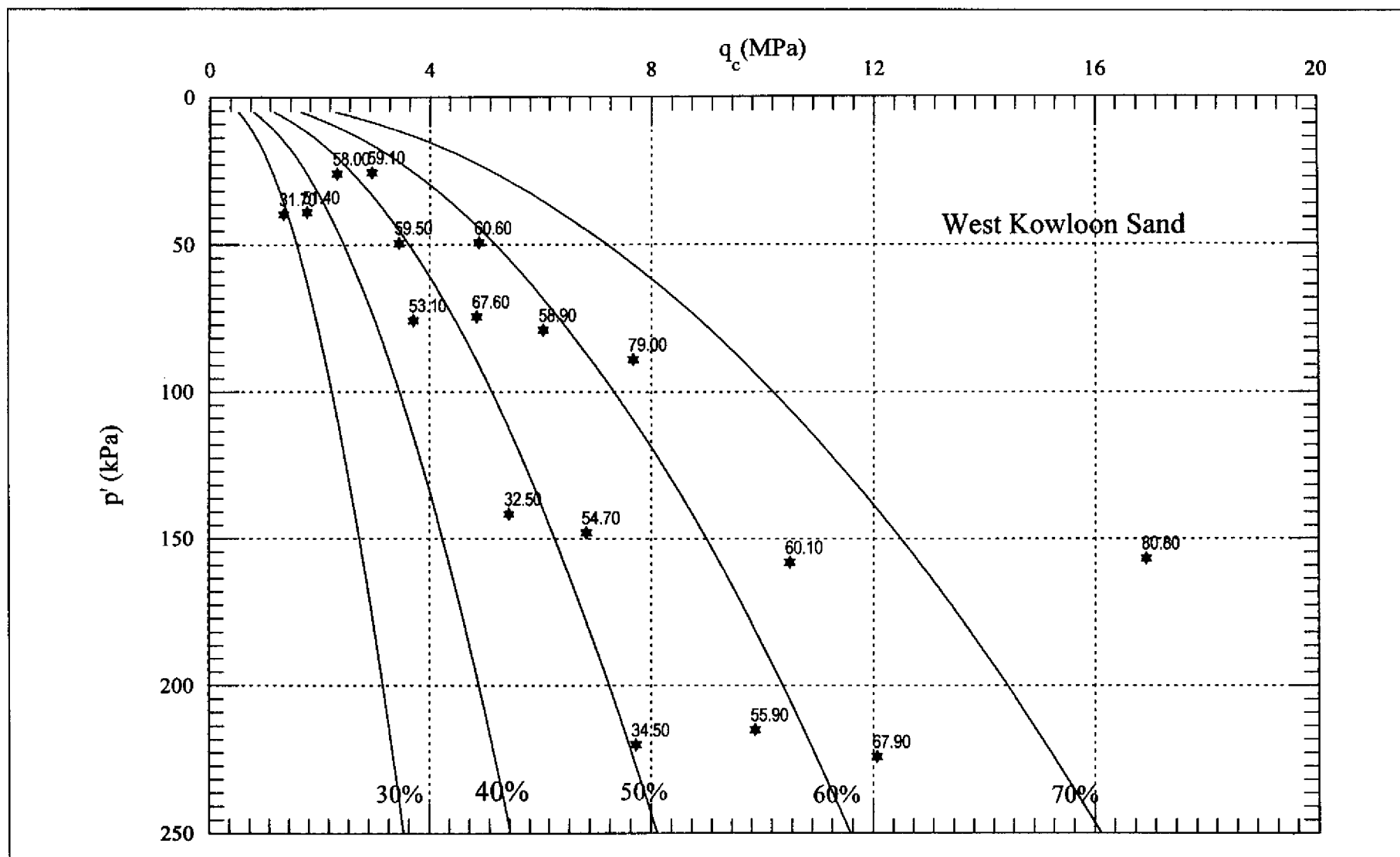


Figure 7.19 - Effective Mean Normal Stress (p') versus Cone Tip Resistance (q_c) with Contours of Relative Density (D_r) and Typical Calibration Test Results (Marked with Laboratory Measured D_r Values in Percentage) for the CS1 Sand

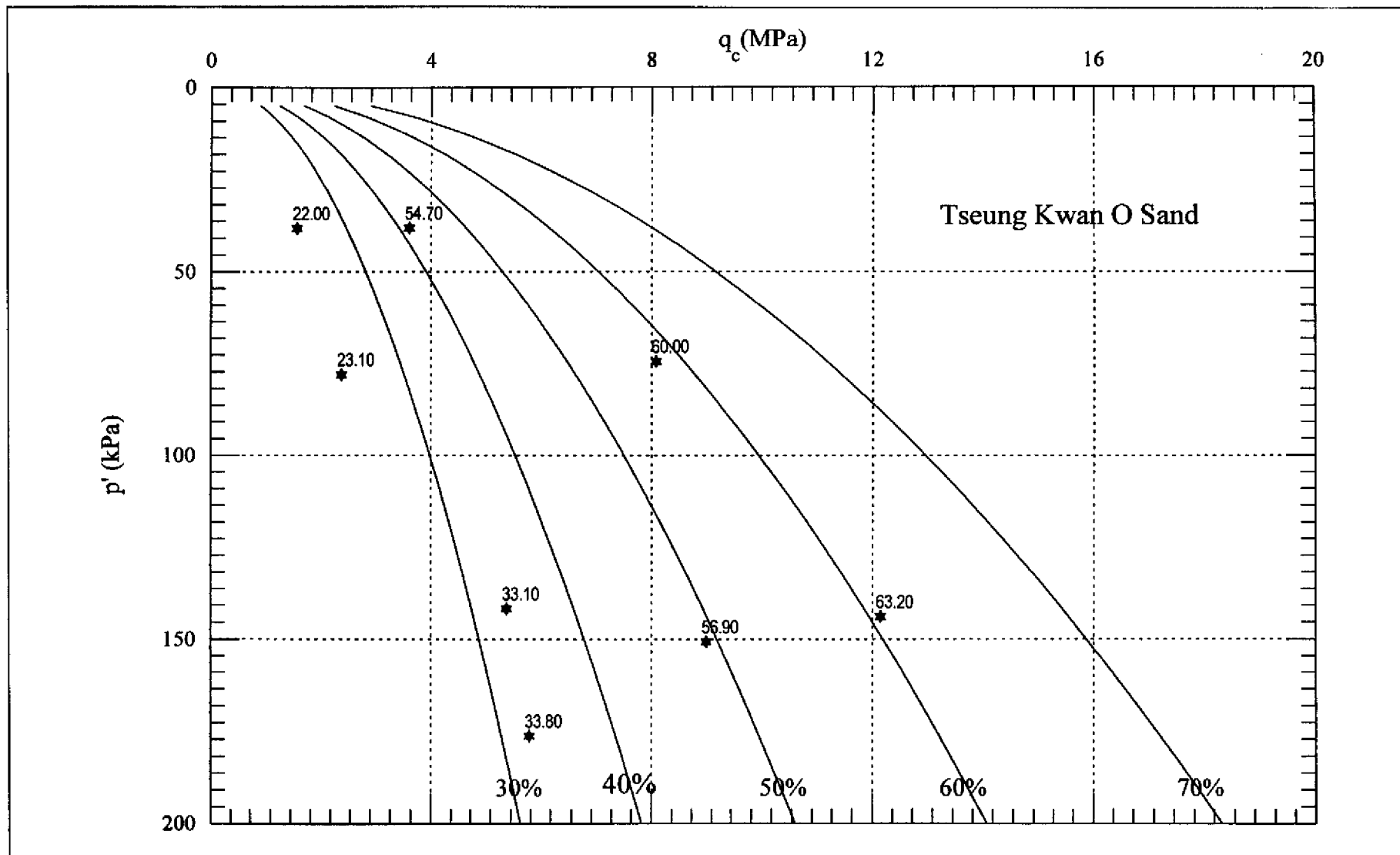


Figure 7.20 - Effective Mean Normal Stress (p') versus Cone Tip Resistance (q_c) with Contours of Relative Density (D_r) and Typical Calibration Test Results (Marked with Laboratory Measured D_r Values in Percentage) for the TKO Sand

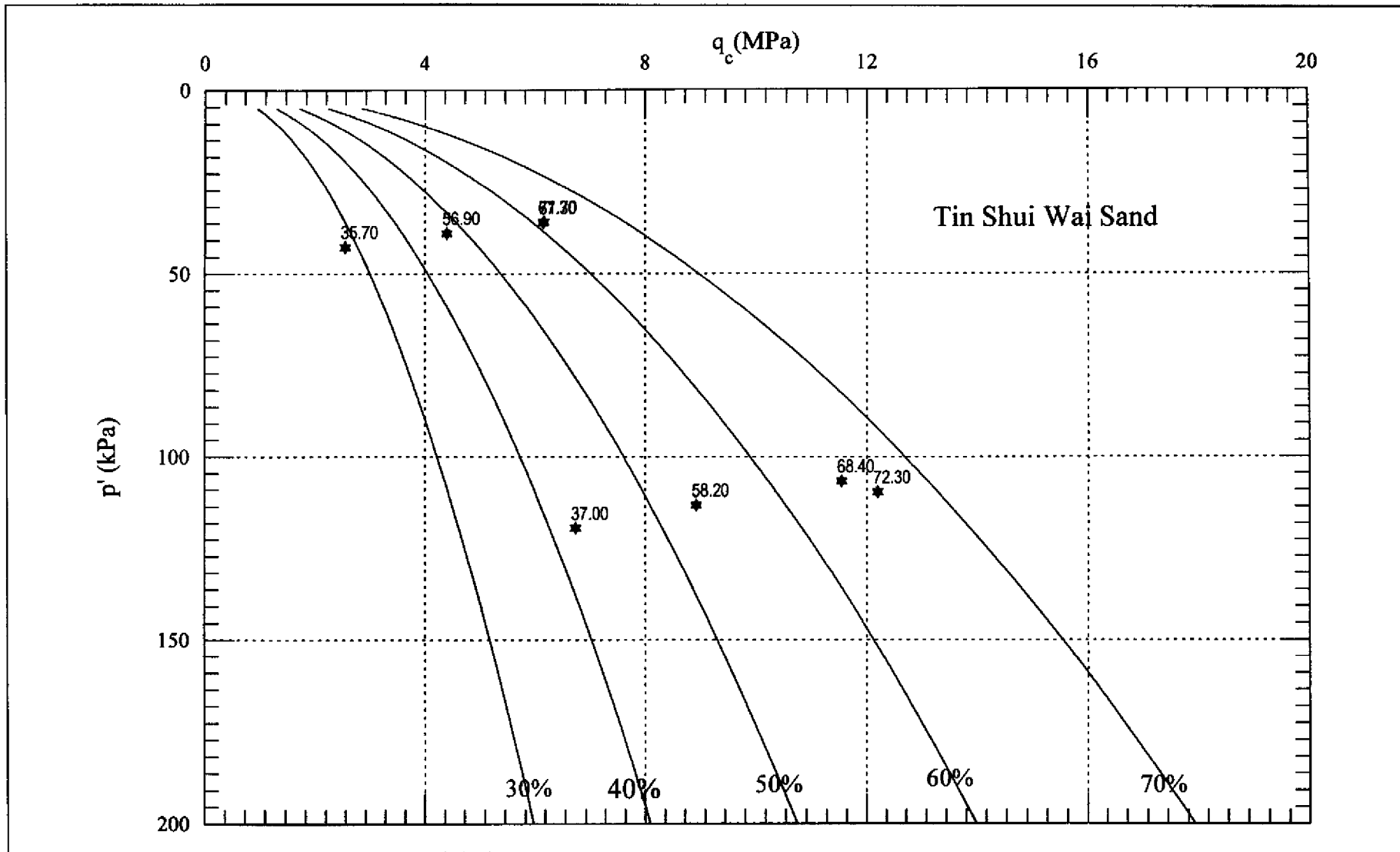


Figure 7.21 - Effective Mean Normal Stress (p') versus Cone Tip Resistance (q_c) with Contours of Relative Density (D_r) and Typical Calibration Test Results (Marked with Laboratory Measured D_r Values in Percentage) for the TSW Sand

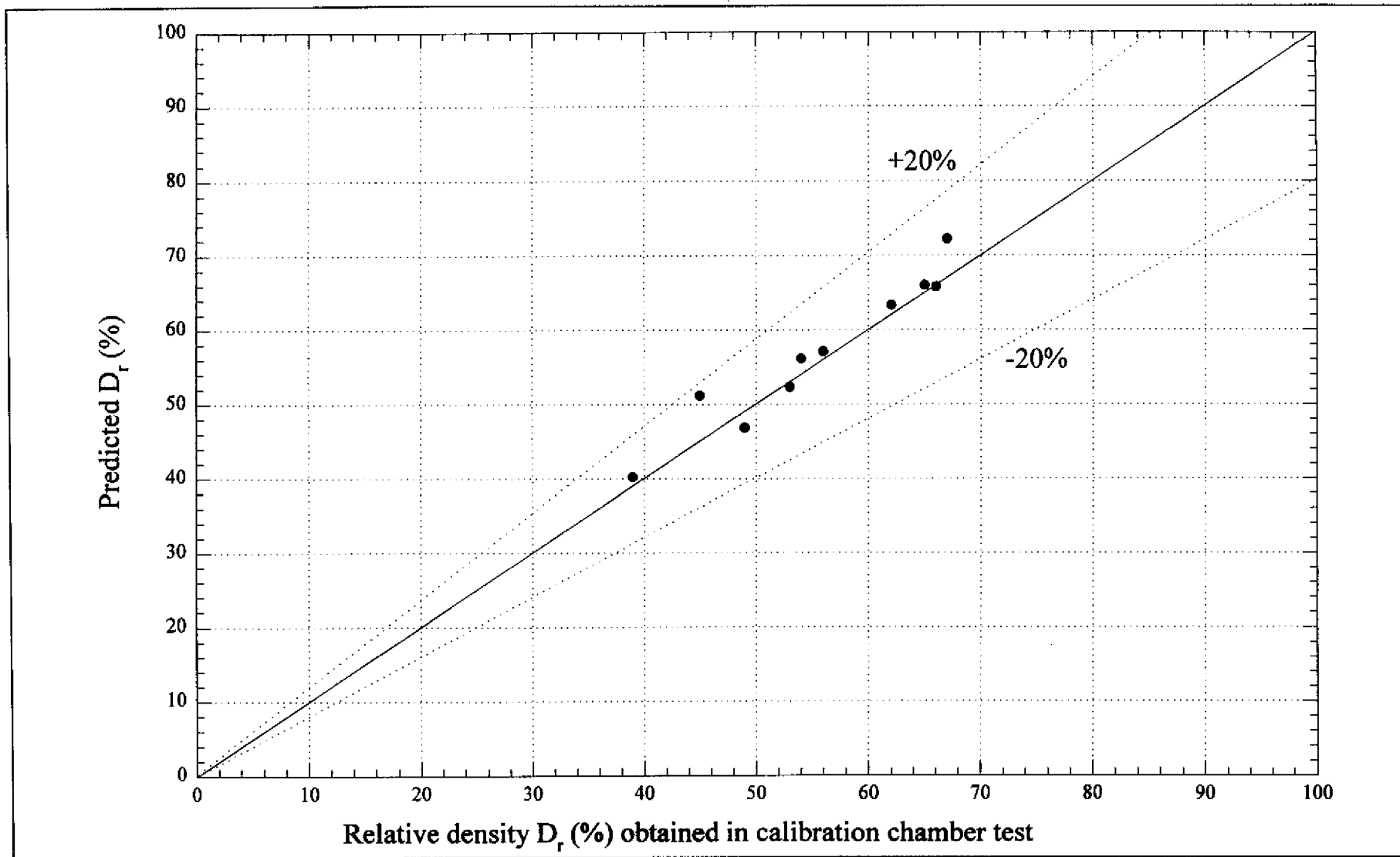


Figure 7.22 - Comparison between Relative Density Obtained in Calibration Chamber Test and That Predicted by Eq. (7.10) for the TC Sand

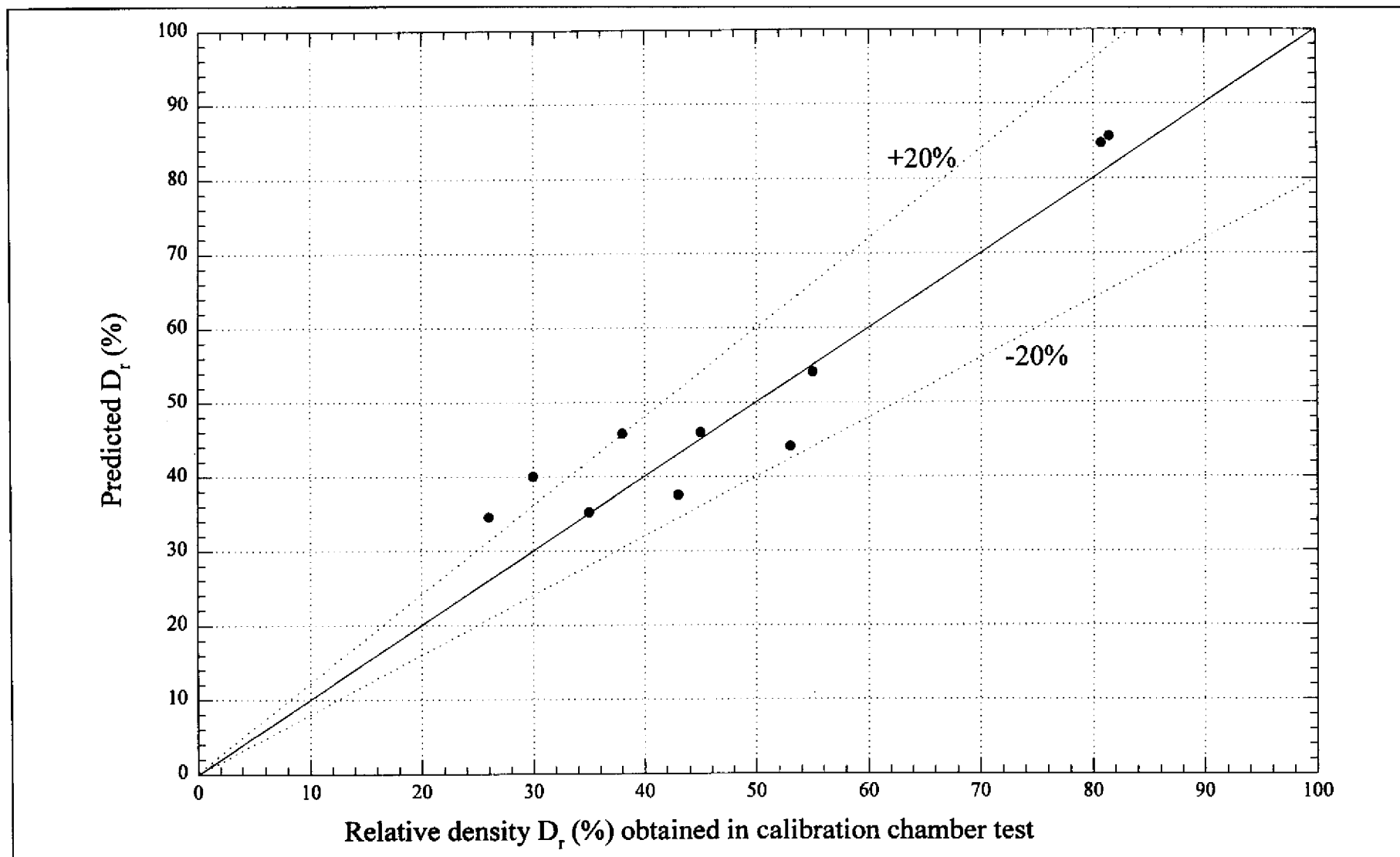


Figure 7.23 - Comparison between Relative Density Obtained in Calibration Chamber Test and That Predicted by Eq. (7.10) for the CLK Sand

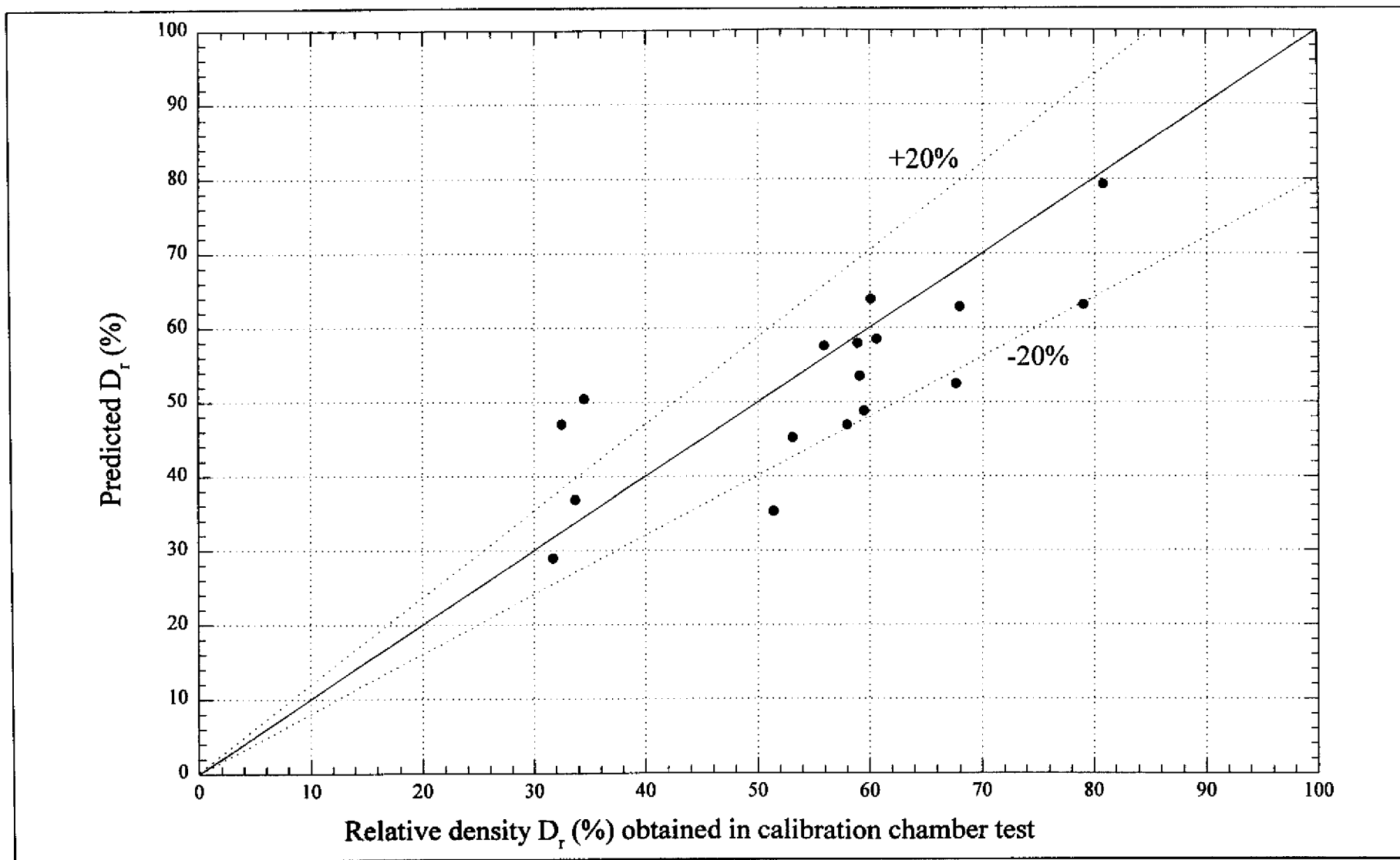


Figure 7.24 - Comparison between Relative Density Obtained in Calibration Chamber Test and That Predicted by Eq. (7.10) for the CS1 Sand

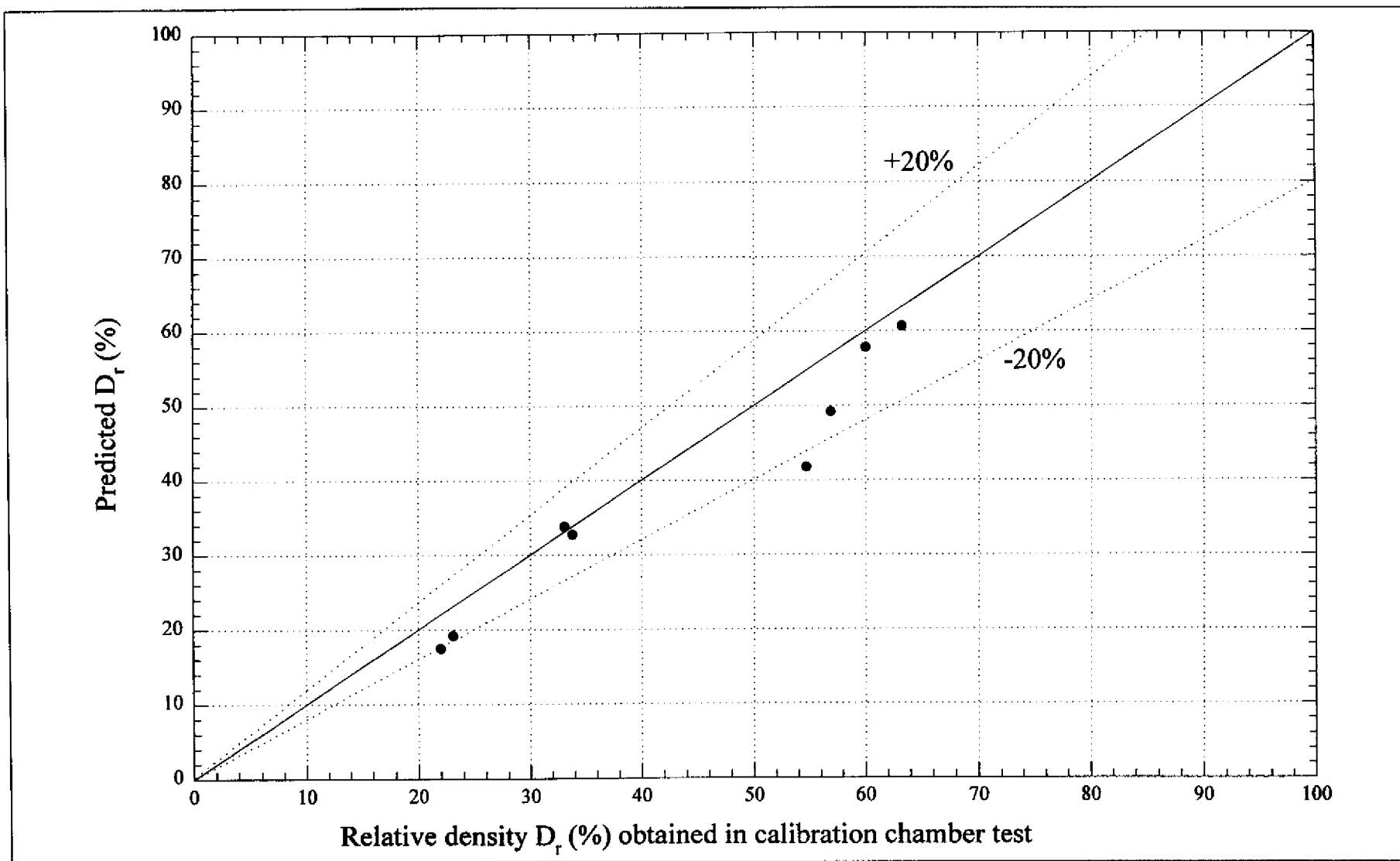


Figure 7.25 - Comparison between Relative Density Obtained in Calibration Chamber Test and That Predicted by Eq. (7.10) for the TKO Sand

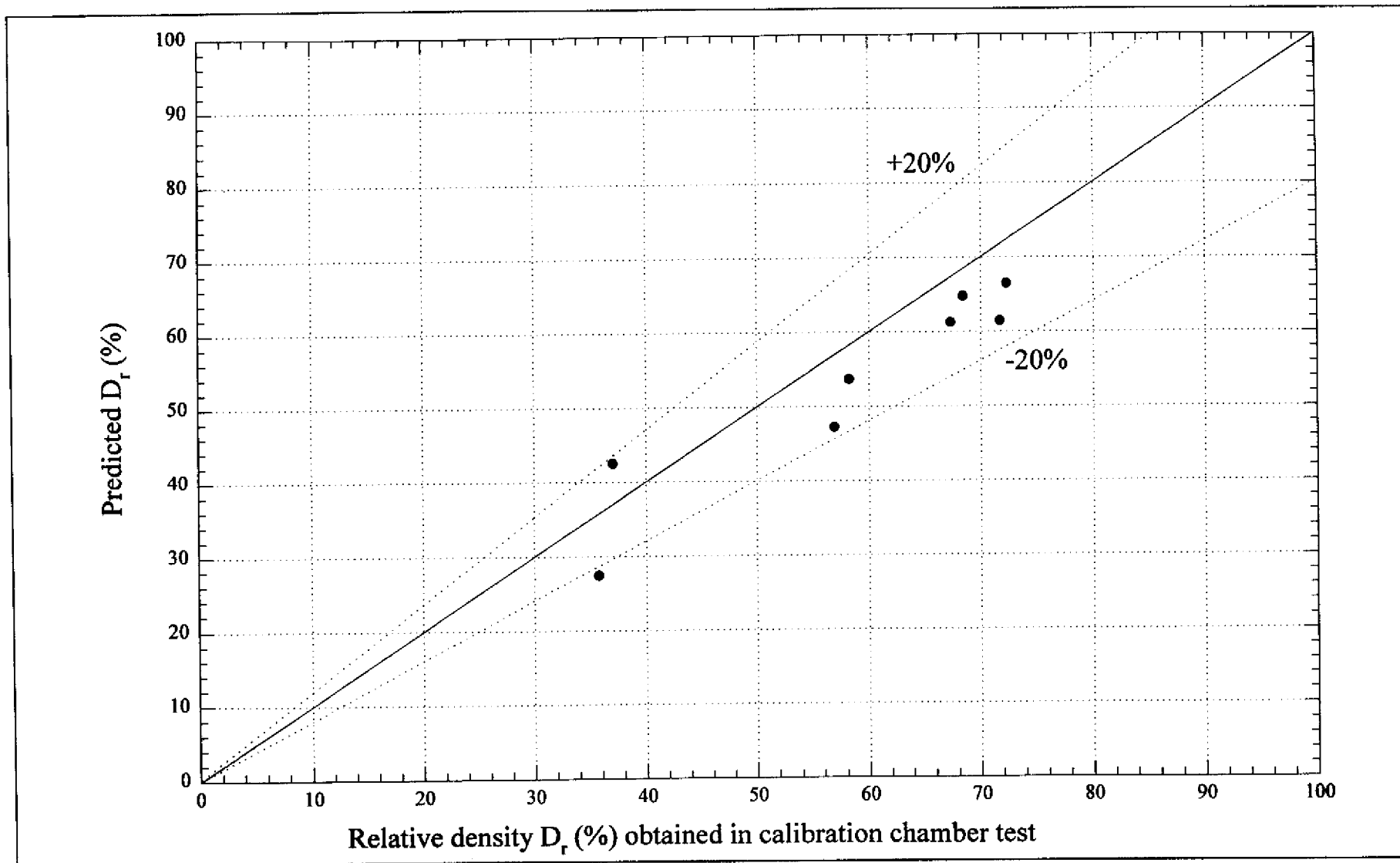


Figure 7.26 - Comparison between Relative Density Obtained in Calibration Chamber Test and That Predicted by Eq. (7.10) for the TSW Sand

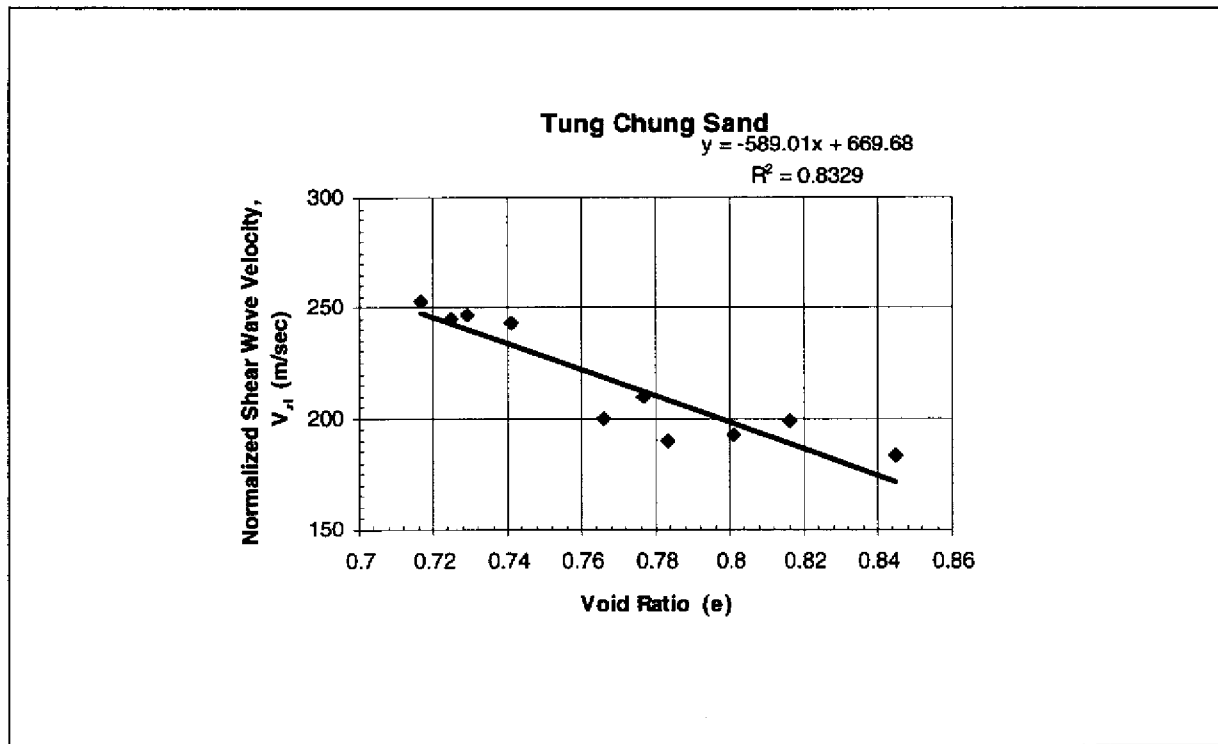


Figure 7.27 - Correlation between Void Ratio and Normalized Shear Wave Velocity for the TC Sand

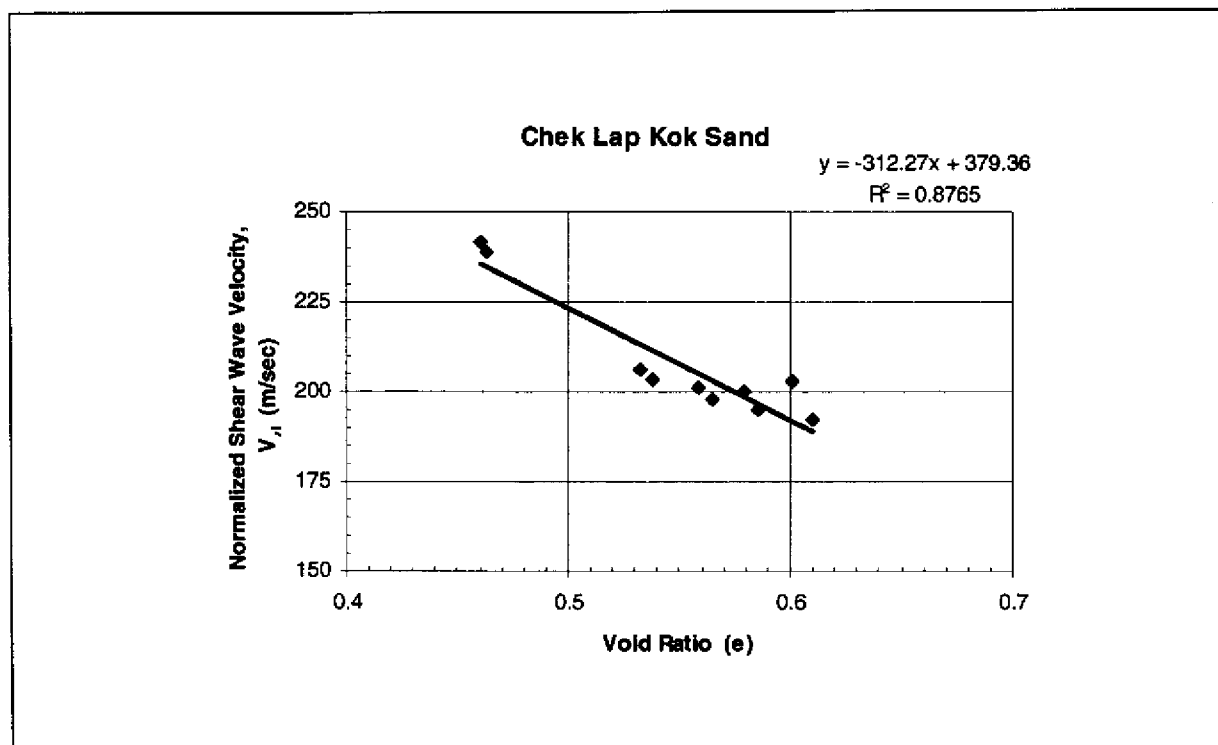


Figure 7.28 - Correlation between Void Ratio and Normalized Shear Wave Velocity for the CLK Sand

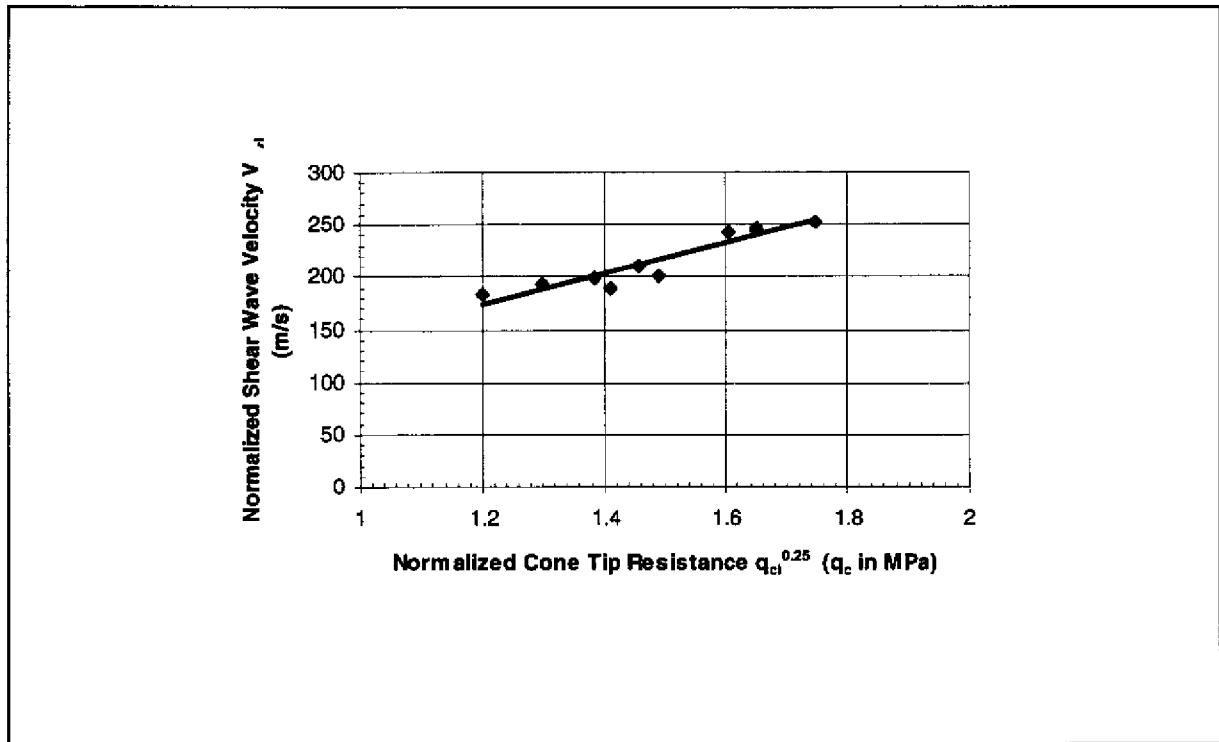


Figure 7.29 - Correlation between Normalized Cone Tip Resistance ($q_{cl}^{0.25}$) and Normalized Shear Wave Velocity (V_{s1}) for the TC Sand

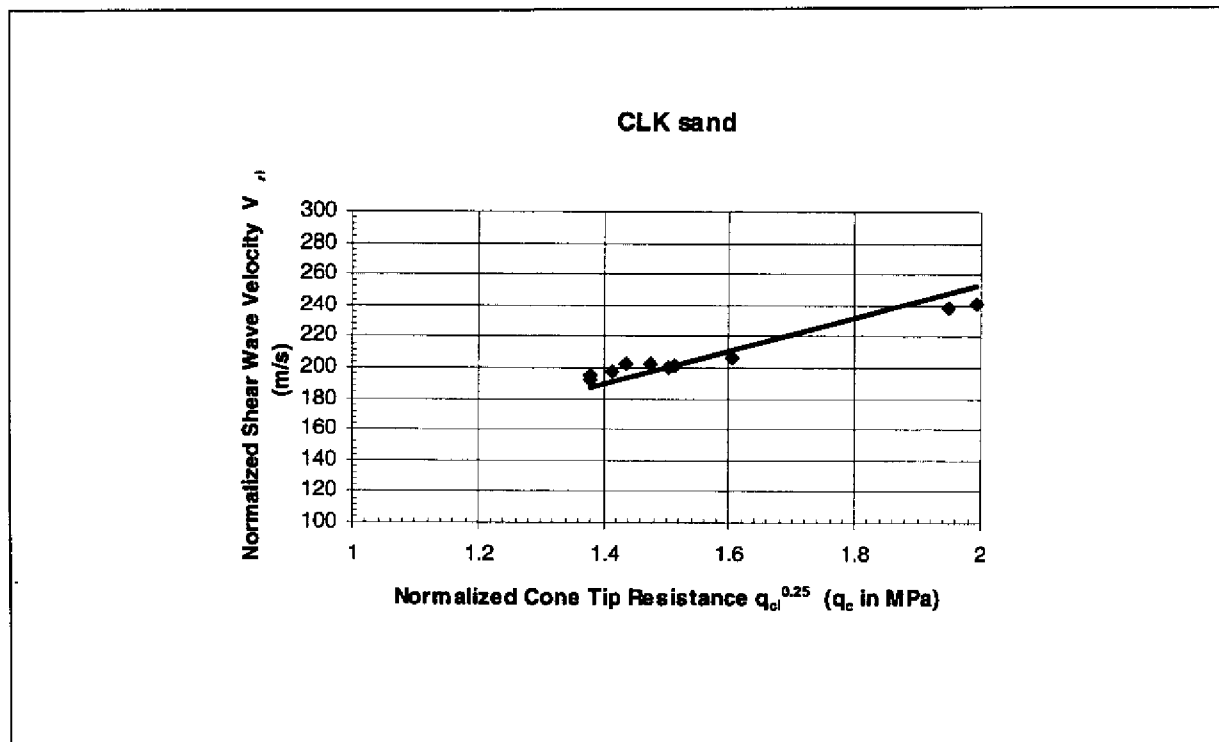


Figure 7.30 - Correlation between Normalized Cone Tip Resistance ($q_{cl}^{0.25}$) and Normalized Shear Wave Velocity (V_{s1}) for the CLK Sand

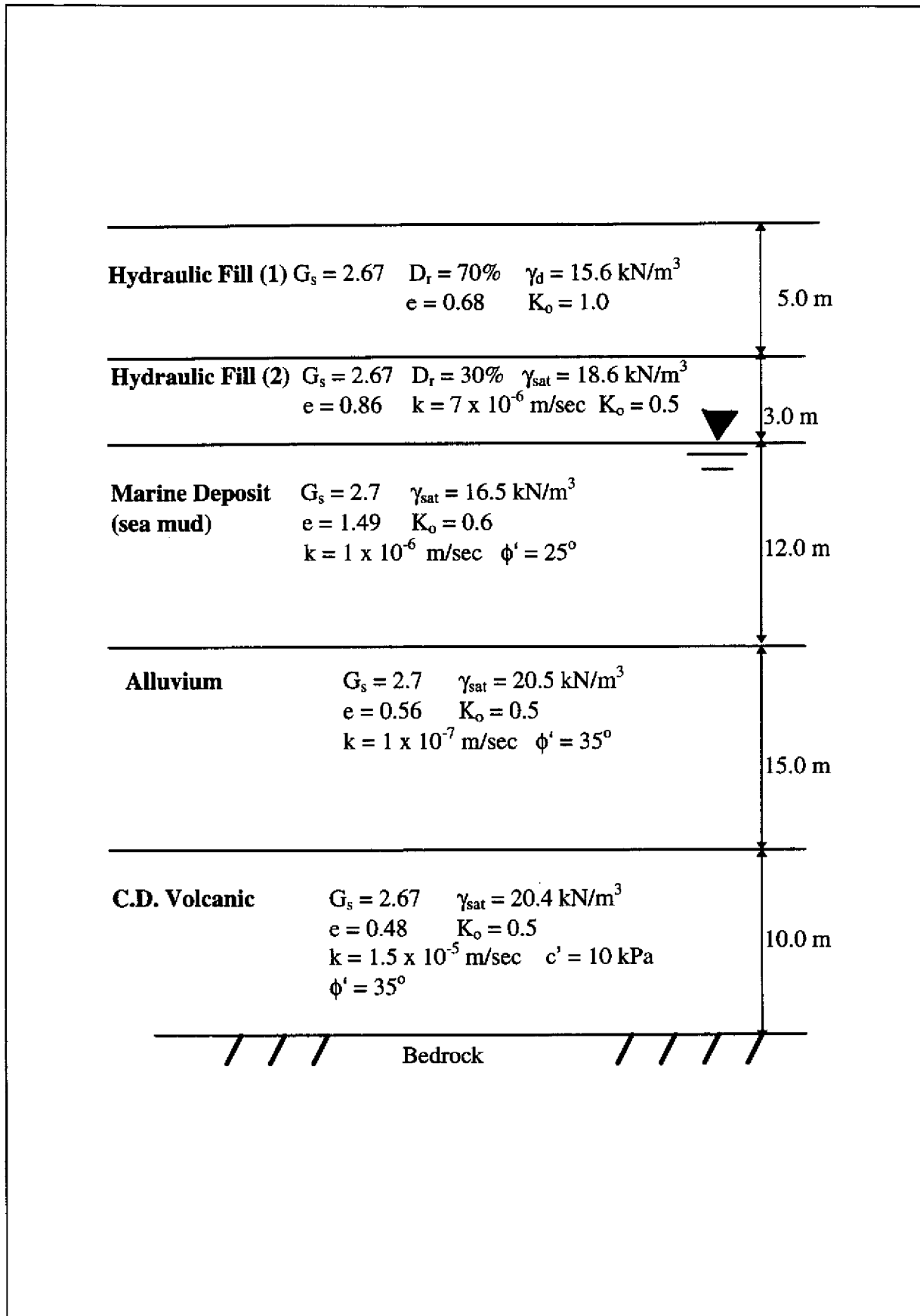


Figure 8.1 - Assumed Soil Profile for Site Response Analysis in the Tung Chung (TC) Site

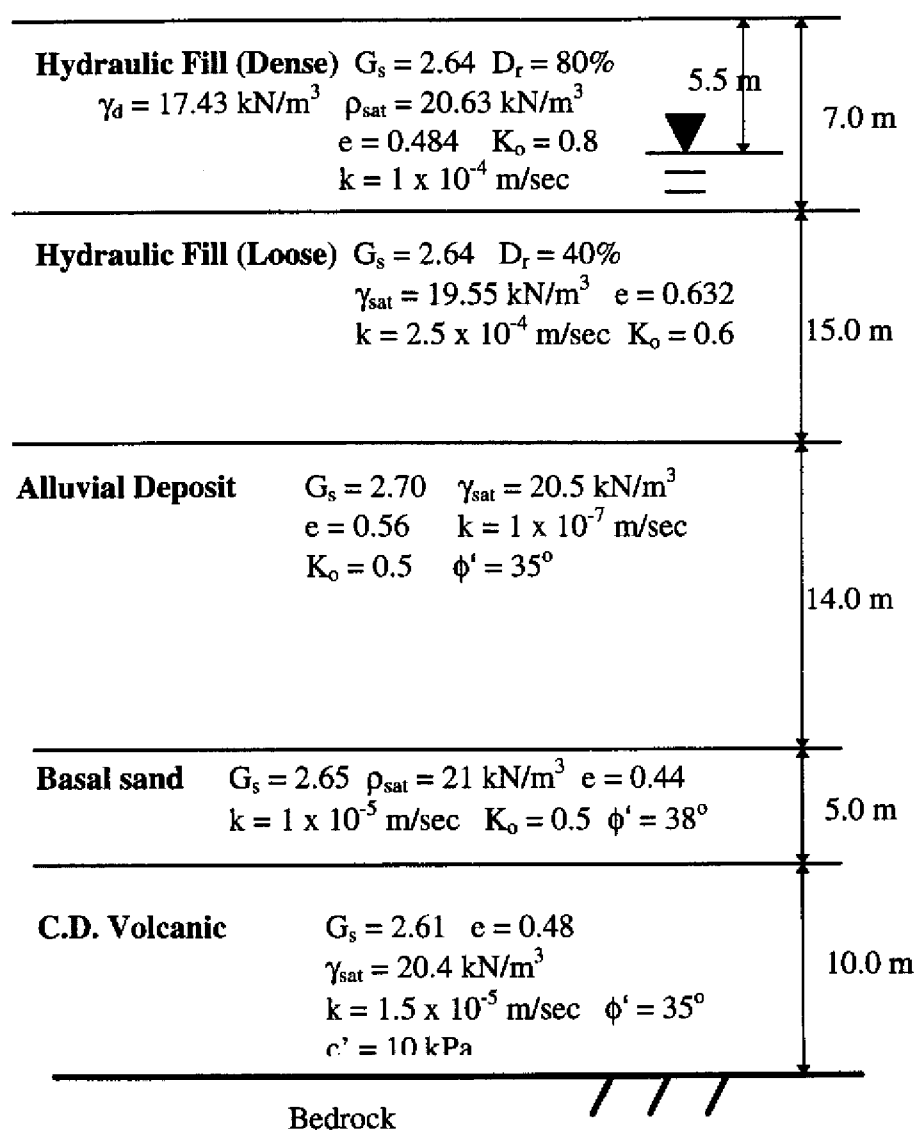


Figure 8.2 - Assumed Soil Profile for Site Response Analysis in the Chek Lap Kok (CLK) Site

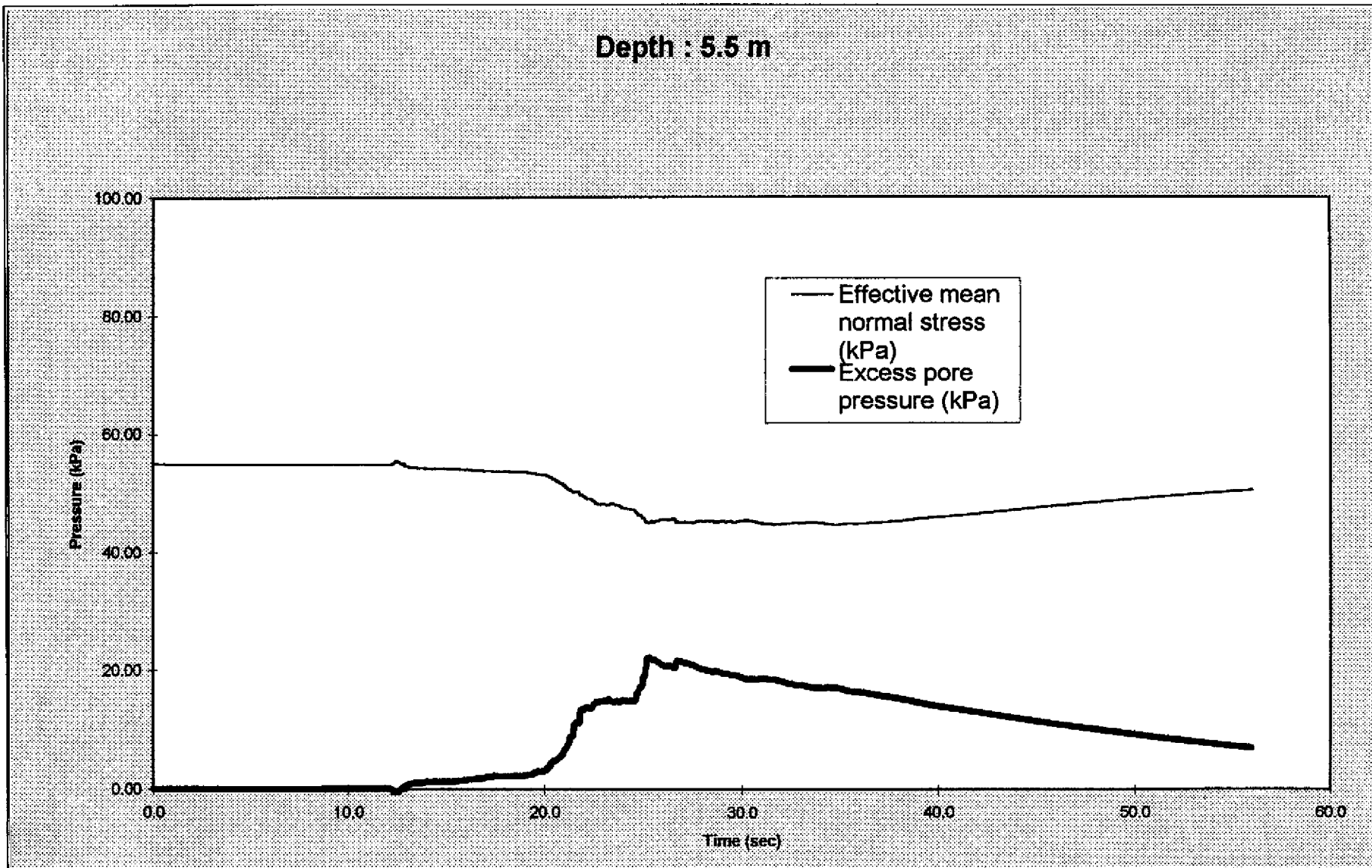


Figure 8.3 - Predicted Effective Mean Normal Stress and Excess Pore Pressure at a Depth of 5.5 m (Tung Chung Site)

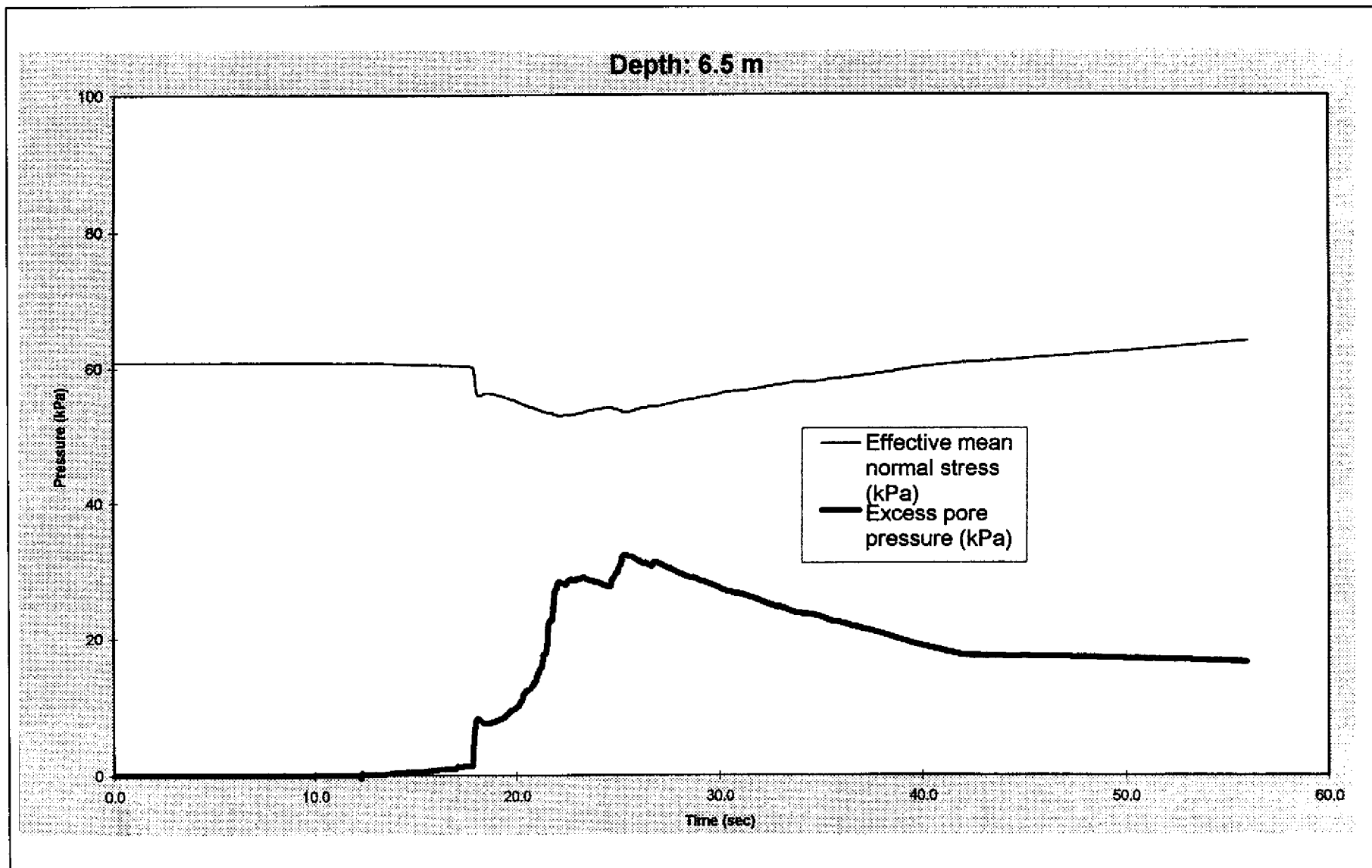


Figure 8.4 - Predicted Effective Mean Normal Stress and Excess Pore Pressure at a Depth of 6.5 m (Tung Chung Site)

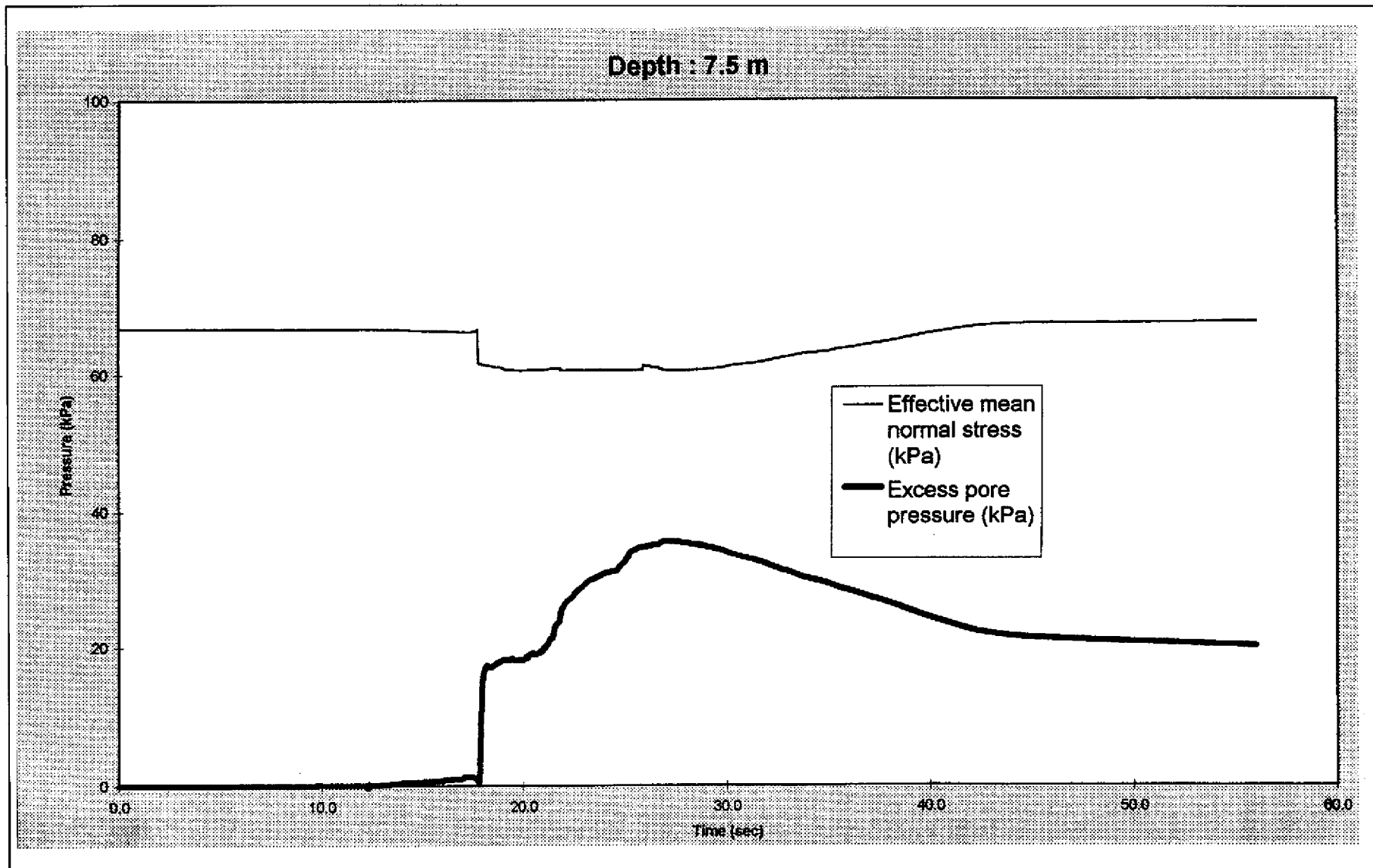


Figure 8.5 - Predicted Effective Mean Normal Stress and Excess Pore Pressure at a Depth of 7.5 m (Tung Chung Site)

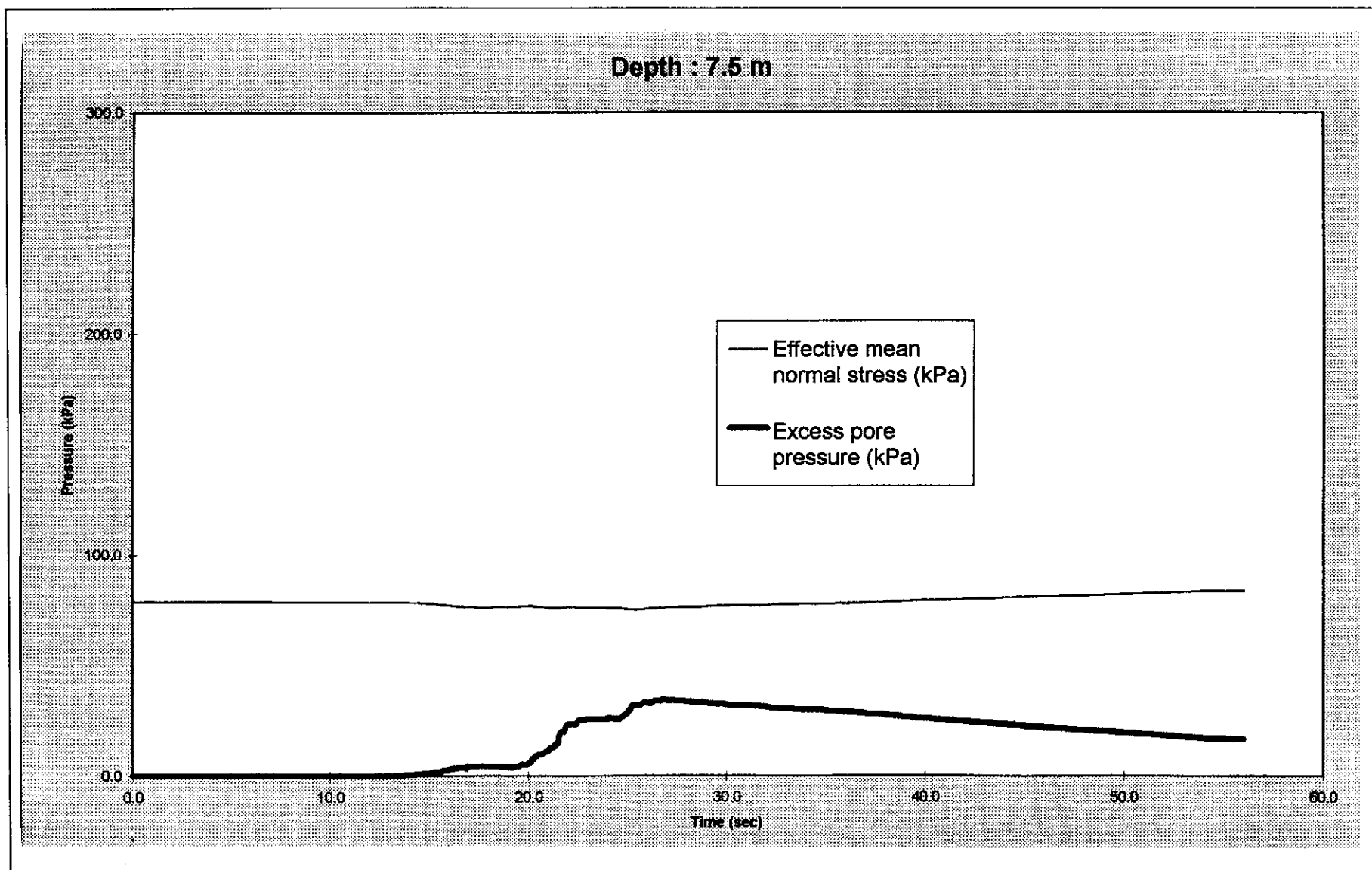


Figure 8.6 - Predicted Effective Mean Normal Stress and Excess Pore Pressure at a Depth of 7.5 m (Chek Lap Kok Site)

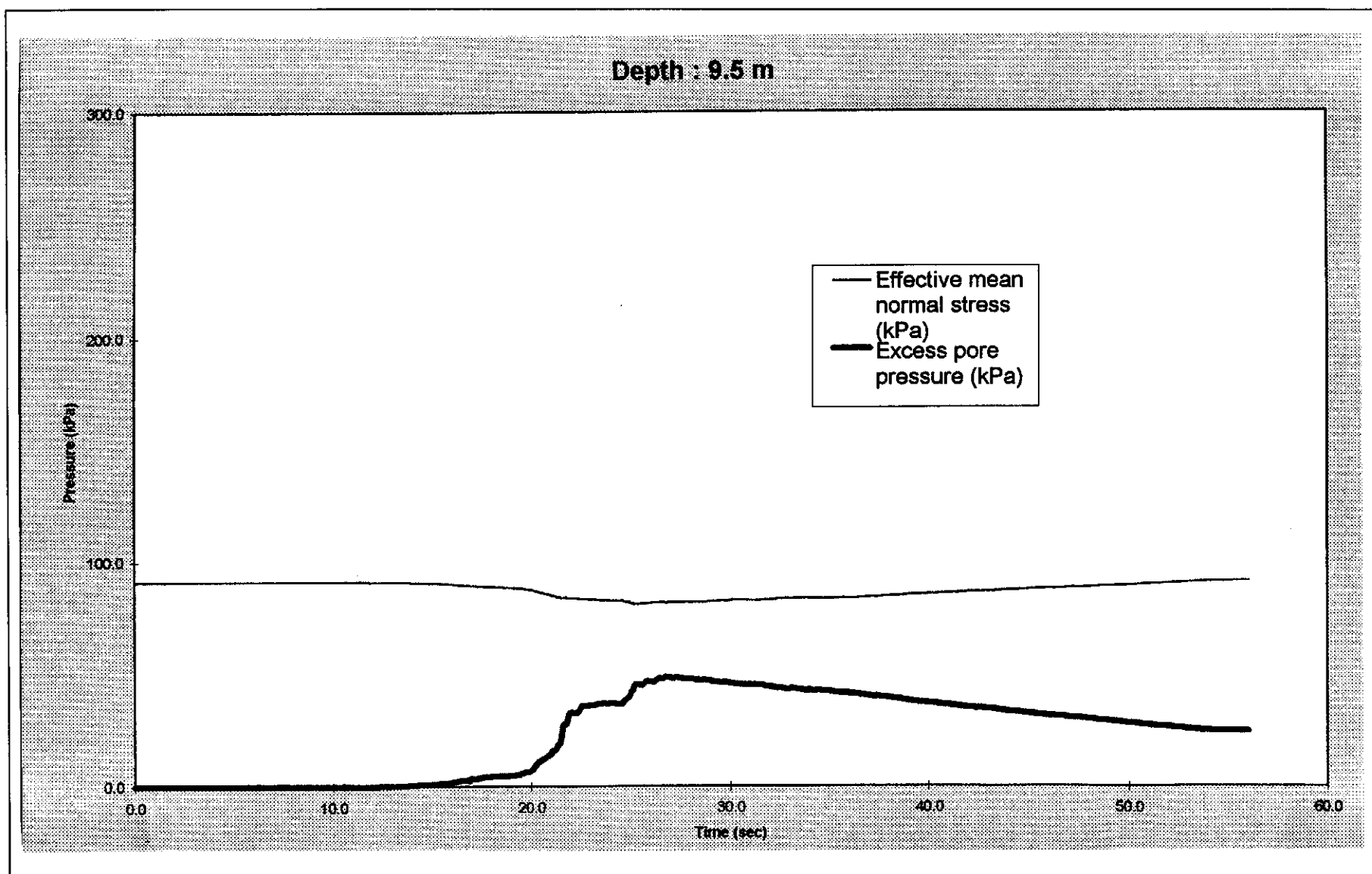


Figure 8.7 - Predicted Effective Mean Normal Stress and Excess Pore Pressure at a Depth of 9.5 m (Chek Lap Kok Site)

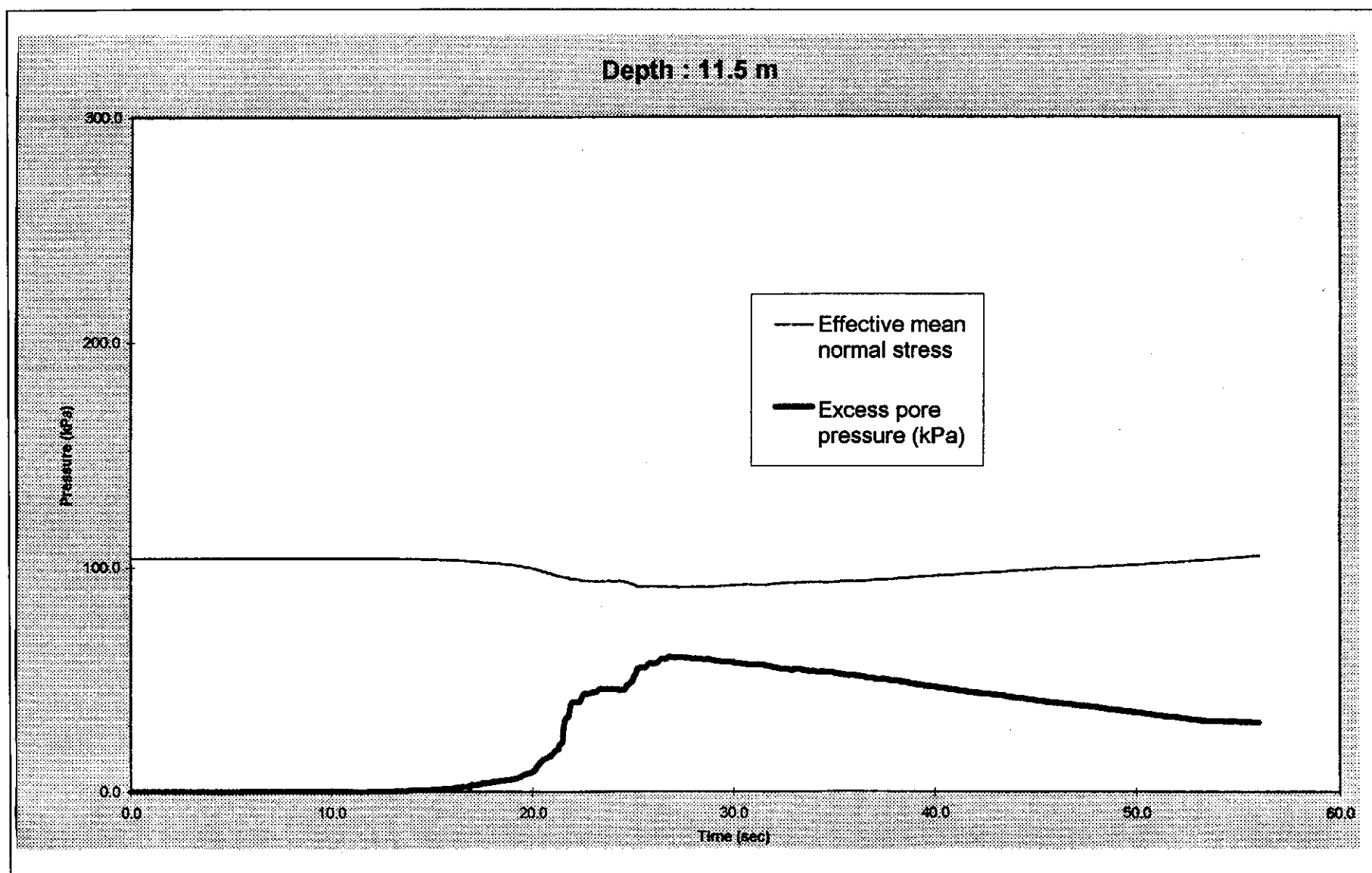


Figure 8.8 - Predicted Effective Mean Normal Stress and Excess Pore Pressure at a Depth of 11.5 m (Chek Lap Kok Site)

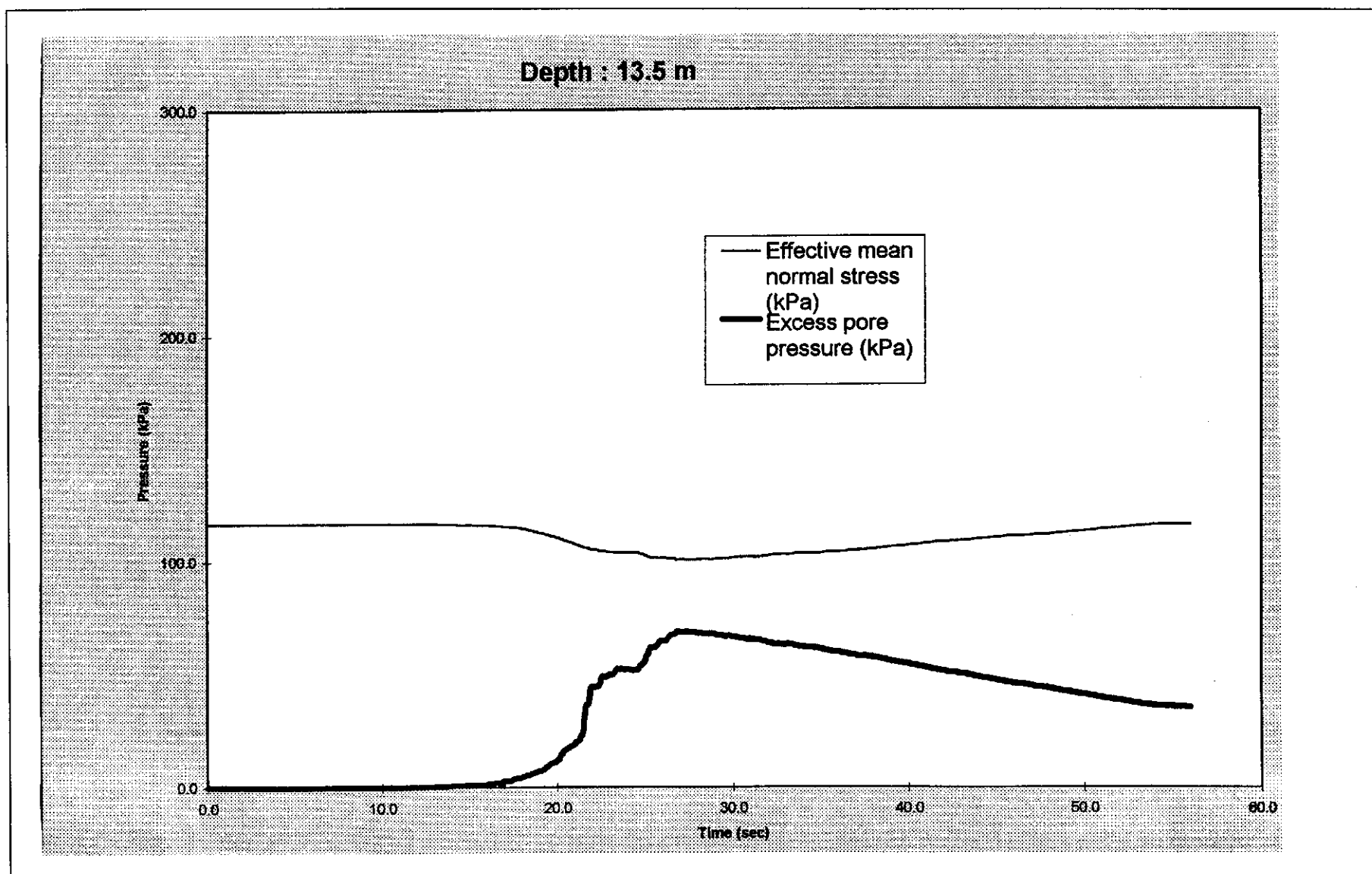


Figure 8.9 - Predicted Effective Mean Normal Stress and Excess Pore Pressure at a Depth of 13.5 m (Chek Lap Kok Site)

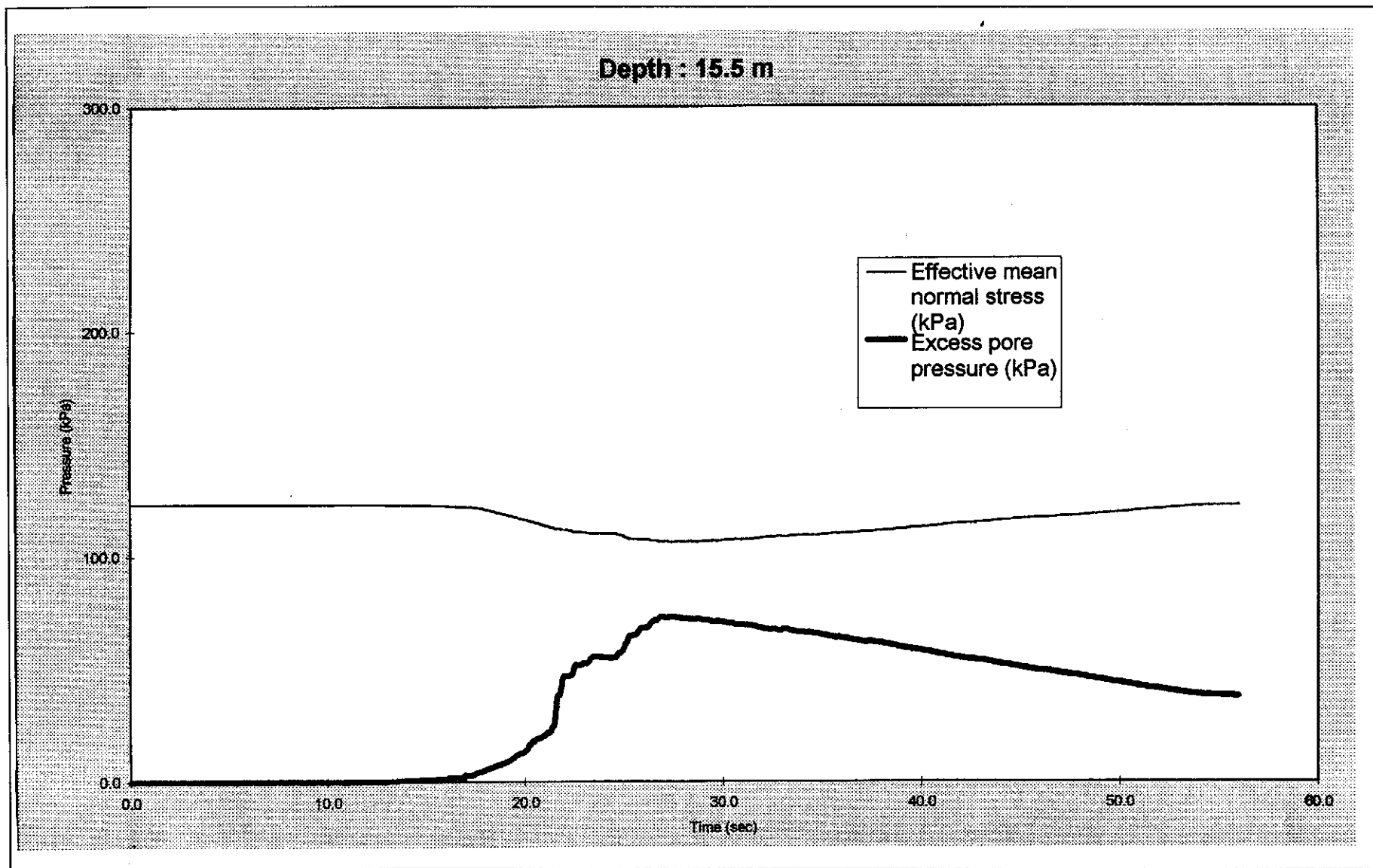


Figure 8.10 - Predicted Effective Mean Normal Stress and Excess Pore Pressure at a Depth of 15.5 m (Chek Lap Kok Site)

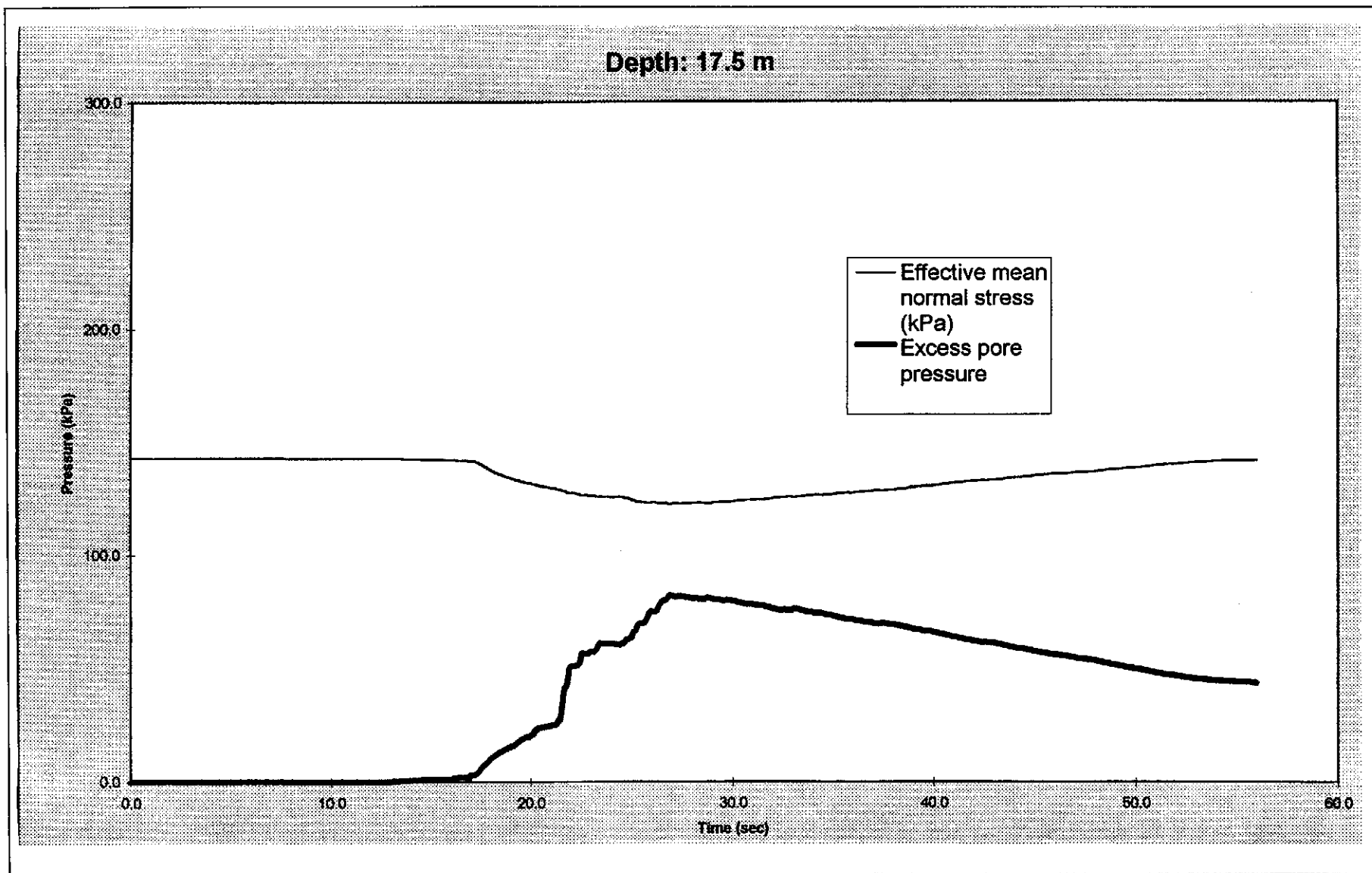


Figure 8.11 - Predicted Effective Mean Normal Stress and Excess Pore Pressure at a Depth of 17.5 m (Chek Lap Kok Site)

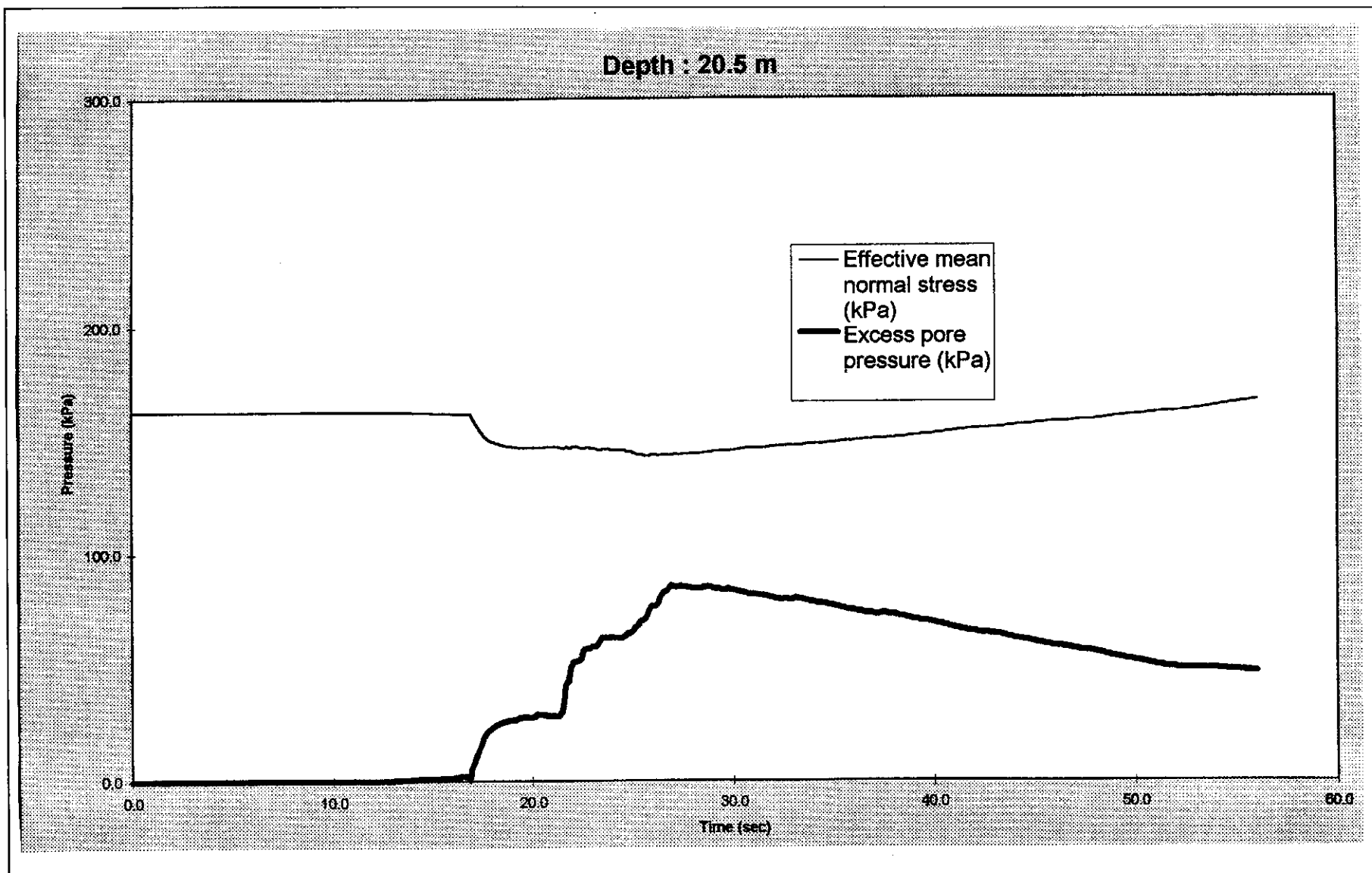


Figure 8.12 - Predicted Effective Mean Normal Stress and Excess Pore Pressure at a Depth of 20.5 m (Chek Lap Kok Site)

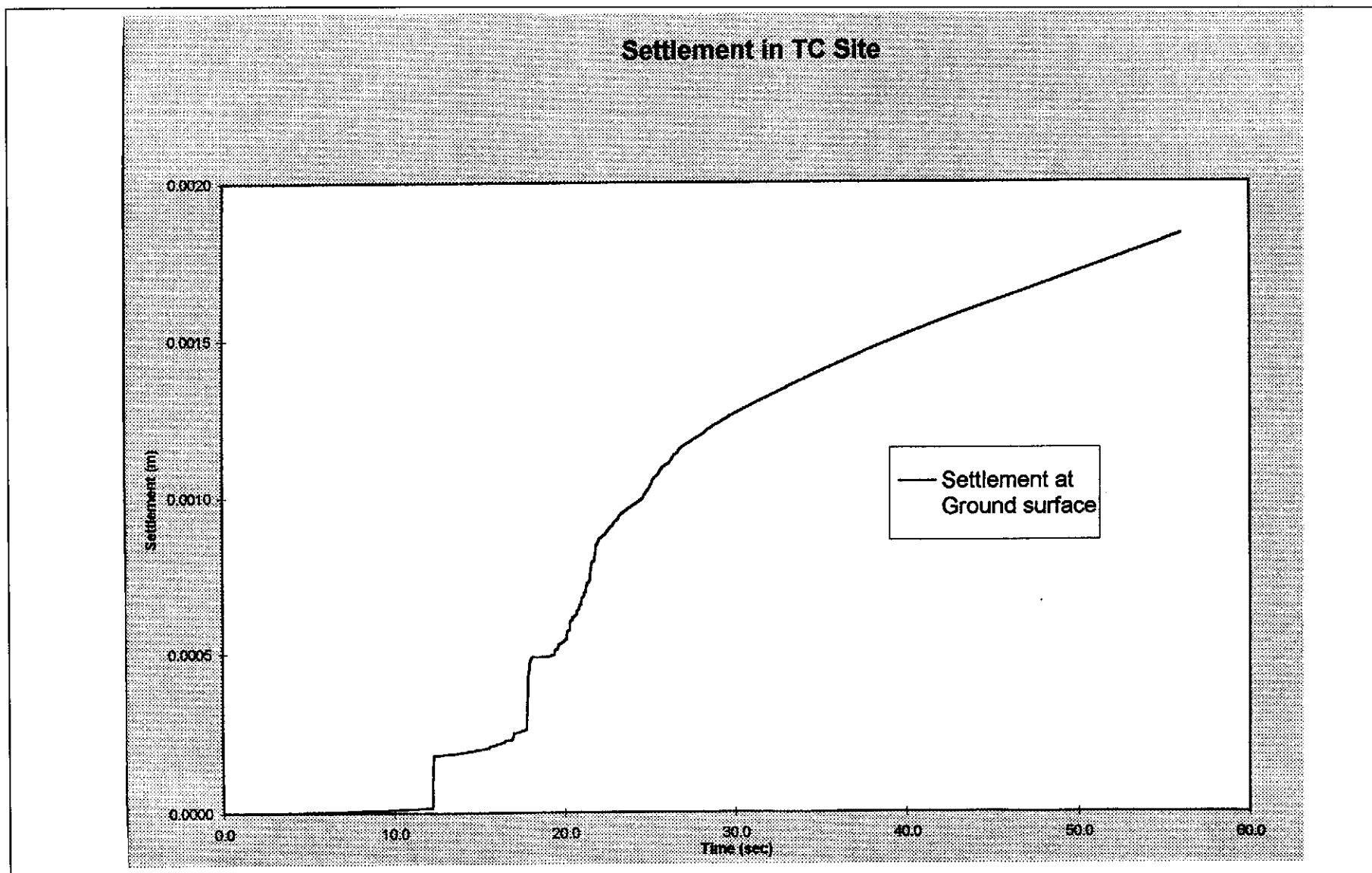


Figure 8.13 - Prediction of Earthquake Induced Surface Settlement in the Tung Chung Site

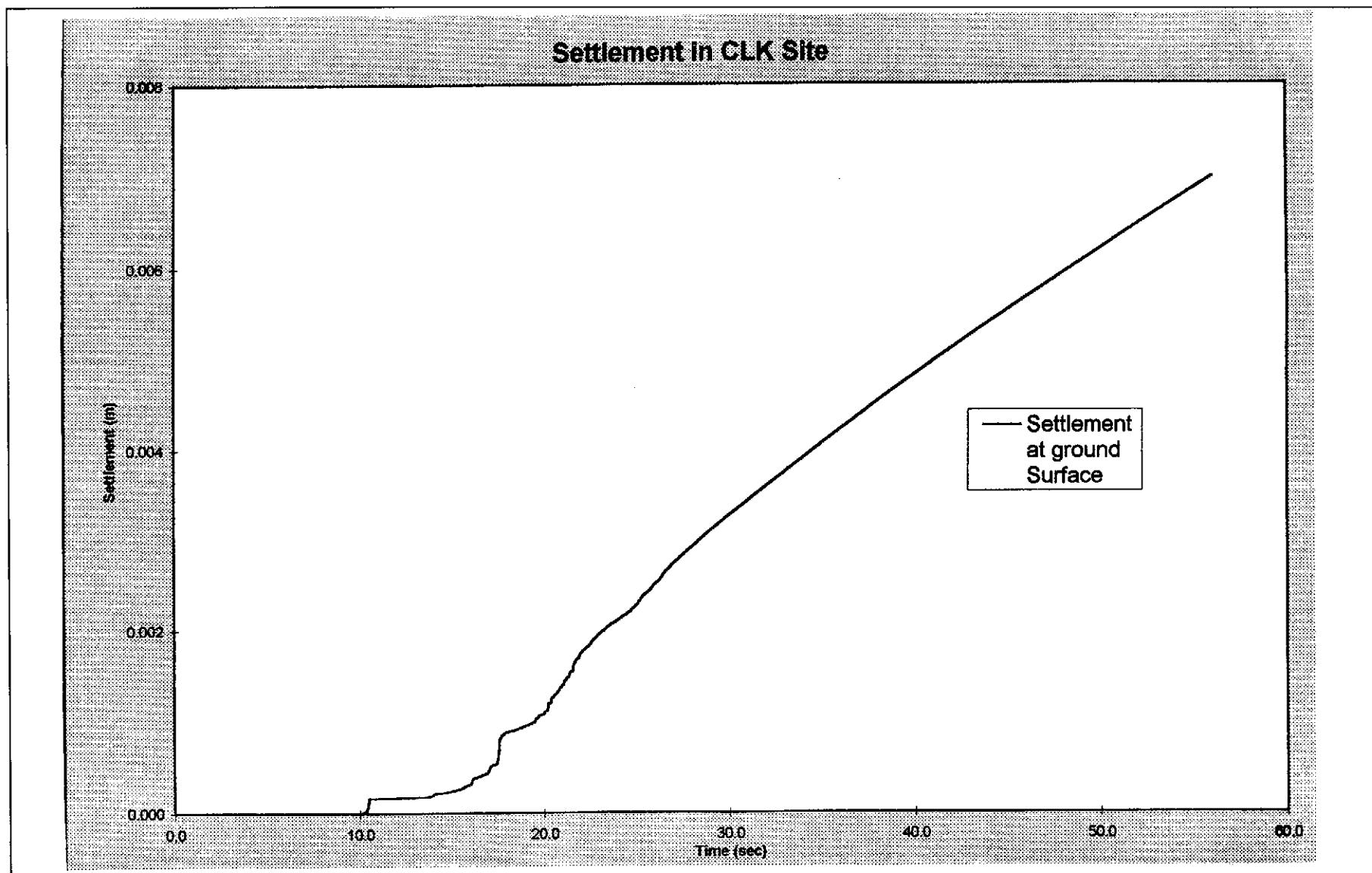


Figure 8.14 - Prediction of Earthquake Induced Surface Settlement in the Chek Lap Kok Site

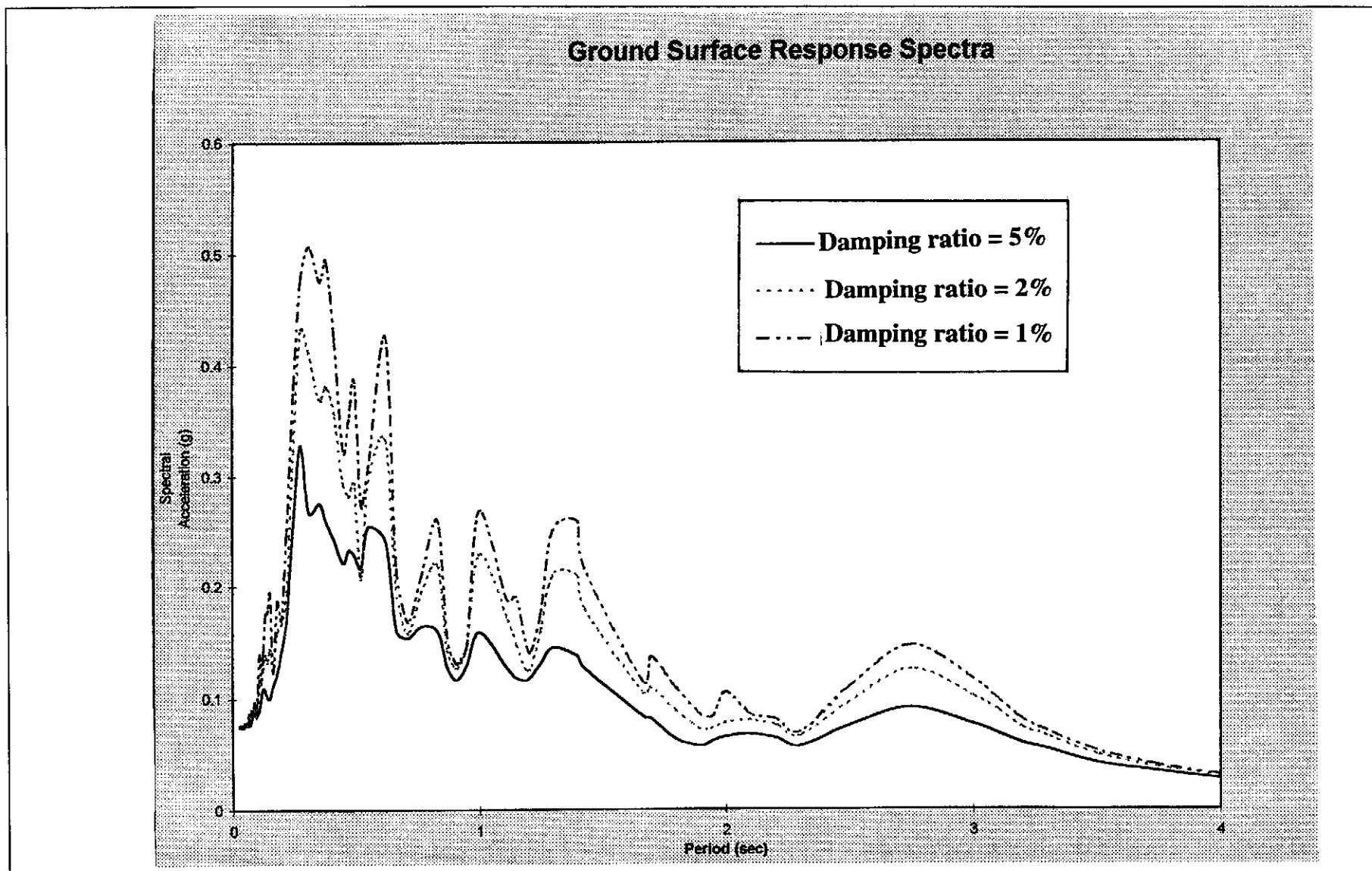


Figure 8.15 - Ground Surface Response Spectra in Tung Chung Site

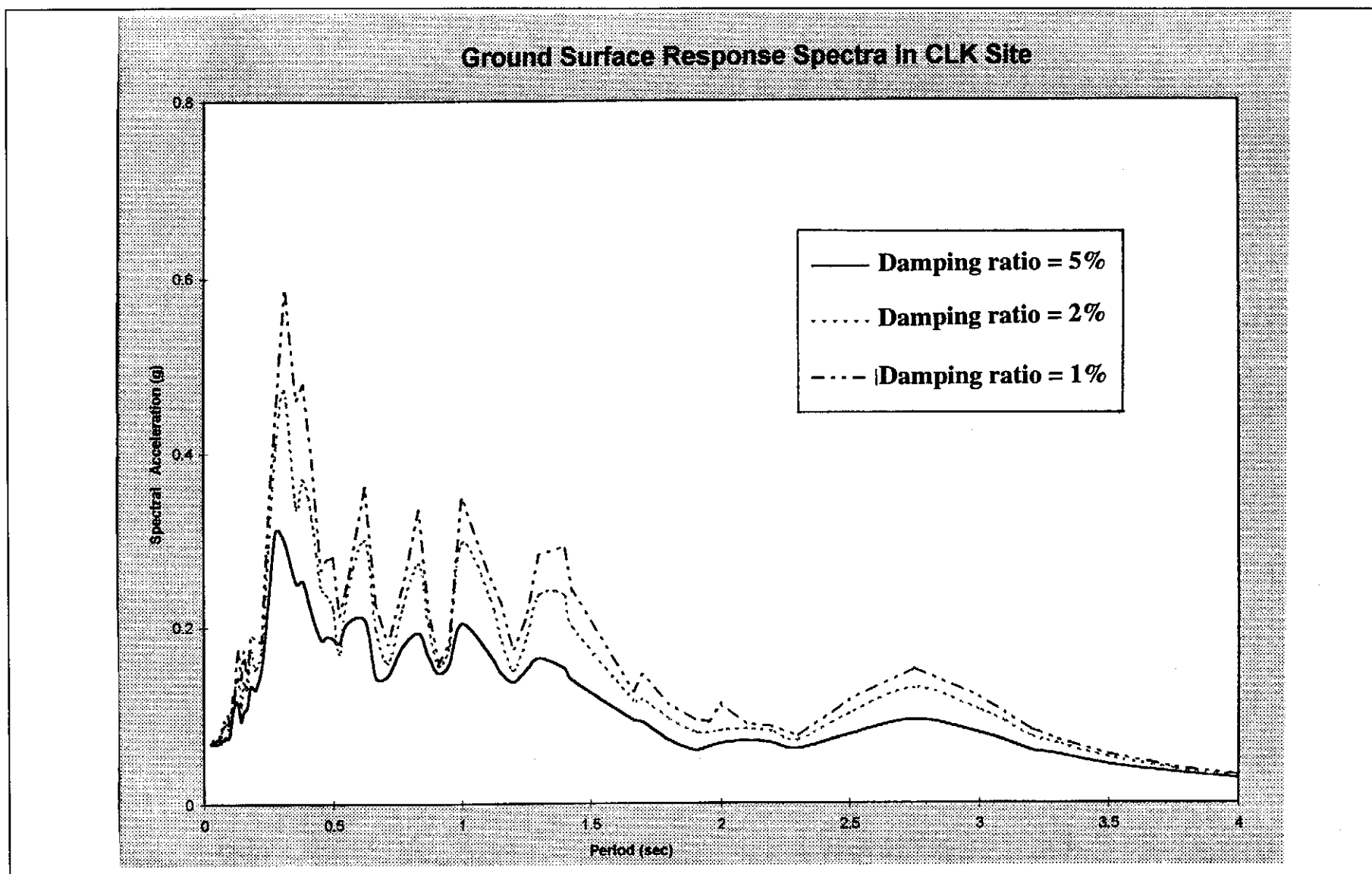


Figure 8.16 - Ground Surface Response Spectra in Chek Lap Kok Site

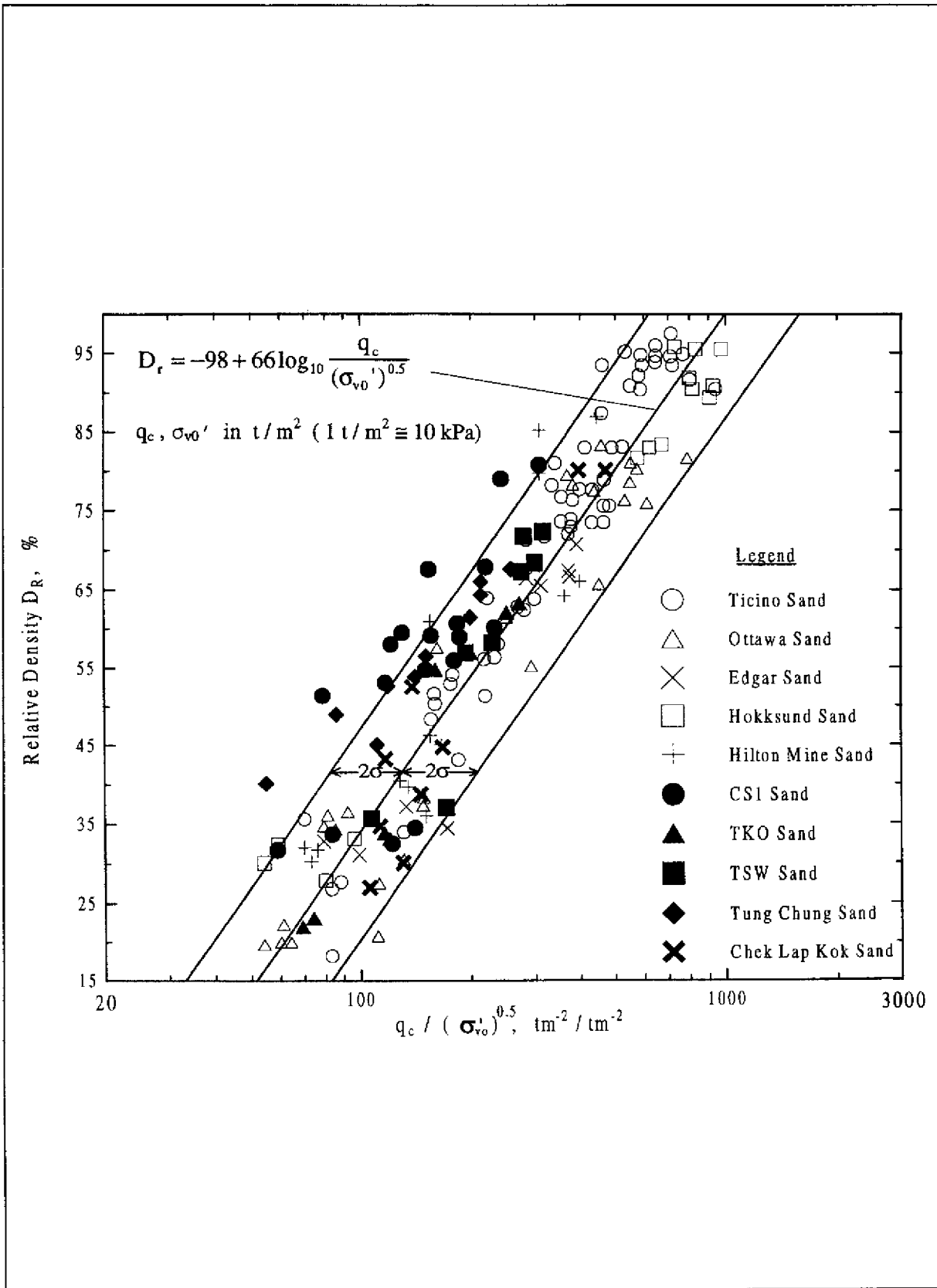


Figure 9.1 - Comparison of the Calibration Chamber Test Results for the Five Hong Kong Marine Sands with the Other Uniformly Graded Quartz Sands (Modified from Jamiolkowski et al, 1985)

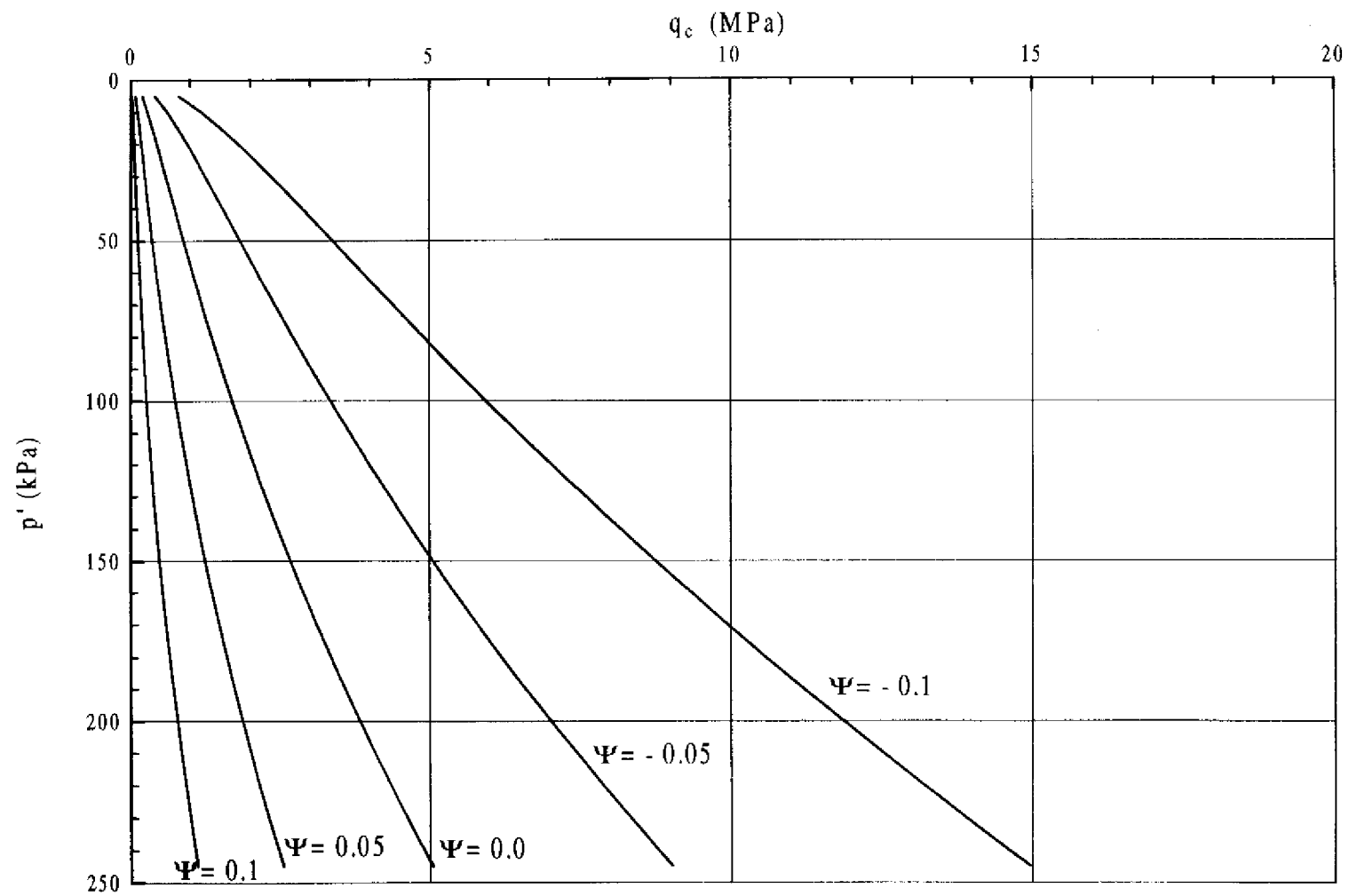


Figure 9.2 - p' versus q_c with Contours of State Parameter (Ψ) Varied from $\Psi = 0.1$ to $\Psi = -0.1$ for the TC Sand

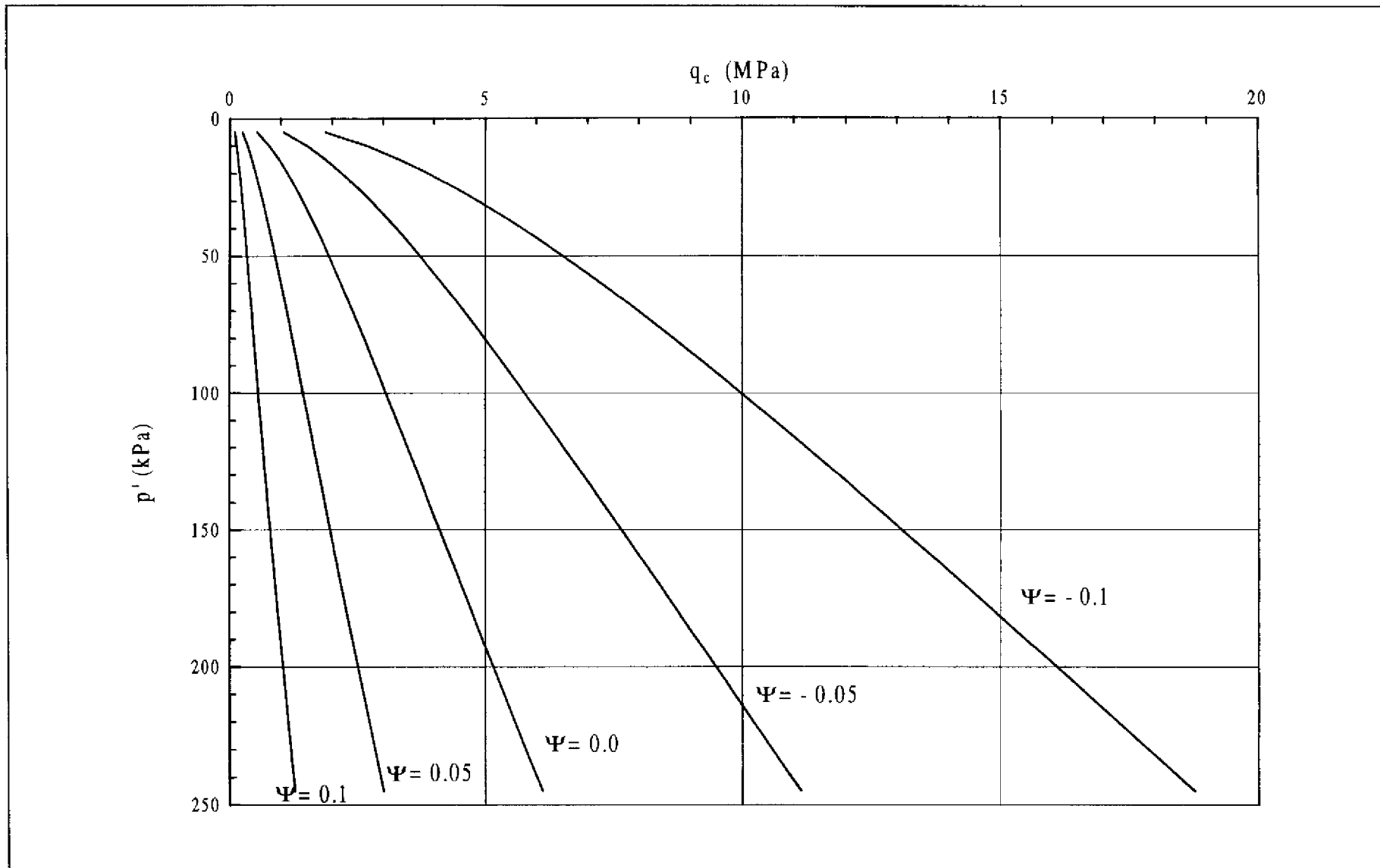


Figure 9.3 - p' versus q_c with Contours of State Parameter (Ψ) Varied from $\Psi = 0.1$ to $\Psi = -0.1$ for the CLK Sand

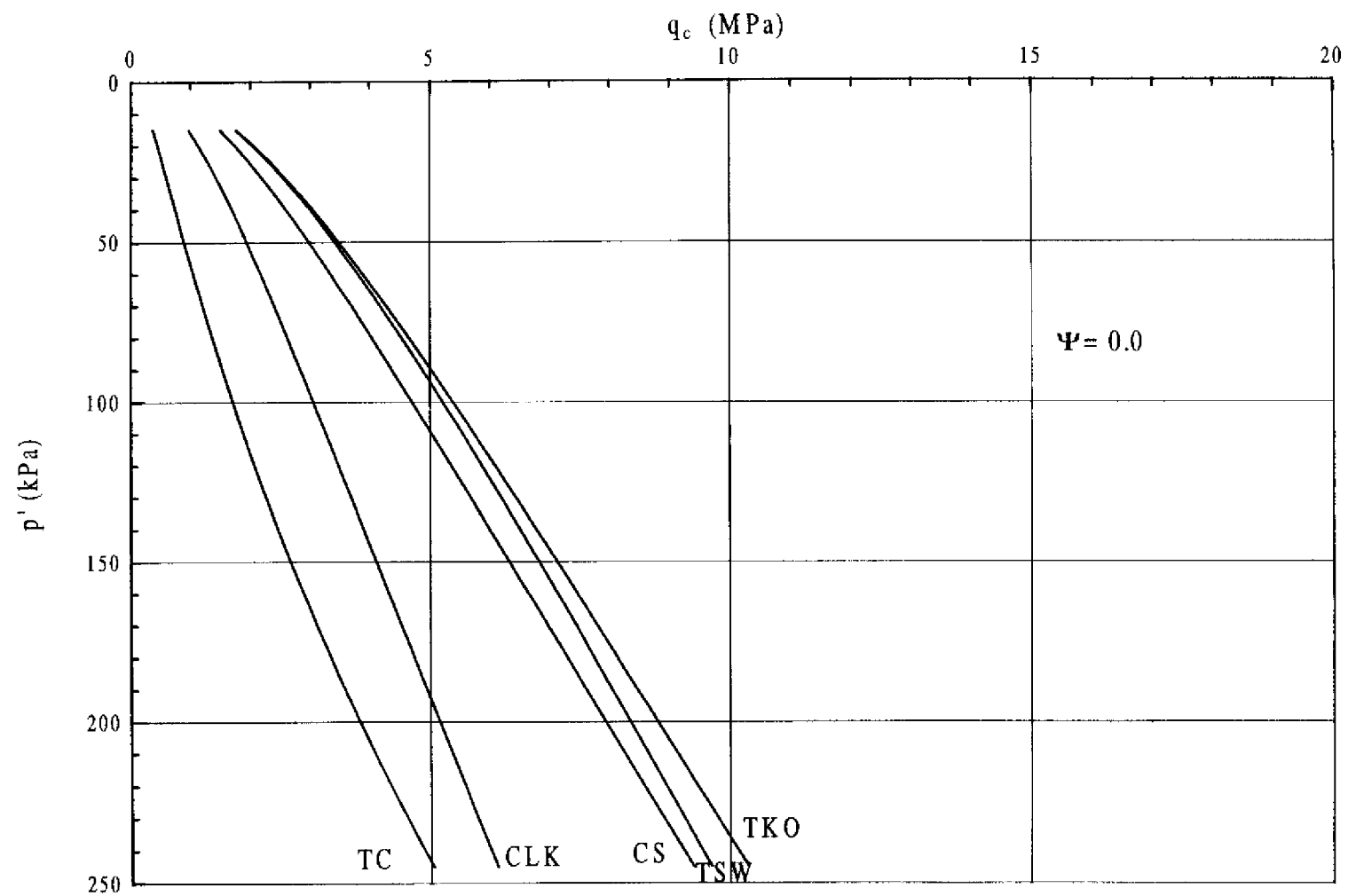


Figure 9.4 - Variation of $\Psi = 0$ Profiles (Contractive/Dilative Boundary) for the Five Hong Kong Marine Sands

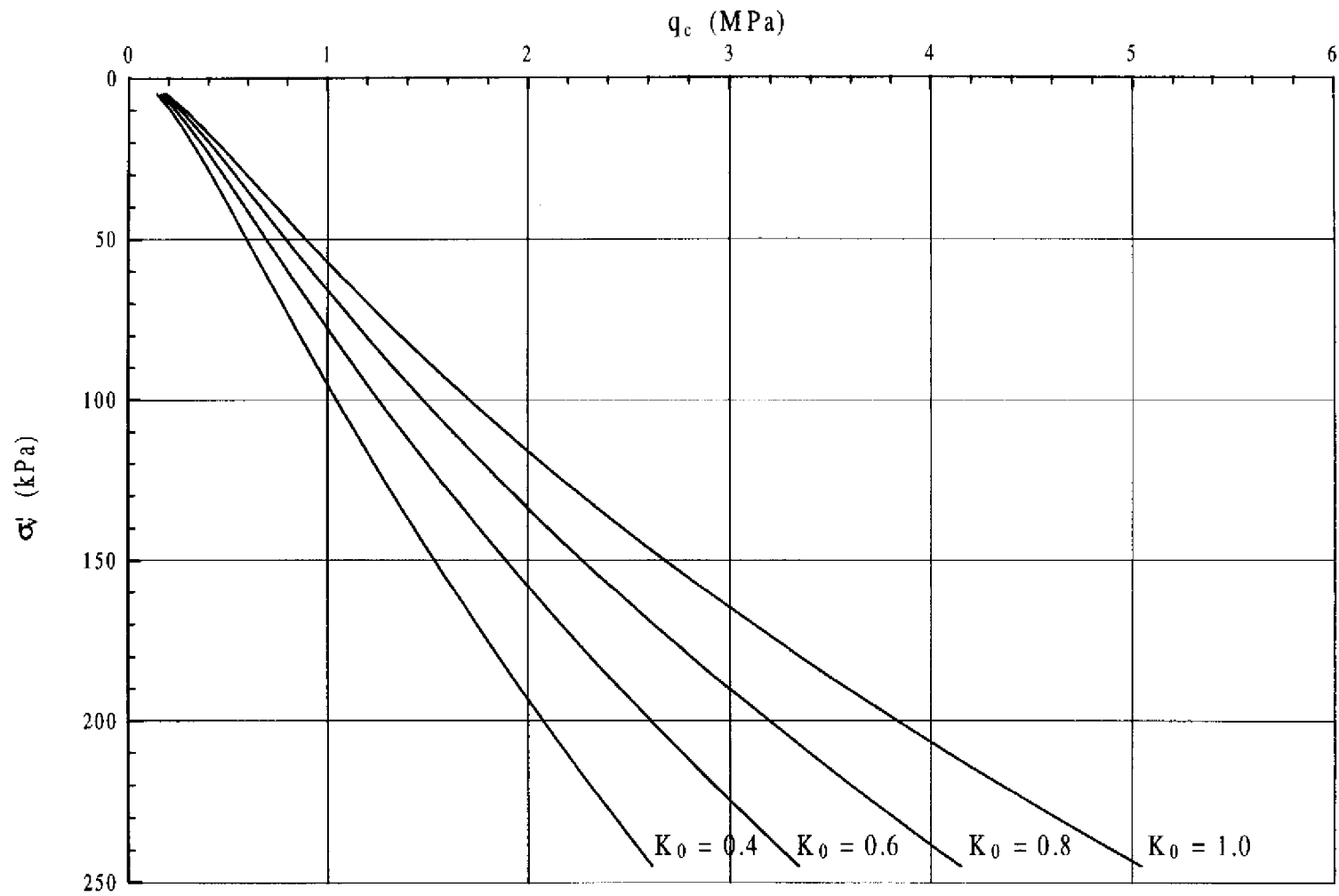


Figure 9.5 - Variation of $\Psi = 0$ Profiles for the TC Sand with $K_0 = 0.4$ to $K_0 = 1.0$

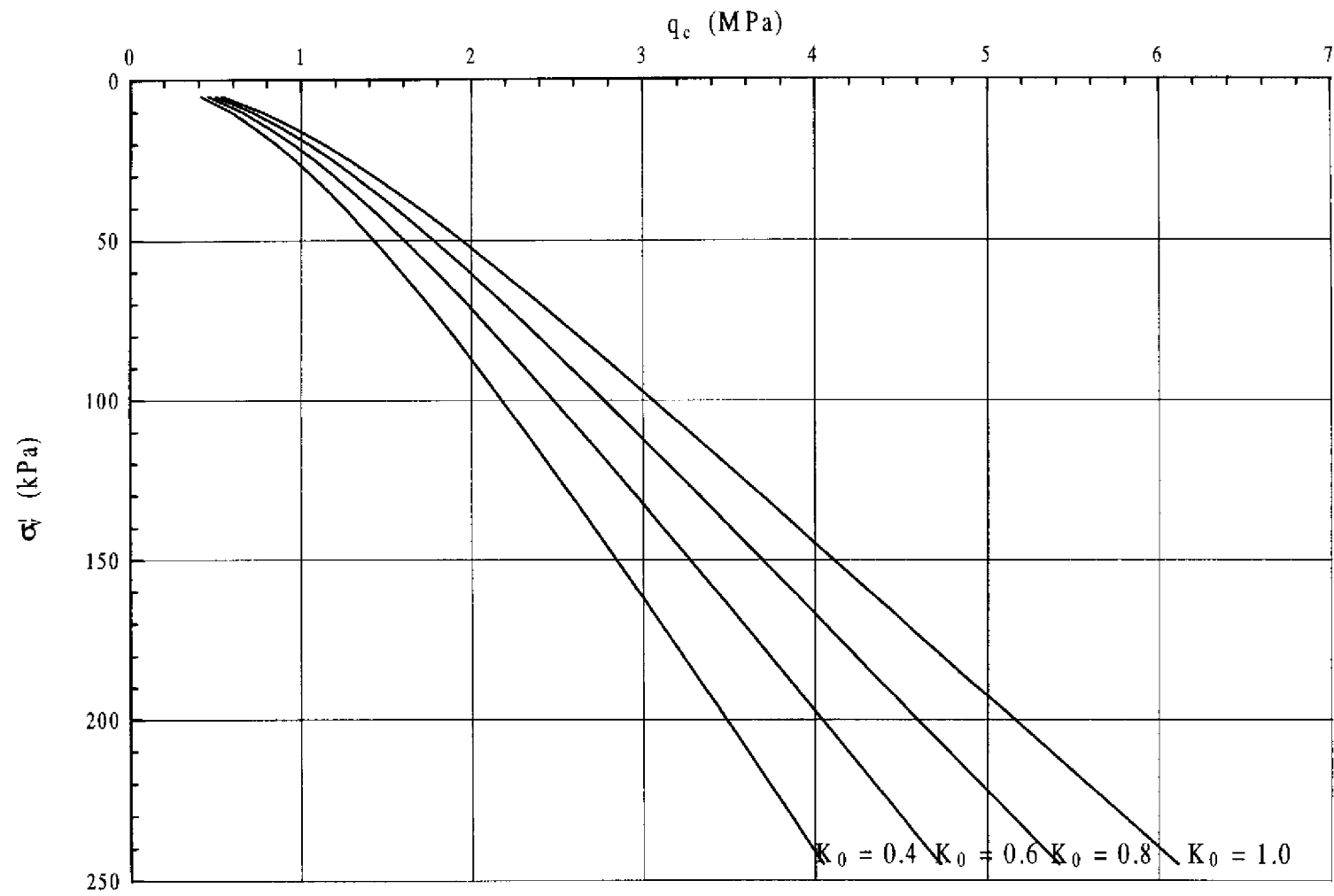


Figure 9.6 - Variation of $\Psi = 0$ Profiles for the CLK Sand with $K_0 = 0.4$ to $K_0 = 1.0$

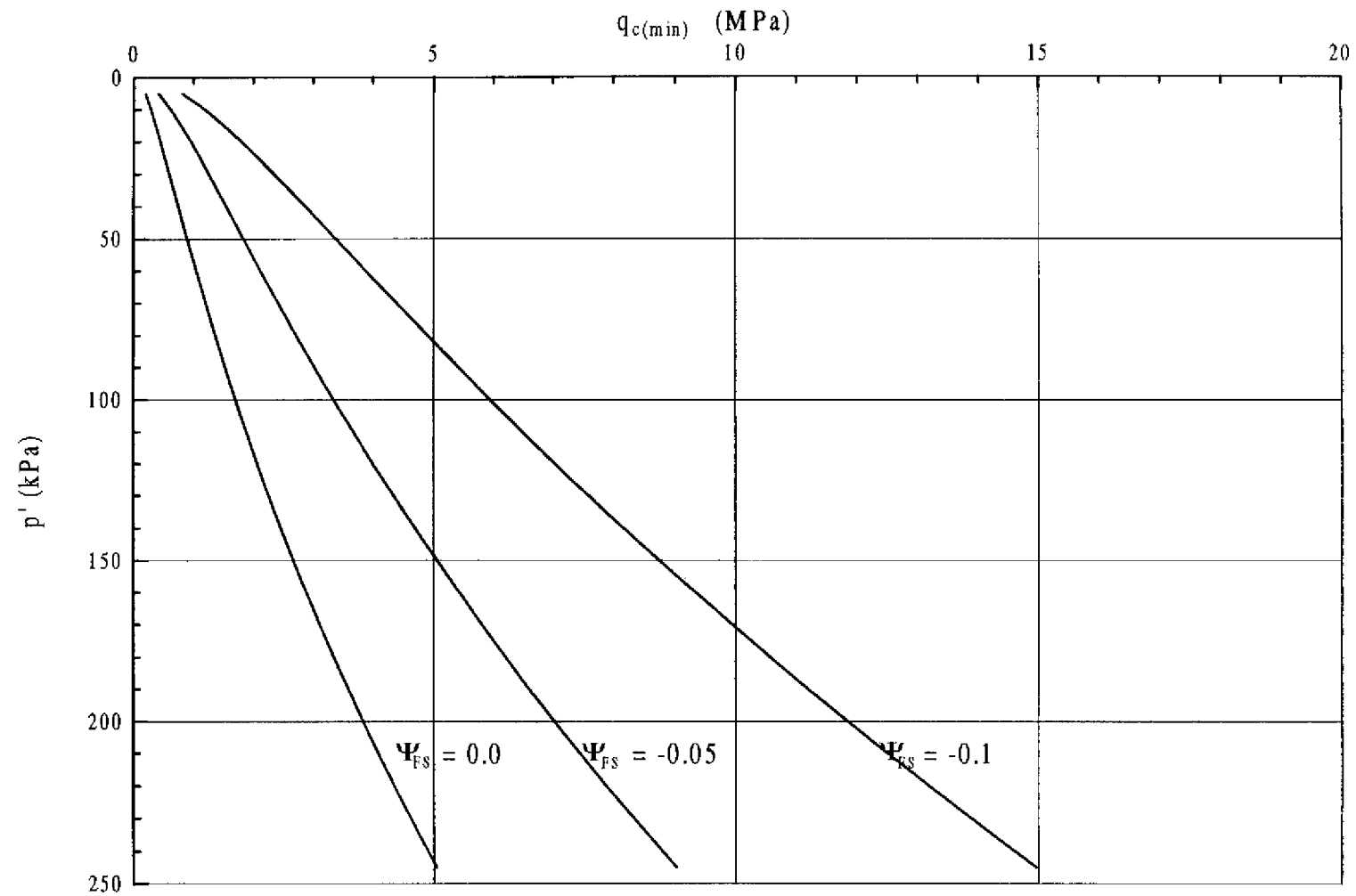


Figure 9.7 - Effects of $\Psi_{FS} = -0.05$ and -0.1 on the $q_{c(\min)}$ for the TC Sand

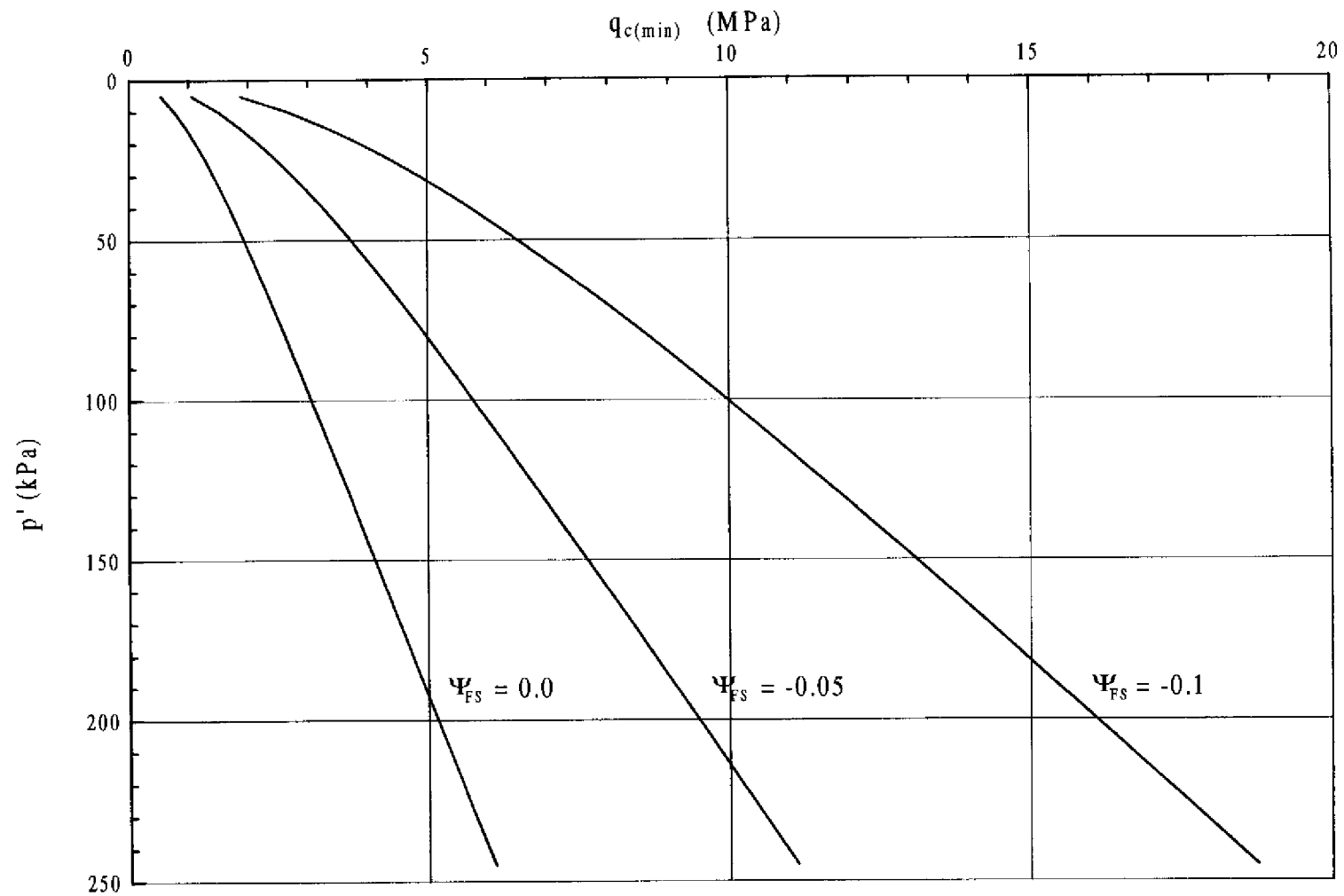


Figure 9.8 - Effects of $\Psi_{FS} = -0.05$ and -0.1 on the $q_{c(min)}$ for the CLK Sand

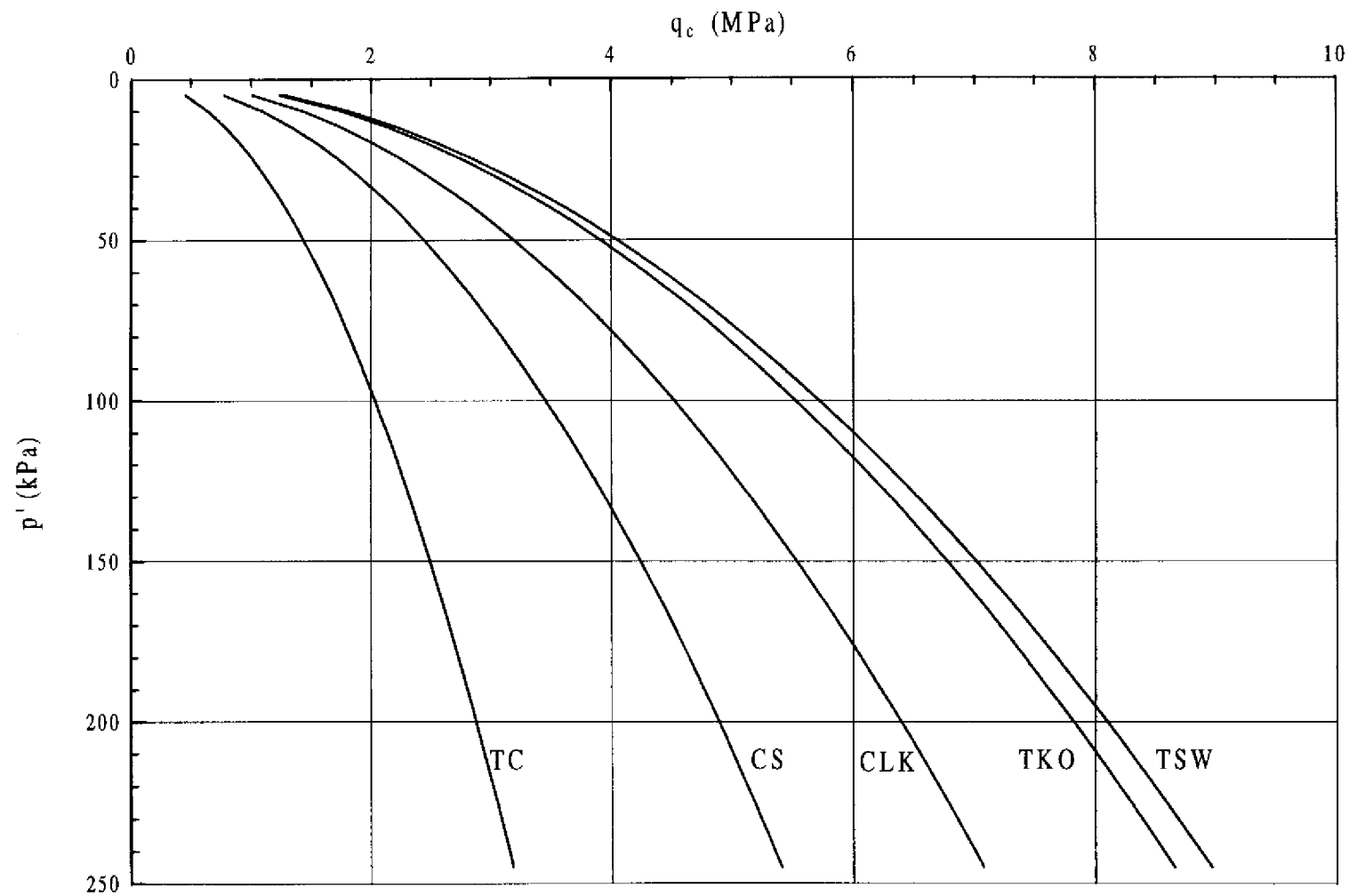


Figure 9.9 - Predicted p' versus q_c Profiles (with Relative Density, D_r of 40%) for the Five Hong Kong Marine Sands

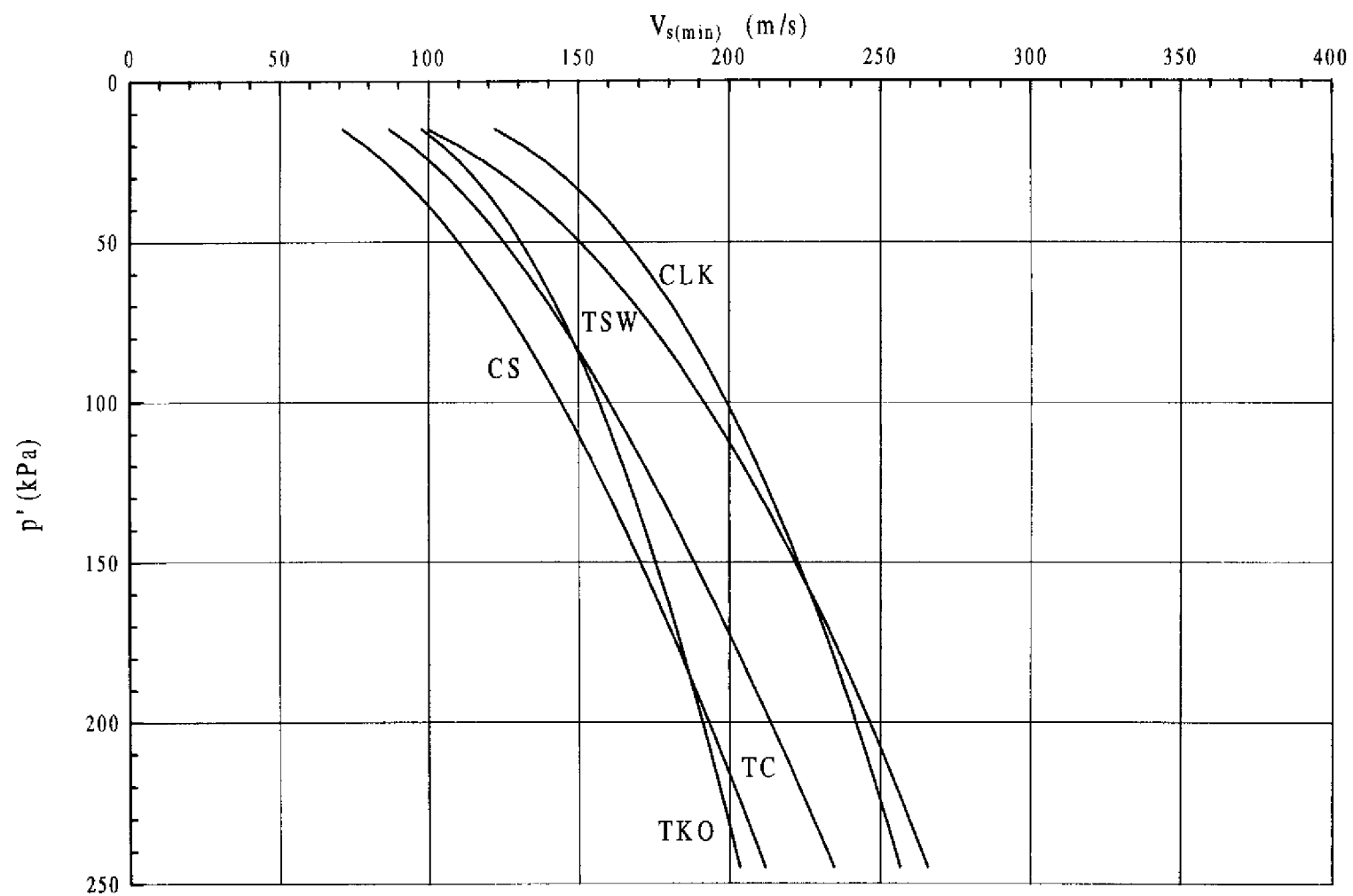


Figure 9.10 - Comparison between $\Psi = 0$ Profiles Based on V_s Correlation for the Five Hong Kong Marine Sands

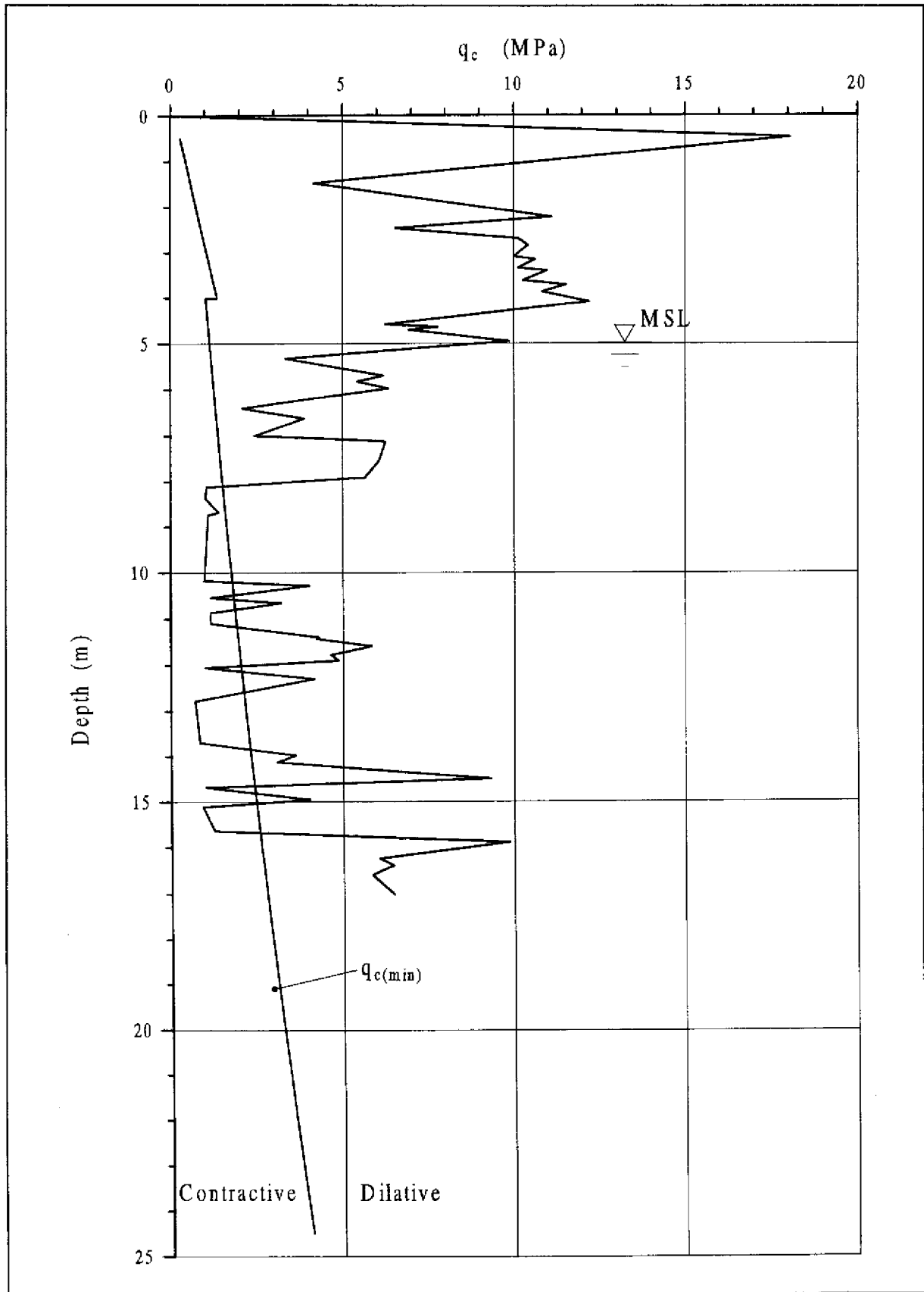


Figure 9.11 - Comparison of the Tung Chung Field CPT Data with $q_{c(min)}$
Defining the Contractive/Dilative Boundary

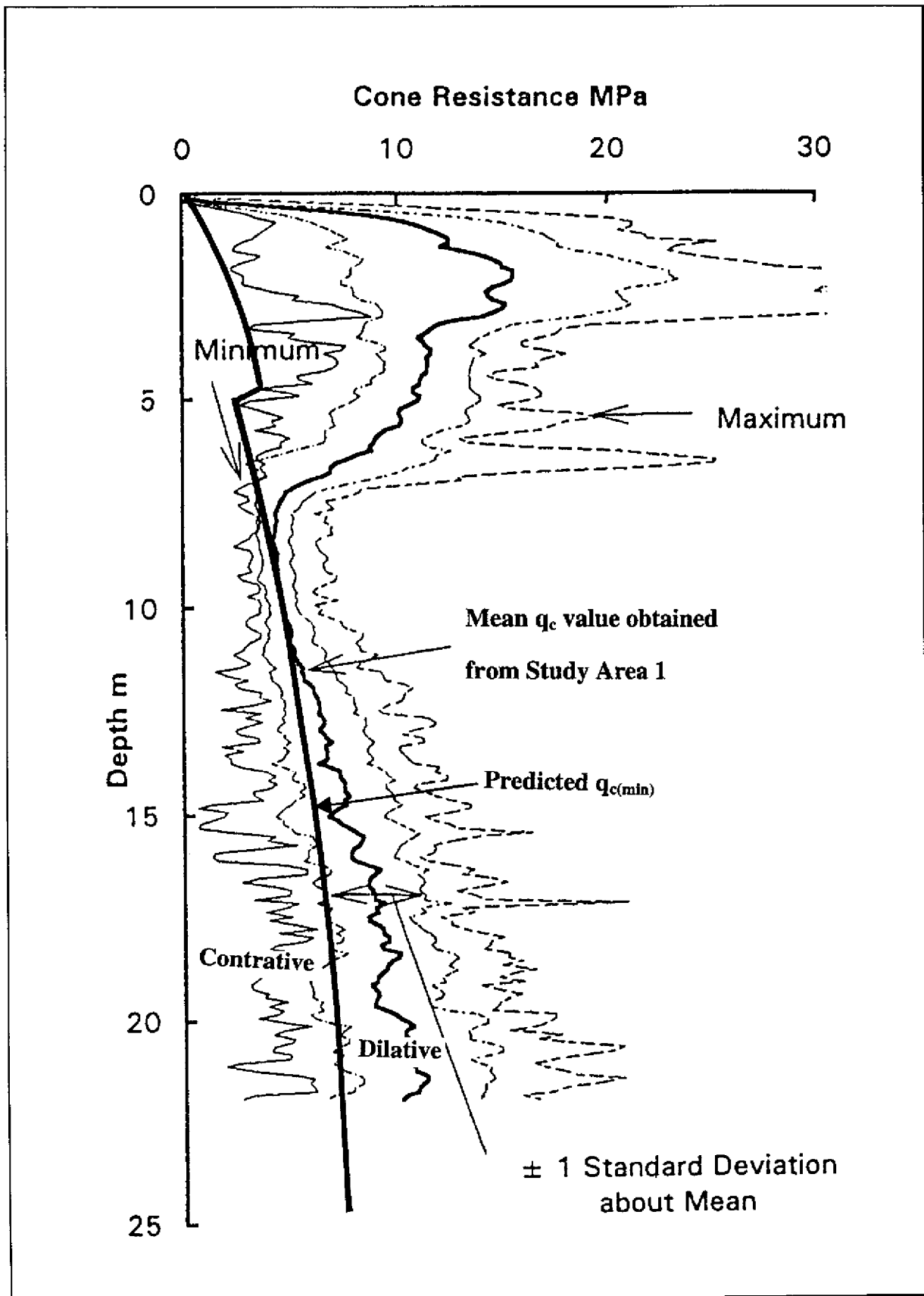


Figure 9.12 - Comparison of the CLK Field CPT Data with $q_{c(min)}$
Defining the Contractive/Dilative Boundary

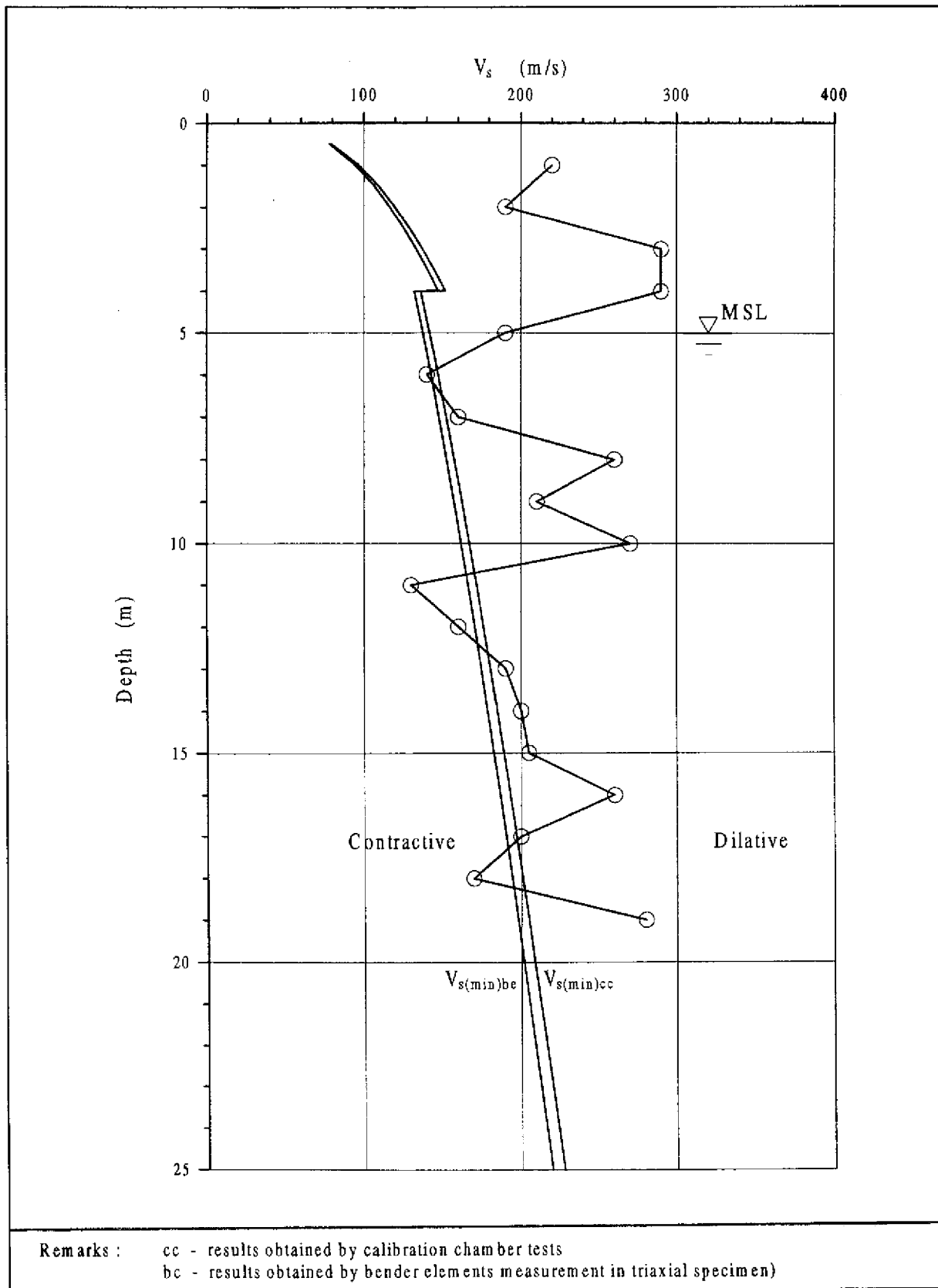


Figure 9.13 - Comparison of the Shear Wave Velocity Profile Determined by SCPT at the Tung Chung Site with the $V_{s(min)}$ Defining the Contractive/Dilative Boundary

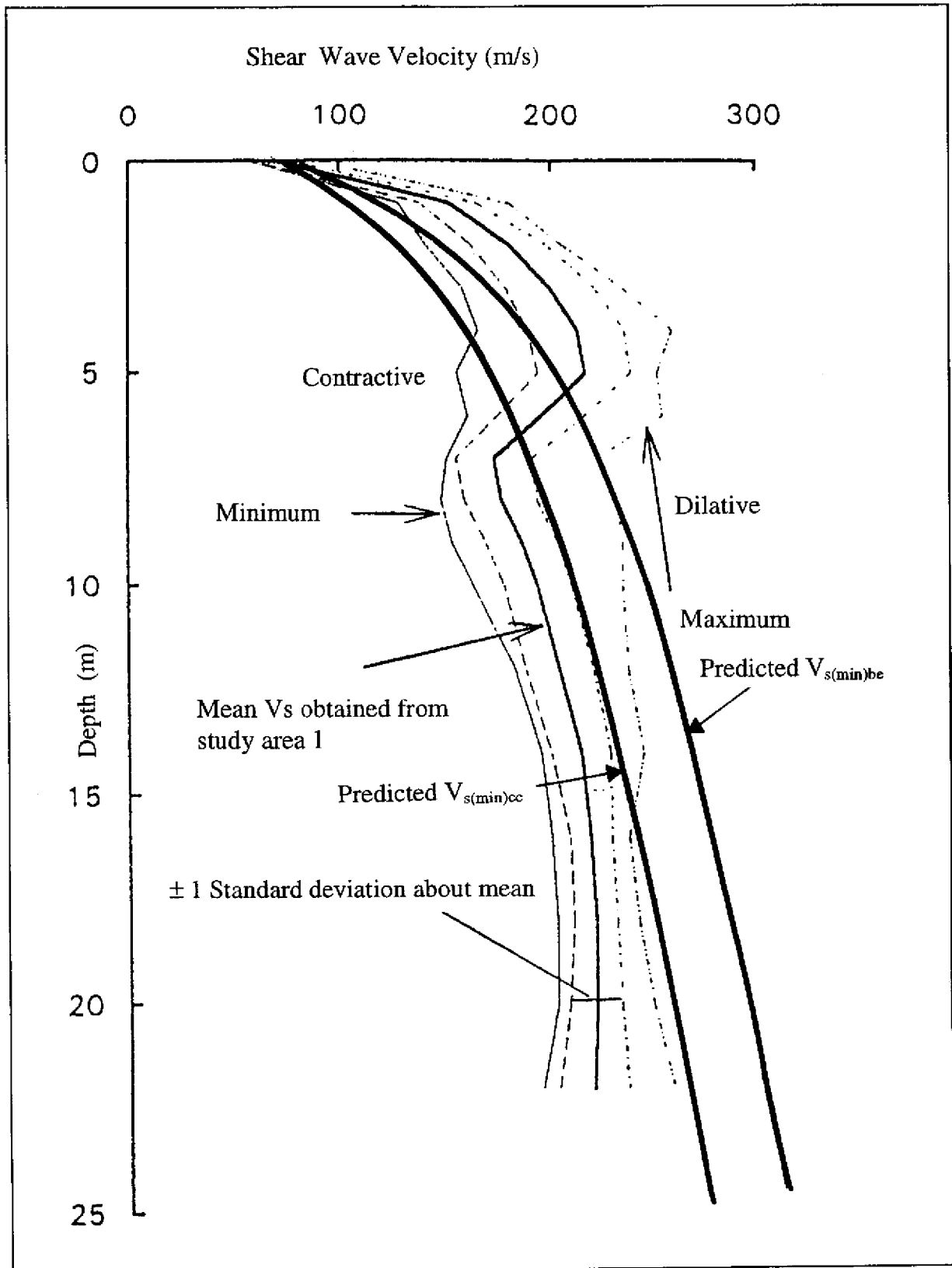


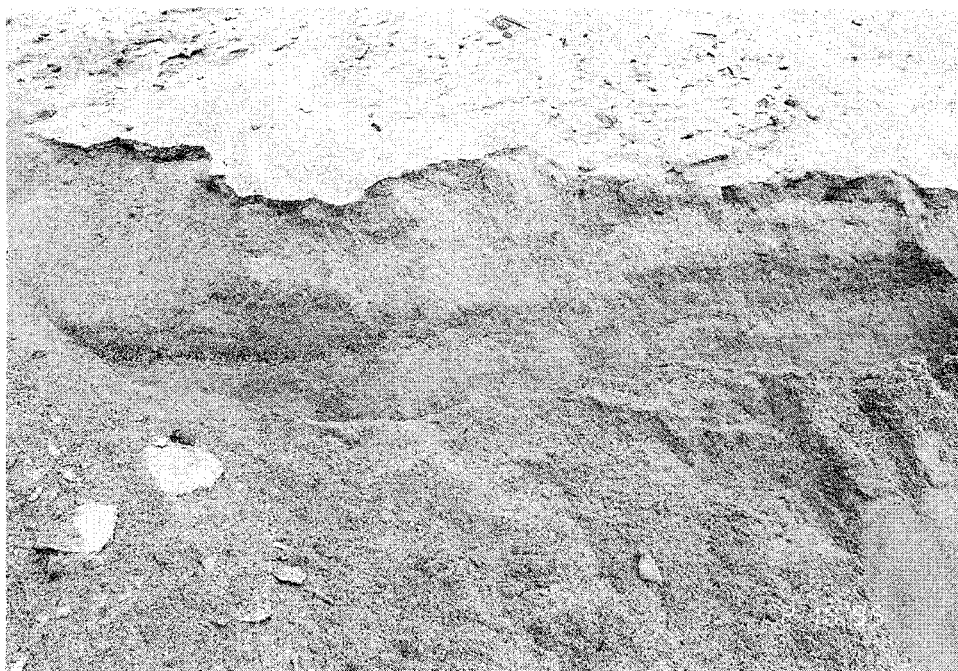
Figure 9.14 - Comparison of the Shear Wave Velocity Profile Determined by SCPT at the CLK Site with the $V_{s(min)}$ Defining the Contractive/Dilative Boundary (cc-results Obtained by Calibration Chamber Tests; Be-results Obtained by Bender Elements Measurement in Triaxial Specimen)

LIST OF PLATES

Plate No.		Page No.
2.1	Bulk Sampling at Chek Lap Kok (CLK) Site	261
2.2	Bulk Sampling at Tung Chung (TC) Site	262
3.1	Sand Extraction in Progress at Soko Sand Borrow Area for the TC Reclamation Site	263
5.1	A Bender Element Mounted on the Top Loading Platen	264
5.2	Triaxial Soil Sample with Bender Elements Mounted on the Top and Bottom Loading Platens	264
5.3	Set-up of Laboratory Shear Wave Velocity Measurement	265



(a) Bulk Sampling in Progress (CLK)

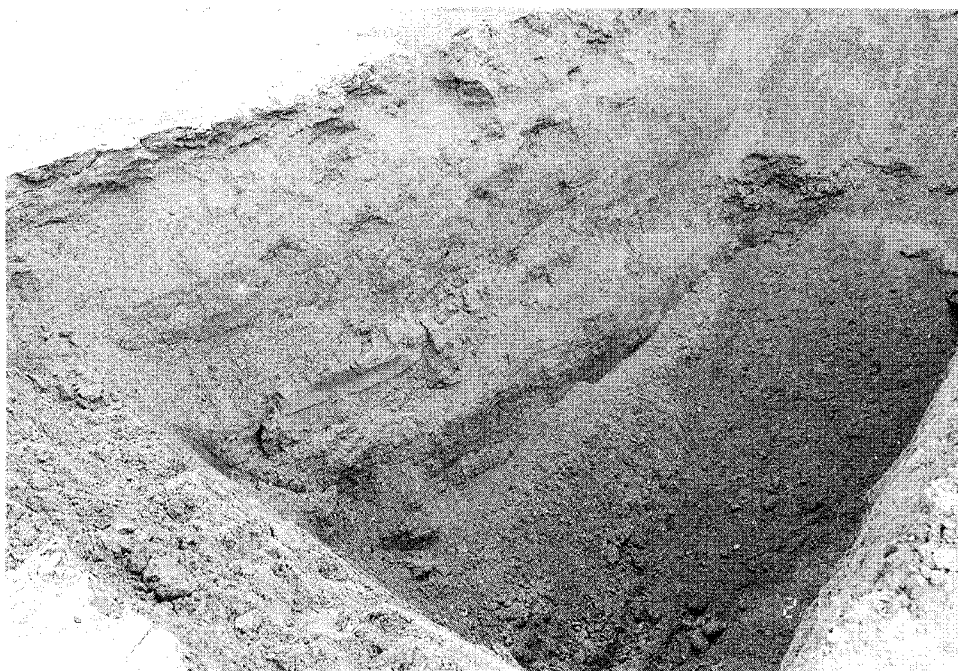


(b) Bulk Sample Taken from Stockpile at CLK

Plate 2.1 - Bulk Sampling at Chek Lap Kok (CLK) Site



(a) Bulk Sampling in Progress (TC)



(b) Bulk Sample Taken at 2 to 3 m below Ground

Plate 2.2 - Bulk Sampling at Tung Chung (TC) Site

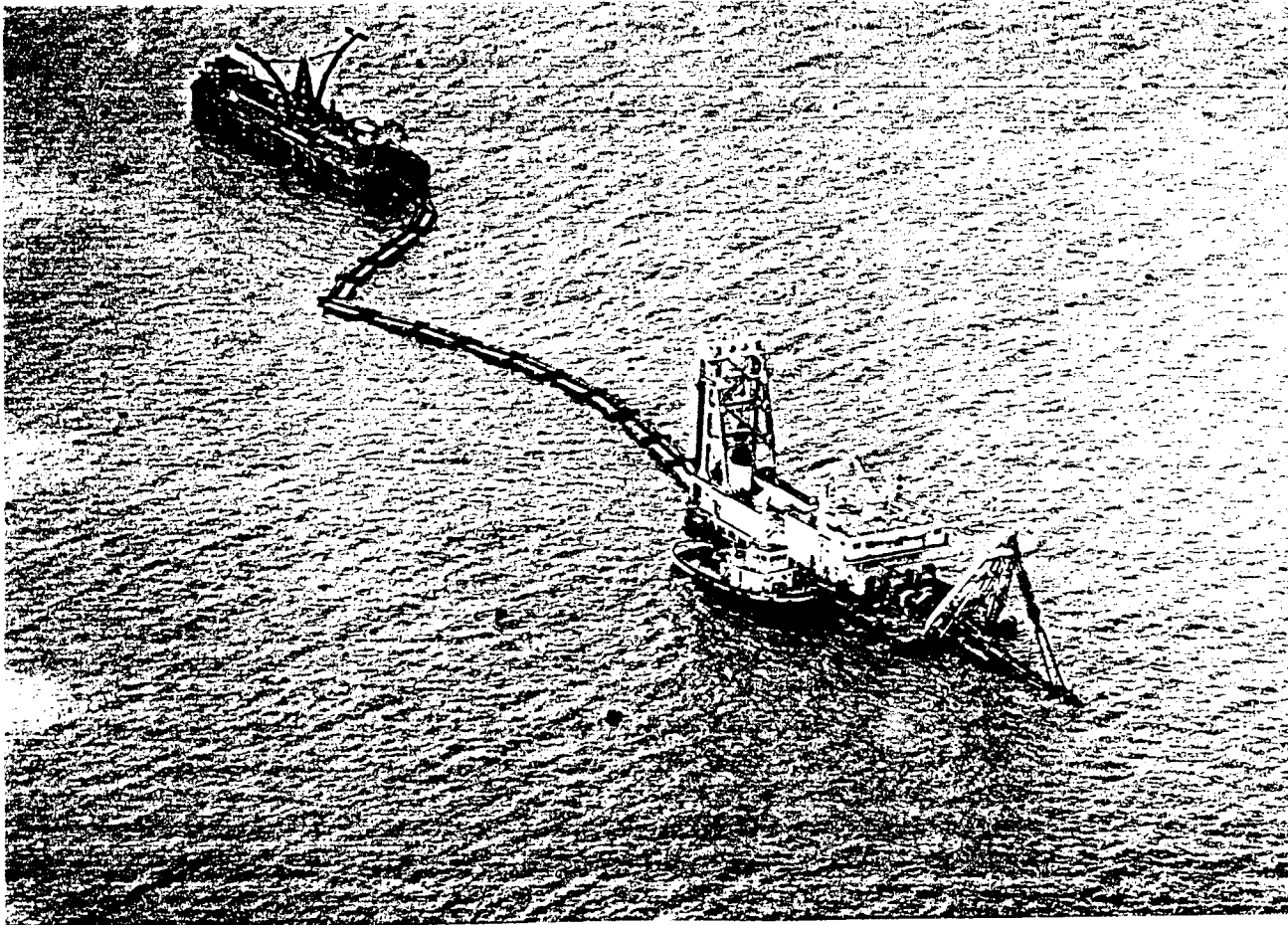


Plate 3.1 - Sand Extraction in Progress at Soko Sand Borrow Area for the TC Reclamation Site

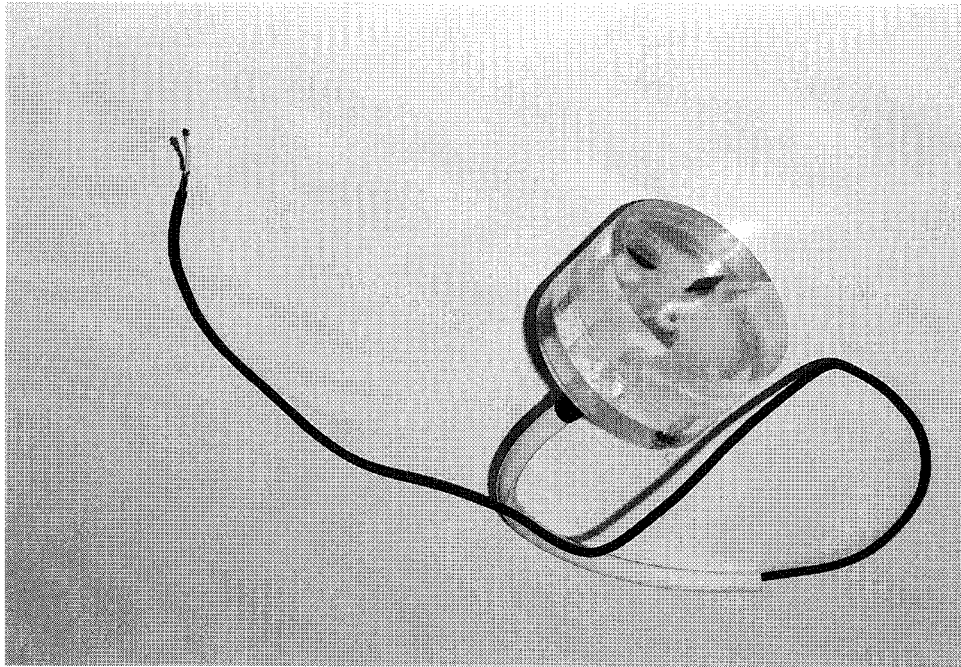


Plate 5.1 - A Bender Element Mounted on the Top Loading Platen

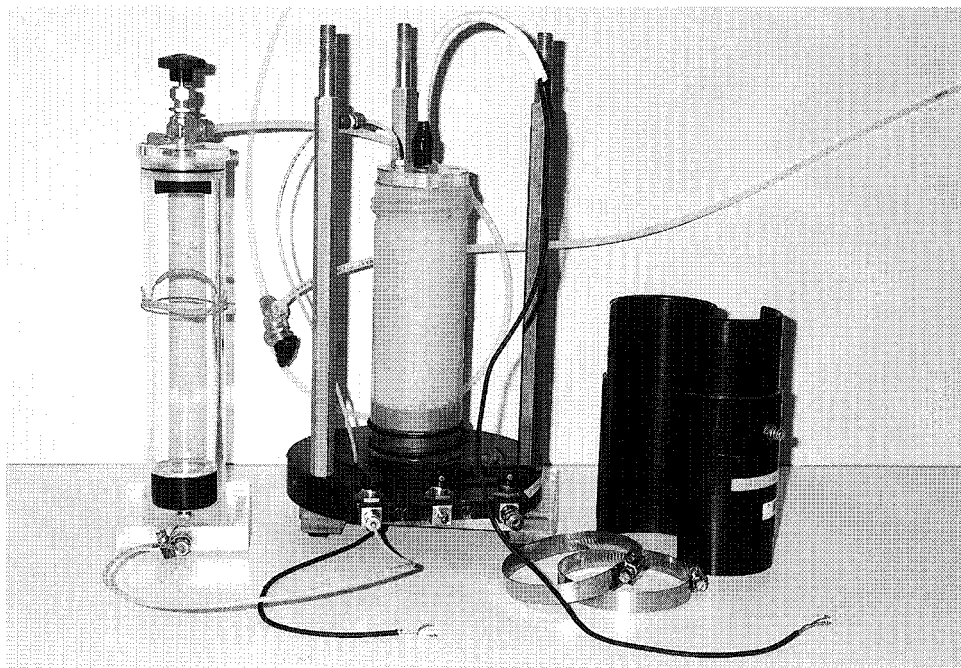


Plate 5.2 - Triaxial Soil Sample with Bender Elements Mounted on the Top and Bottom Loading Platens

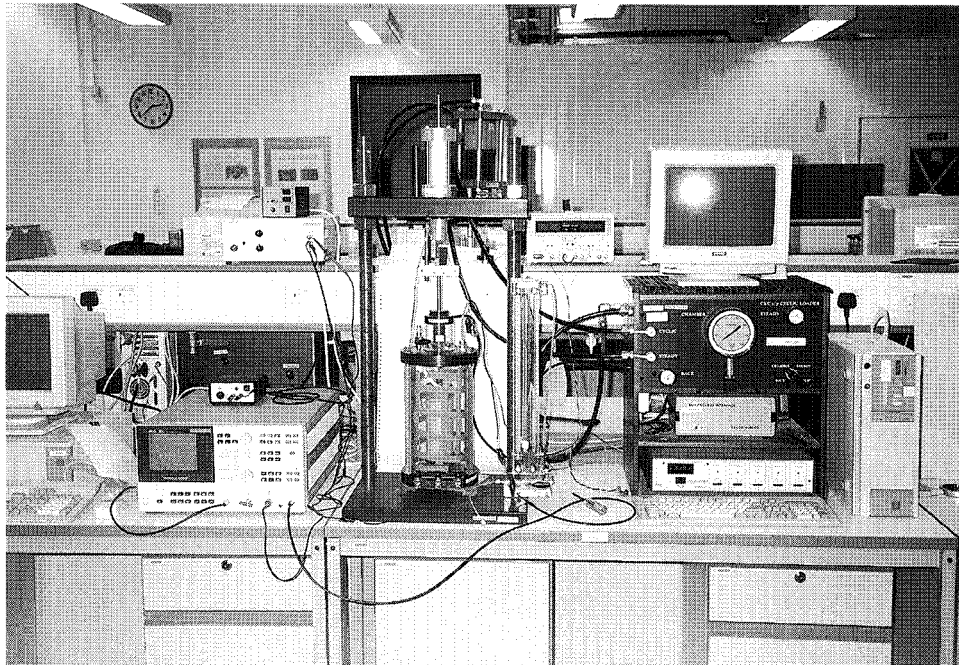


Plate 5.3 - Set-up of Laboratory Shear Wave Velocity Measurement